INVESTIGATION OF CATALYTIC ACTIVITY OF STABLE β-KETOACYL-ACP SUBSTRATE ANALOGS IN QUORUM SENSING SIGNAL SYNTHESIS

by

Nhu Lam

A thesis

submitted in partial fulfillment

of the requirements for the degree of

Master of Science in Chemistry

Boise State University

May 2018

BOISE STATE UNIVERSITY GRADUATE COLLEGE

DEFENSE COMMITTEE AND FINAL READING APPROVALS

of the thesis submitted by

Nhu Lam

Thesis Title: Investigation of Catalytic Activity of Stable β-Ketoacyl-ACP Substrate Analogs in Quorum Sensing Signal Synthesis

Date of Final Oral Examination: 12 October 2017

The following individuals read and discussed the thesis submitted by student Nhu Lam, and they evaluated her presentation and response to questions during the final oral examination. They found that the student passed the final oral examination.

Rajesh Nagarajan, Ph.D.	Chair, Supervisory Committee
Eric Brown, Ph.D.	Member, Supervisory Committee
Owen McDougal, Ph.D.	Member, Supervisory Committee

The final reading approval of the thesis was granted by Rajesh Nagarajan, Ph.D., Chair of the Supervisory Committee. The thesis was approved by the Graduate College.

DEDICATION

I dedicate this thesis work to my supportive family. A special feeling of gratitude to my loving mother, Loan Huynh, for constant support and encourgement during challenges I have experienced through this process. My brother, Tan Lam, who always believes in me. This thesis is also dedicated to my husband, Ryan Nguyen, who is always there for me throughout the struggles of graduate school and life. I'm truly thankful for having you in my life. He has always encouraged me to work hard for the things that I aspire to achieve.

ACKNOWLEDGEMENTS

I would like to thank my committee members, Dr. Rajesh Nagarajan, Dr. Eric Brown, and Dr. Owen McDougal, who were more than generous with their expertise and precious time. I would first like to thank my research mentor, Dr. Rajesh Nagarajan, for his guidance and the opportunities he has offered me. He is an incredible organizer, a great problem solver, and extremely helpful in moving my project forward. Under his mentorship, I have learned to become a better scientist and invaluable tools for my future career. Thank Dr. Eric Brown for always being available and your guidance to help me achieve a great amount of organic chemistry work in this thesis.

I would like to acknowledge and thank the Department of Chemistry and Biochemistry at Boise State University for allowing me to conduct my research and providing any assistance requested. Special thanks go to Dr. Joe Dumais for always being enthusiastic in helping me develop a greater understanding of NMR, and Dr. Shin Pu for his great help in identifying substrates with mass spectrometry.

I would like to recognize the members of Dr. Rajesh Nagarajan's laboratory who have all contributed to the progress I have made. With his hard work in organic synthesis during his post-doc, Dr. Dastagiri Dudekula contributed tremendously to my successful organic synthesis experiments. Also, I would like to acknowledge Bri Durham for always being very helpful whenever I need a hand and always being excited to talk about scientific problems and data. I would like to express my appreciation for the optimistic attitude that

Ashley Poppe and Bradley Lopes bring to the lab; their interesting questions usually bring enjoyable experience to our research lab.

Finally, I would like to acknowledge the support by Institutional Development Awards (IDeA) from the National Institute of General Medical Sciences of the National Institutes of Health under Grants #P20GM103408, P20GM109095, and NIH Grant # 1R15GM117323-01.

ABSTRACT

Quorum sensing is an intercellular mechanism used by many bacterial pathogens to regulate behaviors, such as motility, virulence, and antibiotic production. Disruption of quorum sensing is shown to be deleterious to bacterial pathogenicity, without causing lethality. In Gram-negative bacteria, acyl-homoserine lactone (AHL or acyl-HSL) signal molecules are synthesized by AHL synthase enzymes using acylated-acyl carrier protein (acyl-ACP) and S-adenosyl-L-methionine (SAM) as their substrates. *Pantoea stewartii* EsaI, which causes Stewart's wilt in corn, and *Yersinia pestis* YspI, which causes bubonic plague are AHL synthases that use 3-oxohexanoyl-ACP and 3-oxooctanoyl-ACP as the acyl-substrate to synthesize 3-oxohexanoyl-HSL and 3-oxooctanoyl-HSL signals, respectively. Unfortunately, the instability of the β-ketoacyl-ACP substrate due to the enolate formation at the β-position in the acyl-chain impedes mechanistic investigations for β-ketoacyl-ACP utilizing enzymes. In this thesis, we designed, developed, and evaluated a library of stable β-ketoacyl-ACP mimics for two β-ketoacyl-ACP utilizing AHL synthases, EsaI and YspI. We found that 2-furanacetyl-ACP and 2-benzofuranacetyl-ACP were the best 3-oxoacyl-ACP alternative substrate for EsaI and YspI, respectively, and within an order of magnitude to that observed for well-characterized ACP/CoA-dependent AHL synthases with their native acyl-ACP/ acyl-CoA substrate, such as RhlI, BmaI, and BjaI. The presence of a heteroatom other than oxygen is crucial to retain enzyme activity in both EsaI and YspI. Also, substrate inhibition of 2-thiopheneacetyl-ACP was observed with both enzymes. The success of synthesis and high activity of β-ketoacyl-ACP

mimics for EsaI and YspI should open new doors in characterizing this class of enzymes. Moreover, the β-ketoacyl-ACP substrates could be used as chemical probes to explore and design inhibitors for therapeutically important AHL synthases and several uncharacterized enzymes that impacts human health, such as β-ketoacyl-ACP reductase in fatty acid biosynthesis and polyketide synthase in polyketide synthesis which are targets for antimicrobial, antimalarial, and anti-cancer drugs.

TABLE OF CONTENTS

LIST OF FIGURES

LIST OF TABLES

LIST OF ABBREVIATIONS

QS	Quorum sensing
QSI	Quorum sensing inhibitor
AI	Autoinducer
AIP	Autoinducer peptide
AI-1	Autoinducer-1
AI-2	Autoinducer-2
AHL	Acyl-homoserine lactone
HSL	Homoserine lactone
ACP	Acyl-carrier protein
Acyl-ACP	Acyl-acyl-carrier protein
C6-ACP	Hexanoyl-ACP
C8-ACP	Octanoyl-ACP
C10-ACP	Decanoyl-ACP
CoA	Coenzyme A
SAM	S-adenosyl-L-methionine
MTA	5′-Methylthioadenosine
MTAN	5′-Methylthioadenosine/S-adenosylhomocysteine nucleosidase
XO	Xanthine oxidase
DCPIP	2,6-Dichlorophenolindophenol

UV-Vis	Ultraviolet Visible light
HPLC	High-performance liquid chromatography
Sfp	Surfactin-synthetase activating protein/phosphopantetheinyl transferase
Tris	Tris(hydroxymethyl)aminomethane
EsaI	*Panteoa stewartii* initiator
EsaR	*Panteoa stewartii* receptor
YspI	*Yersinia pestis* initiator
NMR	Nuclear magnetic resonance
COSY	Correlated spectroscopy
HMBC	Heteronuclear Multiple Bond Coherence
HSQC	Heteronuclear single quantum coherence
MS	Mass spectrometry
ESI	Electrospray Ionization
TOF	Time-of-flight

CHAPTER ONE: LITERATURE REVIEW

Quorum Sensing

In many bacterial pathogens, quorum sensing (QS) serves as an intercellular mechanism to establish pathogenic interactions with eukaryotic hosts or to colonize inanimate natural habitats. QS coordinates bacterial behaviors in a cell-density dependent manner. Bacteria communicate with each other by using small, diffusible chemical molecules, called autoinducers.[1,2] These chemical signal molecules help bacteria to count their local population. When the bacterial cells have reached a sufficient quorum, they behave like multicellular species and express virulence.

Thirty years ago, quorum sensing was first discovered in the bioluminescent marine bacterium *Vibrio fischeri*.[1] This bacterium lives in symbiotic relationship with eukaryotic hosts, such as squid *Euprymna scolopes.* When moonlight on a bright clear night penetrates clear water, the bacterium *V. fischeri* provides the squid with counter-illumination to prevent the casting of a shadow underneath and avoid getting noticed from predators. The regulation of light production is correlated with the cell-population density of the bacteria. As the *V. fischeri* bacterial culture grows, concentration of autoinducer molecules increases in the extracellular environment as well as in the intracellular environment. The accumulation of autoinducers activates transcription of luciferase operon responsible for bacterial luminescence.

The bacterial communication systems both within and between species have been shown to be critical for bacterial survival and interaction in natural habitats. Different

groups of bacteria can have different quorum sensing systems.[2,3] Two major classes of autoinducers are species-specific (autoinducer-1, AI-1) and universal (autoinducer-2, AI-2). Gram-negative bacteria produce *N*-acylated-L-homoserine lactones (AHLs), while Gram-positive bacteria produce cyclic or linear peptides as autoinducer peptides (AIP) (Figure 1). The AI-2 quorum sensing system is used by both Gram-negative and Gram-positive bacteria allowing different bacterial species to communicate with each other (Figure 1).

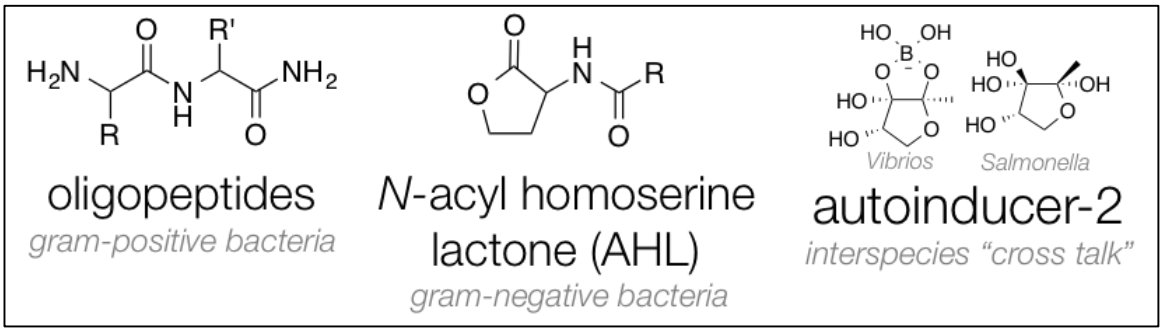

Figure 1. Examples of AHL, AIP, and AI-2 molecules in Gram-negative and Gram-positive bacteria.

AHL-based Quorum Sensing in Gram-negative Bacteria

In the last 30 years, over 50 species of Gram-negative bacteria have been identified to be similar to the quorum sensing system of the symbiotic bacterium *V. fischeri,* which contain homologues of two regulatory proteins called LuxI and LuxR.[1,2,3,4] LuxI-type protein, also called AHL synthase is responsible for the production of *N*-acyl-L-homoserine lactone autoinducer (AHL, AI-1), which can diffuse in and out of the cell either by free diffusion or AHL specific transporters. LuxR-type protein is the receptor for AHLs (Figure 2). When the bacterial cell growth reaches to optimal density, a productive binding of AHL to LuxR activates transcription of target genes, such as bioluminescence, swarming motility, biofilm formation, cell division, stress survival, horizontal DNA transfer,

virulence factors, such as extracellular polysaccharides (EPS), antibiotics, proteases, surfactants, and extracellular enzymes. AHL signal molecules are species-specific. The specificity of AHLs come from variation in acyl-chain. The specific signal production from AHL-synthase allow bacteria to communicate within its own species efficiently.

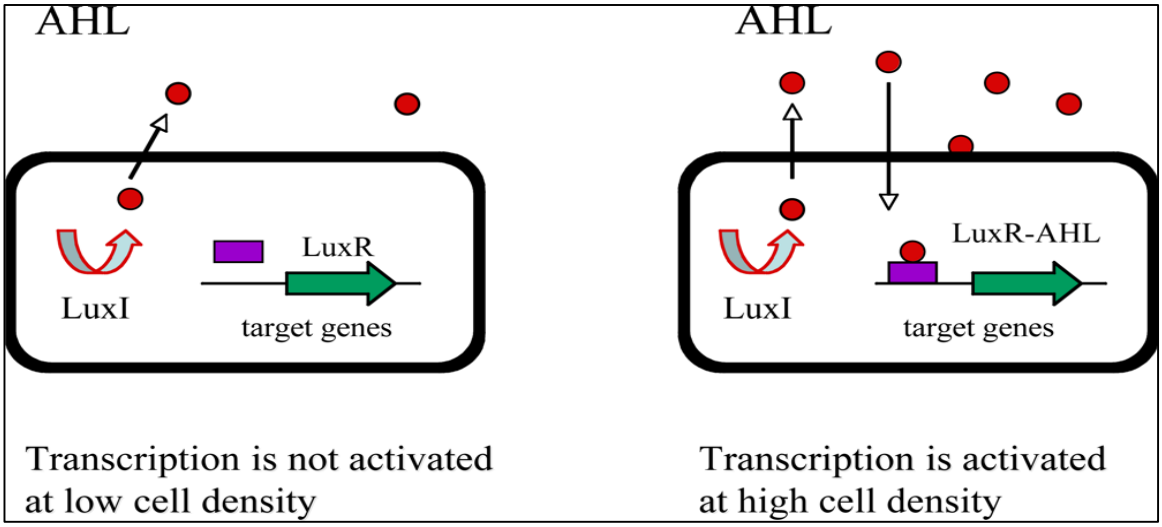

Figure 2. AHL-based quorum sensing in Gram-negative Bacteria (LuxI/LuxR-type). AHLs are represented by red circles, and transcription factors are represented by purple rectangular. The LuxI-type protein is an AHL-synthase responsible for the synthesis of AHLs. AHLs are freely diffusible across the cell membrane and accumulate in proportion to cell density. At high cell density, LuxR-type protein recognizes and binds to AHLs to activate transcription of target genes.

Peptide-based Quorum Sensing in Gram-positive Bacteria

Unlike Gram-negative bacteria, Gram-positive bacteria use oligopeptides as autoinducers for quorum sensing, called autoinducing peptide, AIP.[3] The quorum sensing system is a dephosphorylation-phosphorylation cascade (Figure 3).[1,3] AIPs cannot diffuse freely in and out of the cell membrane but transported through oligopeptide transporter. Two component signaling system, histidine sensor kinase protein and response regulator protein, are the detectors for secretion of peptide signals. The response regulator protein is highly selective for a specific peptide signal, which gives rise to specificity between

bacteria. Histidine sensor kinase detects a specific peptide autoinducer signal and undergoes autophosphorylation cascade. Then, the response regulator protein is activated and phosphorylated. The phosphorylated response regulator protein activates transcription of target genes.

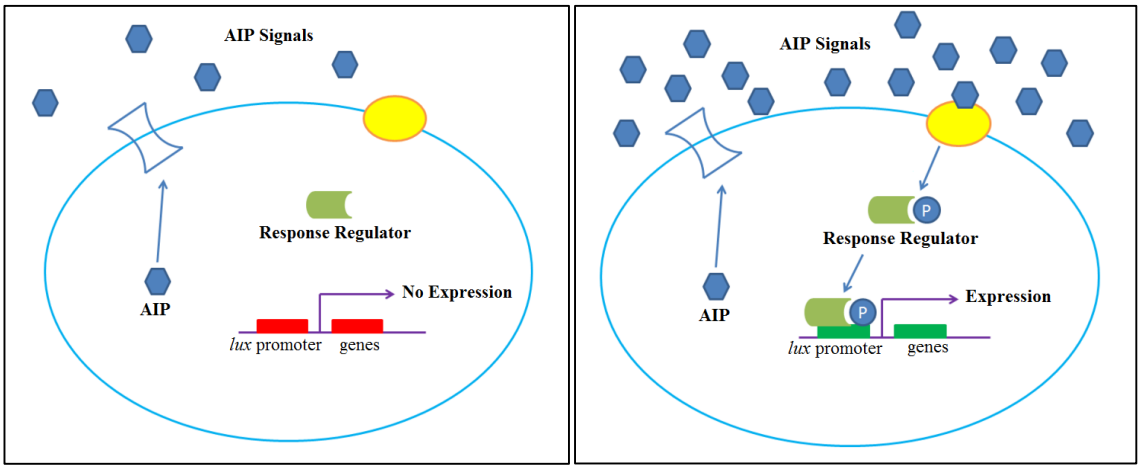

Figure 3. Peptide-based quorum sensing in Gram-positive Bacteria. AIPs are represented by blue hexagon, oligopeptide transporter is represented by cylinder, and surface receptor is represented by yellow oval. Quorum sensing system consists of two-component signal transduction system. The cell membrane consists of oligopeptide transporter that is responsible for secretion of signaling peptide molecules (known as autoinducing peptide, AIP) out of the cell. At high cell density, AIPs bind to a surface receptor, which in turn phosphorylates a response regulator, and regulate gene expression.

Autoinducer-2-based Quorum Sensing

Intra-species communication is advantageous to bacteria themselves because signal synthesis is specific, and the signal to noise ratio is high so that the interference from neighboring bacteria is at minimal. However, *in vivo*, bacteria live in an environment with multiple other different species. Autoinducer-2 (AI-2), synthesized by LuxS is a universal signal molecule used in multispecies communities. AI-2, furanosyl borate diester, was first identified in the marine bacterium *Vibrio harveyi* (Figure 1), and is produced and recognized by many Gram-negative and Gram-positive bacteria.[1,3] Detection of AI-2 molecule takes place either extra- or intracellularly, depending on the bacterium.

Quorum Sensing Inhibitor (QSI) Strategies

At low cellular density, bacteria are singular cells and harmless. When they grow and reach their optimal density, they behave like multicellular organisms. To protect themselves from enemies, such as antibiotics and other chemical or physical stresses, bacteria attach to a surface and grow as a biofilm.[5-7] The bacterial biofilms are composed of biopolymer matrix containing polysaccharides, proteins, and DNA originating from the bacteria. Bacterial biofilms have been demonstrated to be tolerant to antibiotics and involved in chronic infections characterized by persistent inflammation and tissue damage.[8,9]

Current antibiotics in the market kill bacteria that enforces a selective pressure on the bacterium to evolve into a drug-resistant species. Quorum sensing systems are used by bacteria to establish virulence and biofilm formation, but they are not essential for survival.[2] Therefore, quorum sensing inhibitors (QSI) as druggable target is a promising strategy against infectious diseases to decrease pathogenicity without imposing selective pressure associated with antibacterial treatments.[10,11] An effective QSI needs to be chemically stable, highly specific for a given quorum sensing regulator with no adverse effects on the bacteria or the host, and resistant to degradation by various host metabolic systems.[11] Quorum sensing can be inhibited or disrupted by several different methods: 1) inhibiting AHL cognate receptor, 2) inhibiting the production of AHL signal molecules, 3) inactivating quorum sensing signals by enzymatic degradation, such as lactonases and acylases, 4) mimicking signal molecules using synthetic analogs, 5) scavenging quorum sensing molecules by quorum sensing quenching antibodies as vaccination strategy.[11-16]

Effort to understand and disrupt quorum sensing by inhibiting the activity of AHL-synthases is explored in this thesis.

Over the past decades, there have been a lot of debates on whether bacteria will eventually evolve and develop resistance to quorum sensing inhibitors.[17,18,19] Quorum sensing is the mechanism by which the accumulation of small diffusible signaling molecules drive the expression of genes coding virulence factors. The production of the virulence factors has been shown to be a group-beneficial trait that provides a benefit to the local population of bacterial cells. Human infections generally have group-beneficial selective environment. There are two barriers obstructing bacteria from developing resistance to quorum sensing inhibitors (Figure 4).[20] The first barrier is that QSI-resistant mutants receive insufficient signals to express their quorum sensing. As bacterial cells depend on the production of autoinducers from other cells to reach to a quorum, QSI-sensitive cells do not produce enough quorum signals to allow the QSI-resistant bacteria to thrive. The second barrier is that even if QSI-resistant strains are able to express their quorum sensing, the group-beneficial traits, which are formed at the cost of the QSI-resistant strains, will be shared ("cheated off") by all neighboring nonresistant strains, giving the QSI-resistant strains no selective advantage. Thus, the resistant strains would likely to be outcompeted by "cheaters" and failed to spread resistance.

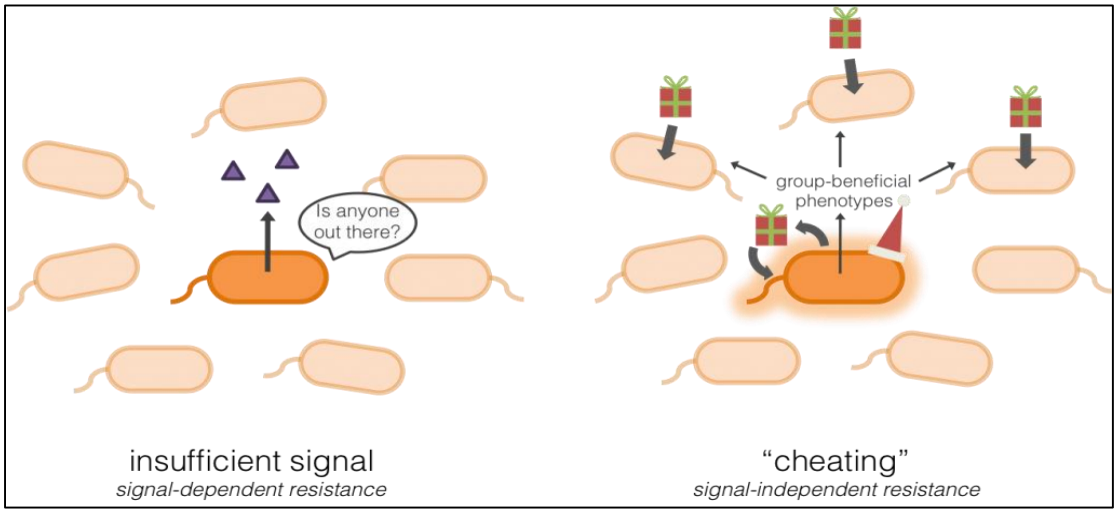

Figure 4. Two barriers blocking bacteria from spreading resistance to quorum sensing inhibitors (QSI). Left: Signal-dependent resistance. Quorum sensing depends on group-beneficial behavior. Insufficient signals prevent rare QSI-resistant from expressing quorum sensing. Right: Signal-independent resistance. Assuming the rare QSI-resistant mutant is able to express quorum sensing and produces group-beneficial phenotypes, QSI-sensitive neighbors would benefit the public goods by cheating off the mutant. Eventually, the mutants are outcompeted by the cheaters.[20]

AHL-synthase Proposed Mechanism

In Gram-negative bacteria, *N*-acyl homoserine lactones (AHLs) are the most common class of autoinducers. The LuxI-type protein in quorum sensing mechanism that are responsible for the synthesis of AHLs are called AHL-synthases. AHL-synthases are bi-substrates enzymes utilizing S-adenosyl-L-methionine (SAM) and acyl-acyl-carrier protein (acyl-ACP) or acyl-CoA substrates to synthesize AHL signals (Scheme 1).[21] The proposed mechanism of AHL signal synthesis have two chemical steps: acylation and lactonization. The acylation step involves a direct nucleophilic attack of the amine of SAM on the α-carbonyl carbon of acyl-ACP/acyl-CoA, resulting in cleavage of the acyl-thioester bond to release holo-ACP/ free CoA. Lactonization occurs by the nucleophilic attack on the γ-carbon of SAM by its own carboxylate oxygen to produce L-homoserine lactone product and release methylthioadenosine (MTA).

SAM is a substrate common to all AHL-synthases. SAM is often thought to be a substrate involved in methyl group transfers. In an interesting way, AHL-synthases use SAM to form lactone ring in AHL product. Acyl-ACP substrate is synthesized from bacterial fatty acid biosynthesis.[21-23] Both acyl-ACP and acyl-CoA substrates have a phosphopantetheine linker that forms a thioester bond to either a variable length acyl-chain or an acetyl group. In acyl-ACP, the phosphopantetheine linker is connected to the hydroxyl oxygen of Ser36 via a phosphodiester bond (Figure 5). In acyl-CoA, the phosphopantetheine linker (pantetheine is colored in blue in Figure 5) is connected to the adenosine 3´,5´-diphosphate. AHL signal specificity is derived from acyl-chain of the acyl-ACP/acyl-CoA that are either unsubstituted or carry modifications such as a 3-oxo, 3-hydroxy group .[21-31]

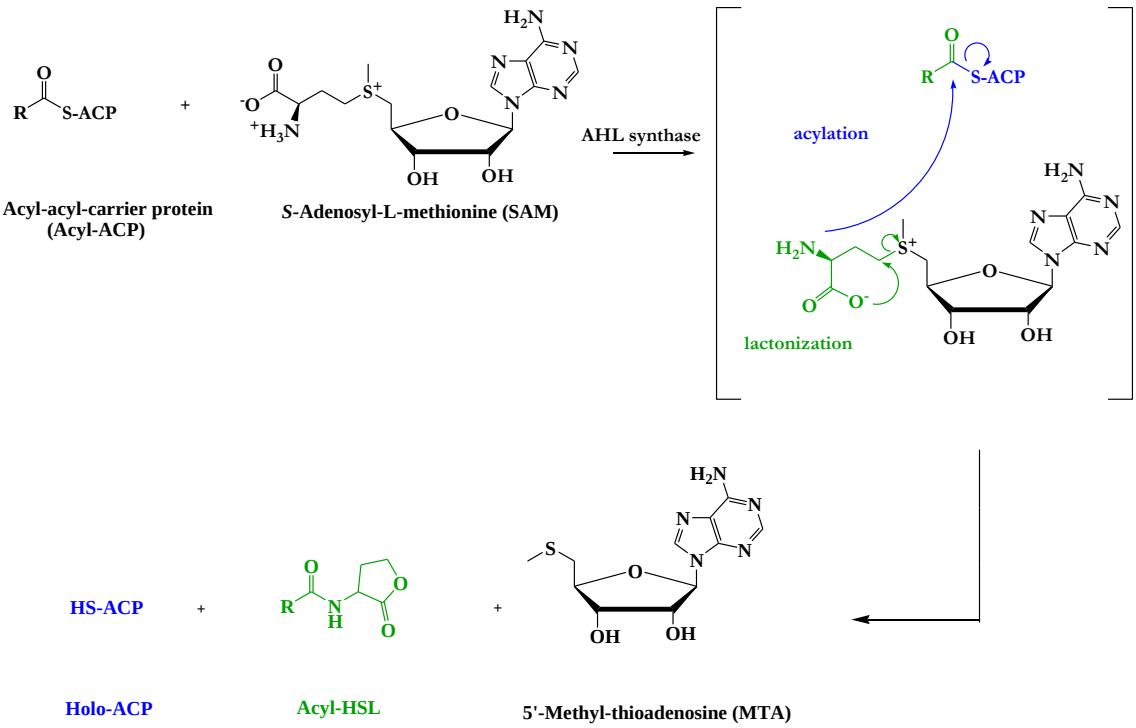

Scheme 1. The proposed AHL-synthase signal synthesis mechanism. AHL synthases react with two substrates SAM and acyl-ACP/acyl-CoA to produce three

products holo-ACP/ free-CoA, acyl-homoserine lactone (acyl-HSL), and MTA via two chemical steps: lactonization and acylation. The acyl-chain length in the AHL signal is specific for each bacterial species.

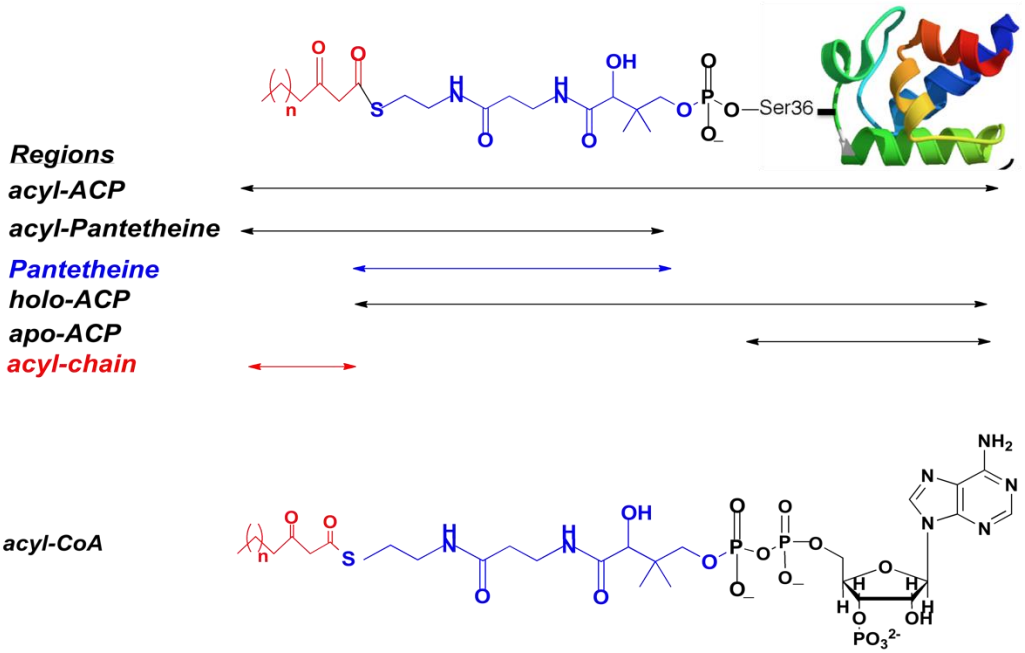

Figure 5. Structures of acyl-CoA, acyl-ACP, holo-ACP, and apo-ACP.

AHL-synthase Crystal Structures

To date, LuxI-type AHL synthase family is the most widespread and most studied. Yet, only four X-ray structures of *Pseudomonas aeruginosa* LasI (uses 3-oxododecanoyl-ACP), *Pantoea stewartii* EsaI (uses 3-oxohexanoyl-ACP), *Burkholderia glumae* TofI (uses octanoyl-ACP), and *Bradyrhizobium japonicum* BjaI (uses isovaleryl-CoA) have been identified previously (Figure 6).[27-32] Unfortunately, crystallization structures of acyl-ACP substrate bound to AHL synthases have not been published. Thus, the understanding of AHL synthases including binding site of acyl chain, phosphopantethiene moiety, and protein core of ACP are based on other enzymes and locations of conserved residues.

AHL synthases have notable structural similarities to *N*-acetyltransferases and defines a common phosphopantetheine binding fold as the catalytic core.[28-32] The topology

of AHL synthases is a mixed α-β-α sandwich with a V-shaped cleft and a deep cavity/tunnel (Figure 6). The ribbon structures of these AHL synthases reveal conserved regions of substrate binding sites and share similarities in binding sites for ACP, acyl-chain in acyl-ACP, and SAM.

ACP/CoA binding site

Acyl-carrier protein (ACP) is a cofactor protein that shuttles covalently bound fatty acid intermediates in its hydrophobic pocket to various partner enzymes.[22,23] The ACP has the negatively charged helix II function as the recognition helix for interaction with the partner enzyme. The interactions between the partner enzyme and ACP are largely electrostatic. In all ACP-dependent AHL synthases, the putative ACP binding site is identified by highly conserved basic residues that form a positively charged patch on the surface (Figure 6).[28-31] Interestingly, BjaI uses isovaleryl-CoA as the native substrate and shows no activity with isovaleryl-ACP.[24] Binding of isovaleryl-CoA is supported through π-stacking interactions between the adenine ring of isovaleryl-CoA and Trp142 located at the beginning of helix α5. The residue stacks with Trp143 resulting in the formation of an "indole platform", providing a foundation for binding to the adenine ring of CoA.[32]

SAM binding site

The N-terminal region of these AHL-synthases is highly conserved and forms a binding pocket for SAM, a substrate common to all AHL synthases. The binding pocket of SAM is located between helices α1 and α2 (Figure 6). In the four crystal structures of AHL synthases (LasI, EsaI, BjaI, and TofI), the strictly conserved residue Trp33 in LasI and TofI (Trp34 in EsaI and BjaI) on helix α2 is important in positioning the SAM amine nitrogen for acylation at the C1 position of acyl-ACP. The side chain of conserved residue Arg103

in BjaI (Arg100 in EsaI, Arg 104 in TofI and LasI) is in close proximity of the adenine ring of the bound SAM and significant in hydrogen-bonding network with the adenine moiety of SAM. [28-32]

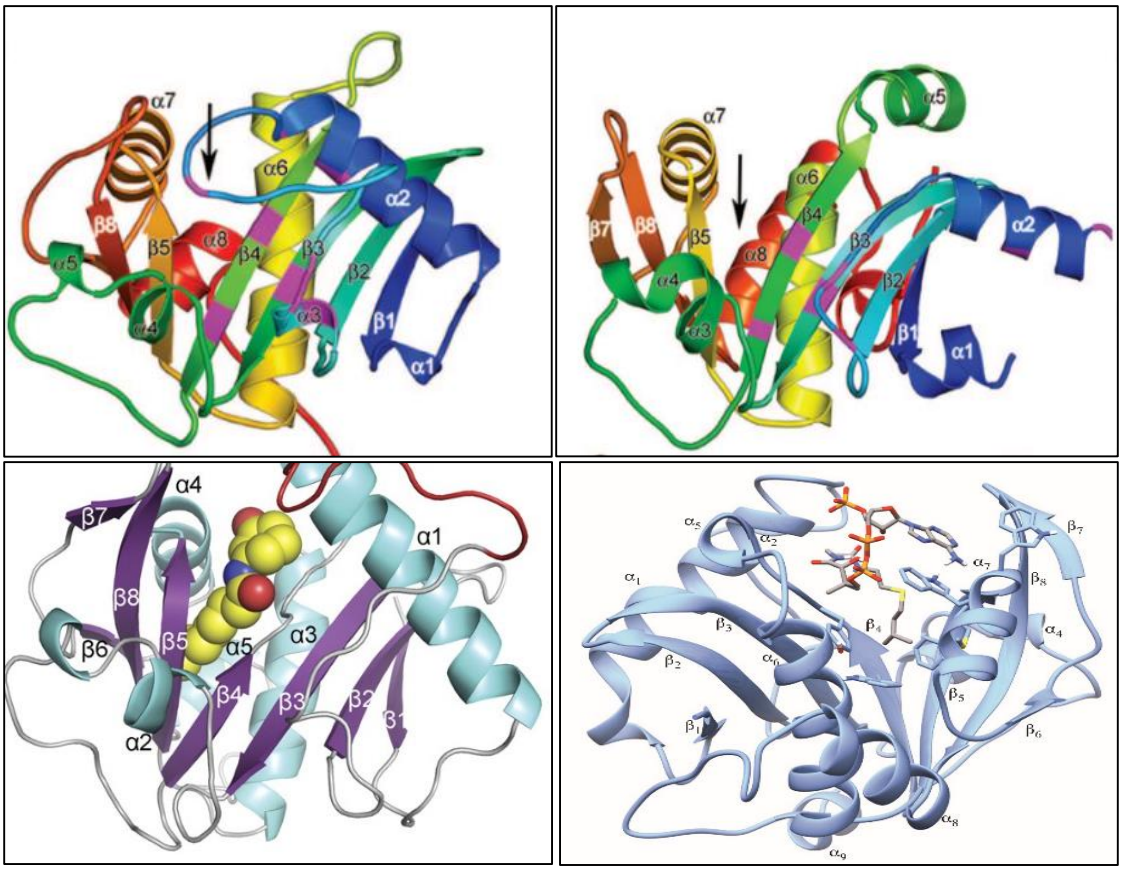

Figure 6. Crystal structures of AHL-synthases. *Pseudomonas aeruginosa* LasI (top left), *Pantoea stewartii* EsaI (top right), *Burkholderia glumae* TofI (bottom left) and *Bradyrhizobium japonicum* BjaI (bottom right). The common V-cleft for acyl-chain binding pocket formed between β5 and β4 (shown in arrow for LasI and EsaI) is observed in all four structures. LasI crystal structure shows a much deeper V-cleft than EsaI, TofI, and BjaI, which allow the enzyme to accommodate long acyl-chain (3-oxododecanoyl-ACP). BjaI structure is crystallized with isovaleryl-CoA native substrate bound.

Acyl-chain binding site

The C-terminal region is less conserved among AHL synthases and involved in recognition of variable acyl-chain of acyl-ACP substrate. The analyses of these AHL-synthase crystal structures (LasI, EsaI, TofI, and BjaI) reported an active site V-shaped

cleft that can accommodate variety of acyl-chain of acyl-ACP/acyl-CoA substrate (Figure 6). The acyl-chain specificity of AHL-synthases depend on the size and shape of this V-shaped acyl-chain binding pocket.

The acyl-chain binding pocket in EsaI structure is an enclosed cavity consisting of conserved residues (Ser98, Met126, Thr140, Val142, Met146, and Leu176) interacted 3-oxohexanoyl portion of the substrate.[28,30] Many other residues within the protein core but not necessarily in direct contact with the hexanoyl chain direct the size and shape of the cavity through hydrophobic packing, resulting in the limitation of acyl chain in EsaI to six carbons. Nonetheless, LasI can accommodate up to 12-carbon acyl-chain (3-oxododecanoyl-ACP) due to the elongated acyl-chain binding pocket that is formed by hydrophobic residues on helices α6, α7, and α8 (Trp69, Leu102, Phe105, Met125, Thr144, Met151, Met152, Ala155, Leu157, and Leu188).[29,30] There is no steric restriction on the acyl-chain length of acyl-ACP that could bind to LasI. In TofI structure, only five α-helices were identified. The acyl-chain binding pocket is enclosed by helices α1, α3, and α4.[31] The octanoyl-chain is surrounded by hydrophobic residues of β4, β5, α4, and α1. Comparing to the pocket of LasI and EsaI, sequence variations in and near the pocket area as well as localized structural differences in α3 and α4 lead to high specificity for the octanoyl chain substrate in TofI.

AHL-synthases from different bacteria can have different preferences for unsubstituted, 3-oxo-, or 3-hydroxyl-acyl-ACPs due to the selectivity of the AHL-synthases in a pool of available acyl-ACP substrates in fatty acid biosynthesis. RhlI produces unsubstituted C4-HSL, while LasI makes predominantly 3-oxoC12-HSL and EsaI synthesizes 3-oxoC6-HSL. The preference of AHL synthases for 3-oxo-substituted

acyl-ACP substrates is due to hydrogen bonding interactions between the 3-oxo- carbon in acyl chain of 3-oxoacyl-ACP and residues in the acyl-chain binding site.[28-30] Structural studies revealed that in the acyl-chain binding pocket, two hydrogen bonds are formed between the enzyme and the 3-oxo- group of the 3-oxoacyl-ACP substrate. One is from Thr140 in EsaI or Thr142 in LasI, and the other hydrogen bond is from the main chain carbonyl group of the adjacent residue (Ile141 in EsaI or Ile 145 in LasI). The mutation of threonine to alanine leads to a loss of specificity without any loss of enzyme activity, indicating the role of Thr140 (or Thr142) is in restricting the acyl-ACPs that can bind to the enzyme, rather than enhancing the affinity of the enzyme for 3-oxoacyl-ACPs.[26] Furthermore, enzymes that produce 3-hydroxy-HSLs have serine at this position (for example, *Rhizoboum leguminosarum* CinI) or unsubstituted HSLs have either glycine or alanine in this position (for example, *Bradyrhizobium japonicum* BjaI).[28-32]

As a result, the difference in hydrophobic residues and orientation of these catalytic residues make up the difference in size and shape of acyl-chain binding pocket. This allows AHL synthase to be able to accommodate a certain acyl-chain length in the active site and also discriminate its native substrate among a pool of acyl-ACPs.

Bi-substrates Enzyme Kinetics

The enzyme-catalyzed reaction with a single substrate can be represented as:

$$E + S \rightleftharpoons ES \rightarrow E + P$$

where E is an enzyme, S is a substrate, *ES* is an enzyme-substrate complex, and *P* is product released after catalysis. The initial rate of the reaction (*V*) can be related to K_m and V_{max} as:[30]

$$V = \frac{V_{max}[S]}{[S]+K_m} \quad (1)$$

where V_{max} is the maximal velocity of the enzyme-catalyzed reaction, [S] is the substrate concentration, and K_m is the amount of substrate required to reach half of V_{max}. By plotting the initial rate of the reaction against substrate concentration, V_{max} and K_m can be determined.

With bisubstrate enzymes, the situation is more complicated. The intital velocity equation becomes:

$$V = \frac{V_{max}[A][B]}{K_{iA}K_B + K_B[A] + K_A[B] + [A][B]} \quad (2)$$

where K_{iA} is the dissociation constant for substrate A in the absence of B, and K_B and K_A are the Michaelis-Menten constants for substrate B and A, respectively, at saturating conditions of the other fixed substrate. If one substrate is held at saturation (for example, substrate B), the above equation is simplified as:

$$V = \frac{V_{max}[A][B]}{K_A[B] + [A][B]} \quad (3)$$

By factoring out the common [B] variable, the above equation is simplified to the single substrate Michaelis-Menten equation as:

$$V = \frac{V_{max}[A]}{[A] + K_a} \quad (4)$$

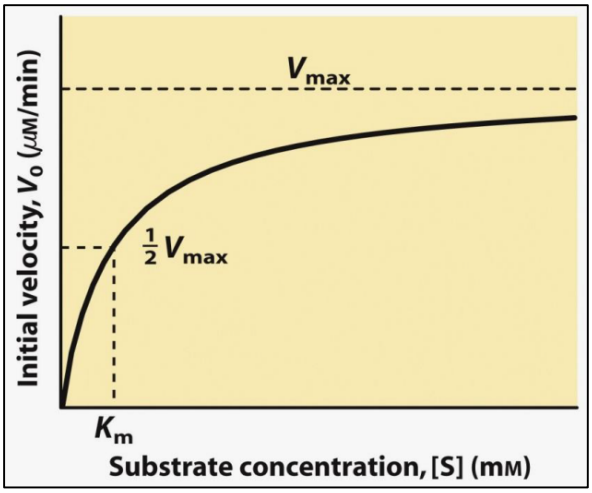

Figure 7. Hyperbolic Michaelis-Menten curve. Substrate concentration, [S], is plotted against intial reaction velocity V_0. V_{max} is the maximal velocity when enzyme is saturated at high substrate concentration and indicated by plateau. K_m is defined as substrate concentration at half of V_{max}.[33]

At high substrate concentrations, some inhibit the enzyme activity because two molecules of substrate can bind to the enzyme and block its activity. The substrate inhibition equation can be expressed as:

$$V = \frac{V_{max}[S]}{K_m + [S]\left(1 + \frac{[S]}{K_i}\right)} \quad (5)$$

Furthermore, the maximum number of substrate molecules converted to product per enzyme molecule per second is calculated as:

$$k_{cat} = \frac{V_{max}}{[E]} \quad (6)$$

Hence, the catalytic efficiency or substrate specificity of the enzyme can be obtained by calculating $\frac{k_{cat}}{K_m}$. A larger $\frac{k_{cat}}{K_m}$ value refer to a more efficient substrate for the enzyme.

AHL-synthase Assays

Enzyme reaction rates can be determined either by the accumulation of product and depletion of substrate over time. Three assays discussed in this thesis are colorimetric assay (DCPIP assay), coupled assay, and HPLC assay.

DCPIP Assay

A colorimetric assay using 2,6-dichlorophenolindophenol (DCPIP) was adapted from Tipton and his group.[34,35] DCPIP is an oxidizing agent with maximum absorption at 600 nm. In this assay, acylation of acyl-ACP and SAM substrates releases holo-ACP product, which in turn reduces the blue DCPIP dye to colorless $DCPIPH_2$ (Scheme 2). The decrease in absorbance at 600 nm due to the reduction of DCPIP can be used to measure the concentration of holo-ACP thiol released in the enzyme-catalyzed reaction.

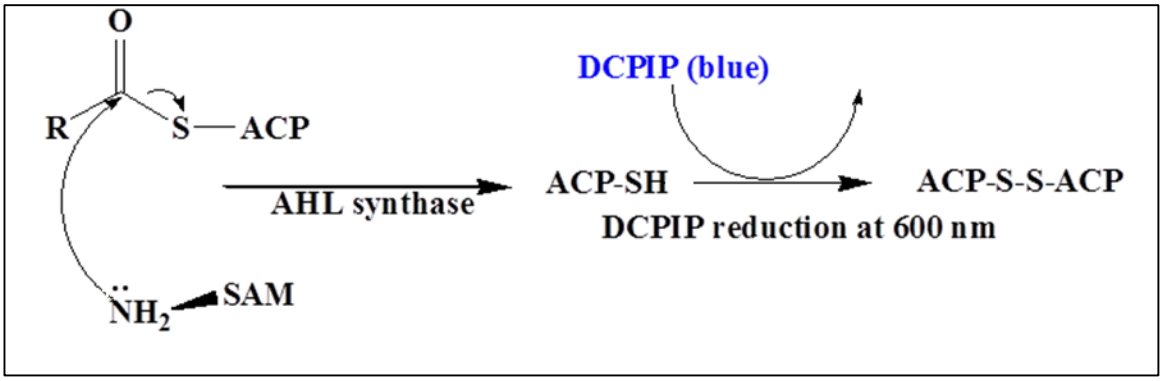

Scheme 2. DCPIP assay using UV-Vis spectrophotometry. (Left) Holo-ACP product is released from acylation chemical step in AHL-synthase signal synthesis mechanism. The free thiol group of holo-ACP reduces the blue DCPIP to colorless $DCPIPH_2$ at 600 nm.

MTAN-Xanthine Oxidase Assay

A coupled assay is designed to follow the release of MTA from lactonization reaction of acyl-ACP and SAM indirectly by coupling it to methylthioadenosine nucleosidase-xanthine oxidase (MTAN-XO) reactions (Scheme 3).[36] The concentrations

of nucleosidase and xanthine oxidase are made to keep the AHL-synthase reaction rate-limiting. In this assay, the MTA product from AHL-synthase reaction first reacts with MTAN to form adenine and methylthioribose (MTR). Addition of xanthine oxidase to the reaction mixture further increase assay sensitivity because the conversion of adenine to 2,8-dihydroxyadenine is accompanied by a large change in extinction coefficient. For instance, the extinction coefficient for the nucleosidase reaction ($\Delta\ \varepsilon_{274}$) is 1600 $M^{-1}cm^{-1}$, while the extinction coefficient for xanthine oxidase reaction ($\Delta\ \varepsilon_{305}$) is 15500 $M^{-1}cm^{-1}$. MTA and adenine react with nucleosidase and xanthine oxidase, respectively, as soon as they are formed. Thus, the increase in rate due to the release of 2,8-dihydroxyadenine signal at 305 nm reflects the rate of AHL synthesis (Figure 7).

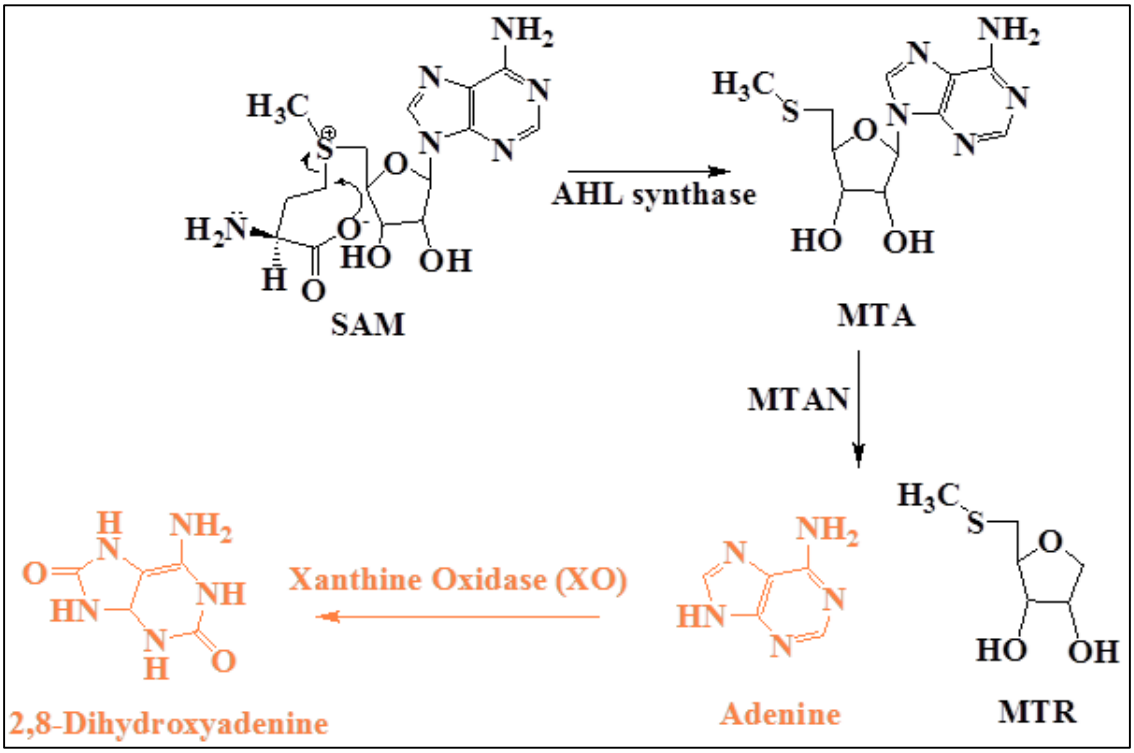

Scheme 3. MTAN-xanthine oxidase coupled assay using UV-Vis spectrometry. Lactonization step in AHL-synthase mechanism releases MTA product, which in turn reacts with methylthioadenosine nucleosidase (MTAN) to form adenine and methylthioribose (MTR). Adenine is converted to 2,8-dihydroxyadenine by xanthine oxidase. The coupled reaction is monitored at 305 nm.

HPLC Assay

Two separate methods were designed for separating protein-based substrates form small molecule substrates.[36] The HPLC method used to monitor acylation half-reaction detects protein-based analytes (holo-ACP, acyl-ACP), while the HPLC method for monitoring lactonization half-reaction resolves small molecules (MTA, SAM). In lactonization assay, SAM is the reactant, and MTA is the product. In acylation assay, acyl-ACP is the reactant, and holo-ACP is the product (Scheme 4). To calculate reaction rate, the concentration of product formed over time is monitored. A calibration curve for each assay is generated by taking known concentrations of product and measuring peak area on HPLC. In the enzyme-catalyzed reaction, the reaction is quenched with 6 M HCl (lactonization) or 4 M acetate buffer, pH 3.7 (acylation) after 4 minutes. Then, peak area of product is calculated and converted to product concentration formed over time using standard calibration curve.

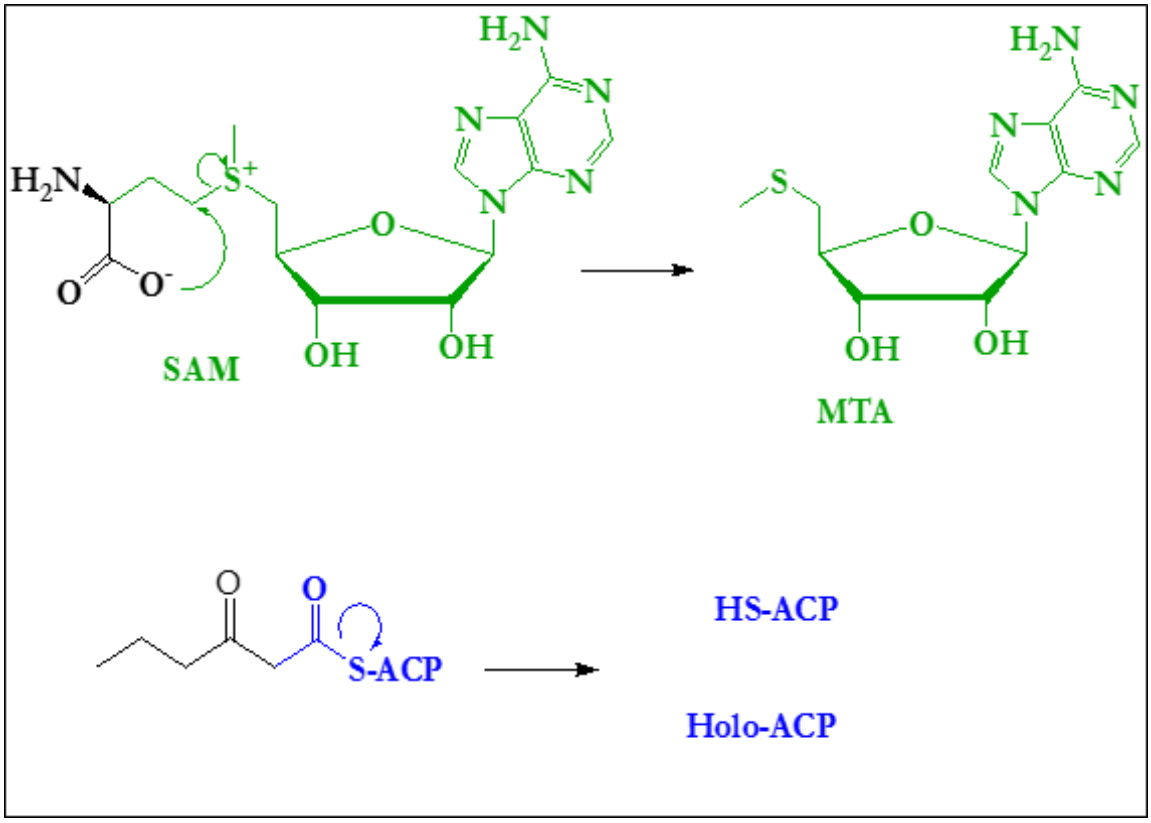

Scheme 4. Lactonization and acylation assays using HPLC. In lactonization (shown in green), the substrate SAM produces MTA product, while in acylation (shown in blue), the substrate acyl-ACP produces holo-ACP product.

β-Ketoacyl-ACP Utilizing AHL-synthases

AHL-synthases use two substrates SAM and acyl-ACP to produce acyl-homoserine lactones (AHLs). To design inhibitors of AHL-synthases, the enzymes need to be characterized with their native substrate. Unfortunately, many therapeutically relevant AHL synthases prefer acyl-ACPs that have 3-oxo substitution at the β-carbon in the acyl-chain (hence named β-ketoacyl-ACPs). For example, opportunistic pathogen *Pseudomonas aeruginosa* LasI use 3-oxoC12-ACP, plant pathogen *Pantoea stewartii* EsaI uses 3-oxoC6-ACP, and bubonic plague causing *Yersinia pestis* YspI uses 3-oxoC8-ACP to make the corresponding AHL signals for each of these bacteria (Scheme 5).

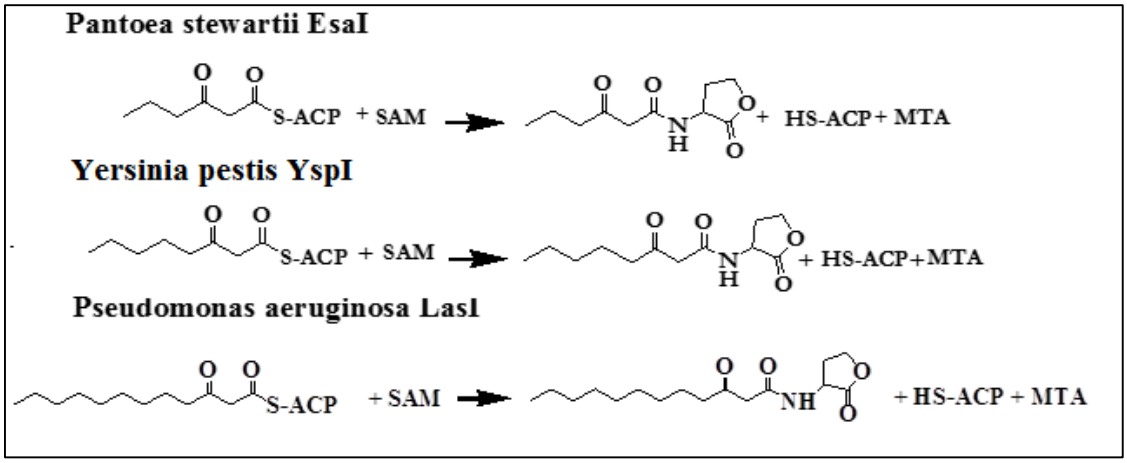

Scheme 5. Examples of β-ketoacyl-ACP utilizing AHL-synthases. SAM is the conserved substrate in all AHL-synthases. *Pantoea stewartii* EsaI, *Yersinia pestis* YspI, and *Pseudomonas aeruginosa* LasI use 3-oxohexanoyl-ACP, 3-oxooctanoyl-ACP, and 3-oxododecanoyl-ACP, respectively.

The β-ketoacyl-ACP in its stable form has not been synthesized *in vitro* because the keto group at C-3 position is an electron withdrawing group, enhancing the acidity of protons at C-2 position. The deprotonation of one of the protons at C-2 forms an intermediate enolate (Scheme 6). Even though C=O bond of the carbanion intermediate is more stable than C=C bond of the enolate intermediate, resonance stabilization of the resulting carbanion favors the tautomer with a negative charge on enolate oxygen. The negatively charged oxygen of the enolate intermediate can attack carbonyl carbon of another nearby 3-oxoacyl-ACP to cause cleavage of the reactive thioester bond.[37,38]

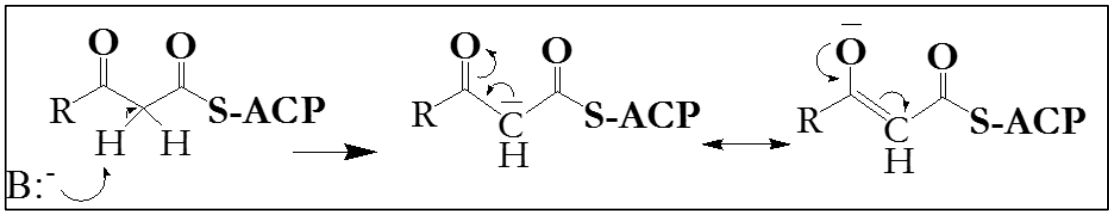

Scheme 6. Tautomerization of keto to enolate of β-ketoacyl-ACP substrate.

The instability of the β-ketoacyl-ACP substrate creates an obstacle to investigate EsaI and other important drug targets such as LasI (*Pseudomonas aeruginosa*), YspI

(*Yersinia pestis*), etc. As mentioned earlier, threonine-140 in the active site of EsaI (or threonine-142 in LasI) is important in recognizing the oxygen atom at C-3 position for catalytic activity. Although substrates devoid of 3-oxo group are easier to make, they would be expected to show low activity (or possibly inactive) to β-ketoacyl-ACP substrate utilizing enzymes. Hence, an investigation of alternative 3-oxoacyl-ACP substrates that carry oxygen or heteroatom in the acyl-chain must be developed to study these signal synthases. Finally, it is worth mentioning that in addition to AHL synthases, medicinally important enzymes such as β-ketoacyl-ACP reductase, polyketide synthase, etc. remain unexplored due to lack of access to β-ketoacyl-ACP substrate. We expect this study will open new avenues (beyond quorum sensing) for researchers to explore and discover inhibitors for several uncharacterized enzymes that impacts human health.

Thesis Objectives

The main objective of this thesis is to develop alternative 3-oxoacyl-ACP substrates and determine the catalytic activity of these substrates with *Pantoea stewartii* EsaI and *Yersinia pestis* YspI. To achieve the objective, several aspects of designing the alternative substrates are taken into consideration: (1) masking C-2 hydrogens with methyl groups in 3-oxoacyl-ACP, (2) changing position of 3-oxo- group in the acyl-chain, (3) changing the heteroatom at the C-3 position, (4) changing the hybridization of C-3 from sp^2 to sp^3, (5) turning the 3-oxo acyl-chain into 3-oxo aromatic analogs, (6) removing the carbonyl oxygen at C-3, (7) changing the acyl-chain length from C6 to C8 and C10 and vice versa. Chapters 2 and 3 in this thesis, respectively, will focus on the design and evaluation of 3-oxoacyl-ACP alternative substrates for EsaI and YspI enzymes.

CHAPTER TWO: INVESTIGATION OF ALTERNATIVE SUBSTRATES FOR EsaI

Introduction

Overview Plant Pathogen *Panteoa stewartii*

Pantoea stewartii subsp. *Stewartii* is the plant-pathogenic Gram-negative bacterium causing Stewart's wilt and leaf blight disease of sweet corn and maize.[39,40] Plant-to-plant transmission does not occur without the presence of the corn flea beetle. Thus, the disease incident is correlated directly with the numbers of corn flea beetles present in cornfields. The Stewart's wilt is transmitted by the corn flea beetle *Chaetocnema pulicaria.*[41] The infected corn flea beetle feeds on the host plant and deposits the pathogenic bacterium directly into the feeding wounds. The bacterium colonizes both the intercellular spaces of the leaf tissue, where it causes water-soaked lesion, and the xylem vessels, which leads to systemic spread and wilting.[41,42] For proliferation, the bacterium preferentially colonizes the xylem tissue and establishes dense biofilms encased in an extracellular polysaccharide (EPS) and slime.[41-43] These dense biofilms block the water flow in the xylem and lead to the wilting and death of the host plant.

According to the United States Department of Agriculture in 2017, more than 90 million acres of land are planted to corn. The United States is a major player in the world corn trade market, with up to 20 percent of the corn crop exported to other countries. Corn is the major component of livestock feed and can also be processed into multitude of food and industrial products, including starch, sweetener, corn oil, beverage, industrial alcohol, and fuel ethanol.

Stewart's wilt is the most serious bacterial disease of sweet corn and maize in the North-Central and Eastern USA.[39-43] Even though the importance of the disease has diminished in the USA due to the use of resistant corn hybrids, Stewart's wilt remains a problem because some desirable sweet corn hybrids and some elite inbred lines used for hybrid corn seed production remain highly susceptible to Stewart's wilt.

AHL-synthase in Plant Pathogen *Pantoea stewartii*: EsaI

EPS production is the major pathogenicity factor responsible for the vascular streaking, bacterial oozing, and wilting caused by *P. stewartii* subsp. *stewartii.*[39-43] The anionic EPS is composed of galactose, glucose, and glucuronic acid in a 3:3:1 ratio.[42] *P. stewartii* subsp. *stewartii* possesses a quorum sensing system containing two homologues of LuxI and LuxR, which are EsaI and EsaR.[39-45] EsaI is the AHL-synthase responsible for synthesis of 3-oxohexanoyl-homoserine lactone (3-oxoC6-HSL) signal molecule. In the quorum sensing system described for *Vibrio fischeri* (LuxI/LuxR), LuxR binds to DNA and acts as transcriptional activator in the presence of AHL signal molecules. Interestingly, EsaR acts as a repressor of transcription of target genes in the absence of quorum sensing signal or at low cell density.[44-46] In other words, EsaR operates as a negative regulator of EPS synthesis. *In vivo* adhesion assay studied by von Bodman and his group showed that surface adhesion and EPS synthesis are governed by inverse coordinate regulation. The delayed EPS synthesis by EsaR enables the bacteria to attach to a surface and transition through the early steps of biofilm development.[44] Hence, quorum sensing in *P. stewartii* subsp. *stewartii* may be a mechanism to delay the expression of EPS during the early stages of infection so that it does not interfere with other mechanisms of pathogenesis.

Mutation studies have shown that disruption of EsaI blocks the synthesis of 3-oxohexanoyl-HSL, which in turn suppresses EPS production and abolishes the capacity of the pathogen to induce Stewart's wilt disease in the plant host.[44,45] EsaI AHL-synthase uses SAM and 3-oxohexanoyl-ACP as substrates. To design effective inhibitors for EsaI, the activity of the enzyme need to be characterized with its native substrate, 3-oxohexanoyl-ACP. Unfortunately, the native substrate in its stable form has not been successfully synthesized. The crystal structure of EsaI revealed that the specific recognition of 3-oxohexanoyl-ACP over hexanoyl-ACP is due to the formation of two hydrogen bonds between the enzyme and the 3-oxo- group of the acyl-ACP substrate.[28,30] One hydrogen bond is formed from Ile141 backbone amide and the other hydrogen bond is formed from threonine Oγ1 at position 140. For enzymes that are known to produce 3-oxo-HSLs, the residue at this position is a threonine. Thus, Thr140 in the active site plays a role as gate keeper for recognizing the oxygen atom at C-3 position of the native substrate via hydrogen bonding (Figure 8 and 9).[28]

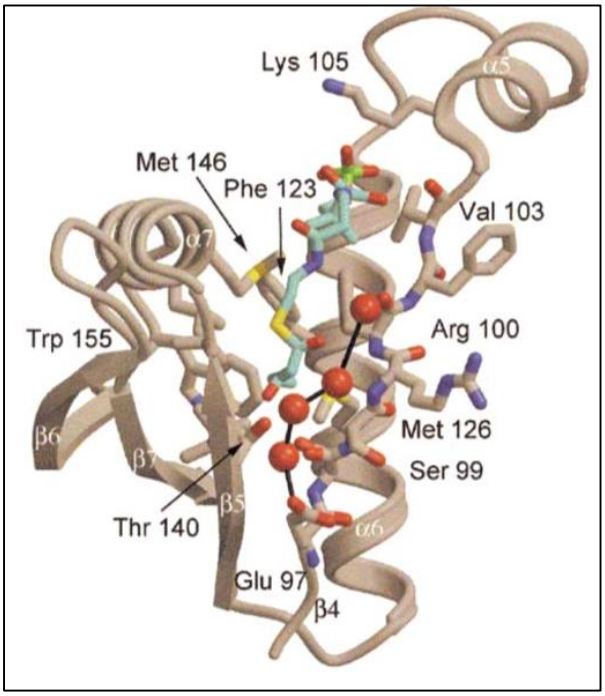

Figure 8. Crystal structure of EsaI active site. EsaI structure in its apo- form shown with 3-oxohexanoyl-phosphopantetheine (cyan color). Four water molecules lie along β4 are shown in red spheres. The conserved residues Ser98, Met126, Thr140, Val142, Met146, and Leu176 (not shown) surrounded by well-ordered water molecules have position the 3-oxo-hexanoyl portion neatly into the hydrophobic cavity in EsaI for catalysis.[28]

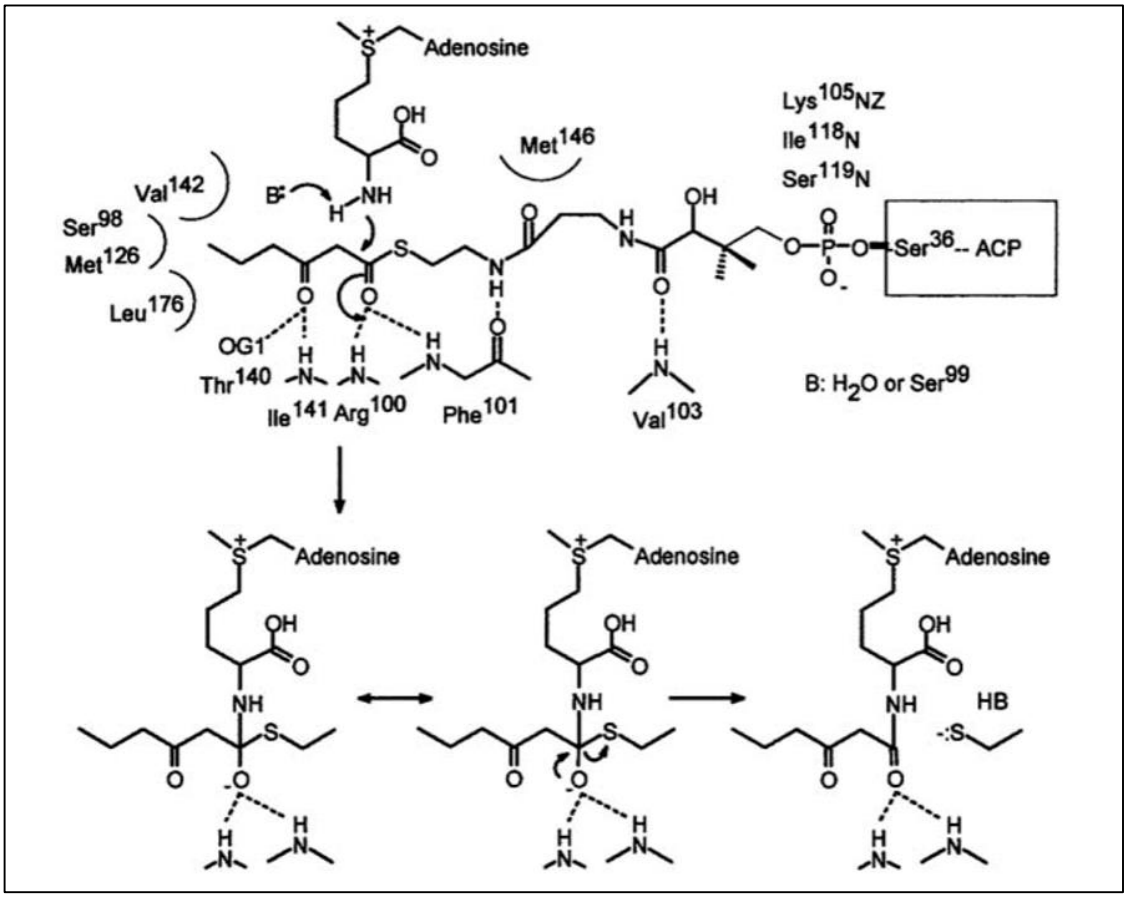

Figure 9. The electrostatic interactions between the bound 3-oxoC6-phosphopantetheine and active site residues of EsaI. The dotted lines are hydrogen bonds and curved lines are for other types of interactions, such as van der Waals. The backbone amide of Val103 forms a hydrogen bond with the carbonyl at C5 position of phosphopantetheine. The carbonyl of Phe101 is a hydrogen bond acceptor for the N3 of phosphopantetheine. The backbone amides of Arg100 and Phe101 stabilize the oxyanion at C-1 through hydrogen bonding during acylation reaction. The Oγ1 of Thr140 and backbone amide of Ille141 form hydrogen bonds with the oxygen at C3 position of 3-oxoC6 part of the substrate. [28]

Substrate Design

Mass spectrometry study of wild-type EsaI and EsaI T140A mutant showed that T140A mutant lost specificity and produced hexanoyl-HSL (C6-HSL) and some other acyl-HSLs instead.[26] Moreover, a kinetic study of wild-type EsaI with C6-ACP resulted in very low or no activity at all due to the lack of hydrogen bonding of C6-ACP with T140. In contrast, the activity of EsaI T140A mutant with C6-ACP showed an increase in activity

by 55-fold because the mutant did not require hydrogen bonding interaction with C6-ACP. This result suggested the presence of oxygen in the acyl-chain might play an important role in β-ketoacyl-ACP substrate recognition. Yet, the specificity for hybridization at the C-3 position, position of oxygen at α, γ, and δ positions, and oxygen vs. other heteroatoms in the acyl-chain of the substrate have not been investigated. One objective is to design, synthesize, and evaluate the activity of alternative 3-oxoacyl-ACP substrates that have oxygen or heteroatom in the acyl-chain with EsaI (Figure 10). 2-Furanacetyl-ACP **(1),** a 3-oxo-aromatic analog of 3-oxohexanoyl-ACP has an oxygen atom and a sp^2-hybridzed carbon at the β-position of the acyl-chain. The β-carbon in the fully reduced ring analog of **(1)**, the 2-tetrahydrofuranacetyl-ACP **(2)** also carries an oxygen atom at the β-position, but is instead sp^3 hybridized. Two other 3-oxo-aromatic analogs are 2-thiopheneacetyl-ACP **(3)** and 2-pyridylacetyl-ACP **(4)**, which have sulfur and nitrogen atom, respectively, at C-3 are designed to evaluate the specificity for oxygen vs. other heteroatoms at the C-3 position. 2-Furoyl-ACP (**5),** 4-oxohexanoyl-ACP **(6)**, and 5-oxohexanoyl-ACP **(7)** are designed to investigate the importance of the position of the oxygen in the acyl-chain. 2,2′-Dimethyl-3-oxohexanoyl-ACP **(8)** is dimethylated at C-2 to avoid deprotonation of α-hydrogens and enolate formation observed in β-ketoacyl-ACPs. Hexanoyl-ACP **(9)** does not have oxygen atom at C-3 position. Furthermore, specificity of EsaI towards C6 vs C8 was also explored by designing 4-oxooctanoyl-ACP **(10)**, 5-oxooctanoyl-ACP **(11)**, octanoyl-ACP **(12)**, and 2-benzofuranacetyl-ACP **(13)**.

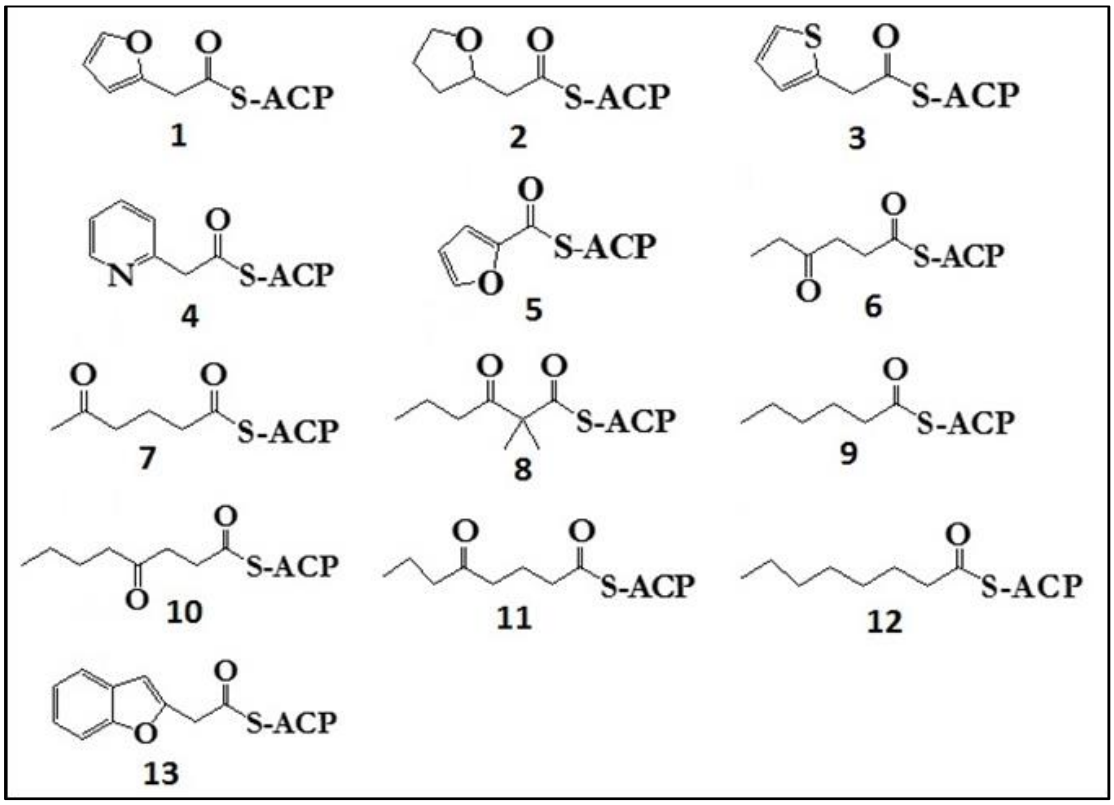

Figure 10. Structures of alternative 3-oxoacyl-ACP substrates designed to study with EsaI.

Materials and Methods

General

All chemical reagents and solvents were purchased from Sigma Aldrich and used without further purification. C6-CoA and C8-CoA were purchased from Sigma Aldrich. Ethyl butyrylacetate was purchased from Acros. Ni^{+}-NTA resin was purchased from Qiagen. Silica gel 230-400 mesh from Fisher was used for flash column chromatography. A Thermo Scientific Evolution 260 Bio UV-Vis spectrophotometer was used to measure concentration of analytes. HPLC data was analyzed by Chromeleon 7.2 software on a Thermo Scientific Dionex UltiMate-3000 HPLC system. Thermo Scientific Hypersil Gold C18 reverse-phase analytical UHPLC column (25002-054630) and preparative HPLC column (25005-159070) were used in acyl-ACP and acyl-CoA syntheses, respectively.

Deuterated chloroform solvent was obtained commercially through Cambridge Isotope Laboratories, Inc. NMR spectra were recorded at 298 K using BRUKER AVANCE III 300 MHz and 600 MHz spectrometers. Chemical shifts for ^{1}H NMR and ^{13}C NMR spectra were expressed in parts per million (ppm) and referenced to residual $CHCl_3$ in $CDCl_3$.

Esai Wild-Type and T140a Mutant Growth, Expression, and Purification

Recombinant EsaI wild-type and T140A mutant in *E. coli* were grown in LB media containing 100 μg/mL ampicillin at 37 °C to an OD_{600} of 0.6-0.8. Expression was induced by addition of 0.5 mM isopropyl-β-D-1-thiogalactopyranoside (IPTG) at room temperature. After 4 hours, the growth cultures were then centrifuged to pellet at 5000 xg at 4 °C for 10 minutes and stored at -20 °C prior to lysis. The cell pellets were thawed on ice for 30-60 minutes before lysis. The cell pellets were suspended in 3 mL B-PER reagent per gram pellet, 1 mL of lysozyme, 40 μL of 4 mg/mL DNAse per gram pellet, 40 μL of 4 mg/mL RNAse per gram pellet, and 60 μL of (13 μg/ 750 μL isopropanol) phenyl methyl sulfonyl fluoride (PMSF) per gram pellet. Lysate was incubated at room temperature with gentle shaking for 15 minutes and centrifuged to collect supernatant at 20,000 xg at 4 °C for 30 minutes. Ni^{2+}-NTA affinity chromatography column was used to purify the protein. The Ni^{2+}-NTA column was first equilibrated with 10X bed volumes of 0.5 M NaCl in 50 mM Tris/HCl, pH 7.5 buffer (Buffer A). The clear supernatant was loaded onto the column to allow the protein of interest to bind to the resin. The column was then washed with 40 mM imidazole in Buffer A. The EsaI protein was eluted using 15 mL of 200 mM imidazole in Buffer A. The presence and purity of EsaI was confirmed by SDS-PAGE gel analysis. Concentration of EsaI was determined via UV-Vis (ε_{280} = 34170 $M^{-1}cm^{-1}$).

Apo-ACP Growth, Expression, and Purification[25]

Apo-ACP in BL21 *E. coli* competent cell was grown in LB broth containing 25 μg/mL kanamycin, 50 μg/mL streptomycin, 50 μg/mL spectinomycin, and 25 μg/mL chloramphenicol at 37 °C to an OD_{600} of 0.6-0.8. An addition of 0.1 mM IPTG was added to induce expression. The growth culture was incubated for another 3 hours and then centrifuged to pellets at 5000 xg at 4 °C for 10 minutes. The cell pellets were suspended in 3 mL B-PER reagent per gram pellet, 1 mL of lysozyme, 40 μL of 4 mg/mL DNAse per gram pellet, 40 μL of 4 mg/mL RNAse per gram pellet, and 60 μL of (13 μg/ 750 μL isopropanol) PMSF per gram pellet. Lysate was incubated at room temperature with gentle shaking for 20 minutes and centrifuged to collect clear supernatant at 20,000 xg at 4 °C for 60 minutes. Then, $MnSO_4$ (1.2 mM) and $MgCl_2$ (25 mM) were added to the clear supernatant. The mixture was incubated at 37 °C for 4 hours to convert all holo-ACP to the apo-ACP form. Cellular protein was precipitated by adding isopropanol slowly to 50% volume with gentle shaking on ice for 1 hour. The precipitated protein was removed by centrifugation at 20,000 xg for 45 minutes. The clear supernatant was then stirred with DEAE-sepharose resin overnight at 4°C. The media was packed into a column and washed with of 0.25 mM LiCl in 10 mM lithium 4-morpholineethane-sulfonate (MES), pH 6.1 buffer. The protein of interest was eluted with 0.5 M LiCl in 10 mM MES, pH 6.1 buffer. Using SDS-PAGE analysis, fractions containing pure protein were pooled and precipitated using 0.02 % (0.2 mg/mL) sodium deoxycholate and 5 % (50 mg/mL) trichloroacetate (w/v). The mixture was incubated for 60 minutes with gentle shaking at 37 °C and centrifuged to pellet at 20,000 xg for 30 minutes. The apo-ACP pellet was resuspended in 0.5 M Tris-HCl, pH 8.0 buffer and concentrated using 3 kD molecular weight cutoff spin

filter column. Concentration of apo-ACP was determined using UV-Vis (ε_{280} = 1490 $M^{-1}cm^{-1}$).

Sfp Growth, Expression, and Purification

Bacillus subtilis sfp was expressed in BL21 *E. coli* competent cells. Sfp was grown in LB media containing 100 μg/mL kanamycin at 37 °C to an OD_{600} of 0.6-0.8. Expression was induced by addition of 0.5 mM IPTG and continued at 37 °C for another 3 hours. The growth cultures were then centrifuged to pellet at 5000 xg at 4 °C for 10 minutes and stored at -20 °C prior to lysis. The cell pellets were thawed on ice for 30-60 minutes before lysis. The cell pellets were suspended in 3 mL B-PER reagent per gram pellet, 1 mL of lysozyme, 40 μL of 4 mg/mL DNAse per gram pellet, 40 μL of 4 mg/mL RNAse per gram pellet, and 60 μL of (13 μg/ 750 μL isopropanol) PMSF per gram pellet. Lysate was incubated at room temperature with gentle shaking for 15 minutes and then centrifuged to collect supernatant at 20,000 xg at 4 °C for 30 minutes. Ni^{2+}-NTA affinity chromatography column was used to purify the protein. The Ni^{2+}-NTA column was first equilibrated with 10X bed volumes of 0.5 M NaCl in 50 mM Tris/HCl, pH 7.5 buffer (Buffer A). The clear supernatant was loaded onto the column to allow the protein of interest to bind to the resin. The column was then washed with 10 mM imidazole in Buffer A. The sfp protein was eluted using 15 mL of 200 mM imidazole in Buffer A. The presence and purity of Sfp was confirmed by SDS-PAGE gel analysis. Concentration of sfp was determined using UV-Vis (ε_{280} = 29130 $M^{-1}cm^{-1}$).

Synthesis of 2-furanacetyl-succinimide ester (1-succ)[47]

To a solution of 2-furanacetic acid (0.20 g, 1.58 mmol) in 1,4-dioxane (3 mL), *N*-hydroxysuccinimide (0.18 g, 1.58 mmol) and *N,N´*-dicyclohexylcarbodiimide (0.33 g, 1.58

mmol) were added and stirred for 24 hours. Diethyl ether (2 mL) was added to the reaction mixture, and then the white cloudy solution was filtered and concentrated under reduced pressure. Warm methanol (3 mL) was added quickly into the residue to precipitate out urea by-product and then concentrated under reduced pressure. Cold 1,4-dioxane (2 mL) was added to the residue to repeat removal of urea and then concentrated under reduced pressure to give 2-furanacetyl-succinimide ester product as pale-yellow liquid (0.19 g, 0.85 mmol, 54% yield). ^{1}H NMR (300 MHz, $CDCl_3$) δ 7.40 (t, *J* = 1.3 Hz, 1H), 6.37 (d, *J* = 1.4 Hz, 2H), 4.01 (s, 2 H), 2.85 (s, 4H). ^{13}C NMR (300 MHz, $CDCl_3$) δ 169.0, 164.8, 144.9, 142.9, 110.9, 109.4, 31.1, 25.8. ESI-TOF: expected m/z $[M+Na]^+$ 246.0373, observed 246.0389.

Synthesis of 2-tetrahydrofuranacetyl-succinimide ester (2-succ)[47]

To a solution of 2-tetrahydrofuranacetic acid (0.043 g, 0.33 mmol) in 1,4-dioxane (3 mL), *N*-hydroxysuccinimide (0.038 g, 0.33 mmol) and *N,N′*-dicyclohexylcarbodiimide (0.068 g, 0.33 mmol) were added and stirred for 24 hours. Diethyl ether (2 mL) was added to the reaction mixture, and then the white cloudy solution was filtered and concentrated under reduced pressure. Warm methanol (3 mL) was added quickly into the residue to precipitate out urea by-product and then concentrated under reduced pressure. Cold 1,4-dioxane (2 mL) was added to the residue to repeat removal of urea and then concentrated under reduced pressure to give 2-tetrahydrofuranacetyl-succinimide ester product as clear syrupy-like liquid (0.050 g, 0.21 mmol, 62% yield). ^{1}H NMR (600 MHz, $CDCl_3$) δ 4.34 (quint, *J* = 6.7 Hz, 1H), 3.94 (q, *J* = 8.0, 7.0 Hz, 1H), 3.81 (q, *J* = 7.9, 6.4 Hz, 1H), 2.94 (dd, *J* = 15.4, 6.4 Hz, 1H), 2.86 (s, 4H), 2.78 (dd, *J* = 15.4, 6.7 Hz, 1H), 2.23 – 2.18 (m, 1H), 2.17 – 1.95 (m, 2H), 1.72 – 1.69 (m, 1H). ^{13}C NMR (600 MHz, $CDCl_3$) δ 169.1, 166.4,

74.8, 68.5, 37.6, 31.4, 25.8, 25.8. ESI-TOF: expected m/z $[M+Na]^+$ 250.0686, observed 250.0709.

Synthesis of 2-thiopheneacetyl-succinimide ester (3-succ)[47]

To a solution of thiopheneacetic acid (0.20 g, 1.41 mmol) in 1,4-dioxane (3 mL), *N*-hydroxysuccinimide (0.16 g, 1.41 mmol) and *N,N′*-dicyclohexylcarbodiimide (0.29 g, 1.41 mmol) were added and stirred for 24 hours. Diethyl ether (2 mL) was added to the reaction mixture, and then the white cloudy solution was filtered and concentrated under reduced pressure. Warm methanol (3 mL) was added quickly into the residue to precipitate out urea by-product and then concentrated under reduced pressure. Cold 1,4-dioxane (2 mL) was added to the residue to repeat removal of urea and then concentrated under reduced pressure to give thiopheneacetyl-succinimide ester product as tan-brown solid (0.27 g, 1.15 mmol, 82% yield). ^{1}H NMR (300 MHz, $CDCl_3$) δ 7.26 (d, *J* = 1.2 Hz, 1H), 7.05 (dd, *J* = 2.5, 1.1 Hz, 1H), 6.97 (dd, *J* = 5.1, 3.5 Hz, 1H), 4.14 (d, *J* = 0.7 Hz, 2H), 2.82 (s, 4H). ^{13}C NMR (300 MHz, $CDCl_3$) δ 169.0, 165.9, 131.9, 128.1, 127.3, 126.0, 32.2, 25.8. ESI-TOF: expected m/z $[M+Na]^+$ 262.0145, observed 262.0276.

Synthesis of 2-pyridylacetyl-succinimide ester (4-succ)[47]

To a solution of 2-pyridylacetic acid (0.50 g, 2.88 mmol) in 1,4-dioxane (10 mL), *N*-hydroxysuccinimide (0.33 g, 2.88 mmol) and *N,N′*-dicyclohexylcarbodiimide (0.59 g, 2.88 mmol) were added and stirred for 24 hours. Diethyl ether (5 mL) was added to the reaction mixture, and then the white cloudy solution was filtered and concentrated under reduced pressure. Warm methanol (3 mL) was added quickly into the residue to precipitate out urea by-product and then concentrated under reduced pressure. Cold 1,4-dioxane was added to the residue to repeat removal of urea and then concentrated under reduced

pressure. The residue was purified by column chromatography (hexane/ethyl acetate) to give 2-pyridylacetyl-succinimide ester product as orange-brownish syrupy-like liquid (0.23 g, 0.98 mmol, 29 % yield). ^{1}H NMR (600 MHz, $CDCl_3$) δ 8.59 (d, *J* = 4.3 Hz, 1H), 7.73 (td, *J* = 7.7, 1.4 Hz, 1H), 7.40 (d, *J* = 7.8 Hz, 1H), 7.26 (dd, *J* = 6.9, 5.3 Hz, 1H), 4.16 (s, 2H), 2.83 (s, 4H). ^{13}C NMR (600 MHz, $CDCl_3$) δ 168.9, 165.9, 151.9, 149.7, 137.1, 123.8, 122.8, 40.4, 25.6. ESI-TOF: expected m/z $[M+Na]^+$ 257.0533, observed 257.0500.

Synthesis of 2-furoyl-succinimide ester (5-succ)[47]

To a solution of 2-furoic acid (0.50 g, 4.46 mmol) in 1,4-dioxane (10 mL), *N*-hydroxysuccinimide (0.51 g, 4.46 mmol) and *N*,*N*′-dicyclohexylcarbodiimide (0.92 g, 4.46 mmol) were added and stirred for 24 hours. Diethyl ether (5 mL) was added to the reaction mixture, and then the white cloudy solution was filtered and concentrated under reduced pressure. Warm methanol (3 mL) was added quickly into the residue to precipitate out urea by-product and then concentrated under reduced pressure. Cold 1,4-dioxane (2 mL) was added to the residue to repeat removal of urea and then concentrated under reduced pressure to give 2-furoyl-succinimide ester product as yellow solid (0.71 g, 3.39 mmol, 76% yield). ^{1}H NMR (600 MHz, $CDCl_3$) δ 7.71 (dd, *J* = 1.6, 0.7 Hz, 1H), 7.47 (dd, *J* = 3.7, 0.7 Hz, 1H), 6.61 (dd, *J* = 3.6, 1.7 Hz, 1H), 2.89 (s, 4H). ^{13}C NMR (600 MHz, $CDCl_3$) δ 169.2, 153.7, 148.9, 139.9, 122.4, 112.8, 25.8. ESI-TOF: expected m/z $[M+Na]^+$ 232.0216, observed 232.0249.

Synthesis of 4-oxohexanoic acid (6-acid)[48]

Gamma-hexalactone (0.233 mL, 2.0 mmol) was hydrolyzed overnight with 0.5 M NaOH in EtOH (1:1, 8 mL). The solvent was removed under reduced pressure. The residue was then dissolved in 40 mL buffer solution (5.52 g NaH_2PO_4 and 1.60 g

Na_2HPO_4). Concentrated NaOCl 10-15% (8 mL) was then added to the reaction mixture and stirred for 20 hours at room temperature. The reaction mixture was acidified with concentrated HCl solution, washed with diethyl ether (2 x 20 mL) and brine solution (40 mL). The organic layer was dried with anhydrous $MgSO_4$, filtered, and concentrated under reduced pressure to afford 4-oxohexanoic acid product as yellow liquid (0.21 g, 1.61 mmol, 81% yield). ^{1}H NMR (600 MHz, $CDCl_3$) δ 2.71 (t, *J* = 6.4 Hz, 2H), 2.62 (t, *J* = 6.4 Hz, 2H), 2.46 (q, *J* = 7.3 Hz, 2H), 1.06 (t, *J* = 7.3 Hz, 3H). ^{13}C NMR (600 MHz, $CDCl_3$) δ 209.7, 178.3, 36.6, 36.1, 27.9, 7.9.

Synthesis of 4-oxohexanoyl-succinimide ester (6-succ)[47]

To a solution of 4-oxohexanoic acid (0.21 g, 1.61 mmol) in 1,4-dioxane (3 mL), *N*-hydroxysuccinimide (0.19 g, 1.61 mmol) and *N,N′*-dicyclohexylcarbodiimide (0.33 g, 1.61 mmol) were added and stirred for 24 hours. Diethyl ether (2 mL) was added to the reaction mixture, and then the white cloudy solution was filtered and concentrated under reduced pressure. Warm methanol (3 mL) was added quickly into the residue to precipitate out urea by-product and then concentrated under reduced pressure. Cold 1,4-dioxane (2 mL) was added to the residue to repeat removal of urea and then concentrated under reduced pressure to give 4-oxohexanoyl-succinimide ester product as brown-yellow liquid (0.15 g, 0.66 mmol, 41% yield). ^{1}H NMR (600 MHz, $CDCl_3$) δ 2.89 (t, *J* = 6.4 Hz, 2H), 2.84 (t, *J* = 6.4 Hz, 2H), 2.82 (s, 4H), 2.47 (q, *J* = 7.3 Hz, 2H), 1.07 (t, *J* = 7.3 Hz, 3H). ^{13}C NMR (600 MHz, $CDCl_3$) δ 207.9, 169.2, 168.5, 36.4, 35.9, 25.8, 25.3, 7.9. ESI-TOF: expected m/z $[M+Na]^+$ 250.0686, observed 250.0700.

Synthesis of 5-oxohexanoic acid (7-acid)[48]

Delta-hexalactone (0.44 mL, 4.0 mmol) was hydrolyzed overnight with 0.5 M NaOH in EtOH (1:1, 16 mL). The solvent was removed under reduced pressure. The residue was then dissolved in 80 mL buffer solution (11.04 g NaH_2PO_4 and 3.2 g Na_2HPO_4). Concentrated NaOCl 10-15% (16 mL) was then added to the reaction mixture and stirred for 20 hours at room temperature. The reaction mixture was acidified with concentrated HCl solution, washed with diethyl ether (2 x 20 mL) and brine solution (40 mL). The organic layer was dried with anhydrous $MgSO_4$, filtered, and concentrated under reduced pressure to afford 5-oxohexanoic acid product as dark brown liquid (0.15 g, 1.15 mmol, 29% yield). ^{1}H NMR (300 MHz, $CDCl_3$) δ 2.51 (t, *J* = 7.2 Hz, 2H), 2.38 (t, *J* = 7.2 Hz, 2H), 2.13 (s, 3H), 1.88 (quint, *J* = 7.2 Hz, 2H). ^{13}C NMR (300 MHz, $CDCl_3$) δ 208.5, 179.0, 42.5, 33.0, 30.2, 18.7.

Synthesis of 5-oxohexanoyl-succinimide ester (7-succ)[47]

To a solution of 5-oxohexanoic acid (0.15 g, 1.15 mmol) in 1,4-dioxane (3 mL), *N*-hydroxysuccinimide (0.13 g, 1.15 mmol) and *N,N′*-dicyclohexylcarbodiimide (0.24 g, 1.15 mmol) were added and stirred for 24 hours. Diethyl ether (2 mL) was added to the reaction mixture, and then the white cloudy solution was filtered and concentrated under reduced pressure. Warm methanol (3 mL) was added quickly into the residue to precipitate out urea by-product and then concentrated under reduced pressure. Cold 1,4-dioxane (2 mL) was added to the residue to repeat removal of urea and then concentrated under reduced pressure to give 5-oxohexanoyl-succinimide ester product as black liquid (0.15 g, 0.66 mmol, 56% yield). ^{1}H NMR (600 MHz, $CDCl_3$) δ 2.82 (s, 4H), 2.64 (t, *J* = 7.0 Hz, 2H), 2.59 (t, *J* = 7.1 Hz, 2H), 2.14 (s, 3H), 1.98 (quint, *J* = 7.1 Hz, 2H). ^{13}C NMR (600 MHz, $CDCl_3$) δ 207.6,

169.3, 168.5, 41.7, 30.2, 30.1, 25.8, 18.7. ESI-TOF: expected m/z $[M+Na]^+$ 250.0686, observed 250.0700.

Synthesis of ethyl-2,2′-dimethyl-3-oxohexanoate (8-ester)[49,50]

To a reaction flask under nitrogen atmosphere, one equivalent of NaH 60% in mineral oil (0.5 g, 12.6 mmol) and dry THF (60 mL) were added. The mixture solution was refluxing while ethyl-3-oxohexanoate (2.02 mL, 12.6 mmol) was adding dropwise. Then, one equivalent of methyl iodide (0.8 mL, 12.6 mmol) was added dropwise into the reaction solution. The reaction was refluxed overnight at 70 °C in mineral oil bath. Next day, the second equivalent of NaH 60% in mineral oil and methyl iodide were added into the same reaction flask and stirred overnight. The completion of reaction was checked using TLC (5% ethyl acetate: 95% hexane). Under nitrogen atmosphere, saturated ammonium chloride solution was added dropwise until all white precipitate dissolved. The product mixture was then extracted with dichloromethane (3 x 70 mL). The organic layer was dried with anhydrous sodium sulfate, filtered, and concentrated under reduced pressure. The residue was purified by silica gel column chromatography (99:1 hexane/ethyl acetate) to give ethyl-2,2′-dimethyl-3-oxohexanoate as a white solid (2.13 g, 11.4 mmol, 91% yield). ^{1}H NMR (600 MHz, $CDCl_3$) δ 4.15 (q, *J* = 7.1 Hz, 2H), 2.40 (t, *J* = 7.2 Hz, 2H), 1.62 – 1.57 (m, 2H), 1.33 (s, 6H), 1.23 (t, *J* = 7.1 Hz, 3H), 0.87 (t, *J* = 7.4 Hz, 3H). DEPT-135 NMR (600 MHz, $CDCl_3$) δ 61.2, 39.8, 21.9, 17.3, 14.0, 13.6.

Synthesis of 2,2′-dimethyl-3-oxohexanoic acid (8-acid)[51]

To a solution of 1 N NaOH (4.3 mL), ethyl-2,2′-dimethyl-3-oxohexanoate (0.2 g, 1.1 mmol) was added and stirred overnight. The reaction mixture was then washed twice with ethyl acetate (2 x 8 mL). The organic layer was collected and cooled on ice. 2 N HCl

solution was added into the cool aqueous solution until the clear solution turned cloudy or pH 2-3. The cloudy solution was filtered and extracted with petroleum ether. The clear aqueous phase from extraction was lyophilized to afford the dried 2,2′-dimethyl-3-oxohexanoic acid product as white powder (0.12 g, 0.79 mmol, 74% yield). ^{1}H NMR (300 MHz, MeOD-d_4) δ 2.46 (t, *J* = 7.1 Hz, 2H), 1.55 – 1.48 (m, 2H), 1.26 (s, 6H), 0.83 (t, *J* = 7.4 Hz, 3H). ^{13}C NMR (300 MHz, MeOD-d_4) δ 209.1, 175.6, 55.1, 39.3, 21.0, 16.9, 12.5.

Synthesis of 2,2′-dimethyl-3-oxohexanoyl-succinimide ester (8-succ)[47]

To a solution of 2,2′-dimethyl-3-oxohexanoic acid (0.15 g, 0.92 mmol) in 1,4-dioxane (3 mL), *N*-hydroxysuccinimide (0.11 g, 0.92 mmol) and *N,N′*-dicyclohexylcarbodiimide (0.19 g, 0.92 mmol) were added and stirred for 24 hours. Diethyl ether (2 mL) was added to the reaction mixture, and then the white cloudy solution was filtered and concentrated under reduced pressure. Warm methanol (3 mL) was added quickly into the residue to precipitate out urea by-product and then concentrated under reduced pressure. Minimal amount of cold 1,4-dioxane was added to the residue to repeat removal of urea and then concentrated under reduced pressure. The residue was purified by silica gel column chromatography (1:1 hexane/ethyl acetate) to give 2,2′-dimethyl-3-oxohexanoyl-succinimide ester product as clear solid (0.062 g, 0.24 mmol, 26 % yield). ^{1}H NMR (600 MHz, $CDCl_3$) δ 2.81 (s, 4H), 2.64 (t, *J* = 7.1 Hz, 2H), 1.66 – 1.60 (m, 2H), 1.48 (s, 6H), 0.89 (t, *J* = 7.4 Hz, 3H). ^{13}C NMR (600 MHz, $CDCl_3$) δ 205.5, 169.7, 168.9, 54.7, 40.3, 25.6, 22.1, 17.3, 13.6. ESI-TOF: expected m/z $[M+Na]^+$ 278.0999, observed 278.1107.

Synthesis of 4-oxooctanoic acid (10-acid)[48]

Gamma-octalactone (0.51 mL, 3.5 mmol) was hydrolyzed overnight in 0.5 M NaOH in EtOH (1:1, 14 mL). The solvent was removed under reduced pressure. The residue was then dissolved in 70 mL buffer solution (9.70 g NaH_2PO_4 and 2.81 g Na_2HPO_4). Concentrated NaOCl 10-15% (14 mL) was then added to the reaction mixture and stirred for 20 hours at room temperature. The reaction mixture was adjusted to pH 3 with concentrated HCl solution, washed with diethyl ether (2 x 20 mL) and brine solution (40 mL). The organic layer was dried with anhydrous $MgSO_4$, filtered, and concentrated under reduced pressure to afford 4-oxooctanoic acid product as pale-yellow liquid (0.26 g, 1.6 mmol, 48 % yield). ^{1}H NMR (300 MHz, $CDCl_3$) δ 2.69 (t, *J* = 5.9 Hz, 2H), 2.60 (t, *J* = 5.9 Hz, 2H), 2.42 (t, *J* = 7.5 Hz, 2H), 1.55 (quint, *J* = 7.5 Hz, 2H), 1.35 – 1.23 (m, 2H), 0.88 (t, *J* = 7.3 Hz, 3H). ^{13}C NMR (300 MHz, $CDCl_3$) δ 209.3, 178.8, 42.6, 36.9, 27.9, 26.1, 22.5, 14.0.

Synthesis of 4-oxooctanoyl-succinimide ester (10-succ)[47]

To a solution of 4-oxooctanoic acid (0.078 g, 0.49 mmol) in 1,4-dioxane (3 mL), *N*-hydroxysuccinimide (0.057 g, 0.49 mmol) and *N,N′*-dicyclohexylcarbodiimide (0.10 g, 0.49 mmol) were added and stirred for 24 hours. Diethyl ether (2 mL) was added to the reaction mixture, and then the white cloudy solution was filtered and concentrated under reduced pressure. Warm methanol (3 mL) was added quickly into the residue to precipitate out urea by-product and then concentrated under reduced pressure. Cold 1,4-dioxane was added to the residue to repeat removal of urea and then concentrated under reduced pressure to give 4-oxooctanoyl-succinimide ester product as yellow liquid (0.11 g, 0.43 mmol, 88% yield). ^{1}H NMR (300 MHz, $CDCl_3$) δ 2.88 (t, *J* = 2.6 Hz, 2H), 2.84 (t, *J* = 5.9 Hz, 2H), 2.79

(s, 4H), 2.42 (t, *J* = 7.4 Hz, 2H), 1.54 (quint, *J* = 7.5 Hz, 2H), 1.34 – 1.21 (m, 2H), 0.86 (t, *J* = 7.3 Hz, 3H). ^{13}C NMR (300 MHz, $CDCl_3$) δ 207.6, 169.2, 168.4, 42.5, 36.8, 26.0, 25.7, 25.2, 22.4, 13.9. ESI-TOF: expected m/z $[M+Na]^+$ 278.0999, observed 278.1009.

Synthesis of 5-oxooctanoic acid (11-acid)[48]

Delta-octanolactone (0.10 g, 0.79 mmol) was hydrolyzed overnight with 0.5 M NaOH in EtOH (1:1, 3 mL). The solvent was removed under reduced pressure. The residue was then dissolved in 16 mL buffer solution (2.18 g NaH_2PO_4 and 0.63 g Na_2HPO_4). Concentrated NaOCl 10-15% (3 mL) was then added to the reaction mixture and stirred for 20 hours at room temperature. The reaction mixture was acidified with concentrated HCl solution, washed with diethyl ether (2 x 20 ml) and brine solution (40 mL). The organic layer was dried with anhydrous $MgSO_4$, filtered, and concentrated under reduced pressure to afford 5-oxooctanoic acid product as pale-yellow liquid (0.084 g, 0.53 mmol, 67% yield). ^{1}H NMR (600 MHz, $CDCl_3$) δ 2.47 (t, *J* = 7.2 Hz, 2H), 2.36 (q, *J* = 7.1 Hz, 4H), 1.88 (quint, *J* = 7.2 Hz, 2H), 1.61 – 1.55 (m, 2H), 0.88 (t, *J* = 7.4 Hz, 3H). ^{13}C NMR (600 MHz, $CDCl_3$) δ 210.5, 178.8, 45.0, 41.5, 33.1, 18.8, 17.5, 13.9.

Synthesis of 5-oxooctanoyl-succinimide ester (11-succ)[47]

To a solution of 5-oxooctanoic acid (0.028 g, 0.18 mmol) in 1,4-dioxane (3 mL), *N*-hydroxysuccinimide (0.020 g, 0.18 mmol) and *N,N′*-dicyclohexylcarbodiimide (0.037 g, 0.18 mmol) were added and stirred for 24 hours. Diethyl ether (2 mL) was added to the reaction mixture, and then the white cloudy solution was filtered and concentrated under reduced pressure. Warm methanol (3 mL) was added quickly into the residue to precipitate out urea by-product and then concentrated under reduced pressure. Cold 1,4-dioxane (2 mL) was added to the residue to repeat removal of urea and then concentrated under

reduced pressure to give 5-oxooctanoyl-succinimide ester product as orange-yellowish liquid (0.038 g, 0.15 mmol, 84% yield). ^{1}H NMR (600 MHz, $CDCl_3$) δ 2.81 (s, 4H), 2.64 (t, *J* = 7.1 Hz, 2H), 2.55 (t, *J* = 7.1 Hz, 2H), 2.37 (t, *J* = 7.4 Hz, 2H), 1.99 (quint, *J* = 7.1 Hz, 2H), 1.60 – 1.57 (m, 2H), 0.89 (t, *J* = 7.4 Hz, 3H). ^{13}C NMR (600 MHz, $CDCl_3$) δ 209.7, 169.0, 168.3, 44.8, 40.5, 30.0, 25.6, 18.6, 17.3, 13.7. ESI-TOF: expected m/z $[M+Na]^+$ 278.0999, observed 278.1012.

General preparation of 3-oxoacyl-CoA analogs[52-54]

Under inert condition, acyl-succinimide ester analog (0.2 mmol) was dissolved in mixture solution of water: dimethylformamide (1:1, 3 mL). A pea-size amount of K_2CO_3 was added to make the reaction solution basic, pH 8-9. To this reaction mixture, free CoA (0.1 mmol) was added after gentle mixing. The reaction was stirred at room temperature overnight under nitrogen atmosphere. The reaction mixture was washed twice with diethyl ether to remove any organic contaminants. The aqueous layer was collected and filtered through a 0.22 μm centrifugal spin filter. Acyl-CoA was purified by a preparative C-18 reverse-phase HPLC with gradient beginning at 95% buffer B (25 mM ammonium acetate, pH 5) and ending at 95% solvent D (acetonitrile + 0.1% TFA) at flow rate of 3 mL/min over a period of 25 minutes.

Synthesis of 2-benzofuranacetyl-CoA (13-CoA)[55]

To a solution of acetonitrile (3 mL) at -5℃, 2-benzofuranacetic acid (10 mg, 0.057 mmol) and 1,1'-carbonyldiimidazole (12 mg, 0.073 mmol) were added. The reaction mixture was stirred at below 0℃ for 1.5 hours. In a separate flask containing 1:1 acetonitrile: water solution (2 mL), free CoA (22 mg, 0.037 mmol) was dissolved under nitrogen environment. The reaction mixture was transferred into the free CoA solution and

continued to stir under nitrogen environment for another 3-5 hours at the same temperature condition. The crude product was collected and filtered through a 0.22 μm centrifugal spin filter. 2-Benzofuranacetyl-CoA was purified by a preparative C-18 reverse-phase HPLC with gradient beginning at 95 % buffer B (25 mM ammonium acetate, pH 5) and ending at 95 % solvent D (99.9 % acetonitrile + 0.1 % TFA) at flow rate of 3 mL/min over a period of 25 minutes.

General preparation of 3-oxoacyl-ACP analogs[56,57]

Acyl-ACP can be synthesized by enzymatic modification of apo-ACP with acyl-CoA using phosphopantheinyl transferase, *B. subtilis* Sfp. The reaction contained nanopure water, 50 mM Tris-HCl, pH 6.8, 10 mM $MgCl_2$, apo-ACP, acyl-CoA (1.25X apo-ACP), and 3 μM Sfp. Acyl-CoA was added in partition over 15 minute intervals. The reaction was incubated at 37 °C and monitored by analytical C-18 reverse-phase UHPLC for completion. Acyl-ACP separation using UHPLC began with 75 % solvent A (99.9 % H_2O + 0.1 % TFA) and 25% solvent D (99.9 % acetonitrile + 0.1 % TFA), and ended with 25% solvent A and 75% solvent D over a period of 10 minutes at flow rate of 600 μL/min. The reaction time varied from 1 hour to 4 hours. Once the reaction went to completion, ammonium sulfate was added to the reaction mixture to 75 % saturation to precipitate out Sfp.[58] After at least 1 hour of stirring at 4 °C, the reaction solution was centrifuged to pellet out Sfp at 13000 xg for 15 minutes. The clear supernatant containing acyl-ACP solution was desalted and concentrated by multiple washes with nanopure water and then 10 mM MES, pH 6 + 20 % glycerol buffer using a 3kD molecular cutoff spin filter column. Concentration of acyl-ACP was determined using UV-Vis (ε_{280} = 1490 $M^{-1}cm^{-1}$).

Mass determination of Acyl-CoA molecules

Acyl-CoA molecules were analyzed on an ultra-high-resolution Quadrupole Time of Flight (QTOF) instrument (Bruker maXis, Bruker Corporation, Billerica, Massachusetts) using direct injection to the MS. The ESI source was operated under the following conditions: positive ion mode, nebulizer pressure: 0.4 Bar; flow rate of drying gas (N_2): 4L/min; drying gas temperature: 200 °C; voltage between HV capillary and HV end-plate offset: 3000 V to -500 V; and the quadrupole ion energy 4.0 eV. Sodium formate was used to calibrate the system in the mass range. All MS data was analyzed using the Compass Data Analysis software package (Bruker Corporation, Billerica, Massachusetts). The Bruker Compass Isotope Pattern application was used to calculate the expected molecular mass of each acyl-CoA molecule based on the most abundant isotopes of the provided molecular formula of each acyl-CoA. **2-Furanacetyl-CoA (1-CoA):** expected $[M+H]^+$ 876.1436, observed $[M+H]^+$ 876.1451. 2-**Tetrahydrofuranacetyl-CoA (2-CoA):** expected $[M+H]^+$ 880.1749, observed 880.1721. **2-Thiopheneacetyl-CoA (3-CoA):** expected $[M+H]^+$ 892.1208, observed 892.1194. **2-Pyridylacetyl-CoA (4-CoA):** expected $[M+H]^+$ 887.1596, observed 888.0821. **2-Furoyl-CoA (5-CoA):** expected $[M+H]^+$ 862.1280, observed 862.1309. **4-Oxohexanoyl-CoA (6-CoA):** expected $[M+H]^+$ 879.1671, observed 879.1881. **5-Oxohexanoyl-CoA (7-CoA):** expected $[M+H]^+$ 879.1671, observed 879.1877. **2,2´-Dimethyl-3-oxohexanoyl-CoA (8-CoA):** expected $[M+H]^+$ 908.2062, observed 908.2022. **4-Oxooctanoyl-CoA (10-CoA):** expected $[M+H]^+$ 907.1984, observed 907.1887. **5-Oxooctanoyl-CoA (11-CoA):** expected $[M+H]^+$ 907.1984, observed 907.1878. **2-Benzofuranacetyl-CoA (43):** expected $[M+H]^+$ 926.1593, observed 926.1626.

Mass determination of Acyl-ACP proteins

Molecular mass of ACP and its derivatives were determined by high performance liquid chromatography mass spectrometry (HPLC-MS) using an ultra-high-resolution Quadrupole Time of Flight (QTOF) instrument (Bruker maXis, Bruker Corporation, Billerica, Massachusetts). The electrospray ionization (ESI) source was operated under the following conditions: positive ion mode; nebulizer pressure: 1.2 Bar; flow rate of drying gas (N2): 8 L/min; drying gas temperature: 200 °C; voltage between HV capillary and HV end-plate offset: 3000 V to −500 V; and the quadrupole ion energy was 4.0 eV. Low concentration ESI tuning mix (Agilent Technologies, Santa Clara, California) was used to calibrate the system in the mass range. HPLC separation was achieved using a Dionex UltiMate® 3000 uHPLC system (Dionex Corporation, Sunnyvale, California). Ten microliters of samples were injected onto a Phenomenex Kinetex XB-C18 column (100 x 2.1 mm, 2.6μm) (Phenomenex Corporation, Torrance, California) at a flow rate of 0.3 mL/min followed by a simple linear gradient for sample desalting and separation. The initial eluent was 98% mobile phase A (99.9% water, 0.1% formic acid) and 2% B (99.9% acetonitrile, 0.1% formic acid) for 5 min and then mobile phase B was increased to 50% in 25 min. LC eluent was diverted to the waste during the first five minutes of the gradient to eliminate salts in the sample buffer. Obtained mass spectra were deconvoluted using Bruker Data Analysis 4.0 software to obtain charge state (N) of protein ions. To calculate the molecular mass of ACP and its derivatives, the measured m/z values were multiplied by corresponding charge state (N) of protein ions and were subtracted by the mass of N protons (N x 1.0079). **Apo-ACP (16):** calculated mass 8508.1636 Da, observed mass 8508.2138 Da; **2-furanacetyl-ACP (1):** calculated mass 8957.2798 Da, observed mass

8957.6844 Da; **2-tetrahydrofuranacetyl-ACP (2):** calculated mass 8961.3068 Da, observed mass 8961.2978 Da; **2-thiopheneacetyl-ACP (3):** calculated mass: 8972.5905 Da, observed mass: 8972.5293 Da; **2-pyridylacetyl-ACP (4):** calculated mass 8969.2168 Da, observed mass 8969.1140 Da; **2-furoyl-ACP (5):** calculated mass 8942.6020 Da, observed mass 8942.5198 Da; **4-oxoC6-ACP (6):** calculated mass 8960.3228 Da, observed mass 8960.4226 Da; **5-oxoC6-ACP (7):** calculated mass 8960.3224 Da, observed mass 8960.6268 Da; **2,2´-dimethyl-3-oxoC6-ACP (8):** calculated mass 8988.6773 Da, observed mass 8988.9023 Da; **C6-ACP (9):** calculated mass 8946.8127 Da, observed mass 8946.5601 Da; **4-oxoC8-ACP (10):** calculated mass 8988.3234 Da, observed mass 8988.3352 Da; **5-oxoC8-ACP (11):** calculated mass 8988.3225 Da, observed mass 8988.4745 Da; **C8-ACP (12):** calculated mass 8974.8667 Da, observed mass 8974.5376 Da; **2-benzofuranacetyl-ACP (13):** calculated mass 9006.2867 Da, observed mass 9006.0533 Da.

HPLC assay

Two chemical steps, lactonization and acylation, could be resolved independently using analytical C-18 reverse-phase UHPLC. MTA peak from SAM lactonization was monitored using a gradient beginning at 100 % A (99.9% water, 0.1% formic acid) : 0 % D (99.9% acetonitrile, 0.1% formic acid) and ending at 70 % A: 30 % D over a period of 10 minutes at flow rate of 500 μL/min. Holo-ACP from acylation half-reaction was monitored using a gradient beginning at 75 % A: 25 % D and ending at 25 % A: 75 % D over a period of 10 minutes at flow rate of 600 μL/min. Standard calibration curves for MTA and holo-ACP were generated by serial dilution of known analyte concentrations in buffer with quench solution, 6 M HCl (lactonization) or 4 M acetate buffer, pH 3.7

(acylation). Peak areas at each MTA and holo-ACP concentration were determined from HPLC chromatograms at 260 nm (SAM and MTA) or 220 nm (acyl-ACP and holo-ACP). A typical enzyme-catalyzed reaction (100 μL) contained nanopure water, 100 mM HEPES pH 7.3 buffer, fixed SAM concentration at 500 μM, varied acyl-ACP concentrations. The mixture was split into two equal portions for background and reaction. After incubation at room temperature for 5 minutes, the reaction and background aliquots were initiated, respectively with 1 μM EsaI enzyme (2 μM EsaI for 4-oxo-C8-ACP, 5-oxo-C8-ACP, and C8-ACP) and nanopure water. Both aliquots were quenched after 4 minutes of initiation using 6 M HCl (lactonization) or 4 M acetate buffer pH 3.7 (acylation) with final concentration of 0.4 M HCl or 0.4 M acetate buffer. Peak areas of MTA and holo-ACP at each acyl-ACP concentration were determined from HPLC chromatograms. The difference between background and reaction in peak area per minute was converted to initial reaction rate in μM/min using standard calibration curves. MTA standard curve had linear fit equation of $y = 0.198x$; holo-ACP standard curve had linear fit equation of $y = 0.4058x$, where y = peak area of analyte, x = known concentration of analyte. The initial rate was fitted to Michaelis-Menten equation (Eq. 4) or substrate inhibition equation (Eq. 5) using GraphPad Prism 7.00. All experiments were repeated duplicated to check for reproducibility and to estimate errors.

Results and Discussion

Purification of EsaI wild-type and T140A mutant

Inoculation of BL21 (DE3) *E. coli* EsaI WT and T140A on agar plates containing 100 μg/ mL ampicillin antibiotic showed appearance of small white circular colonies. An isolated colony of WT and T140A mutant was picked to inoculate mini growths and then

large growths with the same antibiotic concentration. The large growths of WT and T140A mutant reached to OD of 0.6-0.8 within three hours of shaking at 37 °C. Chemical lysis using B-PER, lysozyme, DNase, RNase, and PMSF gave clear yellow lysate in both large growths. EsaI protein was purified using Ni-NTA affinity column chromatography. The molecular weight of EsaI (WT and T140A) is ~ 25 kDa. It was confirmed that the clean EsaI WT and T140A proteins were obtained indicating by a band at 25 kDa on SDS-PAGE gel (Figure 11 and 12).

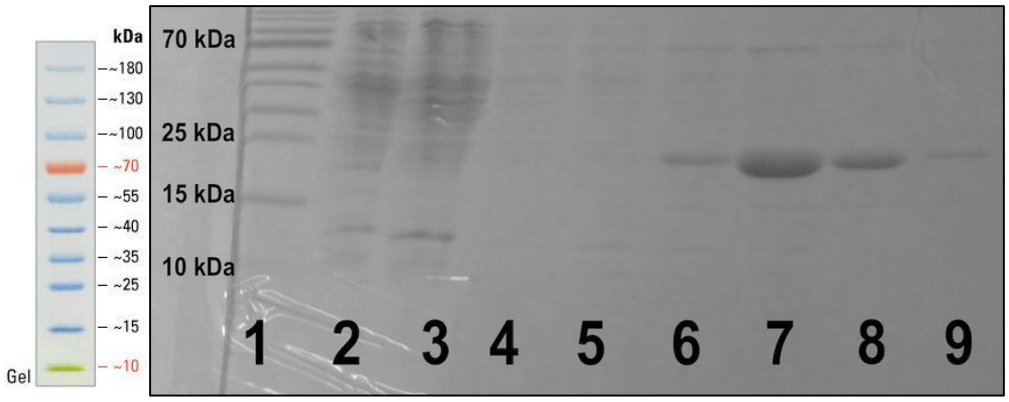

Figure 11. SDS-PAGE of EsaI wild-type fractions using Ni-NTA affinity column chromatography. Lane 1: EZ prestained protein ladder from Fisher; 2: run through of EsaI crude; 3: 40 mM imidazole in Tris-HCl buffer wash of EsaI; 4-9: 200 mM imidazole in Tris-HCl buffer elutions 1-6. The elutions in lanes 6-9 were on the 25 kDa marker indicating the presence of clean EsaI from purification.

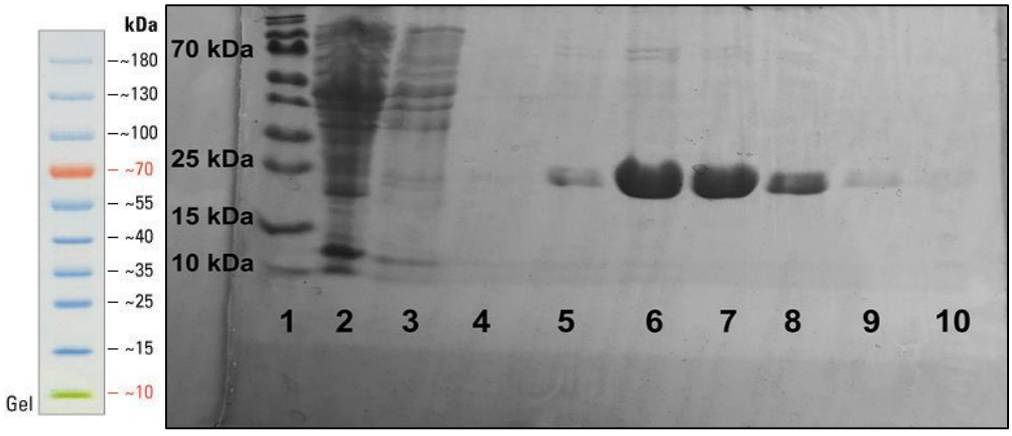

Figure 12. SDS-PAGE of EsaI T140A mutant fractions using Ni-NTA affinity column chromatography. Lane 1: EZ prestained protein ladder from Fisher; 2: run

through of T140A crude; 3: 40 mM imidazole in Tris-HCl buffer wash of T140A; 4-10: 200 mM imidazole in Tris-HCl buffer elutions 1-7. The elutions in lanes 5-10 were on the 25 kDa marker indicating the presence of clean T140A from purification.

Purification of apo-ACP

Inoculation of BL21 (DE3) *E. coli* apo-ACP on agar plate containing 25 μg/mL kanamycin, 50 μg/mL streptomycin, 50 μg/mL spectinomycin, and 25 μg/mL chloramphenicol antibiotics showed appearance of small white circular colonies. An isolated colony was picked to inoculate mini growth and then large growth with the same antibiotic concentrations. The large growth reached to OD of 0.6-0.8 within three hours of shaking at 37 °C. Chemical lysis using B-PER, lysozyme, DNase, RNase, and PMSF gave clear yellow lysate. Due to the fact that production of holo-ACP is common during fatty acid biosynthesis, conversion of holo-ACP to apo-ACP by ACP-hydrolase, which was inserted in apo-ACP plasmid, was done by addition of $MgCl_2$ and $MnSO_4$ to the clear lysate. The conversion of holo-ACP to apo-ACP resulted in a cloudy solution. ACP-hydrolase was precipitated with isopropyl alcohol and removed by centrifugation to afford clear solution. Anion exchange chromatography using DEAE-sepharose resin was successfully used to isolate pure apo-ACP from other cellular debris. The molecular weight of apo-ACP is 8639.5 Da or ~ 9 kDa. It was confirmed that the clean apo-ACP protein was obtained indicating by a band at ~ 9 kDa on SDS-PAGE gel (Figure 13).

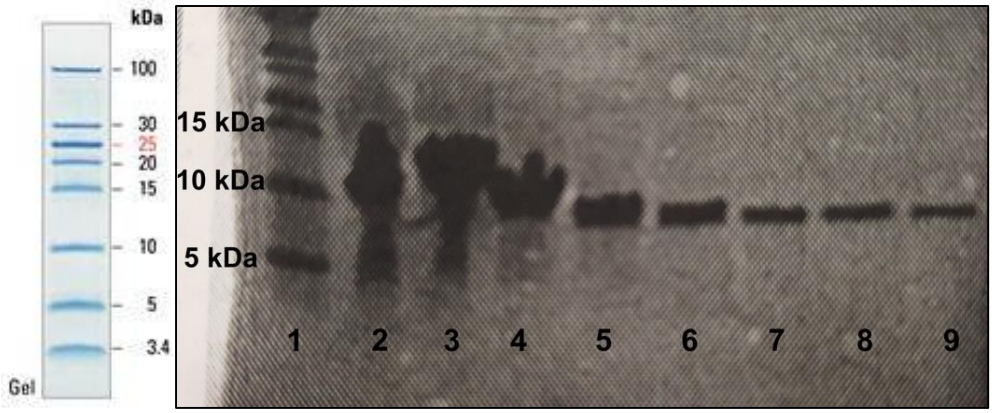

Figure 13. Tris-Tricine SDS-PAGE of apo-ACP fractions using DEAE-cellulose anion exchange column chromatography. Lane 1: EZ prestained low range protein ladder from Fisher; 2: run through of apo-ACP crude; 3: 0.25 mM LiCl in 10 mM MES, pH 6.1 buffer wash of apo-ACP; 4-9: 0.5 M LiCl in 10 mM MES, pH 6.1 buffer elutions 1-6. The elutions in lanes 4-9 showed banding at ~ 9 kDa, indicated that clean apo-ACP was successfully isolated by anion exchange chromatography.

Purification of Sfp

Inoculation of BL21 (DE3) *E. coli* sfp on agar plate containing 100 μg/ mL kanamycin antibiotic showed appearance of small white circular colonies. An isolated colony was picked to inoculate mini growth and then large growth with the same antibiotic concentration. The large growth reached to OD of 0.6-0.8 within three hours of shaking at 37 °C. Chemical lysis using B-PER, lysozyme, DNase, RNase, and PMSF gave clear yellow lysate. Sfp was purified using Ni-NTA affinity column chromatography. The molecular weight of Sfp is 26990.5 Da or ~ 27 kDa. It was confirmed that the clean sfp protein was obtained indicating by a band at ~ 27 kDa on SDS-PAGE gel (Figure 14).

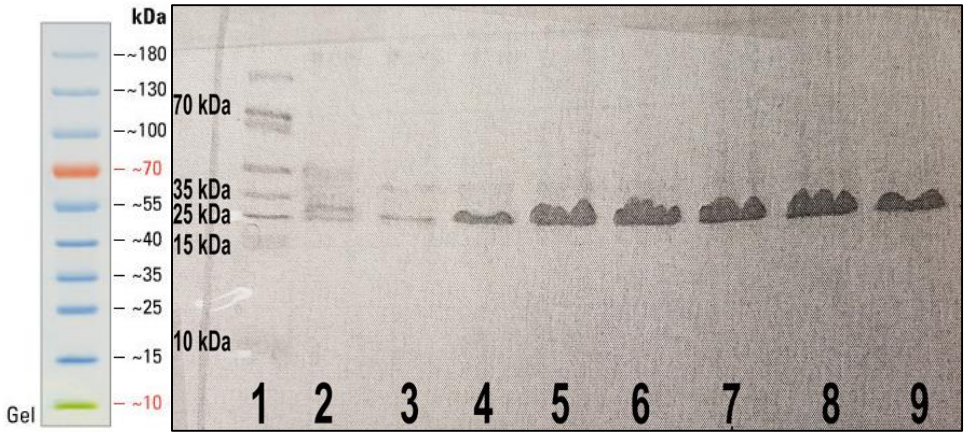

Figure 14. SDS-PAGE of Sfp fractions using Ni-NTA affinity column chromatography. Lane 1: EZ prestained protein ladder from Fisher; 2: run through of sfp crude; 3: 10 mM imidazole in Tris-HCl buffer wash of sfp; 4-9: 200 mM imidazole in Tris-HCl buffer elutions 1-6. The elutions in lanes 4-9 were on ~ 27 kDa indicating the presence of clean sfp from purification.

Syntheses of acyl-succinimide ester molecules

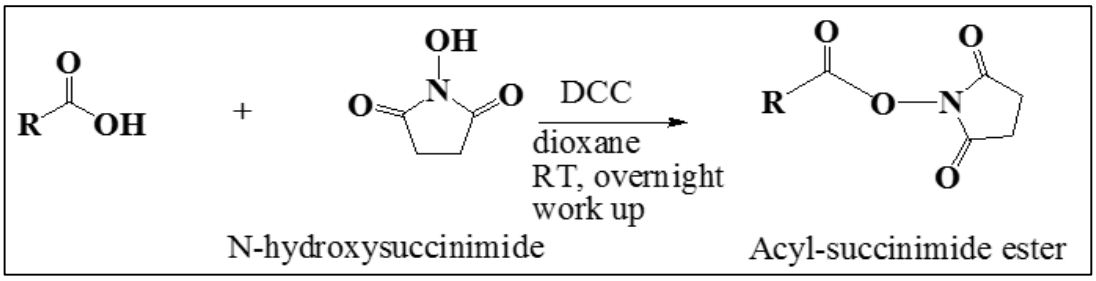

Scheme 7. Synthesis of acyl-succinimide ester using DCC and N-hydroxysuccinimide.

Chemical syntheses of acyl-succinimide ester molecules were prepared by treating commercially available carboxylic acids with dehydrating agent *N,N′*-dicyclohexylcarbodiimide (DCC) and *N*-hydroxysuccinimide (Scheme 7).[47] In the reaction, the coupling reagent DCC was used to activate the carboxylic acids, forming the highly reactive intermediate O-acylisourea with an activated leaving group. Then, O-acylisourea reacted with *N*-hydroxysuccinimide to form the desired acyl-succinimide ester product and *N,N′*-dicyclohexylurea by-product. DCC was chosen in this type of coupling reaction because it is inexpensive and high yielding. The *N,N′*-dicyclohexylurea by-

product was insoluble in organic solvents, such as warm methanol and cold dioxane, and was easily removed by simple filtration**.** NMR characterization of all acyl-succinimide esters was achieved using ^{1}H-NMR, COSY, and ^{13}C-NMR (Figures A1-A30). The diagnostic feature indicating the presence of acyl-succinimide ester molecule is the singlet signal at 2.82 ppm, which integrates to 4 protons in the ^{1}H-NMR, and the signal at 25.8 ppm in the ^{13}C-NMR, which corresponds to the two methylene (-CH_2-) groups of the succinimide ring. Additionally, in the synthesis of 2,2′-dimethyl-3-oxoC6-succinimide ester (**8-succ**), it was difficult to remove trace amounts of urea even though silica gel column chromatography was performed. Hence, in order to absolutely confirm the presence of 2,2′-dimethyl-3-oxoC6-succinimide ester, HSQC experiment was done (Figure A18). ESI-MS-TOF of all acyl-succinimide ester molecules were obtained to confirm their identities (Figures B1-B11).

Synthesis of 4-oxo- and 5-oxo- acids (**6-acid**, **7-acid**, **10-acid** and **11-acid**)

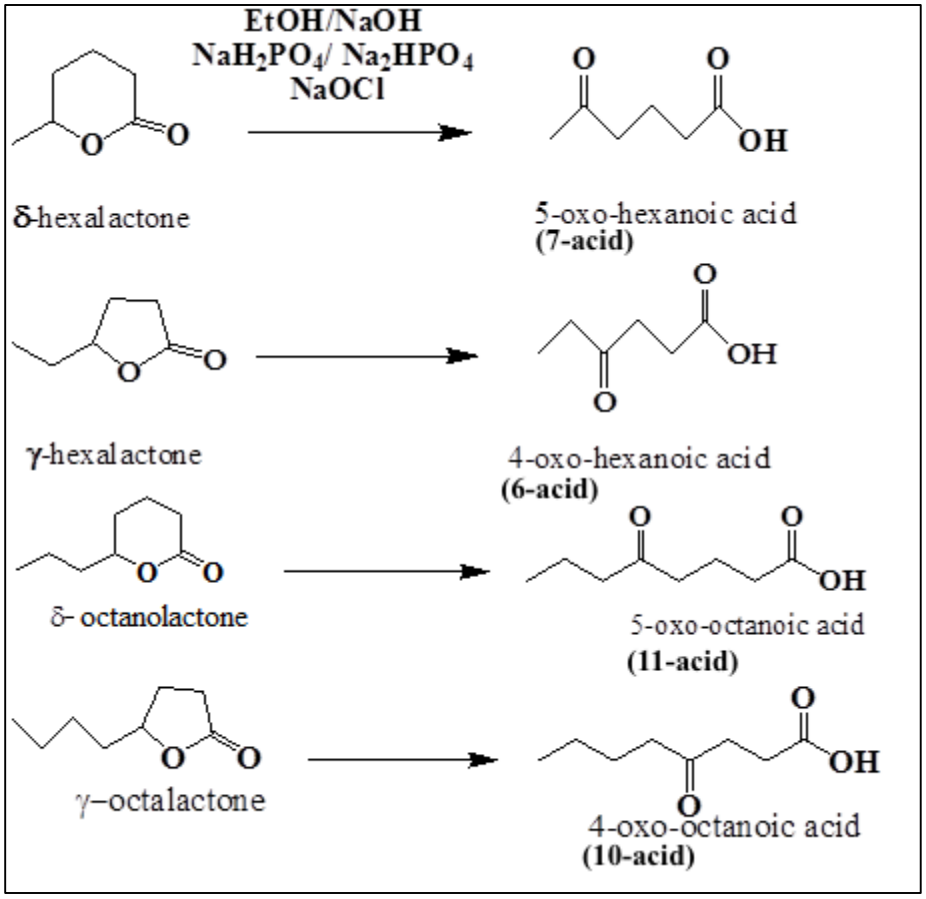

Scheme 8. Syntheses of 5-oxohexanoic acid/ octanoic acid and 4-oxohexanoic acid/ octanoic acid by oxidation of respective δ- and γ-lactones in buffered sodium hypochlorite.

In some cases, carboxylic acids were not commercially available to achieve synthesis of acyl-succinimide esters, such as 5-oxohexanoic acid (**7-acid**), 5-oxooctanoic acid (**11-acid**), 4-oxohexanoic acid (**6-acid**), and 4-oxooctanoic acid (**10-acid)**. The 5-oxocarboxylic acids and 4-oxocarboxylic acids were prepared chemically by oxidation of respective δ- and γ-lactones by buffered sodium hypochlorite (Scheme 8).[48] Hypochlorous acid was a cheap oxidant and is commonly used for conversion of secondary alcohols to ketones. In the reaction, the lactone ring was first hydrolyzed under basic conditions

(EtOH/NaOH) to afford its open form (hydroxyl-carboxylate salt). A buffer solution of sodium dihydrogen phosphate/ disodium hydrogen phosphate at pH 6.6 with hypochlorous acid was used to oxidize the 2° alcohols to ketones with reasonable yield. The characterization of **6-acid**, **7-acid**, **10-acid** and **11-acid** by NMR spectroscopy (^{1}H, ^{13}C and COSY) were obtained to confirm their identities (Figures A35-A45). Compounds **6-acid**, **7-acid**, **10-acid** and **11-acid** were then used to prepare the corresponding succinimide esters **6-succ**, **7-succ**, **10-succ** and **11-succ**.

Synthesis of 2,2′-dimethyl-3-oxohexanoic acid (**8-acid**)

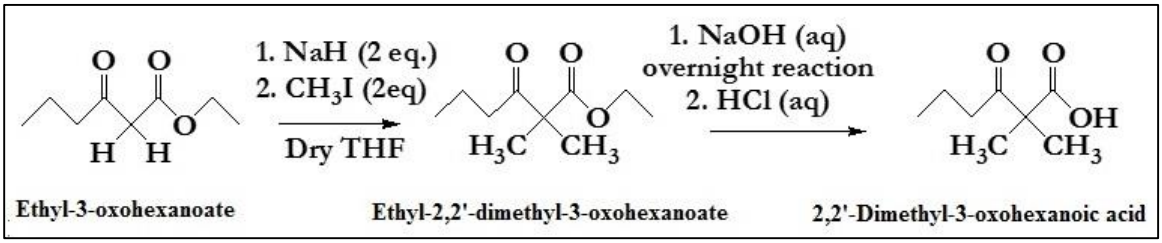

Scheme 9. Synthesis of 2,2′-dimethyl-3-oxohexanoic acid.

Similar to the 5-oxo- and 4-oxo- acids, 2,2′-dimethyl-3-oxohexanoic acid was not commercially available and was prepared chemically using commercially available ethyl-3-oxohexanoate as starting material (Scheme 9).[49,50] Iodomethane was used as the methylating reagent because the iodide ion was the least basic and thus the best leaving group among the halogens. Sodium hydride NaH was used as a strong base to deprotonate the acidic protons at the C-2 position of ethyl-3-oxohexanoate, forming the carbanion intermediate. Then, the reactive carbanion nucleophile attacked the electrophilic carbon in iodomethane and displaced iodide in an S_N2 reaction. The reaction was done under inert condition due to the reactivity of sodium hydride. The dimethylation reaction of ethyl-3-oxohexanoate gave a successful reaction with high yield (91%). Also, the monomethylated

product of the reaction was not observed, indicating the reaction had gone to completion. One of the important indication of the success of the dimethylation reaction was the singlet at 1.33 ppm, which integrates to 6 protons in the ^{1}H-NMR (Figure A31). In addition, in the DEPT135-NMR, the height of signal at 21.9 ppm, which was about twice as high as other methyl group signal, indicated the two methyl groups at C-2 overlapped (Figure A32).

Furthermore, the dimethylated ethyl-3-oxohexanoate was then hydrolyzed using 1N NaOH and 2N HCl solutions to obtain 2,2´-dimethyl-3-oxohexanoic acid (Scheme 9).[51] In the ^{1}H-NMR, the complete disappearance of the two signals at 4.15 and 1.23 ppm indicated that ethyl group of the dimethylated ethyl-3-oxohexanoate staring material was hydrolyzed successfully (Figure A33). In the ^{13}C-NMR, the appearance of signals at 209.1 ppm and 175. 6 ppm were observed for the respective ketone and carboxylic acid functional groups of the desired product **8-acid** (Figure A34).

Syntheses of acyl-CoA molecules

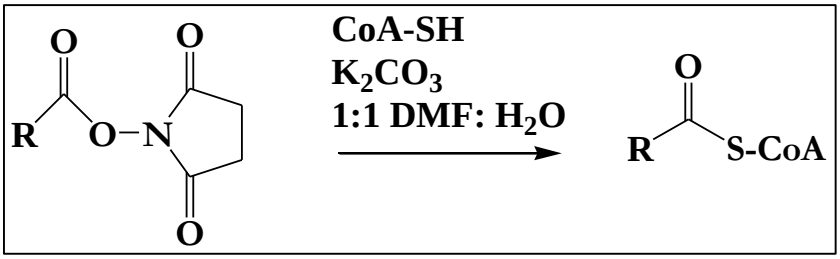

Scheme 10. Synthesis of acyl-CoA molecules using free CoA acid and acyl-succinimide ester under nitrogen atmosphere.

The rationale for preparing acyl-succinimide ester molecules was because the molecules are activated acids containing an excellent leaving group that could be used to prepare acyl-CoA analogs. The syntheses of acyl-CoA molecules were achieved by treating the synthesized acyl-succinimide esters with free coenzyme A (CoA) acid under a nitrogen environment (Scheme 10).[53-55] The free CoA acid was deprotonated under basic conditions

and readily attacked the carbonyl carbon of the acyl-succinimide ester starting material, substituting for the succinimide group. The crude product from the acyl-CoA reaction was extracted and ran on preparative HPLC to collect the desired pure acyl-CoA product. HPLC chromatograms of all synthesized acyl-CoA molecules were obtained and are shown in Figure 14 (Panels A-J). Molecules with higher polarity or smaller in molecular size eluted earlier in reverse-phase HPLC (Figure 15, Panels B-F, H). 2-Thiopheneacetyl-CoA (Panel G) is less polar than 2-furanacetyl-CoA (Panel E) and had a retention time at 7.5 minutes. 2,2′-Dimethyl-3-oxoC6-CoA (Panel A) is more hydrophobic compared to 4-oxoC6-CoA (Panel B) and 5-oxoC6-CoA (Panel C) due to the presence of two methyl groups at C-2 and had a retention time at 8.5 minutes. 4-oxoC8-CoA (Panel I) and 5-oxoC8-CoA (Panel J) had retention times at 8.7 minutes due to the presence of two additional carbons in the acyl-chain, causing them to be more non-polar than the other acyl-CoA molecules. Mass spectral data using ESI-TOF for all acyl-CoA molecules were also obtained to confirm their identities (Figures B12-B22).

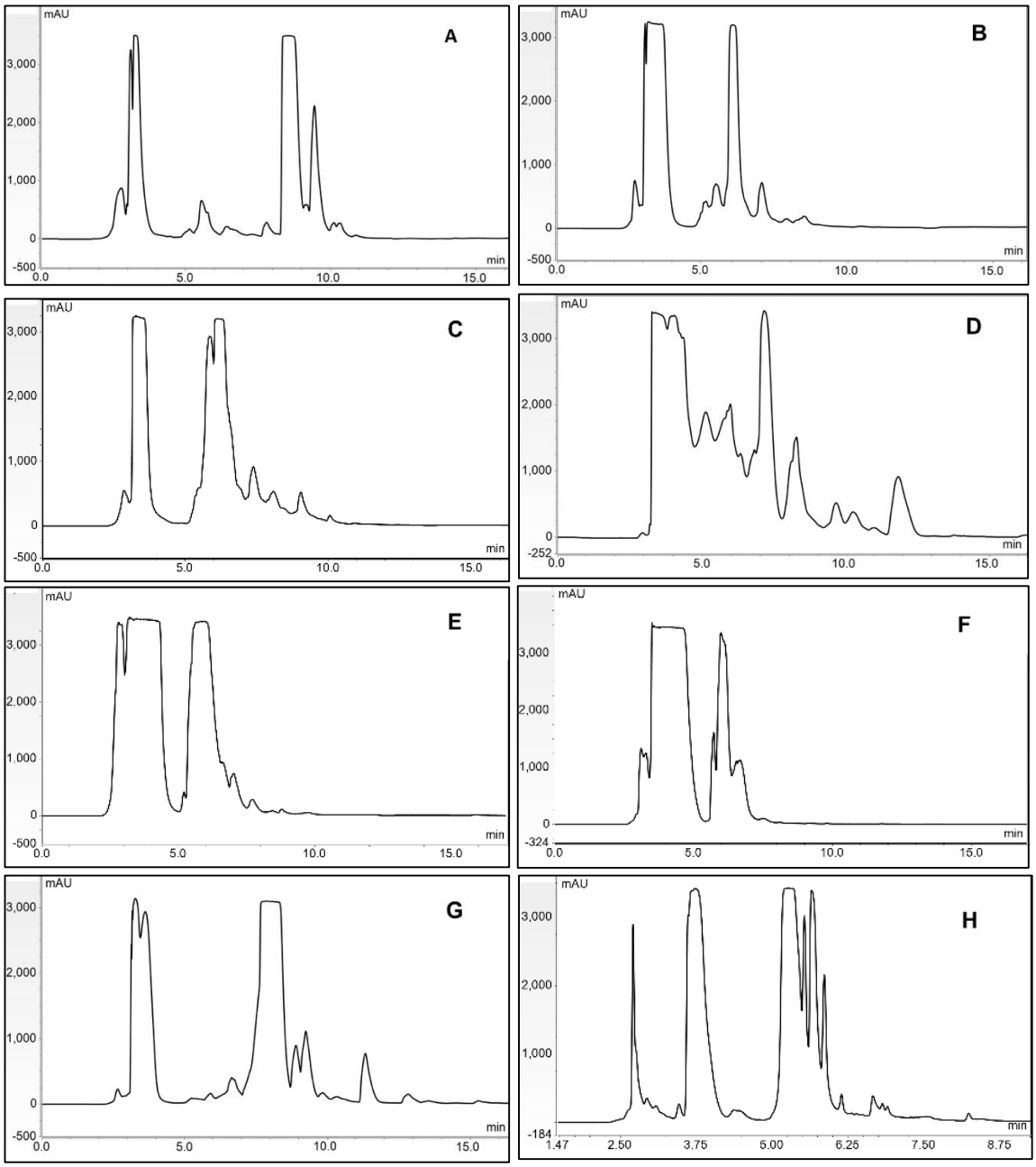
A
mAU
3,000
2,000
1,000
0
-500
0.0
5.0
10.0
15.0
min
B
mAU
3,000
2,000
1,000
0
-500
0.0
5.0
10.0
15.0
min
C
mAU
3,000
2,000
1,000
0
-500
0.0
5.0
10.0
15.0
min
D
mAU
3,000
2,000
1,000
0
-252
0.0
5.0
10.0
15.0
min
E
mAU
3,000
2,000
1,000
0
-500
0.0
5.0
10.0
15.0
min
F
mAU
3,000
2,000
1,000
0
-324
0.0
5.0
10.0
15.0
min
G
mAU
3,000
2,000
1,000
0
-500
0.0
5.0
10.0
15.0
min
H
mAU
3,000
2,000
1,000
-184
1.47
2.50
3.75
5.00
6.25
7.50
8.75
min

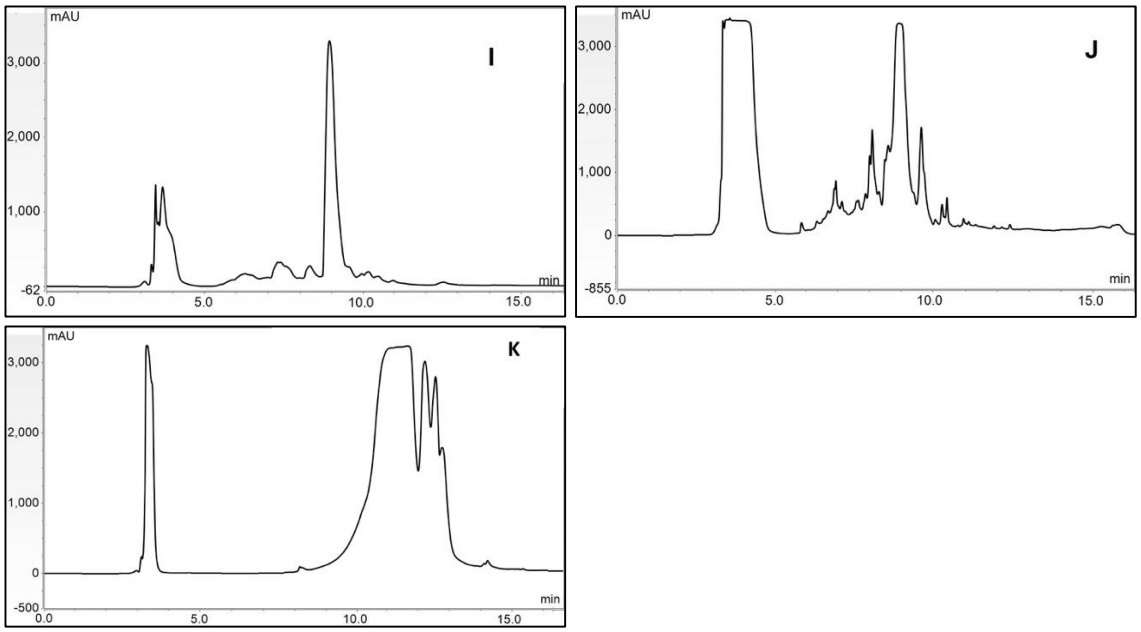

Figure 15. HPLC chromatograms of synthesized alternative 3-oxo-acyl-CoA molecules using preparative HPLC. Excess of starting material, acyl-succinimide ester and unreacted CoA eluted from 2.5 – 4.8 minutes. Only peak corresponding to the acyl-CoA product of interest was collected by fraction collector. (A) 2,2′-Dimethyl-3-oxohexanoyl-CoA eluted at 8.5 – 9.2 minutes (B) 4-Oxohexanoyl-CoA eluted at 5.3 – 7.1 minutes (C) 5-Oxohexanoyl-CoA eluted at 5.4 – 7.2 minutes (D) 2-Furoyl-CoA eluted at 6.1 – 9.9 minutes (E) 2-Furanacetyl-CoA eluted at 5.2 – 6.8 minutes (F) 2-Tetrahydrofuranacetyl-CoA eluted at 5.5 – 6.5 minutes (G) 2-Thiopheneacetyl-CoA eluted at 7.5 – 9.1 minutes (H) 2-Pyridylacetyl-CoA eluted at 5.0 – 6.0 minutes (I) 4-Oxooctanoyl-CoA eluted at 8.7 – 10.0 minutes (J) 5-Oxooctanoyl-CoA eluted at 8.7 – 9.3 minutes (K) 2-Benzofuranacetyl-CoA eluted at 8.4 – 12.0 minutes.

Interestingly, 2-benzofuranacetyl-succinimide ester was synthesized from 2-benzofuranacetic acid and treated with free CoA acid did not yield the desired 2-benzofuranacetyl-CoA product. Mass spectral data confirmed that 2-benzofuranacetyl-CoA product was not observed under this reaction condition. A different approach was attempted to afford the 2-benzofuranacetyl-CoA product. Synthesis of 3-oxo-acid *N*-acetylcysteamine thioester was reported using 1,1′-carbonyldiimidazole and *N*-acetylcysteamine in dry acetonitrile at below 0 °C.[52] *N*-Acetylcysteamine is similar to the free-CoA molecule, except that *N*-acetylcysteamine only has the cystamine part of free-CoA molecule. By adapting to the reported protocol, the synthesis of 2-benzofuranacetyl-

CoA was successfully done using 2-benzofuranacetic acid, 1,1′-carbonyldiimidazole, and free-CoA (Scheme 11). The HPLC chromatogram was shown in Figure 14 (Panel K). 2-Benzofuranacetyl-CoA is relatively more hydrophobic and bigger in size than 2-furanacetyl-CoA and had retention time at 8.4 minutes. The characterization of 2-benzofuranacetyl-CoA (**13-CoA**) was confirmed by ESI-TOF (Figure B23).

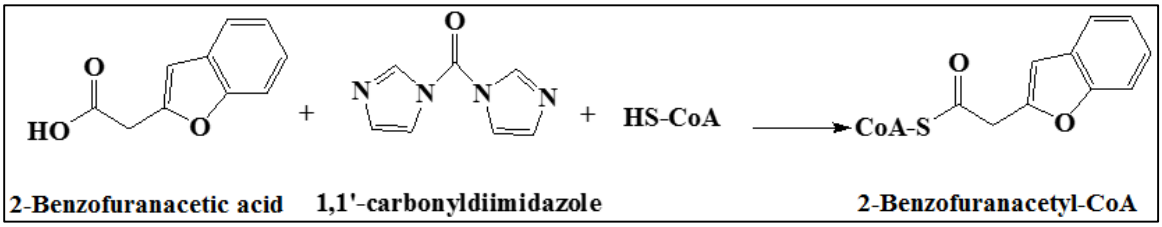

Scheme 11. Synthesis of 2-benzofuranacetyl-CoA using 2-benzofuranacetic acid, 1,1′-carbonyldiimidazole, and CoA-SH in dry acetonitrile.

Syntheses of acyl-ACP proteins

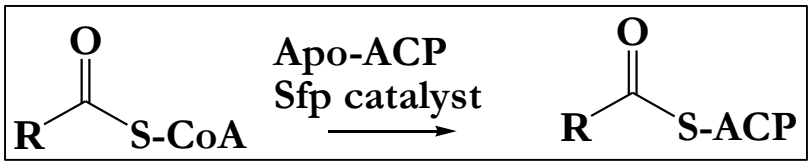

Scheme 12. Enzymatic synthesis of acyl-ACP protein using synthesized acyl-CoA molecule and apo-ACP catalyzed by Sfp enzyme.

Enzymatic synthesis of *E. coli* acyl-ACP proteins was done by using Sfp enzyme (Scheme 12). *Bacillus subtilis* Sfp 4′-phosphopantetheinyl transferase exhibits extraordinarily broad substrate specificity. Sfp transfers the 4′-phosphopantetheinyl group of CoA onto a conserved serine residue of acyl carrier protein (ACP) to convert ACPs from their inactive apo forms into active forms.[56,57] The completion of the reactions was monitored by the depletion of apo-ACP at 7.7 minutes and the growth of corresponding acyl-ACP peak. The addition of acyl-pantetheine linker and various acyl-chain to apo-ACP shifted the retention time for each substrate accordingly (Figure 16, Panels A-J). The Sfp

enzyme eluted at 5.1 minutes. Since acyl-ACP with 6 carbons overlapped with apo-ACP when using 10 min method with flow rate of 600 μL/min, a different method began with 75% solvent A (H_2O + 0.1% TFA) and 25% solvent D (acetonitrile + 0.1% TFA) and ended with 25% solvent A and 75% solvent D at flow rate of 200 μL/min over a period of 60 minutes was optimized to separate C6-ACP, 4-oxoC6-ACP, 5-oxoC6-ACP from apo-ACP (Figure 17, Panels A-C).

Once the acyl-ACP reaction had gone to completion, Sfp enzyme was precipitated out by addition of ammonium sulfate and removed from the reaction mixture by centrifugation. Clean acyl-ACP product from the reaction was obtained by multiple washes with nanopure water to remove excess acyl-CoA and ammonium sulfate. These impurities absorbed at 260 nm while apo-ACP and acyl-ACP proteins absorbed at 280 nm on UV-Vis. The reduction of 260 peak after washes indicated the acyl-ACP protein was free of contamination. All acyl-ACPs were confirmed by ESI-LC/MS (Figures B24-B39).

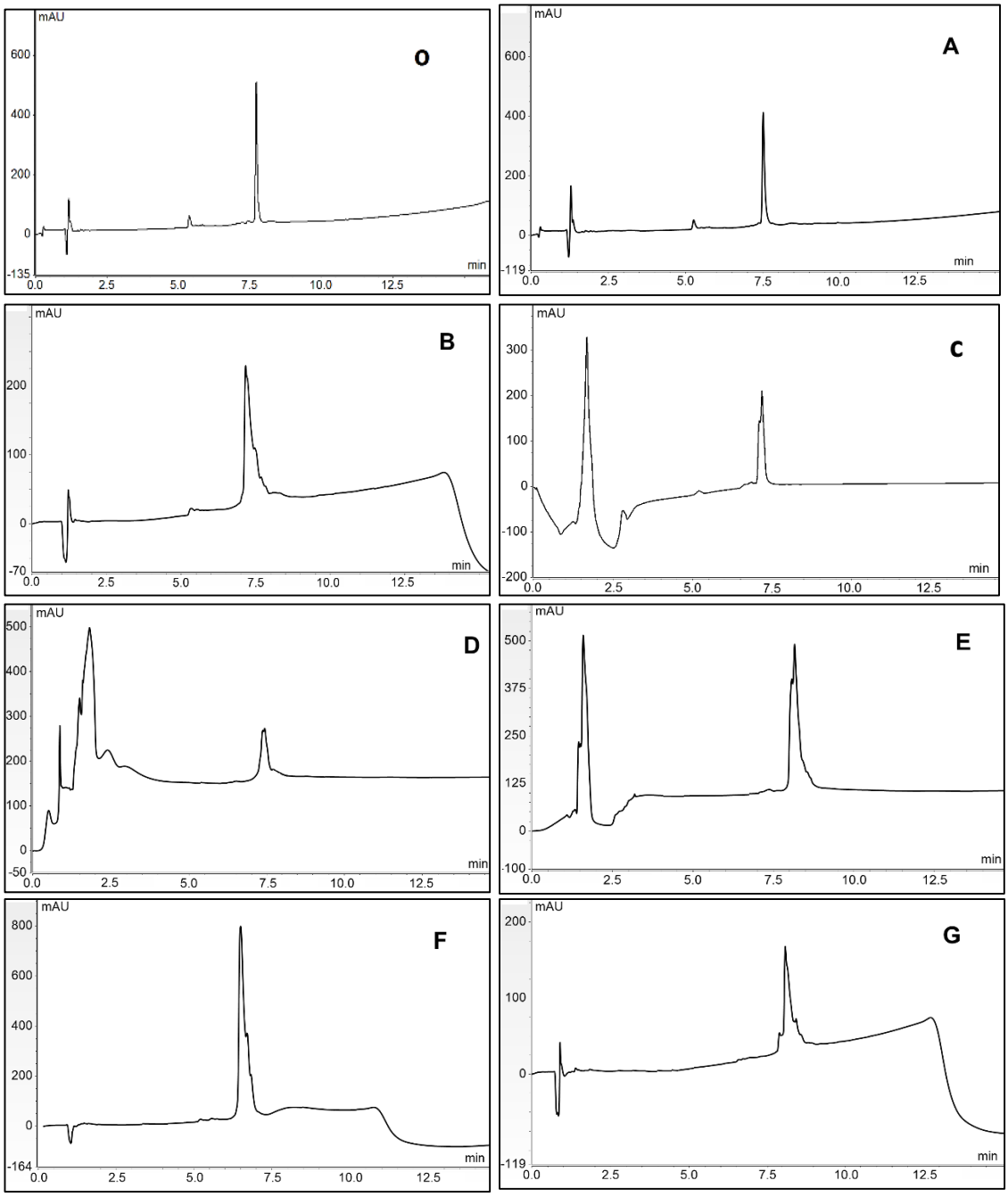
O
A
B
C
D
E
F
G
mAU
min

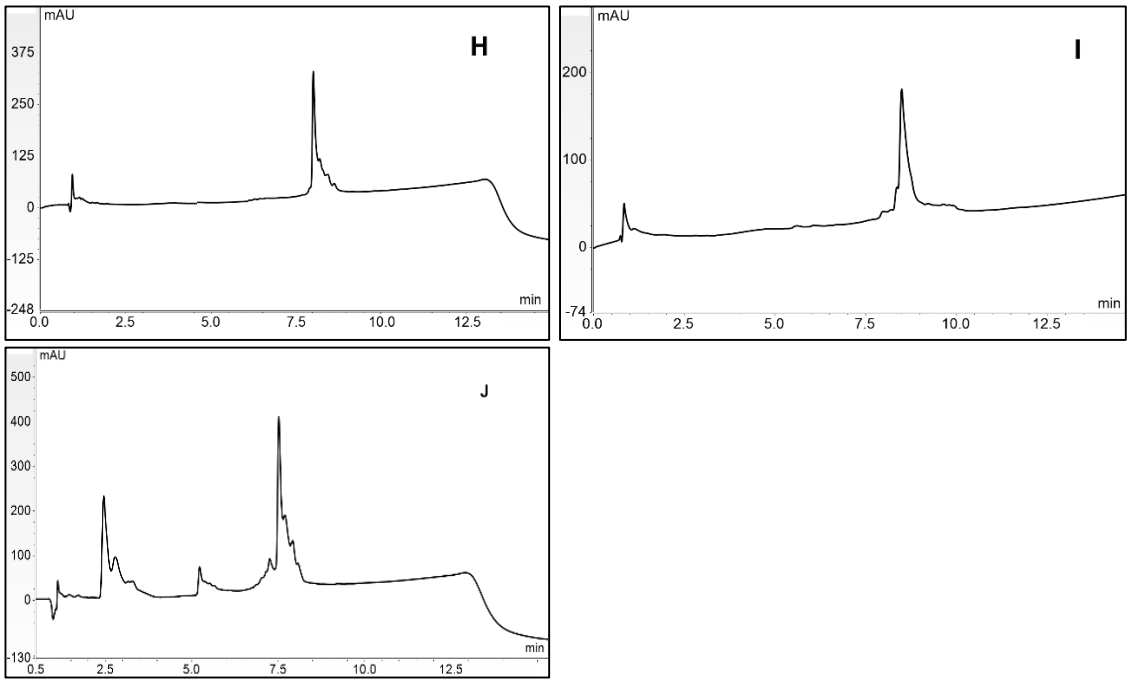

Figure 16. HPLC chromatograms of apo-ACP and alternative 3-oxoacyl-ACPs using analytical HPLC over a period of 10 minutes with flow rate of 600 μL/min. Sfp enzyme eluted at 5.1 minutes. (O) Apo-ACP eluted at 7.7 minutes. The completion of acyl-ACP synthesis reaction was monitored by disappearance of apo-ACP peak over time. (A) 2,2′-Dimethyl-3-oxohexanoyl-ACP eluted at 7.6 minutes. (B) 2-Furoyl-ACP eluted at 7.5 minutes (C) 2-Furanacetyl-ACP eluted at 7.4 minutes. (D) 2-Tetrahydrofuranacetyl-ACP eluted at 7.3 minutes (E) 2-Thiopheneacetyl-ACP eluted at 7.8 minutes. (F) 2-Pyridylacetyl-ACP eluted at 6.5 minutes. (G) 4-Oxooctanoyl-ACP eluted at 8.0 minutes. (H) 5-Oxooctanoyl-ACP eluted at 8.1 minutes. (I) Octanoyl-ACP eluted at 8.7 minutes. (J) 2-Benzofuranacetyl-ACP eluted at 7.5 minutes.

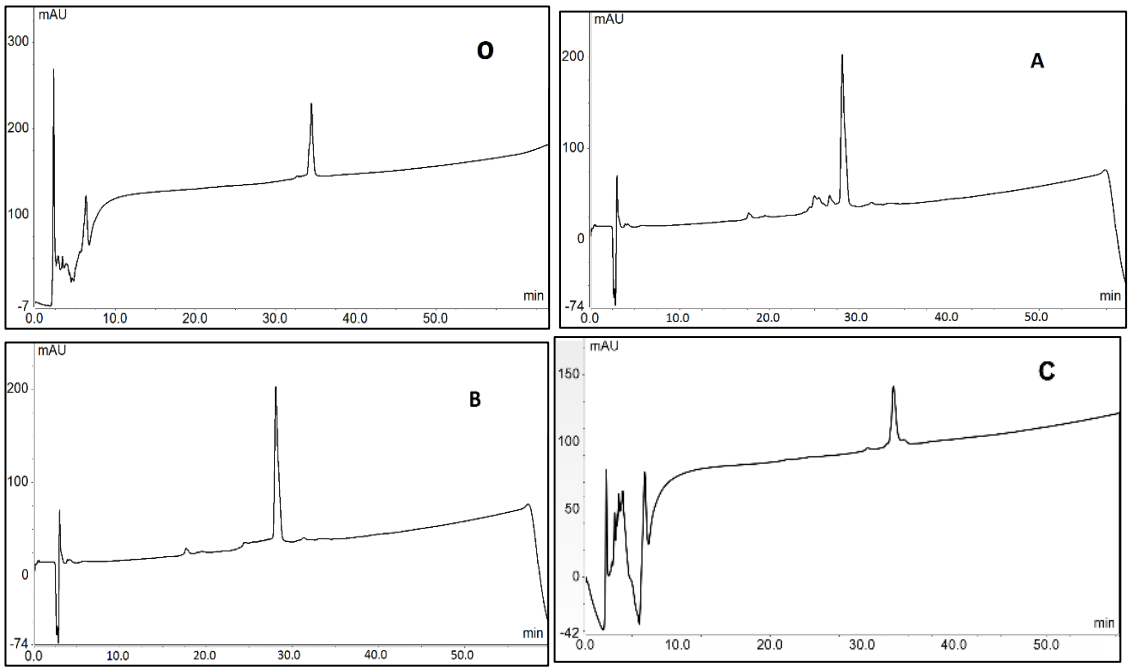

Figure 17. HPLC chromatogram of apo-ACP and alternative 3-oxoacyl-ACPs using analytical HPLC over a period of 60 minutes with flow rate of 200 μL/min. Sfp enzyme eluted at 20.8 minutes. (O) Apo-ACP eluted at 33.1 minutes (A) 4-Oxohexanoyl-ACP eluted at 30.0 minutes (B) 5-Oxohexanoyl-ACP eluted at 30.0 minutes (C) Hexanoyl-ACP eluted at 31.7 minutes.

Enzyme assays

One of the objectives in this thesis is to determine the activity of the alternative 3-oxo-acyl-ACP substrates with EsaI. Different enzymatic kinetic assays were explored, including DCPIP assay, MTAN-XO coupled assay, and HPLC assay. DCPIP assay is the simplest and well-documented in literature to determine kinetic parameters by measuring the decrease in absorbance at 600 nm related to the concentration of holo-ACP product formed over time. Unfortunately, with DCPIP colorimetric assay, the reaction rates did not change when substrate concentration and enzyme concentration were increased (Figure 18). One of the possibility is that the enzyme might have surface-exposed cysteine, which can reduce DCPIP, and thus, the enzyme is dead.

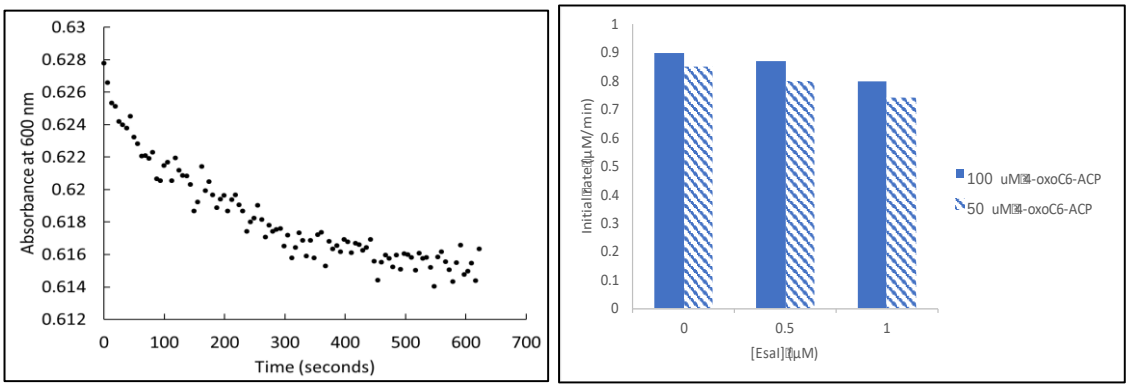

Figure 18. DCPIP assay. (Left) A representative progress curve for 1 μM EsaI reacting with 300 μM SAM and 12 μM 4-oxohexanoyl-ACP. (Right) Plot of initial rate versus EsaI concentrations at fixed 300 μM SAM, 50 μM and100 μM 4-oxohexanoyl-ACP. The reaction rate did not increase when the EsaI concentrations or 4-oxohexanoyl-ACP substrate concentrations increased.

Methylthioadenosine nucleosidase-Xanthine oxidase (MTAN-XO) coupled assay was also tested with EsaI, but collected data was not promising. In MTAN-XO assay, the methylthioadenosine nucleosidase (MTAN) reaction rate is directly dependent on MTA product concentration from AHL synthase reaction. The concentration of MTA from AHL synthase reaction must be low in the beginning, so that the rates for coupling enzymes are lower until MTA concentration reaches steady state levels. Unfortunately, MTA is the common contaminant in commercial SAM. It is possible that the amount of contaminant MTA in SAM had been too high at the beginning, causing difficulty in determining small changes in MTA concentrations in the midst of high background MTA in SAM. Thus, the accurate determination of reaction rate at low amounts of MTA produced from EsaI AHL synthase reaction was impossible.

Due to the limitations of DCPIP assay and MTAN-XO coupled assay discussed above, kinetic data for EsaI substrates were collected using an HPLC method. Lactonization assay and acylation assay using HPLC were another two assays developed to determine the rates of AHL synthesis independently. Lactonization assay follow

production of MTA from SAM substrate, while acylation assay follows production of holo-ACP from acyl-ACP substrate. One of the advantages of HPLC is the assays are not dependent on colorimetric dye or coupling enzyme. Another advantage is that the changes in peak areas give a direct measurement of substrate and product concentrations in the reaction (Figure 19).

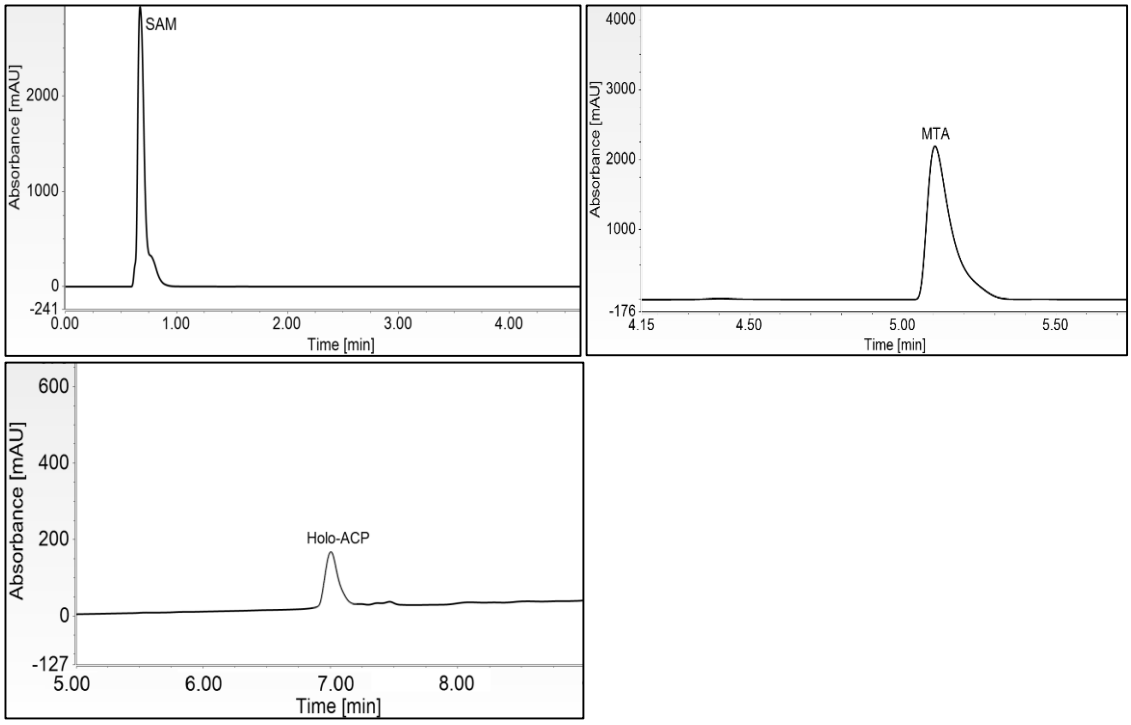

Figure 19. HPLC chromatograms showing retention time of SAM, MTA, and holo-ACP. SAM is eluted at 0.6 minutes; MTA is eluted at 5.05 minutes; holo-ACP is eluted at 6.8 minutes.

MTA and holo-ACP standard curves

To calculate the reaction rate of EsaI synthesis by HPLC assay, standard curves for MTA and holo-ACP products need to be generated (Figure 20). Two HPLC methods were performed to follow small molecules (MTA and SAM) and proteins (holo-ACP and acyl-ACP) independently. MTA peak from SAM lactonization eluted at 5.05 minutes; holo-ACP from acylation half-reaction eluted at 6.8 minutes. Standard calibration curves for

MTA and holo-ACP were generated by plotting serial diluted known analyte concentrations against their respective peak area (Figure 20).

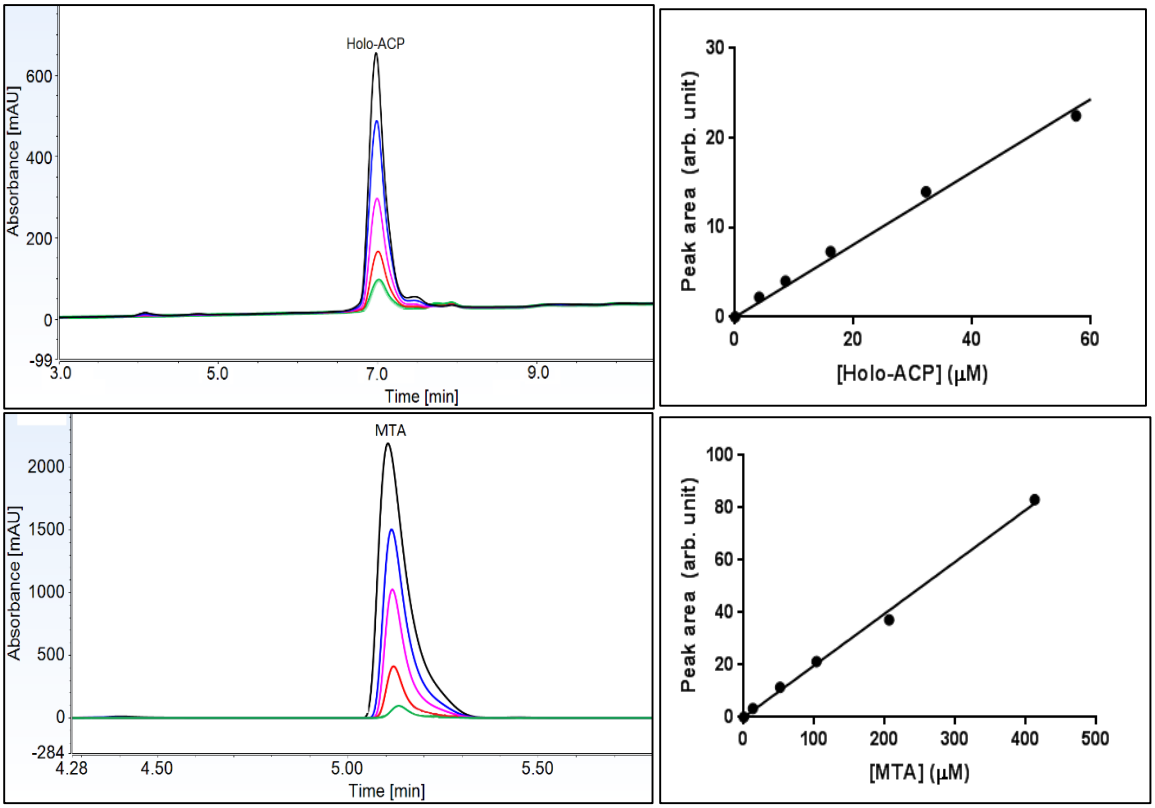

Figure 20. HPLC chromatograms of MTA and holo-ACP in standard calibration curves. MTA peak eluted at 5.05 minutes; holo-ACP eluted at 6.8 minutes. The standard curve of each analyte was generated by plotting serial diluted concentrations of each analyte against their respective peak areas (arbitrary units). MTA was monitored at 260 nm; holo-ACP was monitored at 220 nm.

Lactonization and acylation assay in EsaI-catalyzed reaction

In the EsaI-catalyzed reaction, the formation of MTA and holo-ACP products after quenching the enzyme were measured quantitatively by using the same HPLC methods used to generate the calibration curves. Product formation over a 6 minutes period was linear, indicating that quenching after 4 minutes of incubation with enzyme would be sufficient to determine the initial reaction rate (Figure 21).

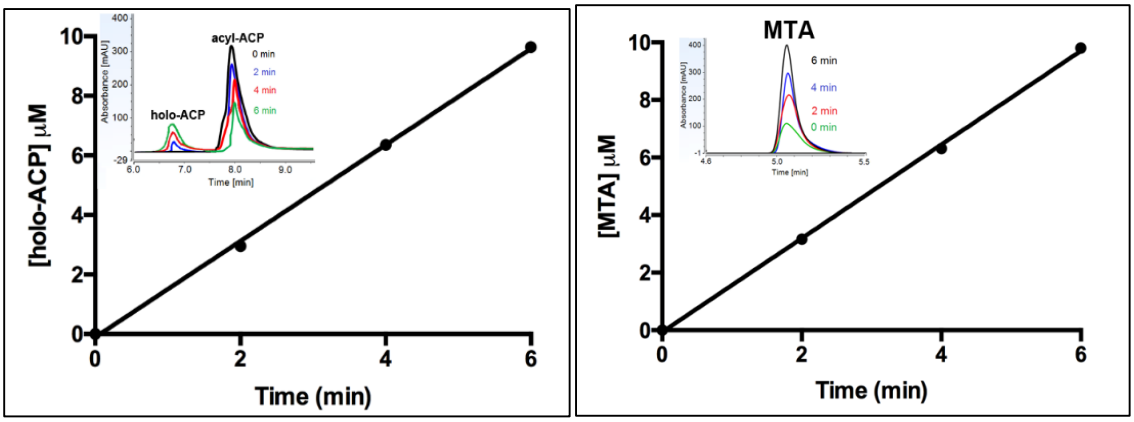

Figure 21. Different quenched time (0, 2, 4, 6 minutes) follwing formation of MTA and holo-ACP in lactonization and acylation half-reactions in EsaI. In the reaction, concentrations of EsaI, SAM, and 2-furoyl-ACP were fixed at 1.3 μM, 500 μM, and 112 μM, respectively. In lactonization, MTA peak at 0 minute corresponded to contaminant MTA in commercially available SAM from Sigma. In acylation, decrease in 2-furoyl-ACP peak area was accompanied by increase in holo-ACP product peak area.

In the lactonization half-reaction, SAM and MTA peaks eluted at 0.6 and 5.0 minutes, respectively (Figure 22). Since MTA is a common contaminant in commercial SAM, the actual amount of MTA produced in the quenched reaction was determined by subtracting the total peak area from the contaminant MTA peak area presented in the background. The MTA concentration produced in the enzymatic reaction was calculated from its respective peak area by using an MTA standard curve. In the acylation half-reaction, holo-ACP and acyl-ACP (2-furanacetyl-ACP in this case) eluted at 6.8 and 7.4 minutes, respectively (Figure 23). The overlaid background and EsaI-catalyzed reaction chromatograms showed that in the presence of EsaI, holo-ACP peak increased while 2-furanacetyl-ACP decreased respectively.

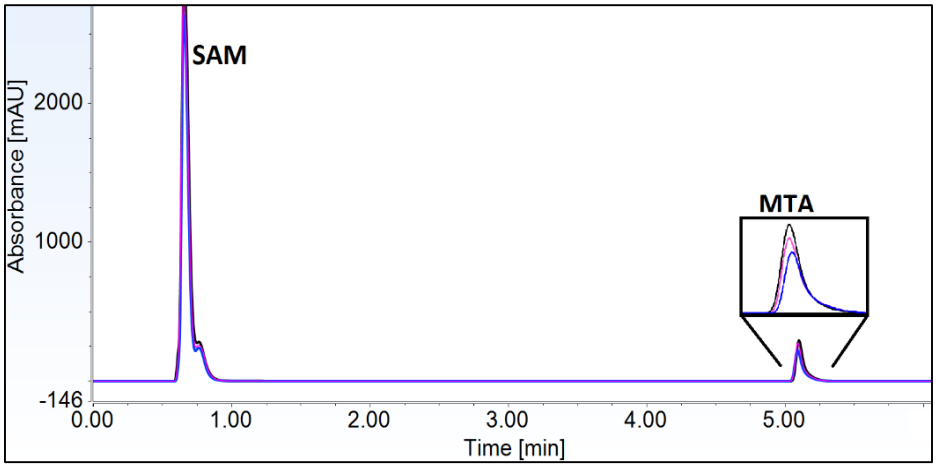

Figure 22. Lactonization assay for EsaI. HPLC chromatogram of MTA product formation in EsaI-catalyzed reaction using 0 µM, 7 µM, and 15µM 2-furanacetyl-ACP substrate concentrations, fixed 500 µM SAM, fixed 1 µM EsaI quenched at 4 minutes with 6 M HCl. SAM eluted at 0.65 minutes; MTA peak from SAM lactonization eluted at 5.05 minutes. The peak areas were reported in arbitrary units. The actual amount of MTA produced in the quenched reaction was determined by subtracting the total peak area from the contaminant MTA peak area presented in the background. The MTA concentration produced in the enzymatic reaction was calculated from its respective peak area by using MTA standard curve.

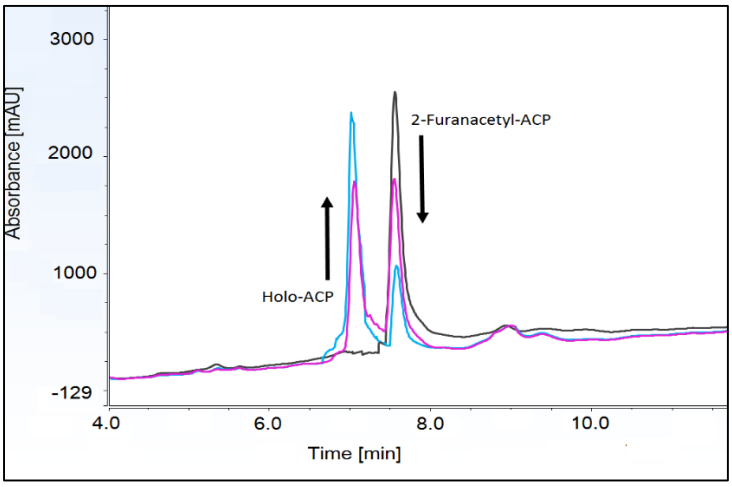

Figure 23. Acylation assay for EsaI. HPLC chromatogram of holo-ACP product formation in EsaI-catalyzed reaction using 80 µM (in blue) and 40 µM (in pink) 2-furanacetyl-ACP substrate concentration, fixed 500 µM SAM, fixed 1 µM EsaI quenched at 4 minutes with 4 M acetate buffer, pH 3.6. Black chromatogram is background with 2-furanacetyl-ACP eluted at 7.4 minutes. Blue and pink chromatograms are EsaI-catalyzed reactions with the appearance of holo-ACP peak at 6.8 minutes. An increase in holo-ACP peak was accompanied with a decrease in 2-furanacetyl-ACP peak area. The peak areas were reported in arbitrary units. The holo-ACP concentration in the quenched reaction mixture was determined from its respective peak area by using holo-ACP standard curve.

Kinetic study of EsaI T140A mutant with C6-ACP

To examine the importance of Thr140 in recognition of 3-oxoC6-ACP substrate in EsaI wild-type, kinetic assays by following lactonization and acylation steps were performed using C6-ACP as the variable substrate. In each kinetic reaction, SAM and EsaI (both wild-type and T140A mutant) were fixed, respectively, at 500 μM and 1 μM. The kinetic constants obtained by following acylation and lactonization assays were comparable (Table 1 and Figure C1). When using EsaI WT with C6-ACP substrate, K_m values for lactonization and acylation were 62.68 ± 9.87 μM and 61.89 ± 7.69 μM, respectively; k_{cat}/K_m value for lactonization and acylation were 0.0082 ± 0.0014 $\mu M^{-1}min^{-1}$ and 0.0083 ± 0.0011 $\mu M^{-1}min^{-1}$. When using EsaI T140A with C6-ACP substrate, K_m values for lactonization and acylation were 3.43 ± 0.52 μM and 3.08 ± 0.33 μM, respectively; k_{cat}/K_m value for lactonization and acylation were 0.445 ± 0.069 $\mu M^{-1}min^{-1}$ and 0.507 ± 0.055 $\mu M^{-1}min^{-1}$. Previously, mass spectrometry study had showed that EsaI T140A mutant lost specificity and produced majority C6-HSL.[26] In this thesis, kinetic studies on T140A with C6-ACP confirmed the earlier observations that the catalytic efficiency of hexanoyl-ACP with T140A mutant was about 57-fold higher than with wild-type EsaI enzyme (Figure 24). The K_m value of WT for C6-ACP was about 19-fold less than that of T140A. The result is reasonable because alanine does not need to form a hydrogen bond with C6-ACP and thus produces high activity with C6-ACP. Therefore, it suggested that Thr140 play an essential role in discriminating 3-oxoacyl-ACP from unsubstituted acyl-ACP substrate in the active site of EsaI.

Table 1. Comparison kinetic parameters of EsaI WT and T140A mutant in the presence of C6-ACP by following lactonization (A) and acylation (B).

(A) Lactonization	K_m (μM)	k_{cat} (min^{-1})	k_{cat}/K_m ($\mu M^{-1}min^{-1}$)
C6-ACP + EsaI T140A	3.43 ± 0.52	1.52 ± 0.06	0.445 ± 0.069
C6-ACP + EsaI WT	62.68 ± 9.87	0.52 ± 0.03	0.0082 ± 0.0014

(B) Acylation	K_m (μM)	k_{cat} (min^{-1})	k_{cat}/K_m ($\mu M^{-1}min^{-1}$)
C6-ACP + EsaI T140A	3.08 ± 0.33	1.56 ± 0.04	0.507 ± 0.055
C6-ACP + EsaI WT	61.89 ± 7.69	0.51 ± 0.02	0.0083 ± 0.0011

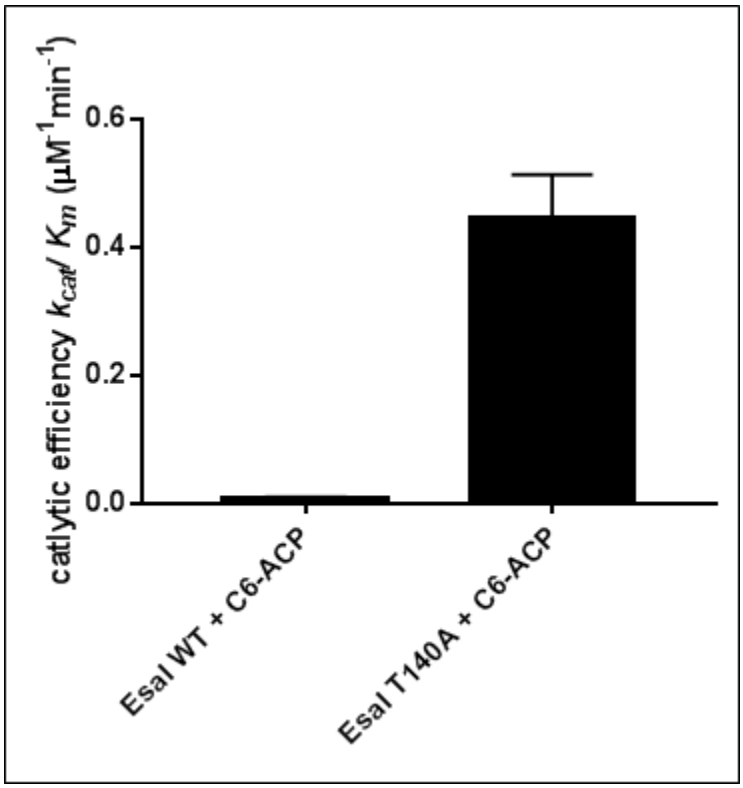

Figure 24. Bar diagram comparing the catalytic efficiencies of hexanoyl-ACP with EsaI WT and T140A mutant. In both reactions, SAM concentration was fixed at 500 μM and EsaI concentration was fixed at 1 μM. K_m (WT + C6-ACP) is 62.68 ± 9.86 μM, k_{cat} is 0.52 ± 0.03 min^{-1}, k_{cat}/K_m is 0.0082 ± 0.0014 $\mu M^{-1}min^{-1}$. K_m (T140A + C6-ACP) is 3.43 ± 0.52 μM, k_{cat} is 1.52 ± 0.06 min^{-1}, k_{cat}/K_m is 0.445 ± 0.069 $\mu M^{-1}min^{-1}$. The catalytic activity of T140A mutant with hexanoyl-ACP was about 57-fold higher than that of wild-type with hexanoyl-ACP.

Determination of kinetic parameters of alternative 3-oxoacyl-ACP substrates in EsaI wild-type study

In this thesis, we were interested in exploring a) the effect of changing the heteroatom (oxygen to sulfur and nitrogen) at the C-3 position, b) methylation of 3-oxoC6-ACP substrate, c) changing the hybridization at C-3, d) changing from straight acyl-chain to aromatic analogs, e) changing the position of the oxygen atom in the acyl-chain, f) changing the acyl-chain length, and g) removal of oxygen atom in the acyl-chain on EsaI activity. The initial rate at each substrate concentration was fitted to the Michaelis-Menten equation to determine kinetic constants (Figures C2 and C3). The K_m, k_{cat}, and k_{cat}/K_m values in lactonization and acylation assay were within error (Table 2). A general trend of K_m and k_{cat} was observed among all alternative substrates: the substrates that carried oxygen at C-3 position had similar range of K_m and k_{cat} values. Besides, when the oxygen atom at C-3 moved to different position (C-2, C-4, and C-5) or was removed or changed to a different heteroatom (nitrogen or sulfur), and acyl chain length changed from 6 carbons to 8 carbons, K_m increased and k_{cat} decreased. The true understanding of this variation in activity is understood when comparing catalytic efficiencies (k_{cat}/K_m) of alternative substrates all together. Figure 25 summarizes the trend of catalytic efficiency of all substrates with EsaI enzyme.

Table 2. Determination of K_m, k_{cat}, k_{cat}/K_m of alternative 3-oxoacyl-ACP substrates on EsaI activity by following (A) lactonization and (B) acylation reactions.

(A) Lactonization	K_m (μM)	k_{cat} (min^{-1})	k_{cat}/K_m ($\mu M^{-1}min^{-1}$)	% activity [a]
2-Furanacetyl-ACP (1)	10.56 ± 1.03	3.49 ± 0.10	0.330 ± 0.034	100.00
2,2′-Dimethyl-3-oxoC6-ACP (8)	7.63 ± 1.34	2.35 ± 0.10	0.308 ± 0.055	93.33
2-Tetrahydrofuranacetyl-ACP (2)	11.12 ± 0.99	2.90 ± 0.07	0.261 ± 0.024	79.09
2-Thiopheneacetyl-ACP (3)	4.34 ± 1.82	0.76 ± 0.15	0.174 ± 0.080	52.73
2-Pyridylacetyl-ACP (4)	9.15 ± 1.54	1.02 ± 0.04	0.112 ± 0.019	33.94
5-oxoC6-ACP (7)	19.61 ± 2.74	2.11 ± 0.09	0.107 ± 0.016	32.42
2-Furoyl-ACP (5)	16.14 ± 2.64	1.43 ± 0.03	0.088 ± 0.015	26.67
4-oxoC6-ACP (6)	23.56 ± 3.55	0.97 ± 0.05	0.041 ± 0.007	12.42
5-oxoC8-ACP (11)	39.76 ± 7.56	0.61 ± 0.04	0.015 ± 0.003	4.55
C6-ACP (9)	62.68 ± 9.86	0.52 ± 0.03	0.0082 ± 0.0014	2.48
4-oxoC8-ACP (10)	47.16 ± 7.06	0.37 ± 0.02	0.0078 ± 0.0012	2.36
C8-ACP (12)	101.50 ± 17.54	0.22 ± 0.02	0.0021 ± 0.0004	0.64
2-Benzofuranacetyl-ACP (13)	16.18 ± 2.24	0.84 ± 0.02	0.0516 ± 0.0073	15.64

[a] % activity = $\frac{k_{cat}/K_m}{0.330} \times 100$

(B) Acylation	K_m	k_{cat}	k_{cat}/K_m	% activity [a]
	(μM)	(min^{-1})	(μM^{-1} min^{-1})	
2-Furanacetyl-ACP (1)	10.83 ± 1.42	3.99 ± 0.14	0.368 ± 0.050	100.00
2,2′-Dimethyl-3-oxoC6-ACP (8)	7.65 ± 1.12	2.30 ± 0.08	0.301 ± 0.045	81.79
2-Tetrahydrofuranacetyl-ACP (2)	11.57 ± 1.51	3.07 ± 0.12	0.266 ± 0.036	72.28
2-Thiopheneacetyl-ACP (3)	4.33 ± 1.52	1.06 ± 0.17	0.244 ± 0.095	66.30
2-Pyridylacetyl-ACP (4)	9.42 ± 0.67	1.08 ± 0.02	0.115 ± 0.008	31.25
5-oxoC6-ACP (7)	18.74 ± 1.89	2.10 ± 0.07	0.112 ± 0.012	30.43
2-Furoyl-ACP (5)	15.39 ± 3.24	1.51 ± 0.10	0.098 ± 0.022	26.63
4-oxoC6-ACP (6)	22.24 ± 5.02	1.11 ± 0.09	0.049 ± 0.012	13.32
5-oxoC8-ACP (11)	38.29 ± 5.52	0.62 ± 0.03	0.016 ± 0.002	4.35
4-oxoC8-ACP (10)	50.23 ± 6.88	0.44 ± 0.02	0.0088 ± 0.0013	2.39
C6-ACP (9)	61.89 ± 7.69	0.51 ± 0.02	0.0083 ± 0.0011	2.26
C8-ACP (12)	102.40 ± 13.05	0.25 ± 0.01	0.0025 ± 0.0003	0.68
2-Benzofuranacetyl-ACP (13)	16.59 ± 1.877	0.84 ± 0.02	0.0505 ± 0.0058	13.73

[a] % activity = $\frac{k_{cat}/K_m}{0.368} \times 100$

Table 3. Effect of 2-thiopheneacetyl-ACP when SAM is fixed on EsaI activity.

Fixed S	Variable S	K_m (μM)	k_{cat} (min^{-1})	k_{cat}/K_m ($\mu M^{-1}min^{-1}$)	K_i (μM)
50 μM SAM	2-Thiopheneacetyl-ACP	6.48 ± 1.81	0.68 ± 0.10	0.105 ± 0.033	74.41 ± 28.72
500 μM SAM	2-Thiopheneacetyl-ACP	4.34 ± 1.82	0.76 ± 0.15	0.174 ± 0.080	100.6 ± 54.57

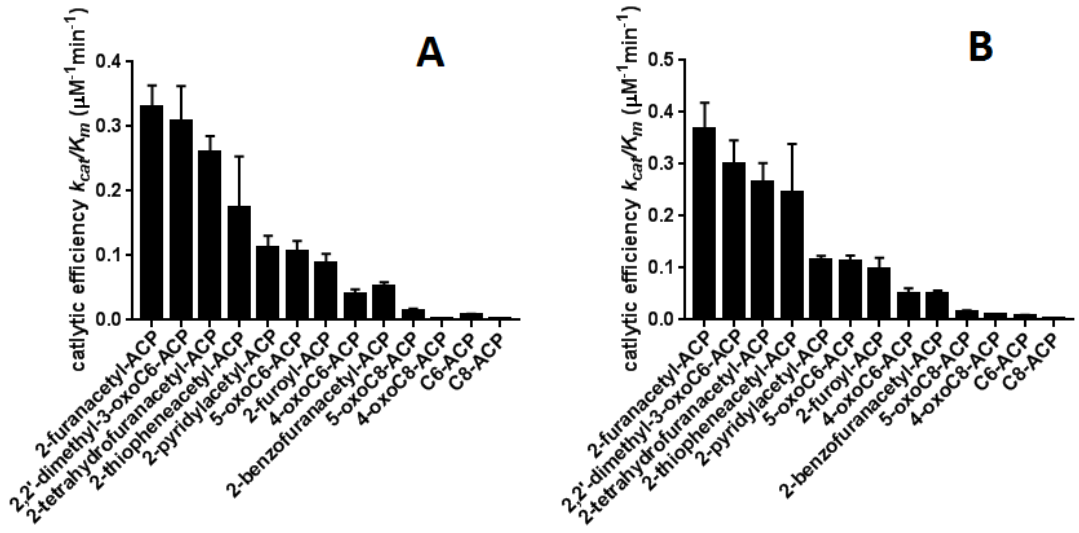

Figure 25. Comparison of catalytic efficiency of the alternative 3-oxoacyl-ACP substrates for EsaI by following Lactonization assay (A) and Acylation assay (B). 2-Furanacetyl-ACP with sp^2 hybridized carbon at C-3 showed the highest catalytic efficiency among all of the tested substrates with EsaI. The second-best substrate was 2,2′-dimethyl-3-oxohexanoyl-ACP. The activity decreased as the hybridization of C-3 converted to sp^3, the change of oxygen atom to sulfur and nitrogen atom, removal of oxygen atom and the change of length in acyl-chain from six carbons to eight carbons.

Among all of the substrates, 2-furanacetyl-ACP showed the highest catalytic efficiency ($0.330 \pm 0.034\ \mu M^{-1}min^{-1}$). 2-Furanacetyl-ACP, 2,2′-dimethyl-3-oxoC6-ACP, and 2-tetrahydrofuranacetyl-ACP substrates all had an oxygen atom at C-3 and 6 carbons in acyl chain. Both 2-furanacetyl-ACP and 2,2′-dimethyl-3-oxoC6-ACP are sp^2 hybridized at C-3 while 2-tetrahydrofuranacetyl-ACP is sp^3 hybridized at C-3. The 2,2′-dimethyl-3-oxoC6-ACP resembles the native 3-oxoC6-ACP substrate of EsaI, except that this substrate has two methyl groups at the C-2 instead of two hydrogens. The catalytic efficiency of 2,2′-dimethyl-3-oxoC6-ACP was relatively close to that of 2-furanacetyl-ACP, indicating that the two methyl groups at C-2 did not introduce steric hindrance in acyl-chain binding site of EsaI.

Notably, the oxygen of 2-furanacetyl-ACP substrate has two lone pairs of electrons: one must involve in part of the π-conjugated system (*p* orbitals); the other is in sp^2 orbital and must involve in hydrogen bonding with Thr140. One of the hypotheses was that if the lone pair of electrons involved in aromaticity of the ring had been positioned in a way to also form hydrogen bond with Thr140 in the active site of EsaI, 2-furanacetyl-ACP would have been a poorer substrate. The kinetic data showed that 2-furanacetyl-ACP had the highest catalytic efficiency among all alternative substrates, suggesting that the lone pair of electrons involved in aromaticity did not affect the hydrogen bonding of the other lone pair with Thr140. The protein structure with the substrate bound has not yet been studied, the possibility of the substrate binding resulted in enzyme's conformational change still cannot be neglected. It may be possible that the aromatic ring of the substrate directed itself to a new binding site and oxygen atom in the ring is no longer in close proximity to Thr140 to establish hydrogen bond. Yet, in turn, the enzyme conformational change was induced by this new interaction might result in a different hydrogen bond acceptor residue closer to Thr140.

Additionally, even though K_m and k_{cat} were somewhat similar between 2-furanacetyl-ACP and 2-tetrahydrofuranacetyl-ACP, the catalytic efficiencies (k_{cat}/K_m) showed that the activity of 2-tetrahydrofuranacetyl-ACP was about 21-28 % less than that of 2-furanacetyl-ACP. There was no significant change in substrate activity between sp^2 and sp^3 of carbon at C-3 position. This suggests that the effect of changing the hybridization of the carbon at the C-3 position on EsaI activity is subtle.

Moreover, when the oxygen atom at C-3 was changed to nitrogen and sulfur in 2-pyridylacetyl-ACP and 2-thiopheneacetyl-ACP substrates, respectively, the catalytic

activity of these two substrates dropped significantly. Comparing 2-pyridylacetyl-ACP to 2-furanacetyl-ACP, the lone pair of electrons of nitrogen is not part of the aromatic ring and can serve either as hydrogen bond acceptor or donor. Although K_m of 2-furanacetyl-ACP and 2-pyridylacetyl-ACP were somewhat similar, k_{cat}/K_m value showed that 2-pyridylacetyl-ACP is less favorable than 2-furanacetyl-ACP when bound to EsaI. One of the possibility for the lower catalytic efficiency observed in 2-pyridylacetyl-ACP is because the binding of a larger 6-membered ring in 2-pyridylacetyl-ACP might induce enzyme's conformational change and cause the necessary reorientation of catalytic residues in the enzyme active site for the reaction to occur, which then results in reduction of enzyme catalysis.

Like 2-furanacetyl-ACP, the sulfur atom in 2-thiopheneacetyl-ACP has two lone pairs of electrons of which one should be involved in aromaticity and the other capable of forming a hydrogen bond with Thr140. However, since the electronegativity of oxygen (3.44) is higher than that of sulfur (2.58), hydrogen bonds to sulfur may be weaker than those to oxygen.[59] Interestingly, among all alternative substrates, 2-thiopheneacetyl-ACP has the lowest K_m and also showed substrate inhibition when the concentrations of 2-thiopheneacetyl-ACP were varied and concentration of SAM was fixed (Figure C2, C3, C6). Also, Table 3 summarizes kinetic parameters when SAM concentrations were fixed at 50 μM and 500 μM. The inhibition constant K_i value when fixed SAM at 500 μM (100.6 ± 54.57 μM) was compared to K_i value when fixed SAM at 50 μM (74.41 ± 28.72 μM). Substrate inhibition was observed in both of the cases and had similar K_i values.

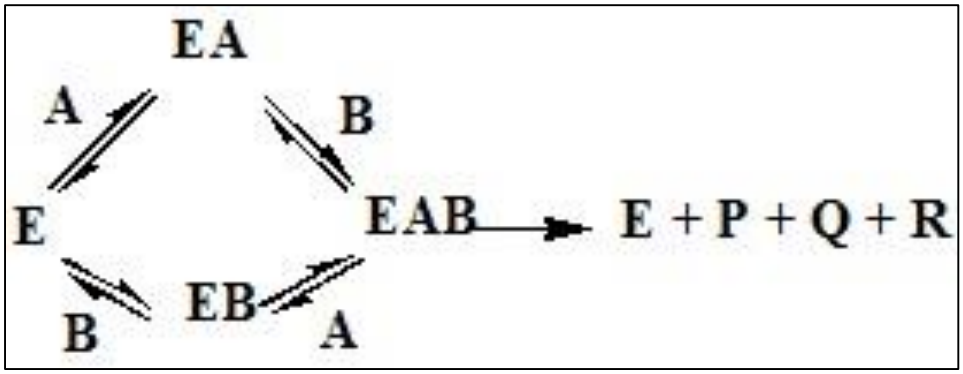

Figure 26. Random sequential mechanism. In this diagram, E is free enzyme; A is 2-thiopheneacetyl-ACP; B is SAM. EA is [E.2-thiopheneacetyl-ACP] complex where 2-thiopheneacetyl-ACP binds first and follows a productive pathway. EB is [E.SAM] complex where SAM binds first and follow a non-productive pathway. EAB is [E.2-thiopheneacetyl-ACP.SAM] ternary complex. P, R, and Q are products released from this mechanism.

Additionally, K_m of SAM when fixed 2-furanacetyl-ACP (111.3 ± 10.7 μM) was determined and compared to K_m of SAM when fixed 2-thiopheneacetyl-ACP (36.09 ± 4.69 μM) (Figure C7). The k_{cat} for fixed concentrations of 2-thiopheneacetyl-ACP with variable concentration of SAM (0.796 ± 0.029 min^{-1}) is 5-fold lower than that for fixed concentrations of 2-furanacetyl-ACP (3.64 ± 0.09 min^{-1}). However, the k_{cat}/K_m for fixed 2-thiopheneacetyl-ACP (0.0221 ± 0.0029 $\mu M^{-1}min^{-1}$) is almost similar to that for fixed 2-furanacetyl-ACP (0.0327 ± 0.0032 $\mu M^{-1}min^{-1}$). Both 2-thiopheneacetyl-ACP and 2-furanacetyl-ACP showed normal hyperbolic curves when SAM was the variable substrate. This data together with substrate inhibition data observed when fixed SAM suggest that all available free enzyme (E) favored the formation of stable EA ([E.2-thiopheneacetyl-ACP] or [E.2-furanacetyl-ACP]) complex, resulting in the binding of SAM to EA to drive the formation of productive EAB ([E.2-thiophenacetyl-ACP.SAM] or [E.2-furanacetyl-ACP.SAM]) ternary complex (Figure 26).

Further experiments will be needed to understand the binding mechanism of 2-thiopheneacetyl-ACP to EsaI. Yet, this observation might suggest a possibility that the substrate addition could have occurred through a random sequential mechanism where one pathway was more productive over the other (Figure 26). Assuming, in the productive pathway, 2-thiopheneacetyl-ACP (A) binds to free enzyme (E) first followed by SAM (B) forming the [E.2-thiopheneacetyl-ACP.SAM] complex (EAB); whereas, in the nonproductive pathway, 2-thiopheneacetyl-ACP binds to [E.SAM] complex and form [E.SAM.2-thiopheneacetyl-ACP] complex. At low concentration of 2-thiopheneacetyl-ACP, free enzyme E can bind to 2-thiophenacetyl-ACP (A) and form a stable EA complex; whereas E binds to SAM (B) to form an unstable EB complex and converted back to E. Most of available E form will bind to A to populate the productive EAB pathway. However, when there is too much A around, it can also bind to the unstable EB complex; thus, the nonproductive pathway would now compete with the productive pathway and result in a lower turnover number (k_{cat}) and decreased the reaction rate.

On the other hands, if acyl-ACP (A) is a poorer substrate, EA complex will be less stable and convert back to free E form at low acyl-ACP concentrations, resulting in the binding of SAM (B) to E to form EB complex. Successive addition of A drives the formation of [E.SAM.acyl-ACP] ternary complex (EBA). The accumulation of nonproductive EBA complex results in a lag phase. Once the concentration of A is high enough, the chance for it to bind to E increases and drives the reaction towards the productive [E.acyl-ACP.SAM] ternary complex (EAB). Hence, sigmoidal curve will be observed.

Furthermore, the C-S bond length in the thiophene ring (1.71 Å) is particularly longer than the C-O bond length in the furan ring (1.36 Å).[60] It can also be possible that the sulfur atom in thiophene found a new binding site in the enzyme active site, causing it to position away from Thr140 and interact with a different hydrogen bond acceptor residue to establish a new hydrogen bond network with Thr140. The enzyme conformational change induced by the interaction between 2-thiopheneacetyl-ACP substrate and the active site residues may result in such a favorable conformation that keeps the substrate occupied in the active site. Thus, an increase in 2-thiopheneacetyl-ACP concentration beyond saturation would force another 2-thiopheneacetyl-ACP to bind to an allosteric site, resulting in inhibition of the enzyme's activity.

Thirdly, the position of the oxygen atom along the acyl-chain was taken in consideration to see how it might affect the hydrogen bonding ability of the substrate to Thr140. Interestingly, k_{cat}/K_m value of 4-oxoC6-ACP (0.041 ± 0.007 $\mu M^{-1}min^{-1}$) was significantly lower than that of 5-oxoC6-ACP (0.107 ± 0.016 $\mu M^{-1}min^{-1}$) and 2-furoyl-ACP (0.088 ± 0.015 $\mu M^{-1}min^{-1}$). The catalytic efficiency of 2-furoyl-ACP was about 1.2-fold less than that of 5-oxoC6-ACP; and, the catalytic efficiency of 4-oxoC6-ACP was about 3-fold less than 5-oxoC6-ACP. The crystal structure of EsaI showed that the oxygen at C-3 in 3-oxohexanoyl-phosphopantetheine substrate formed a hydrogen bond to Thr140. Thus, in order to establish hydrogen bond to Thr140, the distance from the oxygen at C-2, C-4, and C-5 must also be in close proximity. The reason of higher relative catalytic efficiency in 5-oxoC6-ACP compared to 2-furoyl-ACP and 4-oxoC6-ACP may be because the oxygen at C-5 is in the same face with C-3 and was locked in a position where it may be able to establish hydrogen bond network with Thr140. In contrast, the

direction of oxygen at C-2 and C-4 is opposite to C-3 and C-5. Although the acyl chain of the two substrates (4-oxoC6-ACP and 2-furoyl-ACP) have the ability of free rotation, the kinetic data suggested the conformation of enzyme may restrict free rotation of the acyl-chain in 4-oxoC6-ACP and 2-furoyl-ACP, causing the oxygen to point away from Thr140 and reduce the turnover rate of the substrates.

In the crystal structure of EsaI, the V-cleft acyl-chain binding pocket of EsaI was in enclosed form and suggested that the length of acyl-chain was limited to 6 carbons. In this thesis, how alternative substrate activity change with acyl-chain length was also examined experimentally. 2-Benzofuranacetyl-ACP is a derivative of 2-furanacetyl-ACP with 8 carbons instead of 6 carbons. Although 2-benzofuranacetyl-ACP substrate retained some activity (15 % activity), the catalytic efficiency of 2-benzofuranacetyl-ACP had a 7-fold decrease compared to 2-furanacetyl-ACP. The decrease in catalytic efficiency for 2-benzofuranacetyl-ACP can possibly be attributed to the bulkiness of the two fused rings of the substrate, causing a hard time for the interaction between the enzyme and substrate to successfully lock in a productive conformation that is conducive for catalysis. Additionally, 5-oxoC8-ACP and 4-oxoC8-ACP substrates were also examined and compared to 5-oxoC6-ACP and 4-oxoC6-ACP. The 4-oxoC6-ACP had 5-fold higher activity than that of 4-oxoC8-ACP. Similarly, the 5-oxoC6-ACP had about 6.6-fold higher activity than that of 5-oxoC8-ACP. The kinetic data suggested that the acyl-chain binding pocket of EsaI can use alternative 3-oxoacyl-ACP substrates of length consisting of up to, but not exceeding 6 carbons.

Last but not least, the kinetic study of EsaI wild-type with unsubstituted C6-ACP and C8-ACP substrates showed that the activity of C6-ACP dropped down to 2.26 – 2.48

% compared to the highest activity substrate, 2-furanacetyl-ACP. Also, C8-ACP had the lowest catalytic efficiency (less than 1 %) compared to 2-furanacetyl-ACP. Again, the data suggested that the presence of a heteroatom in the acyl-chain (preferably at the C-3 position) plays an essential role in maintaining the activity of EsaI. Also, chain length greater than 6 carbons severely damaged the activity of EsaI.

CHAPTER THREE: INVESTIGATION OF ALTERNATIVE SUBSTRATES FOR YspI

Introduction

Overview human pathogen *Yersinia pestis*

Yersinia pestis, *Yersinia pseudotuberculosis* and *Yersinia enterocolitica* are three pathogenic species in the genus *Yersinia*. *Y. pseudotuberculosis* causes Far East scarlet-like fever in humans, who occasionally get infected zoonotically, most often through the food-borne route. *Y. enterocolitica* causes enterocolitis, which is an inflammation of the small intestine and colon in young children. *Y. pestis* causes bubonic plague in humans, which is one of the deadliest diseases. From analyses of DNA sequences of multiple housekeeping genes, *Y. pseudotuberculosis*-*Y. pestis* evolutionary linkage diverged from *Y. enterocolitica* between 41 and 186 million years ago, while *Y. pestis* diverged from *Y. pseudotuberculosis* within the last 1,500 – 20,000 years ago.[61-63] By Darwinian adaptive evolution, *Y. pestis* evolved from *Y. pseudotuberculosis* into a newly emerged pathogen that is not only able to parasitize insects in part of its life cycle but also highly virulent to rodents and humans, causing pandemics of a systemic and fatal disease. Three adaptive evolution mechanisms involved to gain more pathogenic phenotypes in *Y. pestis* were (1) the horizontal acquisition of genes encoding specific virulence determinants ("gain-of-function" mechanism), (2) an appropriate functional inactivation or loss of preexisting genetic materials ("loss-of-function" mechanism), (3) laterally acquired virulence genes either with or without their own specific regulators, which evolve to

being integrated into the host's regulatory cascades to coordinate expression of virulence factors within global gene regulatory networks for maintaining homeostasis through the infectious life cycle ("regulation-remodeling" mechanism).[61,63]

Plague is primarily a zoonotic disease between mammals by fleas. When a flea bites an infected rodent, *Y. pestis* is ingested with the blood meal. Human usually get plague after being bitten by a rodent flea that is carrying *Y. pestis* or by handling an animal infected with plague.[61-63] *Y. pestis* are subdivided into three biovars (Antiqua, Medievalis, and Orientalis).[61] The biovar Antiqua imported from Africa caused the first pandemic, Justinian's plague, 541-767 AD. The biovar Medievalis imported from central Asia caused the second pandemic, the Black Death from 1346 to the early 19th century. The biovar Orientalis imported from China and via marine shipping from Hong Kong caused the third pandemic in the mid- 19th century and the majority of modern outbreaks of plague. One of the most recent cases was reported in July 2016 in southwestern Idaho. Out of twelve cats who got sick, six of them were infected with plague due to contact with infected squirrels and other wild rodents or rabbits.

AHL-Synthase in *Yersinia pestis:* YspI

Yersinia pestis reproduces and causes blockage in a muscular valve in the gut of the flea by forming a biofilm.[49] The biofilm blocks the passage between the esophagus and the rest of the gut, inhibiting any blood from entering the stomach cavity after intake of blood meals from humans. As a result, infected fleas must feed repeatedly, and each successive feeding attempt helps transmit the bacterium to more hosts. Studies have identified that *Y. pestis* have two types of quorum sensing systems: LuxS makes AI-2 signal molecules and two LuxI/LuxR systems make four different AHL molecules (3-

oxohexanoyl-homoserine lactone, 3-oxooctanoyl-homoserine lactone, hexanoyl-homoserine lactone, and octanoyl-homoserine lactone).[64-66] The two LuxI/LuxR systems in *Y. pestis* are YspI/R and YpeI/R.[65-67] The genome sequence of *Y. pestis* suggests that *yspI* and *ypeI* genes encoding LuxI AHL-synthases have very similar structure.[63,65-67] Analysis of the recombinant YspI and wild-type *Y. pestis* by liquid chromatography-tandem mass spectrometry indicated that YspI AHL-synthase produces 3-oxohexanoyl-homoserine lactone (39%) and 3-oxooctanoyl-homoserine lactone (53%) predominantly.[66] AHL-bioassay study showed that YpeI AHL-synthase is responsible for octanoyl-homoserine lactone (C8-HSL) synthesis.[67-69] The role of YpeI AHL-synthase in AHL production needs further investigation.

Substrate Design

To design quorum sensing inhibitors for YspI, the enzyme needs to be characterized first. Similar to EsaI, the obstacle in studying YspI is that the native 3-oxooctanoyl-ACP substrate is not stable *in vitro.* Since the crystal structure of YspI is unknown, the recognition of YspI towards 3-oxoacyl-ACPs needs to be elucidated. Even though mass spectrometry study showed that YspI produced majority of 3-oxooctanoyl-HSL (53 %) and 3-oxohexanoyl-HSL (39 %), the importance of hybridization at C-3 position and position of oxygen atom have remained unclear. One of the objectives in this thesis is to design, synthesize, and analyze substrate analogues that have high activity with YspI so that it can serve as the foundation in understanding chemistry behind YspI signal synthesis mechanism.

Besides the alternative substrates listed in Figure 9, a few more substrates have been developed to study with YspI (Figure 27). These substrates are slightly larger in the

molecular size compared to EsaI substrates shown in Figure 9, designed to occupy YspI's deeper acyl-chain binding pocket. 2,2′-Dimethyl-3-oxooctanoyl-ACP **(14)** is methylated at the α- position to keep the substrate from deprotonation at C-2 and also mimic the native substrate 3-oxooctanoyl-ACP. Decanoyl-ACP **(15)** has 10 carbons in the acyl-chain length and does not have an oxygen atom at the C-3 position.

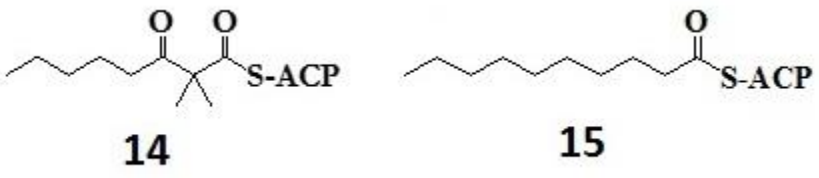

Figure 27. Structures of alternative substrates for YspI.

The reaction rate for each substrate with YspI can be determined directly and independently using HPLC from product concentration of each half-reaction, lactonization and acylation.

Materials and Methods

General

All chemical reagents and solvents were purchased from Sigma Aldrich and used without further purification. C10-CoA was purchased from Sigma Aldrich. Amylose resin was purchased from New England Biolabs, Inc. Silica gel 230-400 mesh from Fisher was used for flash column chromatography. A Thermo Scientific Evolution 260 Bio UV-Vis spectrophotometer was used to measure concentration of analytes. HPLC data was analyzed by Chromeleon 7.2 software on a Thermo Scientific Dionex UltiMate-3000 HPLC system. Thermo Scientific Hypersil Gold C18 reverse-phase analytical UHPLC column (25002-054630) and preparative HPLC column (25005-159070) were used in acyl-ACP and acyl-CoA syntheses, respectively. Deuterated chloroform solvent

was obtained commercially through Cambridge Isotope Laboratories, Inc. NMR spectra were recorded at 298 K using BRUKER AVANCE III 300 MHz and 600 MHz spectrometers. Chemical shifts for ^{1}H NMR and ^{13}C NMR spectra were expressed in parts per million (ppm) and referenced to residual $CHCl_3$ in $CDCl_3$.

YspI Growth, Expression, and Purification

YspI strain was expressed in *E. coli* strain BL21 (DE3) competent cells. The recombinant YspI was grown in LB media containing 50 μg/mL streptomycin and 50 μg/mL spectinomycin at 37 °C to an OD_{600} of 0.6-0.8. Expression was induced by addition of 0.5 mM isopropyl-β-D-1-thiogalactopyranoside (IPTG) at room temperature. After overnight, the growth cultures were centrifuged to pellet at 5000 xg at 4 °C for 10 minutes and stored at -20 °C prior to lysis. The cell pellets were thawed on ice for 30-60 minutes before lysis. The cell pellets were suspended in chilled lysis buffer, containing 50 mM Tris-HCl pH 7.5, 200 mM NaCl, 5 mM DTT, and 1 mM PMSF, with ratio of cell wet weight to buffer volume of 1:1. The cell suspension was cooled on ice for 10 minutes and then sonicated with 10 short bursts of 10 seconds followed by intervals of 30 seconds for cooling. After that, cell debris was removed by centrifugation at 4 °C for 30 minutes at 20,000 xg. Amylose affinity chromatography column was used to purify the protein. The amylose column was first equilibrated with YspI Buffer A (50 mM Tris-HCl pH 7.5, 0.2 M NaCl, 0.1 mM EDTA, 0.1 mM PMSF, 0.1 mM tosyl-L-lysinechloromethyl ketone hydrochloride, 0.4 M sucrose, and 2.5 % (v/v) glycerol). The clear supernatant was loaded onto the equilibrated column to allow the protein of interest to bind to the resin. The column was then washed with YspI Buffer A. The YspI protein was eluted using 35 mL of YspI Buffer A containing 10 mM maltose. The presence and purity of YspI with

maltose binding protein (MBP) was confirmed by SDS-PAGE gel analysis. Concentration of YspI was determined via UV-Vis (ε_{280} = 103710 $M^{-1}cm^{-1}$).

Synthesis of hexyl-Meldrum's acid (14-meldrum's acid)[70]

To a solution of hexanoic acid (0.54 mL, 4.31 mmol) in dry dichloromethane (25 mL), DMAP (0.55 g, 4.52 mmol), DCC (0.98 g, 4.73 mmol), and Meldrum's acid (0.62 g, 4.31 mmol) were added and stirred overnight at room temperature. The cloudy reaction solution was filtered, concentrated under reduced pressure, and redissolved in ethyl acetate. The dissolved solution was washed with 2N HCl, $NaHCO_3$, and brine solutions. The organic layer was dried with anhydrous $MgSO_4$, filtered, and concentrated under reduced pressure to give hexyl-Meldrum's acid product as yellow-brownish oil (0.29 g, 1.19 mmol, 28% yield). ^{1}H NMR (300 MHz, $CDCl_3$) δ 15.27 (s, 1H), 3.04 (t, *J* = 7.5 Hz, 2H), 1.71 (s, 6H), 1.64 (quint, *J* = 3.6 Hz, 2H), 1.40 – 1.32 (m, 4H), 0.88 (t, *J* = 7.0 Hz, 3H).

Synthesis of methyl-3-oxooctanoate (14-ester)[71]

A solution of hexyl-Meldrum's acid (0.29 g, 1.19 mmol) in methanol (15 mL) was refluxed overnight at 65 °C. The solvent was removed under reduced pressure. The residue was purified using silica gel column chromatography (1:1 hexane/ethyl acetate) to give methyl-3-oxooctanoate as yellow liquid (0.15 g, 0.87 mmol, 75% yield). ^{1}H NMR (300 MHz, $CDCl_3$) δ 3.72 (s, 3H), 3.43 (s, 2H), 2.51 (t, *J* = 7.4 Hz, 2H), 1.62 – 1.53 (m, 2H), 1.31 – 1.24 (m, 4H), 0.86 (t, *J* = 6.8 Hz, 3H). ^{13}C NMR (300 MHz, $CDCl_3$) δ 203.1, 167.9, 52.5, 49.2, 43.3, 31.4, 23.4, 22.6, 14.1.

Synthesis of methyl-2,2′-dimethyl-3-oxooctanoate (14-dimethylated)[49,50]

To a reaction flask under nitrogen atmosphere, one equivalent of NaH 60% in mineral oil (0.166 g, 4.15 mmol) and dry THF (50 mL) were added. The mixture solution was refluxing while methyl-3-oxooctanoate (0.714 g, 4.15 mmol) was adding dropwise. Then, one equivalent of methyl iodide (0.209 mL, 4.15 mmol) was added dropwise into the reaction solution. The reaction was refluxed overnight at 70 °C in mineral oil bath. Next day, the second equivalent of NaH 60% in mineral oil and methyl iodide were added into the same reaction flask and stirred overnight. The completion of reaction was checked using TLC (5% ethyl acetate: 95% hexane). Under nitrogen atmosphere, saturated ammonium chloride solution was added dropwise until all white precipitate dissolved. The product mixture was extracted with dichloromethane (3 x 70 mL). The organic layer was dried with anhydrous sodium sulfate, filtered, and concentrated under reduced pressure. The residue was purified by silica gel column chromatography (99:1 hexane/ethyl acetate) to give methyl-2,2′-dimethyl-3-oxooctanoate as white solid (0.6 g, 3.0 mmol, 72 % yield). ^{1}H NMR (600 MHz, $CDCl_3$) δ 3.69 (s, 3H), 2.40 (t, J = 7.3 Hz, 2H), 1.54 – 1.49 (m, 2H), 1.34 (s, 6H), 1.25 – 1.23 (m, 2H), 1.23 – 1.18 (m, 2H), 0.86 (t, J = 7.2 Hz, 3H). ^{13}C NMR (600 MHz, $CDCl_3$) δ 208.3, 174.5, 55.8, 52.6, 38.1, 31.5, 23.7, 22.7, 22.2, 14.1.

Synthesis of 2,2′-dimethyl-3-oxooctanoic acid (14-acid)[51]

To a solution of 1 N NaOH (4.3 mL), methyl-2,2′-dimethyl- 3-oxooctanoate (0.6 g, 3.0 mmol) was added and stirred overnight. The reaction mixture was then washed twice with ethyl acetate (2 x 8 mL). The organic layer was collected and cooled on ice. 2N HCl solution was added into the cool aqueous solution until the clear solution turned

cloudy or pH 2-3. The cloudy solution was extracted with petroleum ether. The organic layer from extraction was dried under reduced pressure to afford the dried 2,2′-dimethyl-3-oxooctanoic acid product as white solid (0.54 g, 2.9 mmol, 97 % yield). ^{1}H NMR (600 MHz, $CDCl_3$) δ 2.51 (t, *J* = 7.3 Hz, 2H), 1.57 (quint, *J* = 7.4 Hz, 2H), 1.39 (s, 6H), 1.31 – 1.22 (m, 4H), 0.86 (t, *J* = 7.2 Hz, 3H). ^{13}C NMR (600MHz, $CDCl_3$) δ 208.4, 178.9, 55.6, 38.2, 31.5, 23.7, 22.7, 22.3, 14.1.

Synthesis of 2,2′-dimethyl-3-oxooctanoyl-succinimide ester (14-succ)

To a solution of 2,2′-dimethyl-3-oxooctanoic acid (0.027 g, 0.15 mmol) in 1,4-dioxane (3 mL), *N*-hydroxysuccinimide (0.017 g, 0.15 mmol) and *N,N′*-dicyclohexylcarbodiimide (0.031 g, 0.15 mmol) were added and stirred for 24 hours. Diethyl ether (2 mL) was added to the reaction mixture, and then the white cloudy solution was filtered and concentrated under reduced pressure. Warm methanol (3 mL) was added quickly into the residue to precipitate out urea by-product and then concentrated under reduced pressure. Cold 1,4-dioxane was added to the residue to repeat the removal of urea and then concentrated under reduced pressure. The residue was purified by column chromatography (hexane/ethyl acetate) to give 2,2′-dimethyl-3-oxooctanoyl-succinimide ester product as clear solid (0.035 g, 0.12 mmol, 83% yield). ^{1}H NMR (600 MHz, $CDCl_3$) δ 2.81 (s, 4H), 2.65 (t, *J* = 7.3 Hz, 2H), 1.59 (quint, *J* = 7.4 Hz, 2H), 1.48 (s, 6H), 1.30 – 1.25 (m, 4H), 0.85 (t, *J* = 7.1 Hz, 3H). ^{13}C NMR (600 MHz, $CDCl_3$) δ 205.6, 169.7, 168.9, 54.7, 38.5, 31.3, 25.8, 23.5, 22.6, 22.2, 14.1. ESI-TOF: expected m/z $[M+Na]^+$ 306.1312, observed 306.1333.

Preparation of 2,2′-dimethyl-3-oxooctanoyl-CoA

The synthesis of 2,2′-dimethyl-3-oxooctanoyl-CoA was prepared in similar fashion mentioned in chapter 2: Materials and Methods-General preparation of 3-oxoacyl-CoA analogs. **2,2′-Dimethyl-3-oxooctanoyl-CoA (14-CoA):** expected $[M+H]^+$ 936.2375, observed 936.2399.

Preparation of 2,2′-dimethyl-3-oxoC8-ACP and C10-ACP

The synthesis of 2,2′-dimethyl-3-oxooctanoyl-ACP and decanoyl-ACP (C10-ACP) were prepared according to methods described in chapter 2: "Materials and Methods-General preparation of 3-oxoacyl-ACP analogs". **2,2′-Dimethyl-3-oxoC8-ACP (14):** calculated mass 9017.3746 Da, observed mass 9017.3185 Da; **C10-ACP (15):** calculated mass 9002.3857 Da, observed mass 9002.3736 Da.

HPLC assay

Two chemical steps, lactonization and acylation, in YspI were followed with the same protocols as discussed in chapter 2: Materials and Methods-HPLC assay.

Results and Discussion

Purification of YspI

Inoculation of BL21 (DE3) *E. coli* YspI on agar plate containing 50 μg/mL streptomycin and 50 μg/mL spectinomycin antibiotics showed appearance of small white circular colonies. An isolated colony was picked to inoculate mini growth and then large growth with the same antibiotic concentration. The large growth reached to OD of 06-0.8 within three hours of shaking at 37 °C. Sonication for cell lysis is a common technique due to its adaptability to different sample volumes and ease of use, allowing pulsed, high frequency sound waves to lyse cells. Since YspI contained maltose-binding protein

(MBP), amylose affinity column chromatography was used. The molecular weight of Ysp with MBP is 67.99 kDa or ~ 68 kDa. It was confirmed that the clean YspI protein was obtained indicating by a band at ~ 68 kDa on SDS-PAGE gel (Figure 28).

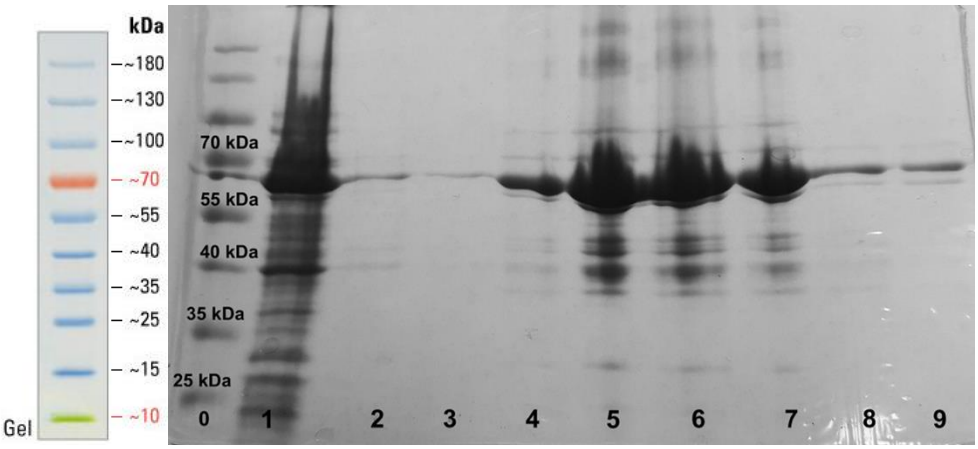

Figure 28. SDS-PAGE of YspI-MBP fractions using amylose column chromatography. Lane 0: EZ prestained protein ladder from Fisher; 1: run through of YspI crude; 2: YspI Buffer A wash of YspI; 3-9: 10 mM maltose in YspI Buffer A elutions 1-7. The elutions in lanes 4-9 had strong banding at ~ 68 kDa indicating the presence of YspI from purification.

Synthesis of 2,2′-dimethyl-3-oxooctanoyl-succinimide ester (**14-succ**)

There was no commercially available methyl or ethyl-3-oxooctanoate ester to make 2,2′-dimethyl-3-oxooctanoic acid. The synthesis of 2,2′-dimethyl-3-oxooctanoic acid was prepared starting from commercially available hexanoic acid and then coupling with DCC, DMAP (4-dimethylaminopyridine) and Meldrum's acid (2,2-dimethyl-1,3-dioxane-4,6-dione) in dry dichloromethane to give hexyl-Meldrum's acid intermediate (**14-Meldrum's acid**) (Scheme 13). The hexyl-Meldrum's acid intermediate gave nearly quantitative yields and was used without further purification. The characterization of the intermediate was confirmed by ^{1}H-NMR and COSY (Figures A46 and A47). The structure of hexyl-Meldrum's acid compound has an active methine hydrogen surrounded by three electron withdrawing groups, allowing for the existence of another

tautomeric form (Scheme 14). Notably, the presence of singlet signal at 15.27 ppm integrated to 1 proton, indicating the H-bonded enolic structure with the enol proton (Figure A46).

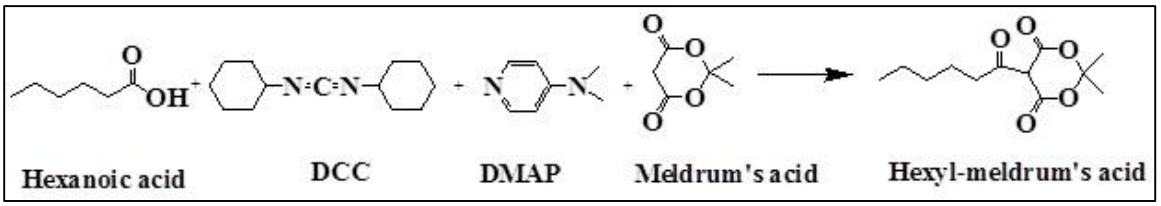

Scheme 13. Synthesis of hexyl-Meldrum's acid using hexanoic acid, DCC, DMAP, and Meldrum's acid.

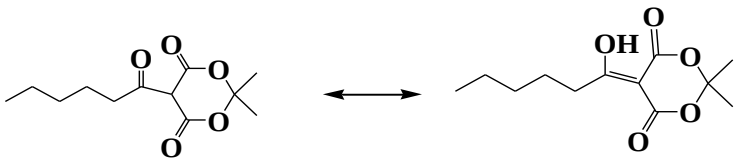

Scheme 14. Tautomeric equilibrium of hexyl-Meldrum's acid, indicating the predomination of enol form.

Then the intermediate hexyl-meldrum's acid was refluxed in the presence of methanol to afford the desired methyl-3-oxooctanoate (**14-ester**) in quantitative yields (Scheme 15). The side product from the reaction was easily removed by silica gel column chromatography. ^{1}H-NMR, COSY, and ^{13}C-NMR spectra were obtained to confirm the identity of **14-ester** (Figures A48-A50). In the ^{1}H-NMR spectrum, the singlet signal at 3.72 ppm that integrates to 3 protons corresponds to the methyl protons of the ester at C-1. Also, the singlet signal at 3.43 ppm, which integrates to 2 protons corresponds to the methylene protons at C-2 because the protons were surrounded by two electron withdrawing groups and resulted in a downfield shift (Figure A48). A small singlet at about 4.95 ppm was observed in the ^{1}H-NMR and may correspond to the α-hydrogen of the enolate tautomer of the product.

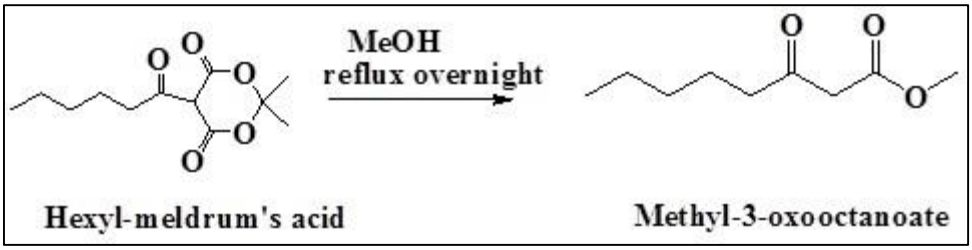

Scheme 15. Synthesis of methyl-3-oxooctanoate (14-ester).

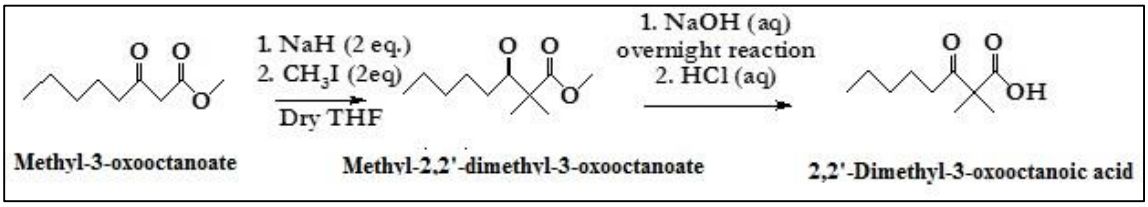

Scheme 16. Synthesis of 2,2′-dimethyl-3-oxooctanoic acid (14-acid).

Once the methyl-3-oxooctanoate ester was synthesized successfully, methyl-2,2′-dimethyl-3-oxooctanoate was chemically synthesized in a similar fashion as discussed in the synthesis of ethyl-2,2′-dimethyl-3-oxohexanoate (Scheme 16). The desired methyl-2,2′-dimethyl-3-oxooctanoate was obtained in quantitative yields and confirmed by ^{1}H-NMR, COSY, ^{13}C-NMR, and DEPT-135 (Figure A51-A54). One of the important indication of the success of the dimethylation reaction was the singlet at 1.34 ppm that integrated to 6 protons and the disappearance of the singlet peak at 3.43 ppm in the ^{1}H-NMR (Figure A51). A small amount of monomethyl-product was also observed in the crude product and separated from the dimethyl-product using silica gel column chromatography. In the ^{1}H-NMR of monomethyl-3-oxooctanoate, a doublet at 1.33 ppm integrated to 3 protons corresponding to one methyl group at C-2 and a quartet at 3.50 ppm integrated to 1 proton corresponding to one hydrogen at C-2 were observed. In addition, in the ^{13}C-NMR and DEPT-135 of the methyl-2,2′-dimethyl-3-oxooctanoate product, the height of the signal at 22.2 ppm, which was about twice as high as other

methyl group signal, indicated the two methyl groups at C-2 overlapped (Figures A52 and A54).

The synthesis of 2,2′-dimethyl-3-oxooctanoic acid was done by hydrolyzing methyl-2,2′-dimethyl-3-oxooctanoate with NaOH and then acidifying with HCl (Scheme 16). ^{1}H-NMR, COSY, and ^{13}C-NMR were obtained to confirm its identity (Figure A55-A57). In ^{1}H-NMR, the complete disappearance of the singlet signal at 3.69 ppm indicated that methyl group at C-1 of the methyl-2,2′-dimethyl-3-oxooctanoate staring material was hydrolyzed successfully (Figure A55). In ^{13}C-NMR, the appearance of signals at 208.4 ppm and 178.9 ppm was observed for the respective ketone and carboxylic acid functional groups of the desired product (Figure A57).

2,2′-Dimethyl-3-oxooctanoyl-succinimide ester was synthesized by treating 2,2′-dimethyl-3-oxooctanoic acid with DCC and *N*-hydroxysuccinimide in dioxane (Scheme 17). Most of the urea by-product was removed by filtration. Remaining trace amounts of the urea by-product was removed by silica gel column chromatography. The desired 2,2′-dimethyl-3-oxooctanoyl-succinimide ester product was afforded in good yields. Characterization by ^{1}H-NMR, COSY, ^{13}C-NMR, and ESI-MS-TOF was obtained to confirm their identity of the product (Figures A58-A60, and B11).

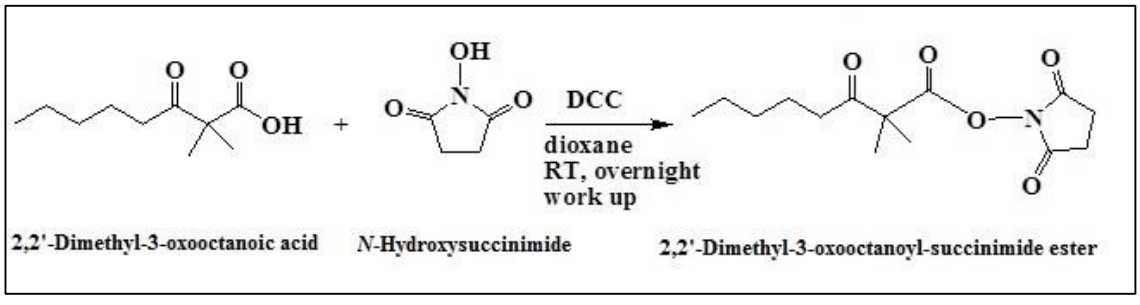

Scheme 17. Synthesis of 2,2′-dimethyl-3-oxooctanoyl-succinimide ester.

Synthesis of 2,2′-dimethyl-3-oxooctanoyl-CoA

Following a similar protocol for the preparation of acyl-CoA compounds in EsaI (chapter 2, Scheme 10), the synthesis of 2,2′-dimethyl-3-oxooctanoyl-CoA molecule was achieved by treating the synthesized 2,2′-dimethyl-3-oxooctanoyl-succinimide ester with free coenzyme A (CoA) acid under nitrogen environment (Scheme 18). The free CoA acid was deprotonated under basic condition and readily attacked the carbonyl carbon of the ester starting material, displacing the succinimide group. The crude product was extracted and ran on preparative HPLC to collect the desired pure 2,2′-dimethyl-3-oxooctanoyl-CoA product. In HPLC chromatogram shown in Figure 29, 2,2′-dimethyl-3-oxooctanoyl-CoA eluted at 11.1 minutes. Mass spectral data using ESI-TOF for 2,2′-dimethyl-3-oxooctanoyl-CoA molecule was also obtained to confirm its identity (Figure B22).

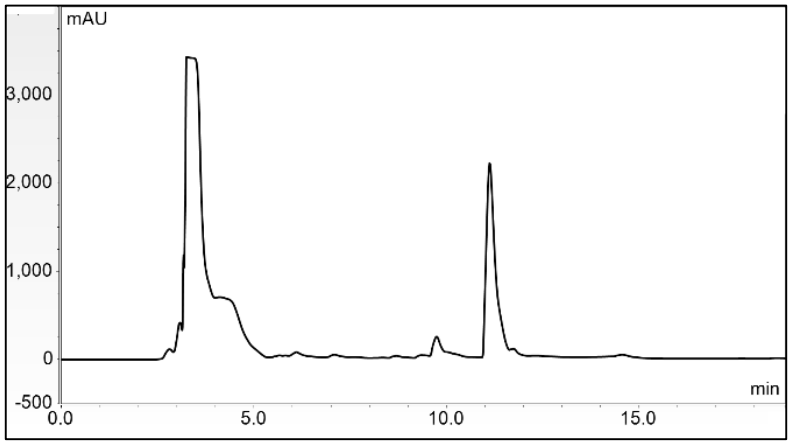

Figure 29. HPLC chromatogram of 2,2′-dimethyl-3-oxoC8-CoA molecule using preparative HPLC. Excess of 2,2′-dimethyl-3-oxoC8-succinimide ester and unreacted free CoA eluted from 2.5 – 4.8 minutes. Only peak corresponding to 2,2′-dimethyl-3-oxoC8-CoA product of interest was collected by fraction collector. 2,2′-Dimethyl-3-oxooctanoyl-CoA eluted at 11.1 – 12.0 minutes.

Syntheses of 2,2′-dimethyl-3-oxoC8-ACP and C10-ACP proteins

Enzymatic syntheses of *E. coli* 2,2′-dimethyl-3-oxoC8-ACP and C10-ACP proteins were in a similar fashion as discussed in acyl-ACP protein syntheses for EsaI (chapter 2, Scheme 12). The syntheses of all acyl-ACPs were confirmed by HPLC and ESI-TOF (Figures 30 and B37).

The completion of the reactions was monitored by the depletion of apo-ACP at 7.5 minutes and the growth of corresponding acyl-ACP peak. The Sfp enzyme eluted at 5.1 minutes. Once the acyl-ACP reaction had gone to completion, Sfp enzyme was precipitated out by addition of ammonium sulfate to 75 % saturation and removed from the reaction mixture by centrifugation.[58] Clean acyl-ACP product from the reaction was obtained by multiple washes with nanopure water to remove excess acyl-CoA and ammonium sulfate. These impurities absorbed at 260 nm while apo-ACP and acyl-ACP proteins absorbed at 280 nm on UV-Vis. The reduction of 260 peak after washes indicated the acyl-ACP protein was free of contamination.

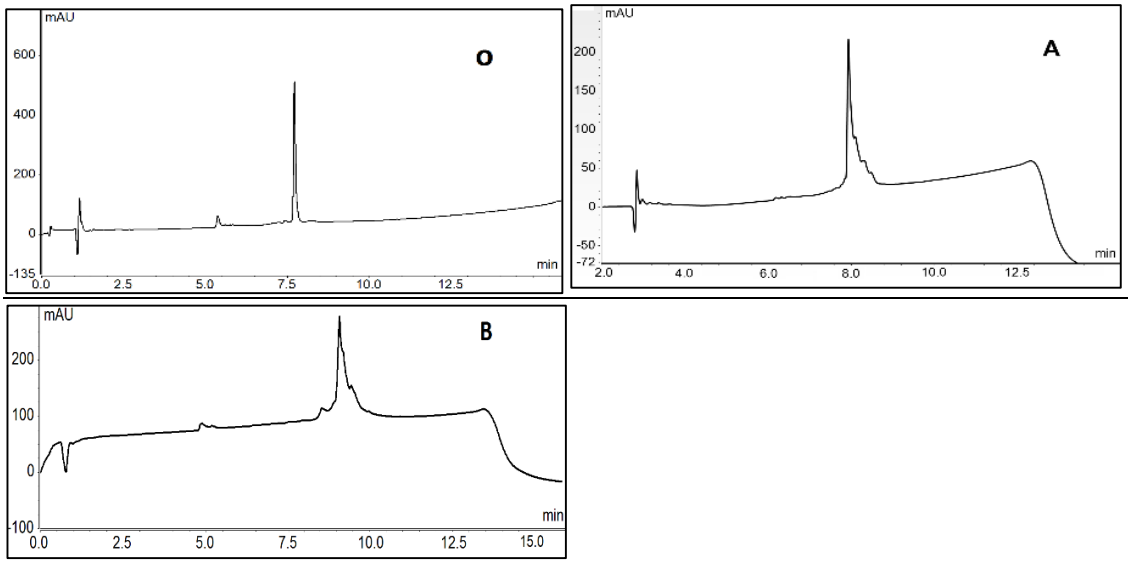

Figure 30. HPLC chromatograms of apo-ACP and alternative 3-oxoacyl-ACPs using analytical HPLC over a period of 10 minutes with flow rate of 600 μL/min. Sfp enzyme eluted at 5.1 minutes (O) Apo-ACP eluted at 7.7 minutes. The completion

of acyl-ACP synthesis reaction was monitored by disappearance of apo-ACP peak over time. (A) 2,2′-Dimethyl-3-oxooctanoyl-ACP eluted at 8.0 minutes (B) Decanoyl-ACP eluted at 9.0 minutes.

Lactonization and acylation assay in YspI-catalyzed reaction

In the YspI-catalyzed reaction, the formation of MTA and holo-ACP products after quenching the enzyme were measured quantitatively by using the same HPLC methods discussed in chapter 2 used for determining rates of EsaI. Product formation over a 6 minutes period was linear, indicating that 4 minutes of incubation with enzyme would be sufficient to determine the initial reaction rate (Figure 31).

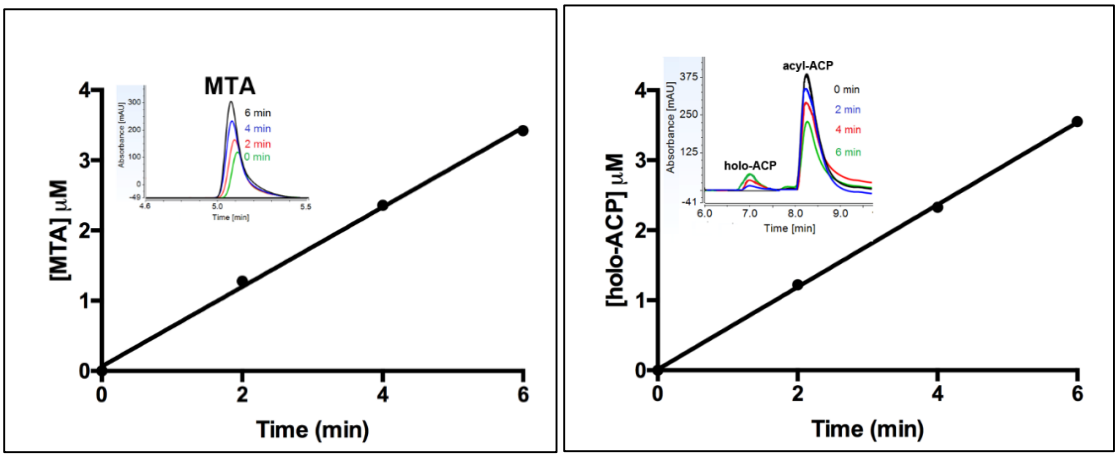

Figure 31. Different quenched time (0, 2, 4, 6 minutes) follwing formation of MTA and holo-ACP in lactonization and acylation half-reactions in YspI. In the reaction, concentrations of YspI, SAM, and 2-furoyl-ACP were fixed at 1.34 μM, 500 μM, and 112 μM, respectively. In lactonization, MTA peak at 0 minute corresponded to contaminant MTA in commercially available SAM from Sigma. In acylation, decrease in furoyl-ACP peak area was accompanied by increase in holo-ACP product peak area.

In the lactonization half-reaction, SAM and MTA peaks eluted at 0.65 and 5.05 minutes, respectively (Figure 32). Since MTA is a common contaminant in commercial SAM, the actual amount of MTA produced in the quenched reaction was determined by subtracting the total peak area from the contaminant MTA peak area presented in the background. The MTA concentration produced in the enzymatic reaction was calculated

from its respective peak area by using MTA standard curve. In acylation half-reaction, holo-ACP and acyl-ACP (2,2′-dimethyl-3-oxoC8-ACP in this case) eluted at 6.8 and 8.0 minutes, respectively (Figure 33). The overlaid background and YspI-catalyzed reaction chromatograms showed that in the presence of YspI, holo-ACP peak increased while 2,2′-dimethyl-3-oxoC8-ACP decreased relatively.

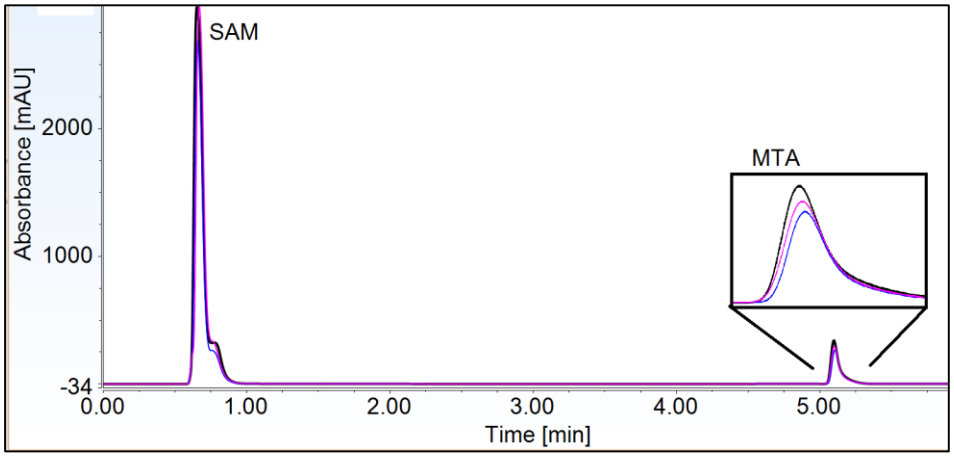

Figure 32. Lactonization assay for YspI. HPLC chromatogram of MTA product formation in YspI-catalyzed reaction using 0 μM, 10 μM, and 20 μM 2,2′-dimethyl-3-oxoC8-ACP substrate concentrations, fixed 500 μM SAM, fixed 1 μM YspI quenched at 4 minutes with 6 M HCl. SAM eluted at 0.65 minutes; MTA peak from SAM lactonization eluted at 5.05 minutes. The peak areas were reported in arbitrary units. The actual amount of MTA produced in the quenched reaction was determined by subtracting the total peak area from the contaminant MTA peak area presented in the background. The MTA concentration produced in the enzymatic reaction was calculated from its respective peak area by using MTA standard curve.

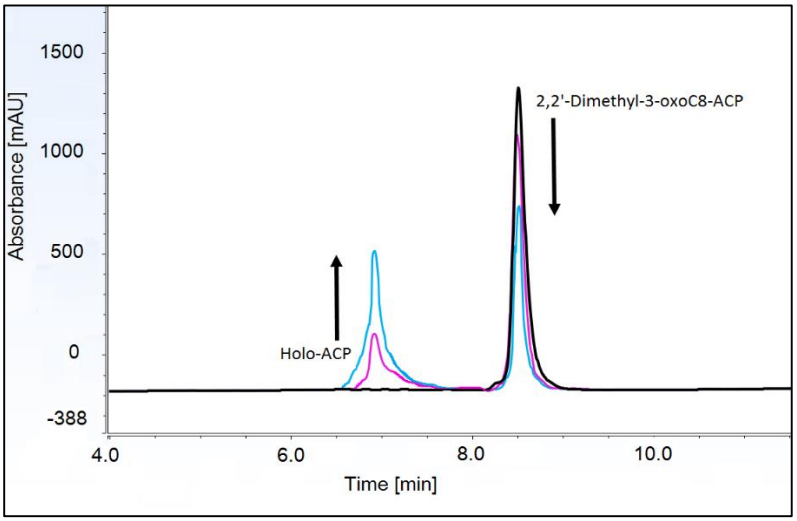

Figure 33. Acylation assay for YspI. HPLC chromatogram of holo-ACP product formation in YspI-catalyzed reaction using 70 μM (in blue) and 20 μM (in pink) 2,2′-dimethyl-3-oxoC8-ACP substrate concentration, fixed 500 μM SAM, fixed 1 μM YspI quenched at 4 minutes with 4 M acetate buffer, pH 3.6. Black chromatogram is background with 2,2′-dimethyl-3-oxoC8-ACP eluted at 8.0 minutes. Blue and pink chromatograms are YspI-catalyzed reactions with the appearance of holo-ACP peak at 6.8 minutes. An increase in holo-ACP peak was accompanied by a decrease in 2,2′-dimethyl-3-oxoC8-ACP peak area in YspI-catalyzed reaction. The peak areas were reported in arbitrary units. The holo-ACP concentration in the quenched reaction mixture was determined from its respective peak area by using holo-ACP standard curve.

Determination of kinetic parameters of alternative 3-oxoacyl-ACP substrates with YspI wildtype

Previously, mass spectrometry study had suggested that YspI produced majority 3-oxoC8-HSL, but the importance of the oxygen and hybridization at C-3 position had not yet been elucidated.[66] In this thesis, we were interested in exploring the effect of change of heteroatom (oxygen to sulfur and nitrogen), methylation of 3-oxoC8-ACP substrate, change of hybridization at C-3, change of straight acyl-chain to aromatic analogs, change of position of oxygen atom in the acyl-chain, change of acyl-chain length, and removal of oxygen atom in the acyl-chain on YspI activity.

The initial rate at each substrate concentration was fitted to Michaelis-Menten equation to determine kinetic constants (Figure C4 and C5). The K_m, k_{cat}, and k_{cat}/K_m

values in lactonization and acylation assay were within error (Table 4). A general K_m trend was observed among all alternative substrates: the substrates that carried oxygen at C-3 position had similar range of K_m value; as the oxygen atom moved to different position (C-2, C-4, and C-5) or removed, or acyl chain length changed from 8 carbons to 6 carbons, K_m increased and k_{cat} decreased. This variation in activity can be truly understood when comparing catalytic efficiencies (k_{cat}/K_m) of alternative substrates all together. The relative catalytic efficiencies of all substrates were compared in Figure 34.

Table 4. Determination of K_m, k_{cat}, k_{cat}/K_m of alternative 3-oxoacyl-ACP substrates on YspI activity by following (A) lactonization and (B) acylation reactions.

(A) Lactonization	K_m (μM)	k_{cat} (min^{-1})	k_{cat} K_m ($\mu M^{-1}min^{-1}$)	% activity [a]
2-Benzofuranacetyl-ACP (13)	7.71 ± 1.19	3.28 ± 0.12	0.425 ± 0.068	100.00
2,2′-Dimethyl-3-oxoC8-ACP (14)	7.78 ± 0.89	1.85 ± 0.05	0.238 ± 0.028	56.03
2-Furanacetyl-ACP (1)	8.35 ± 1.64	0.701 ± 0.032	0.0840 ± 0.0169	19.76
2-Tetrahydrofuranacetyl-ACP (2)	8.19 ± 1.46	0.610 ± 0.029	0.0744 ± 0.0137	17.52
2-Pyridylacetyl-ACP (4)	10.21 ± 1.49	0.742 ± 0.028	0.0727 ± 0.0110	17.12
2-Furoyl-ACP (5)	15.79 ± 3.12	0.574 ± 0.035	0.0364 ± 0.0075	8.56
5-oxoC8-ACP (11)	23.42 ± 3.98	0.788 ± 0.041	0.0336 ± 0.0060	7.92
4-oxoC8-ACP (10)	37.37 ± 5.19	1.12 ± 0.051	0.0299 ± 0.0044	7.06
5-oxoC6-ACP (7)	25.71 ± 2.44	0.619 ± 0.017	0.0241 ± 0.0024	5.67
4-oxoC6-ACP (6)	32.34 ± 4.66	0.593 ± 0.026	0.0183 ± 0.0028	4.32
C8-ACP (12)	87.87 ± 16.83	1.22 ± 0.093	0.0138 ± 0.0028	3.26
C6-ACP (9)	97.72 ± 15.90	0.780 ± 0.055	0.0080 ± 0.0014	1.88
C10-ACP (15)	112.60 ± 16.86	0.562 ± 0.038	0.0050 ± 0.0008	1.18
2-Thiopheneacetyl-ACP (3)	2.81 ± 0.89	0.774 ± 0.115	0.275 ± 0.097	64.84

[a] % activity = $\frac{k_{cat}/K_m}{0.425} \times 100$

(B) Acylation	K_m (μM)	k_{cat} (min^{-1})	k_{cat}/K_m ($\mu M^{-1}min^{-1}$)	% activity [a]
2-Benzofuranacetyl-ACP (13)	7.68 ± 1.11	3.24 ± 0.12	0.422 ± 0.063	100.00
2,2′-Dimethyl-3-oxoC8-ACP (14)	7.09 ± 0.64	1.79 ± 0.04	0.253 ± 0.023	59.91
2-Furanacetyl-ACP (1)	8.86 ± 0.85	0.864 ± 0.020	0.0975 ± 0.0096	23.12
2-Tetrahydrofuranacetyl-ACP (2)	7.49 ± 0.93	0.643 ± 0.019	0.0858 ± 0.0110	20.34
2-Pyridylacetyl-ACP (4)	9.64 ± 0.95	0.768 ± 0.0206	0.0797 ± 0.0081	18.88
5-oxoC8-ACP (11)	21.79 ± 2.80	1.066 ± 0.03917	0.0489 ± 0.0066	11.59
2-Furoyl-ACP (5)	15.90 ± 2.78	0.707 ± 0.036	0.0445 ± 0.0081	10.54
4-oxoC8-ACP (10)	36.56 ± 5.25	1.29 ± 0.061	0.0353 ± 0.0053	8.37
5-oxoC6-ACP (7)	28.05 ± 3.49	0.704 ± 0.027	0.0251 ± 0.00327	5.95
4-oxoC6-ACP (6)	34.22 ± 3.91	0.649 ± 0.025	0.0190 ± 0.0023	4.50
C8-ACP (12)	83.89 ± 16.08	1.34 ± 0.098	0.0159 ± 0.0033	3.78
C6-ACP (9)	97.73 ± 12.07	0.841 ± 0.038	0.0086 ± 0.0011	2.04
C10-ACP (15)	110.50 ± 10.08	0.579 ± 0.018	0.0052 ± 0.0005	1.24
2-Thiopheneacetyl-ACP (3)	1.94 ± 0.51	0.659 ± 0.067	0.339 ± 0.095	80.31
[a] % activity = $\frac{k_{cat}/K_m}{0.422} \times 100$				

Table 5. Effect of 2-thiopheneacetyl-ACP on YspI activity when SAM is fixed.

Fixed S	Variable S	K_m (μM)	k_{cat} (min^{-1})	k_{cat}/K_m ($\mu M^{-1}min^{-1}$)	K_i (μM)
50 μM SAM	2-Thiopheneacetyl-ACP	4.58 ± 2.23	0.48 ± 0.12	0.104 ± 0.058	26.54 ± 12.56
500 μM SAM	2-Thiopheneacetyl-ACP	2.81 ± 0.89	0.774 ± 0.115	0.275 ± 0.097	30.31 ± 9.18

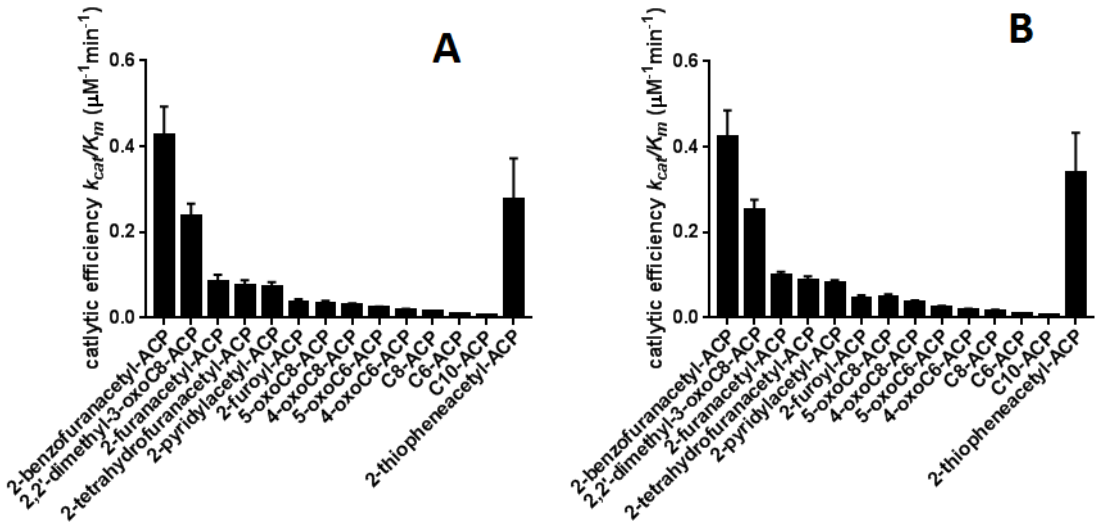

Figure 34. Comparison of catalytic efficiency of the alternative 3-oxoacyl-ACP substrates for YspI by following Lactonization (A) and Acylation assay (B). 2-Benzofuranacetyl-ACP with sp^2 hybridized carbon at C-3 and eight carbons in acyl-chain length showed the highest catalytic efficiency among all of the tested substrates with YspI. The catalytic activity of 2-benzofuranacetyl-ACP was about 4-fold higher than that of 2-furanacetyl-ACP. The change of heteroatom, position of oxygen atom, removal of oxygen atom, and variation in acyl-chain length significantly affected the activity with YspI.

Among all of the substrates, 2-benzofuranacetyl-ACP showed the highest catalytic efficiency (0.425 ± 0.068 $\mu M^{-1}min^{-1}$). Comparing k_{cat}/K_m values of all alternative 3-oxoacyl-ACP substrates, 2-benzofuranacetyl-ACP substrate had the catalytic efficiency within an order of magnitude to that observed for ACP-dependent AHL synthases, such as RhlI (0.3 ± 0.1 $\mu M^{-1}min^{-1}$), BjaI (0.5 ± 0.2 $\mu M^{-1}min^{-1}$), and BmaI1 (0.31 ± 0.05 $\mu M^{-1}min^{-1}$). The second-best substrate with YspI was 2,2′-dimethyl-3-oxoC8-ACP with k_{cat}/K_m value of 0.238 ± 0.028 $\mu M^{-1}min^{-1}$. The 2-benzofuranacetyl-ACP and 2,2′-dimethyl-3-oxoC8-ACP substrates meet the three criteria suggested for YspI activity: 8 carbons in acyl chain, sp^2 hybridized C-3, and oxygen at C-3. However, the catalytic efficiency of 2,2′-dimethyl-3-oxoC8-ACP was 2-fold less active than 2-benzofuranacetyl-ACP. Similar to the situation of 2,2′-dimethyl-3-oxoC6-ACP in EsaI, the two methyl groups at C-2 of 2,2′-

dimethyl-3-oxoC8-ACP may possibly introduce some steric hindrance in acyl-chain binding site of YspI, thus slightly reducing the k_{cat} and k_{cat}/K_m values.

In the YspI-catalyzed reaction, 2-furanacetyl-ACP had only about 19-23 % activity in compared to the EsaI-catalyzed reaction. Yet, 2-furanacetyl-ACP is very similar to 2-benzofuranacetyl-ACP in term of hybridization of C-3 and oxygen at C-3, except that 2-furanacetyl-ACP is smaller than benzofuranacetyl-ACP in molecular size. The catalytic efficiency of 2-furanacetyl-ACP decreased by 4-fold compared to 2-benzofuranacetyl-ACP in YspI because YspI has a deeper acyl-chain binding pocket compared to EsaI that could result in too much fluctuations of acyl chain in the acyl-chain binding pocket of YspI and make it difficult to dock the 2-furanacetyl-ACP substrate in a productive conformation. 2-Tetrahydrofuranacetyl-ACP substrate with sp^3 hybridized C-3 instead of sp^2 had a 5-fold decrease in catalytic efficiency compared to 2-benzofuranacetyl-ACP. There is not much different in catalytic efficiency between 2-tetrahydrofuranacetyl-ACP and 2-furanacetyl-ACP although the hybridization of carbon at C3 position is different.

The alteration of heteroatom from oxygen to nitrogen at C-3 position also affected the k_{cat}/K_m value drastically. The catalytic efficiency of 2-pyridylacetyl-ACP with nitrogen in place of oxygen at C-3 decreased by 6-fold compared to 2-benzofuranacetyl-ACP and 1-fold compared to 2-furanacetyl-ACP. Although the lone pair of electrons of nitrogen center of pyridine is not part of the π-conjugated system and can serve as hydrogen bond acceptor/donor, k_{cat}/K_m value showed that 2-pyridylacetyl-ACP is less favorable than 2-benzofuranacetyl-ACP when bound to YspI.

Unlike EsaI, YspI shows a very distinctive loss in activity when position of oxygen in acyl-chain changed to C-2, C-4, and C-5. 2-Furoyl-ACP, 5-oxoC8-ACP, and 4-oxoC8-

ACP had activity of about 7-12 % compared to 2-benzofuranacetyl-ACP. The k_{cat}/K_m values of 5-oxoC8-ACP and 2-furoyl-ACP were almost similar. The k_{cat}/K_m value of 4-oxoC8-ACP was about 1.2-fold less than that of 5-oxoC8-ACP and 2-furoyl-ACP. Interestingly, when chain length of the substrate was shortened by 2 carbons with the same position of oxygen (5-oxoC6-ACP and 4-oxoC6-ACP), the catalytic efficiencies dropped by 2-fold compared to those of 5-oxoC8-ACP and 4-oxoC8-ACP. In YspI-catalyzed reaction, the k_{cat}/ K_m value of 5-oxoC8-ACP was about 1.4-fold higher than that of 5-oxoC6-ACP. Likewise, the k_{cat}/K_m value of 4-oxoC8-ACP was about 1.6-fold higher than that of 4-oxoC6-ACP. The data may suggest that acyl-chain of 8 carbons is able to reach to the bottom of the acyl-chain binding pocket more easily and produce easier productive conformation. However, the shorter acyl-chain in 4-oxoC6-ACP and 5-oxoC6-ACP may increase the flexibility of acyl-chain in the shorter substrates resulting in a nonproductive binding for the enzyme-substrate ternary complex. This will decrease the turnover number (k_{cat}) of the substrate.

Furthermore, without a heteroatom in the acyl-chain, the activity of C6-ACP, C8-ACP, and C10-ACP dropped significantly (1 – 4 %) compared to the highest activity substrate, 2-benzofuranacetyl-ACP. The data indicated that the presence of a heteroatom plays a role in retaining the activity of YspI. In addition, the preference of YspI for a specific chain length was also examined by looking catalytic efficiencies of C6-ACP, C8-ACP, and C10-ACP. Although these three substrates do not carry any heteroatom in acyl-chain, but the difference in chain length may provide useful information about acyl-chain length specificity of YspI for acyl-ACP substrate. The catalytic efficiencies of these three substrates can be ranked in high to low order: C8-ACP > C6-ACP > C10-ACP. The activity

of C10-ACP was only 1 % compared to 2-benzofuranacetyl-ACP and 3-fold less than C8-ACP. This may be explained that the difference by 2 carbons in C10-ACP compared to C8-ACP may cause the acyl-chain to protrude from the V-cleft binding pocket in YspI. Looking at all 14 substrates together, it is clear that YspI exhibits a strong preference for substrates with length of 8 carbons.

Last but not least, 2-thiopheneacetyl-ACP is an interesting substrate. It exhibited substrate inhibition when SAM was fixed and 2-thiopheneacetyl-ACP was varied (Figure C4, C5, and C8). Table 5 summarizes kinetic parameters when SAM concentrations were fixed at 50 μM and 500 μM. The inhibition constant K_i value when fixed SAM at 500 μM (30.31 ± 9.18 μM) was compared to K_i value when fixed SAM at 50 μM (26.54 ± 12.56 μM). Substrate inhibition was observed in both of the cases and had similar K_i values.

Yet, when 2-thiopheneacetyl-ACP was fixed and SAM was the variable substrate, substrate inhibition was not observed (Figure C9). In addition, K_m of SAM when fixed 2-benzofuranacetyl-ACP (75.98 ± 17.49 μM) was determined and compared to K_m of SAM when fixed 2-thiopheneacetyl-ACP (23.52 ± 4.03 μM) (Figure C9). The k_{cat} for fixed concentrations of 2-thiopheneacetyl-ACP with variable concentration of SAM (0.764 ± 0.029 min^{-1}) is about 5-fold lower than that for fixed concentrations of 2-benzofuranacetyl-ACP (3.21 ± 0.18 min^{-1}). However, the k_{cat}/K_m for fixed 2-thiopheneacetyl-ACP (0.0325 ± 0.0057 $\mu M^{-1}min^{-1}$) is almost similar to that for fixed 2-benzofuranacetyl-ACP (0.0423 ± 0.0100 $\mu M^{-1}min^{-1}$). Both 2-thiopheneacetyl-ACP and 2-benzofuranacetyl-ACP showed normal hyperbolic curves when SAM was the variable substrate. This result together with substrate inhibition data when SAM is fixed indicated that all available free enzyme (E) favored the formation of stable EA (E.2-thiopheneacetyl-ACP or E.2-benzofuranacetyl-

ACP) complex, resulting in the binding of SAM to EA to follow the productive pathway (Figure 25). Product inhibition studies will need to be conducted to determine the order of substrate addition with YspI. One of the explanations for substrate inhibition of 2-thiopheneacetyl-ACP in YspI can be described by random sequential mechanism discussed in chapter 2 (Figure 25). At low concentrations of 2-thiopheneacetyl-ACP, it populated the productive pathway by formation of E.2-thiopheneacetyl-ACP.SAM complex. However, when 2-thiopheneacetyl-ACP reached beyond saturation, the excess of 2-thiopheneacetyl-ACP could also bind to E.SAM complex, pushing the nonproductive pathway to compete with productive pathway. The result is a lower turnover number and the reaction rate decreased. Another explanation is that the binding of 2-thiopheneacetyl-ACP in the acyl-chain binding pocket of YspI partially locks the enzyme in a conformation that the substrate can't be released to perform catalysis, resulting in decrease of released product.

As a result, these data indicated that the presence of heteroatom is important in maintaining activity of YspI, but chain length can also play a critical point in establishing the necessary interactions to position the acyl-chain into a productive conformation to undergo catalysis.

CHAPTER FOUR: CONCLUSIONS

In Gram-negative bacteria, AHL synthases catalyze the synthesis of AHL signal molecules using acyl-ACP and SAM substrates. Many therapeutically relevant AHL synthases utilize β-ketoacyl-ACPs; yet, these enzymes remain uncharacterized with their native substrate due to the instability of the β-ketoacyl-ACP substrate *in vitro*. This thesis work is the first systematic investigation to design and evaluate the alternative 3-oxo-acyl-ACP substrates for *Pantoea stewartii* EsaI and *Yersinia pestis* YspI. This study will open new doors to explore inhibitors for several uncharacterized AHL synthase enzymes as well as other β-ketoacyl-ACP utilizing enzymes that impacts human health.

From the kinetic study of EsaI T140A mutant with C6-ACP, it was confirmed that the acyl-chain binding pocket of EsaI lost specificity with respect to the β- position of the acyl chain when the key threonine residue was mutated to alanine (Figure 34). The kinetic studies of the alternative 3-oxoacyl-ACP substrate analogs with EsaI wild-type suggest that the presence of an oxygen at the β-carbon position and the chain length of six carbons are preferable to yield high catalytic efficiency. When studying kinetics of the alternative 3-oxoacyl-ACP substrate analogs with YspI wild-type, our data indicate that YspI shows a strong preference for substrate with an acyl-chain length of eight carbons and an oxygen heteroatom at the β-carbon. From this thesis work, we found that 2-furanacetyl-ACP and 2-benzofuranacetyl-ACP are the best alternative substrate for EsaI and YspI, respectively. The catalytic efficiencies of these substrates are within an order of magnitude to that observed for ACP/CoA-dependent AHL synthases with their native acyl-ACP/ acyl-CoA

substrate, such as RhlI, BmaI, and BjaI (Figure 35). Also, the presence of heteroatom other than oxygen is crucial to retain enzyme activity in both EsaI and YspI. Surprisingly, our data suggest that the sp^3 hybridization at β-carbon only has a minimal effect on EsaI activity. Finally, the substrate with sulfur atom (2-thiophenacetyl-ACP) in place of oxygen at the β-carbon exhibits substrate inhibition in both EsaI and YspI enzymes, suggesting a possibility of random sequential mechanism. Future product inhibition experiments are needed to confirm this observation.

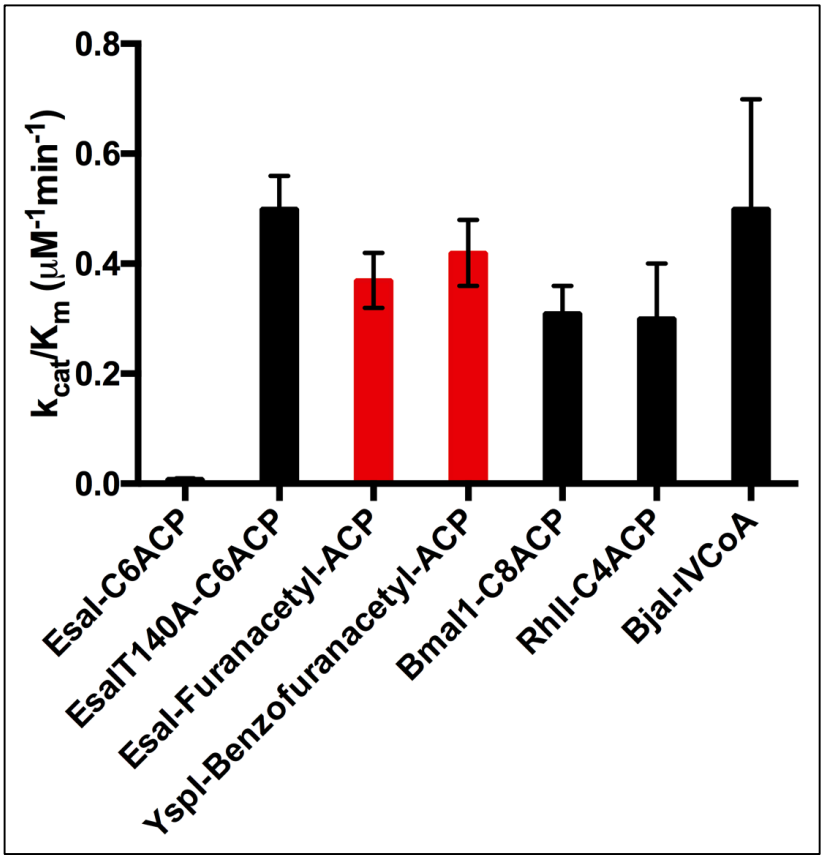

Figure 35. Comparison catalytic efficiency analysis of characterized AHL synthases with their native substrate. 2-Furanacetyl-ACP and 2-benzofuranacetyl-ACP are the best alternative substrate for EsaI and YspI, respectively. The catalytic efficiencies of these two substrates are within an order of magnitude to that observed for ACP/CoA-dependent AHL synthases with their native acyl-ACP/ acyl-CoA substrate, such as RhlI, BmaI, and BjaI.

In summary, this project met the criteria proposed in my thesis objective. The success of synthesis and high activity of β-ketoacyl-ACP mimics for EsaI and YspI should open new doors in characterizing this class of enzymes. Moreover, the β-ketoacyl-ACP substrates could be used as chemical probes to explore and design inhibitors for therapeutically important AHL synthases and several uncharacterized enzymes that impacts human health, such as β-ketoacyl-ACP reductase in fatty acid biosynthesis, polyketide synthase in polyketide synthesis which are targets for antimicrobial, antimalarial, and anti-cancer drugs.

REFERENCES

1. Miller, M. B.; Bassler, B. L. Quorum Sensing in Bacteria. *Annu. Rev. Microbiol.* **2001**, *55*, 165-199.

2. Galloway, W. R. J. D.; Hodgkinson, J. T.; Bowden, S. D.; Welch, M.; Spring, D. R. Quorum Sensing in Gram-Negative Bacteria: Small-Molecule Modulation of AHL and AI-2 Quorum Sensing Pathways. *Chem. Rev.* **2011**, *111*, 28-67.

3. LaSarre, B.; Federle, M. J. Exploiting Quorum Sensing to Confuse Bacterial Pathogens. *Mircobiol. Mol. Rev.* **2013**, *77*, 73-111.

4. Fuqua, C.; Greenberg, E. P. Listening in on Bacteria: Acyl-Homoserine Lactone Signaling. *Nature Rev. Mol. Cell Biol.* **2002**, *3*, 685-695

5. Li, Y.H.; Tian, X. Quorum Sensing and Bacterial Social Interactions in Biofilms. *Sensors* **2012**, *12*, 2519-2538.

6. Ramey, B. E.; Koutsoudis, M.; von Bodman, S. B.; Fuqua, C. Biofilm Formation in Plant-Microbe Associations. Curr. Opin. Microbiol. 2004, 7, 602-609.

7. Parsek, M. R.; Greenberg, E. P. Sociomicrobiology: The Connections Between Quorum Sensing and Biofilms. *TRENDS in Microbiology* **2005**, *13*, 27-33.

8. Høiby, N.; Bjarnsholt, T.; Givskov, M.; Molin, S.; Ciofu, O. Antibiotic Resistance of Bacterial Biofilms. *Int. J. Antimicrob. Agents* **2010**, *35*, 322-332.

9. Chang, C.; Krishnan, T.; Wang, H.; Chen, Y.; Yin, W.; Chong, Y.; Tan, L. Y.; Chong, T. M.; Chan, K. G. Non-Antibiotic Quorum Sensing Inhibitors Acting Against *N*-Acyl Homoserine Lactone Synthase as Druggable Target. *Sci. Rep.* **2014**, DOI: 10.1038/srep07245.

10. Pomianek, M. E.; Semmelhack, M. F. Making Bacteria Behave: New Agonists and Antagonists of Quorum Sensing. *ACS Chem. Biol.* **2007**. DOI: 10.1021/cb700098c.

11. Kalia, V. C. Quorum Sensing Inhibitors: An Overview. *Biotech. Adv.* **2013**, *31*, 224-245.

12. Fetzner, S. Quorum Quenching Enzymes. *J. Biotech.* **2015**, *201*, 2-14.

13. Defoirdt, T.; Boon, N.; Bossier, P.; Verstraete, W. Disruption of Bacterial Quorum Sensing: An Unexplored Strategy to Fight Infections in Aquaculture. *Aquaculture* **2004**, *240*, 69-88.

14. Park, J.; Jagasia, R.; Kaufmann, G. F.; Mathison, J. C.; Ruiz, D. I.; Moss, J. A.; Meijler, M. M.; Ulevitch, R. J.; Janda, K. D. Infection Control by Antibody Disruption of Bacterial Quorum Sensing. *Chem. Biol.* **2007**, *14*, 1119-1127.

15. Amara, N.; Krom, B. P.; Kaufmann, G. F.; Meijler, M. M. Macromolecular Inhibition of Quorum Sensing: Enzymes, Antibodies, and Beyond. *Chem. Rev.* **2011**, *111*, 195-208.

16. Chung, J.; Goo, E.; Yu, S.; Choi, O.; Lee, J.; Kim, J.; Kim, H.; Igarashi, J.; Suga, H.; Moon, J. S.; Hwang, I.; Rhee, S. Small-Molecule Inhibitor Binding to an *N*-Acyl-Homoserine Lactone Synthase. *PNAS* **2011**, *108*, 12089-12094.

17. Defoirdt, T.; Boon, N.; Bossier, P. Can Bacteria Evolve Resistance to Quorum Sensing Disruption? *PLoS Pathog.* **2010**, *6*, 1-6.

18. Popat, R.; Crusz, S. A.; Messina, M.; Williams, P.; West, S. A.; Diggle, S. P. Quorum-sensing and Cheating in Bacterial Biofilms. *Proc. R. Soc. B* **2012**, *279*, 4765-4771.

19. Darch, S. E.; West, S. A.; Winzer, K.; Diggle, S. P. Density-Dependent Fitness Benefits in Quorum-Sensing Bacterial Populations. *PNAS* **2012**, *109*, 8259-8263.

20. Gerdt, J. P.; Blackwell, H. E. Competition Studies Confirm Two Major Barriers That Can Preclude the Spread of Resistance to Quorum-Sensing Inhibitors in Bacteria. *ACS Chem. Biol.* **2014**, *9*, 2291-2299.

21. Val, D. L.; Cronan, J. E. In Vivo Evidence that S-Adenosylmethionine and Fatty Acid Synthesis Intermediates Are the Substrates for the LuxI Family of Autoinducer Synthases. *J. Bacteriol.* **1998**, *180*, 2644-2651.

22. Cronan, J. E.; Thomas, J. Bacterial Fatty Acid Synthesis and Its Relationships with Polyketide Synthetic Pathways. *Methods Enzymol.* **2009**, *459*, 395-433.

23. Beld, J.; Cang, H.; Burkart, M. D. Visualizing the Chain-Flipping Mechanism in Fatty-Acid Biosynthesis. *Angew. Chem. Int. Ed.* **2014**, *53*, 14456-14461.

24. Quin H. Christensen, Ryan M. Brecht, Dastagiri Dudekula, E. Peter Greenberg and Rajesh Nagarajan. Evolution of Acyl-Substrate Recognition by a Family of Acyl-

Homoserine Lactone Synthases. ***PLos One*** (2014), 9 (11) : e112464. doi: 10.1371/journal.pone.0112464.

25. Montebello, A. N.; Brecht, R. M.; Turner, R. D.; Ghali, M.; Pu, X.; Nagarajan, R. Acyl-ACP Substrate Recognition in *Burkholderia mallei* BmaI1 Acyl-Homoserine Lactone Synthase. *Biochemistry* **2014**, *53*, 6231-6242.

26. Gould, T. A.; Herman, J.; Krank, J.; Murphy, R. C.; Churchill, M. E. A. Specificity of Acyl-Homoserine Lactone Synthases Examined by Mass Spectrometry. *J. Bacteriol.* **2006**, *188*, 773-783.

27. Chakrabarti, S.; Sowdhamini, R. Functional Sites and Evolutionary Connections of Acylhomoserine Lactone Synthases. *Protein Engineering* **2003**, *16*, 271-278.

28. Watson, W. T.; Minogue, T. D.; Val, D. L.; Bodman, S. B.; Churchill, M. E. A. Structural Basis and Specificity of Acyl-Homoserine Lactone Signal Production in Bacterial Quorum Sensing. *Mol. Cell* **2002**, *9*, 685-694.

29. Gould, T. A.; Schweizer, H. P.; Churchill, M. E. A. Structure of the *Pseudomonas aeruginosa* Acyl-Homoserinelactone Synthase LasI. *Mol. Microbiol.* **2004**, *53*, 1135-1146.

30. Churchill, M. E. A.; Chen, L. Structural Basis of Acyl-Homoserine Lactone-Dependent Signaling. *Chem. Rev.* **2011**, *111*, 68-85.

31. Chung, J.; Goo, E.; Yu, S.; Choi, O.; Lee, J.; Kim, J.; Kim, H.; Igarashi, J.; Suga, H.; Moon, J.; Hwang, I.; Rhee, S. Small-molecule Inhibitor Binding to an *N*-Acyl-Homoserine Lactone Synthase. *PNAS* **2011**, *108*, 12089-12094.

32. Dong, S.H.; Frane, N. D.; Christensen, Q. H.; Greenberg, E. P.; Nagarajan, R.; Nair, S. K. Molecular Basis for the Substrate Specificity of Quorum Signal Synthases. *PNAS* **2017**, *114*, 9092-9097.

33. Nelson, D. L.; Cox, M. M. Enzymes. *Lehniger Principles of Biochemistry.* Ahr, K.; Rossignol, R.; Shriner, P.; McCaffrey, P.; Geller, E.; Moscatelli, B. W.H. Freeman and Company: New York, 2008; pp 183-205.

34. Raychaudhuri, A.; Tullock, A.; Tipton, P. A. Reactivity and Reaction Order in Acylhomoserine Lactone Formation by *Pseudomonas aeruginosa* RhlI. *Biochemistry* **2008**, *47*, 2893-2898.

35. Raychaudhuri, A.; Jerga, A.; Tipton, P. A. Chemical Mechanism and Substrate Specificity of RhlI, an Acylhomoserine Lactone Synthase from *Pseudomonas aeruginosa*. *Biochemistry* **2005**, *44*, 2974-2981.

36. Shin, D.; Frane, N. D.; Brecht, R. M.; Keeler, J.; Nagarajan, R. A Comparative Analysis of Acyl-Homoserine Lactone Synthase Assays. *ChemBiochem.* **2015**, *16*, 2651-2659.

37. Bouthillette, L. M.; Darcey, C. A.; Handy, T. E.; Seaton, S. C.; Wolfe, A. L. Isolation of the Antibiotic Pseudopyronine B and SAR Evaluation of C3/C6 Alkyl Analogs. *Bioorg. Med. Chem. Lett.* **2017**, *27*, 2762-2765.

38. Mori, T.; Yang, D.; Matsui, T.; Hashimoto, M.; Morita, H.; Fujii, I.; Abe, I. Structural Basis for the Formation of Acylalkylpyrones from Two β-Ketoacyl Units by the Fungal Type III Polyketide Synthase CsyB. *J. Biol. Chem.* **2015**, *290*, 5214-5225.

39. Roper, M. C. *Pantoea stewartii* subsp. *stewartii*: Lessons Learned from a Xylem-Dwelling Pathogen of Sweet Corn. *Mol. Plant Pathol.* **2011**, *12*, 628-637.

40. Bae, C.; Han, S. W.; Song, Y. R.; Kim, B. Y.; Lee, H. J.; Lee, J. M.; Yeam, I.; Heu, S.; Oh, C. S. Infection Processes of Xylem-Colonizing Pathogenic Bacteria: Possible Explanations for the Scarcity of Qualitative Disease Resistance Genes Against Them in Crops. *Theor. Appl. Genet.* **2015**, *128*, 1219-1229.

41. von Bodman, S. B.; Dietz Bauer, W.; Coplin, D. L. Quorum Sensing in Plant-Pathogenic Bacteria. *Annu. Rev. Phytopathol.* **2003**, *41*, 455-482.

42. Chug, R.; Khosla, B.; Singh, M. Modulation of the Extracellular Polymeric Substances (EPS) Production by Quorum Sensing (QS) in Bacteria. *Int. J. Curr. Microbiol. App. Sci.* **2015**, *4*, 884-896.

43. Koutsoudis, M. D.; Tsaltas, D.; Minogue, T. D.; Bodman, S. B. Quorum-sensing Regulation Governs Bacterial Adhesion, Biofilm Development, and Host Colonization in *Pantoea stewartii* subspecies *stewartii*. *PNAS* **2006**, *103*, 5983-5988.

44. von Bodman, S. B.; Farrand, S. K. Capsular Polysaccharide Biosynthesis and Pathogenicity in *Erwinia stewartii* Require Induction by an *N*-Acylhomoserine Lactone Autoinducer. *J. Bacteriol.* **1995**, *177*, 5000-5008.

45. von Bodman, S. B.; Majerczak, D. R.; Coplin, D. L. A Negative Regulator Mediates Quorum-Sensing Control of Exopolysaccharide Production in *Pantoea stewartii* subsp. *stewartii*. *Proc. Natl. Acad. Sci. USA* **1998**, *95*, 7687-7692.

46. Ramachandran, R.; Stevens, A. M. Proteomic Analysis of the Quorum-Sensing Regulon in *Pantoea stewartii* and Identification of Direct Targets of EsaR. *Appl. Environ. Microbiol.* **2013**, *79*, 6244-6252.
47. Higuchi, K.; Yamashina, T.; Ishikawa, K.; Hirofumi, H. Chemistry of Succinimido Esters. IV. A Facile Preparation of N-Succinimidyl Carboxylates Using *N,N′*-Disuccinimidyl Carbonate. *J-Stage* **1987**, 16-20.

48. D'Ambrosio, M.; Guerriero, A. A Simple Oxidation of γ- and δ-lactones to Oxocarboxylic Acids by Buffered Sodium Hypochlorite. *J. Chem. Research* **2002**, 631-633.

49. Huckin, S. N.; Weiler, L. Alkylation of Dianions of β-Keto Esters. *J. Am. Chem. Soc.* **1974**, *96*, 1082-1087.

50. Augelli-Szafran, C. E.; Blankley, C. J.; Roth, B. D.; Trivedi, B. K.; Bousley, R. F.; Essenburg, A. D.; Hamelehle, K. L.; Krause, B. R.; Stanfield, R. L. Inhibitors of Acyl-CoA: Cholesterol Acyltransferase. 5. Identification and Structure-Activity Relationships of Novel β-Ketoamides as Hypocholesterolemic Agents. *J. Med. Chem.* **1993**, *36*, 2943-2949.
51. Marsden, D. M.; Nicholson, R. L.; Skindersoe, M. E.; Galloway, W. R. J. D.; Sore, H. F.; Givskov, M.; Salmond, G. P. C.; Ladlow, M.; Welch, M.; Spring, D. R. Discovery of a Quorum Sensing Modulator Pharmacophore by 3D Small-Molecule Microarray Screening. *Org. Biomol. Chem.* **2010**, *8*, 5313-5323.

52. Azizi, N.; Khajeh Amiri, A.; Bolourtchian, M.; Saidi, M. R. A Green and Highly Efficient Alkylation of Thiols in Water. *J. Iran. Chem. Soc.* **2009**, *6*, 749-753.

53. Kutner, A.; Renstrom, B.; Schnoes, H. K.; DeLuca, H. F. Synthesis of Coenzyme an Ester of Retinoic Acid: Intermediate in Vitamin A Metabolism. *Proc. Natl. Acad. Sci. USA* **1986**, *83*, 6781-6784.

54. Al-Arif, A.; Blecher, M. Synthesis of Fatty Acyl CoA and Other Thiol Esters Using *N*-Hydroxysuccinimide Esters of Fatty Acids. *J. Lipid Res.* **1969**, *10*, 344-345.

55. Sakuda, S.; Higashi, A.; Tanaka, S.; Nihira, T.; Yamada, Y. Biosynthesis of Virginiae Butanolide A, a Butyrolactone Autoregulator from *Streptomyces. J. Am. Chem. Soc.* **1992**, *114*, 663-668.

56. Yin, J.; Straight, P. D.; McLoughlin, S. M.; Zhou, Z.; Lin, A. J.; Golan, D. E.; Kelleher, N. L.; Kolter, R.; Walsh, C. T. Genetically Encoded Short Peptide Tag for Versatile Protein Labeling by Sfp Phosphopantetheinyl Transferase. *PNAS* **2005**, *102*, 15815-15820.

57. Mofid, M. R.; Finking, R.; Marahiel, M. A. Recognition of Hybrid Peptidyl Carrier Proteins/ Acyl Carrier Proteins in Nonribosomal Peptide Synthetase Modules by the 4'-Phosphopantetheinyl Transferases AcpS and Sfp. *J. Biol. Chem.* **2002**, *277*, 17023-17031.

58. EnCor Biotechnology Inc. Ammonium Sulfate Calculator. 2017; http://www.encorbio.com/protocols/AM-SO4.htm. Accessed September 18, 2017.

59. Platts, J. A.; Howard, S. T.; Bracke, B. R. F. Directionality of Hydrogen Bonds to Sulfur and Oxygen. *J. Am. Chem. Soc.* **1996**, *118*, 2726-2733.

60. Tai, J.; Lii, J.; Allinger, N. L. A Molecular Mechanics (MM2) Study of Furan, Thiophene, and Related Compounds. *J. Comput. Chem.* **1989**, *10*, 635-647.

61. Achtman, M.; Zurth, K.; Morelli, G.; Torrea, G.; Guiyoule, A.; Carniel, E. *Yersinia pestis*, the Cause of Plague, is a Recently Emerged Clone of *Yersinia pseudotuberculosis. PNAS* **1999**, *96*, 14043-14048.

62. Atkinson, S.; Sockett, R. E.; Cámara, M.; Williams, P. Quorum Sensing and the Lifestyle of *Yersinia. Curr. Issues Mol. Biol.* **2006**, *8*, 1-10.

63. Parkhill, J. Genome Sequence of *Yersinia pestis*, the Causative Agent of Plague. *Nature.* **2001**, *413*, 523-527.

64. Bobrov, A. G.; Bearden, S. W.; Fetherston, J. D.; Khweek, A. A.; Parrish, K. D.; Perry, R. D. Functional Quorum Sensing Systems Affect Biofilm Formation and Protein Expression in *Yersinia pestis. Advances in experimental medicine and biology*; Perry, R. D., Fetherston, J. D.; Springer Science+Business Media, LLC: New York, 2007; 603, pp 178-191.

65. Atkinson, S.; Sockett, R. E.; Cámara, M.; Williams, P. *N*-Acylhomoserine Lactone-Mediated Quorum Sensing in *Yersinia. Yersinia: Molecular and Cellular Biology* **2004**, 75-90.

66. Kirwan, J. P.; Gould, T. A.; Schweizer, H. P.; Bearden, S. W.; Murphy, R. C.; Churchill, M. E. A. Quorum-Sensing Signal Synthesis by the *Yersinia pestis* Acyl-Homoserine Lactone Synthase YspI. *J. Bacteriol.* **2006**, *188*, 784-788.

67. LaRock, C. N.; Yu, J.; Horswill, A. R.; Parsek, M. R.; Minion, F. C. Transcriptome Analysis of Acetyl-Homoserine Lactone-Based Quorum Sensing Regulation in *Yersinia pestis. PLOS ONE* **2013**, *8*, 1-8.

68. Gelhaus, H. C.; Rozak, D. A.; Nierman, W. C.; Chen, D.; Varga, J. J.; Zadeh, M.; Ulrich, R. L.; Adamovicz, J. J. Exogenous *Yersinia pestis* Quorum Sensing Molecules *N*-Octanoyl-homoserine lactone and *N*-(3-Oxooctanoyl)-homoserine Lactone Regulate the LcrV Virulence Factor. *Microbial Pathogenesis* **2009**, *46*, 283-287.

69. Yates, E. A.; Philipp, B.; Buckley, C.; Atkinson, S.; Chhabra, S. R.; Sockett, R. E.; Goldner, M.; Dessaux, Y.; Cámara, M.; Smith, H.; Williams, P. *N*-Acylhomoserine Lactones Undergo Lactonolysis at a pH-, Temperature-, and Acyl-chain Length-Dependent Manner During Growth of *Yersinia pseudotuberculosis* and *Pseudomonas aeruginosa. IIfect. Immun.* **2002**, *70*, 5635-5646.

70. Chhabra, S. R.; Harty, C.; Hooi, D. S. W.; Daykin, M.; Williams, P.; Telford, G.; Pritchard, D. I.; Bycroft, B. W. Synthetic Analogues of the Bacterial Signal (Quorum Sensing) Molecule *N*-(3-Oxododecanoyl)-L-homoserine Lactone as Immune Modulators. *J. Med. Chem.* **2003**, *46*, 97-104.

71. Hodgkinson, J. T.; Galloway, W. R. J. D.; Casoli, M.; Keane, H.; Su, X.; Salmond, G. P. C.; Welch, M.; Spring, D. R. Robust Routes for the Synthesis of *N*-Acylated-L-Homoserine Lactone (AHL) Quorum Sensing Molecules with High Levels of Enantiomeric Purity. *Tetrahedron Lett.* **2011**, *52*, 3291-3294.

APPENDIX A

NMR Spectra

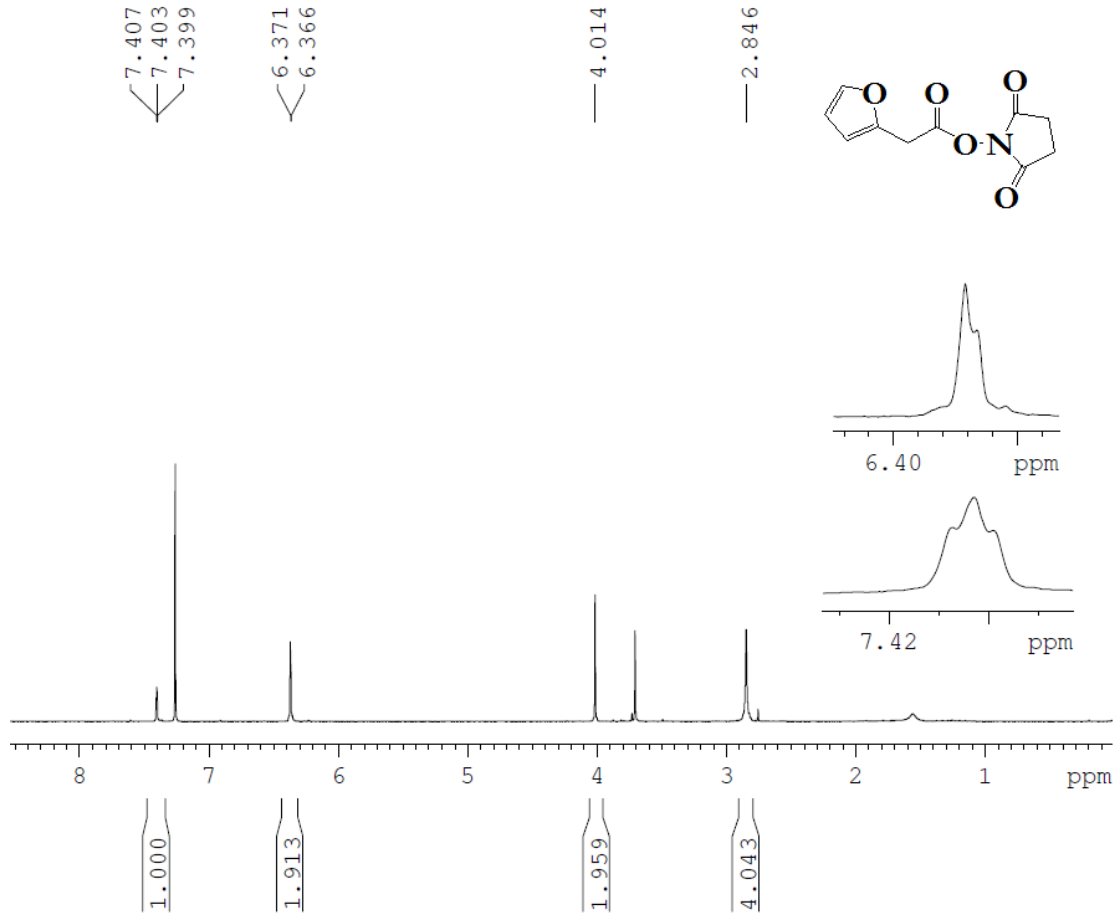

Figure A1. **^{1}H NMR of 2-furanacetyl-succinimide ester in $CDCl_3$ at 300 MHz.**

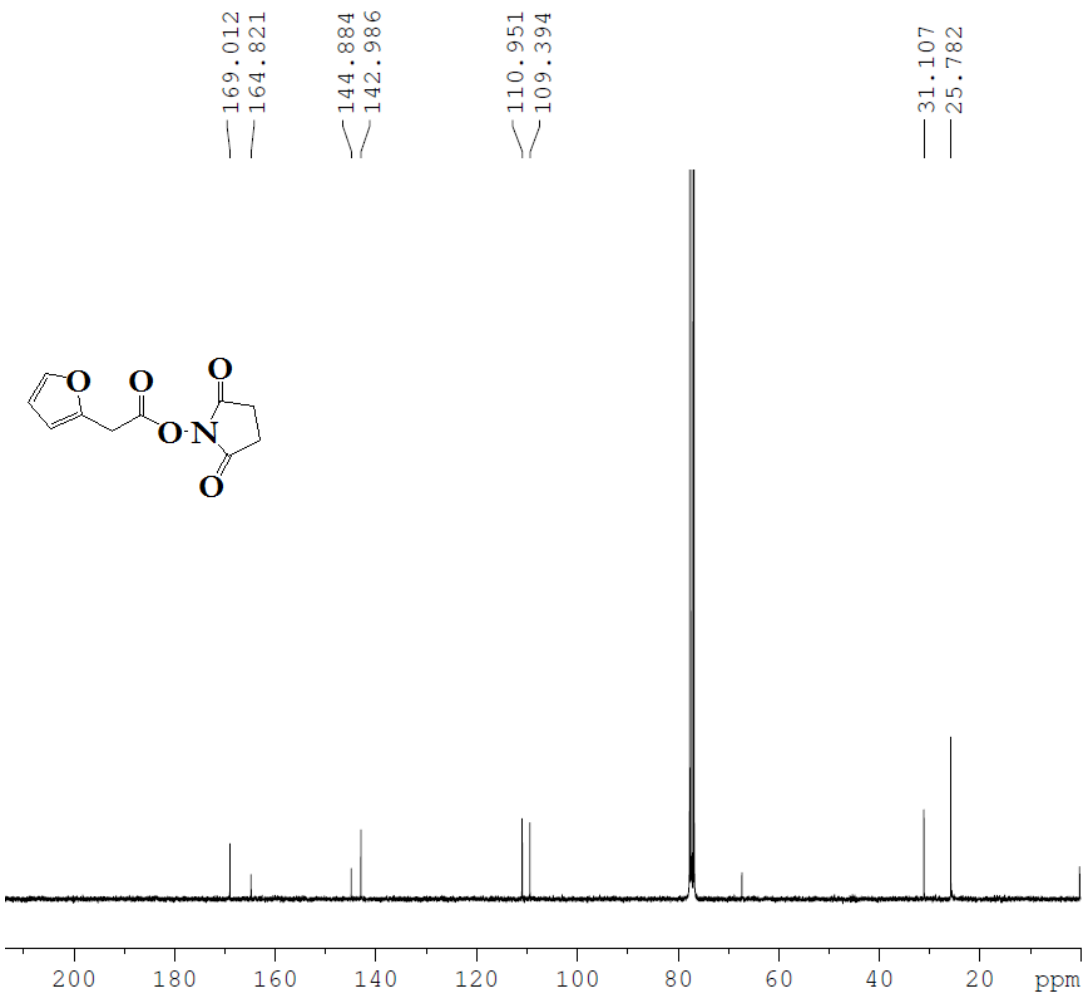

Figure A2. **^{13}C NMR of 2-furanacetyl-succinimide ester in $CDCl_3$ at 300 MHz.**

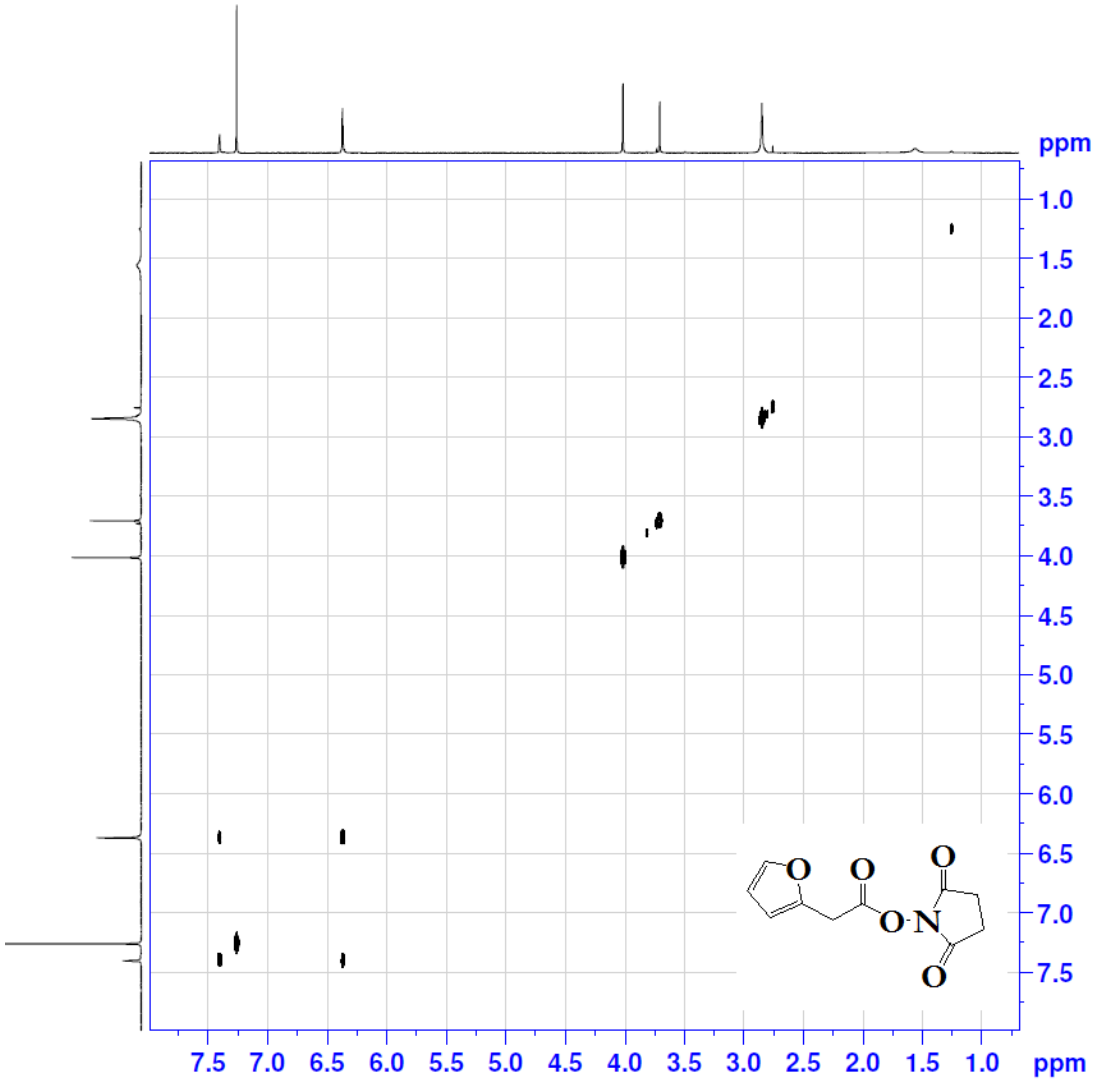

Figure A3. COSY of 2-furanacetyl-succinimide ester in $CDCl_3$ at 300 MHz.

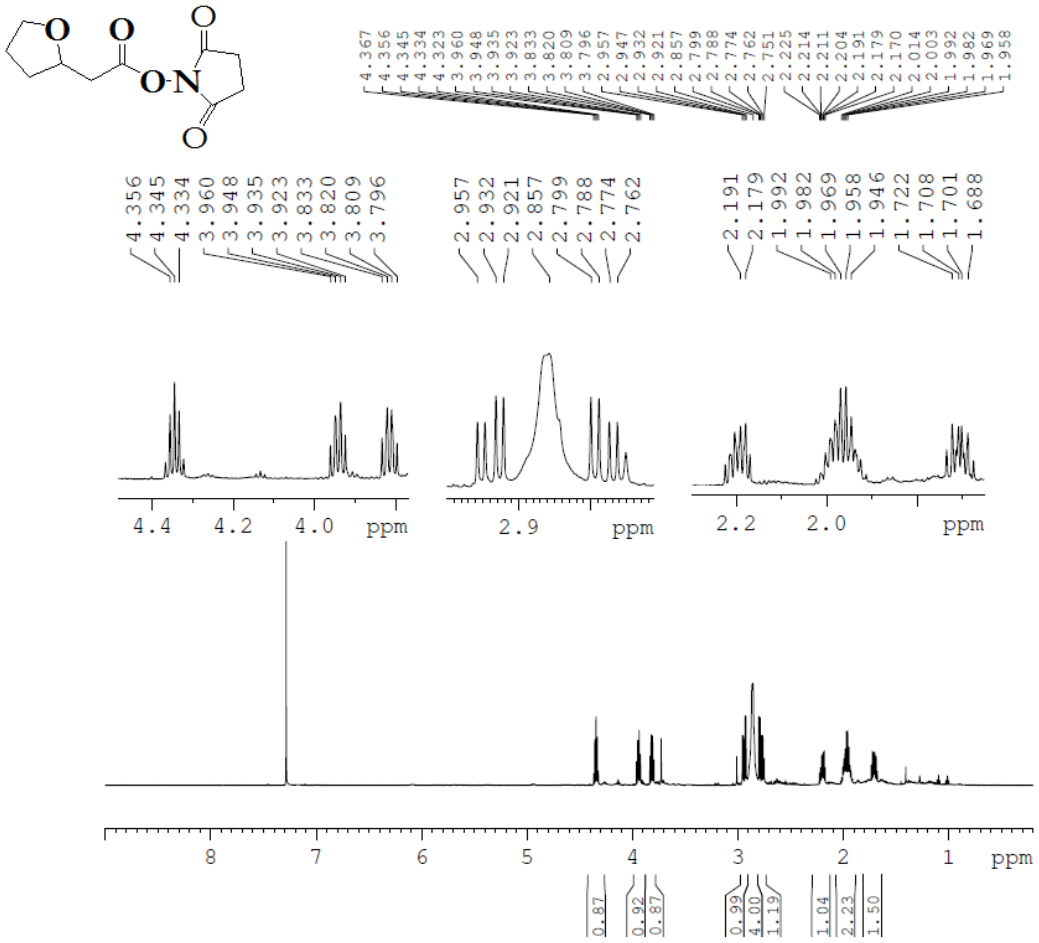

Figure A4. ^{1}H NMR of 2-tetrahydrofuranacetyl-succinimide ester in $CDCl_3$ at 600 MHz.

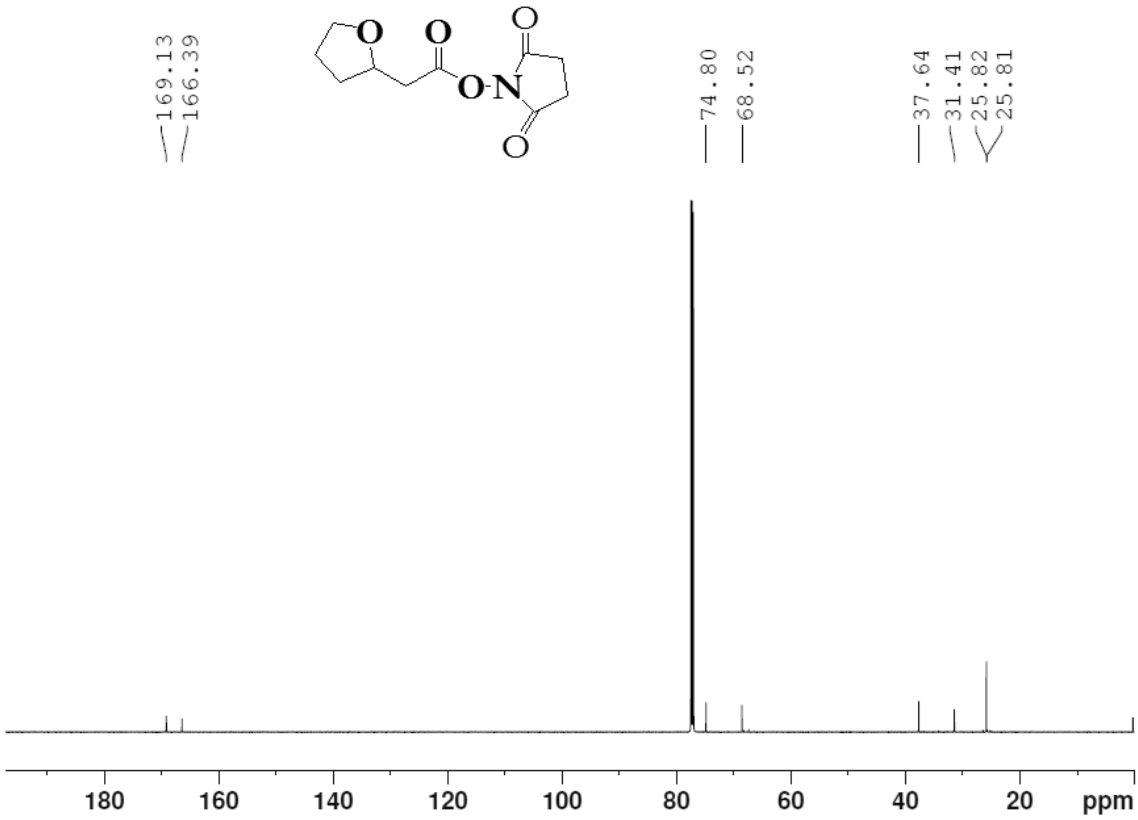

Figure A5. ^{13}C NMR of 2-tetrahydrofuranacetyl-succinimide ester in $CDCl_3$ at 600 MHz.

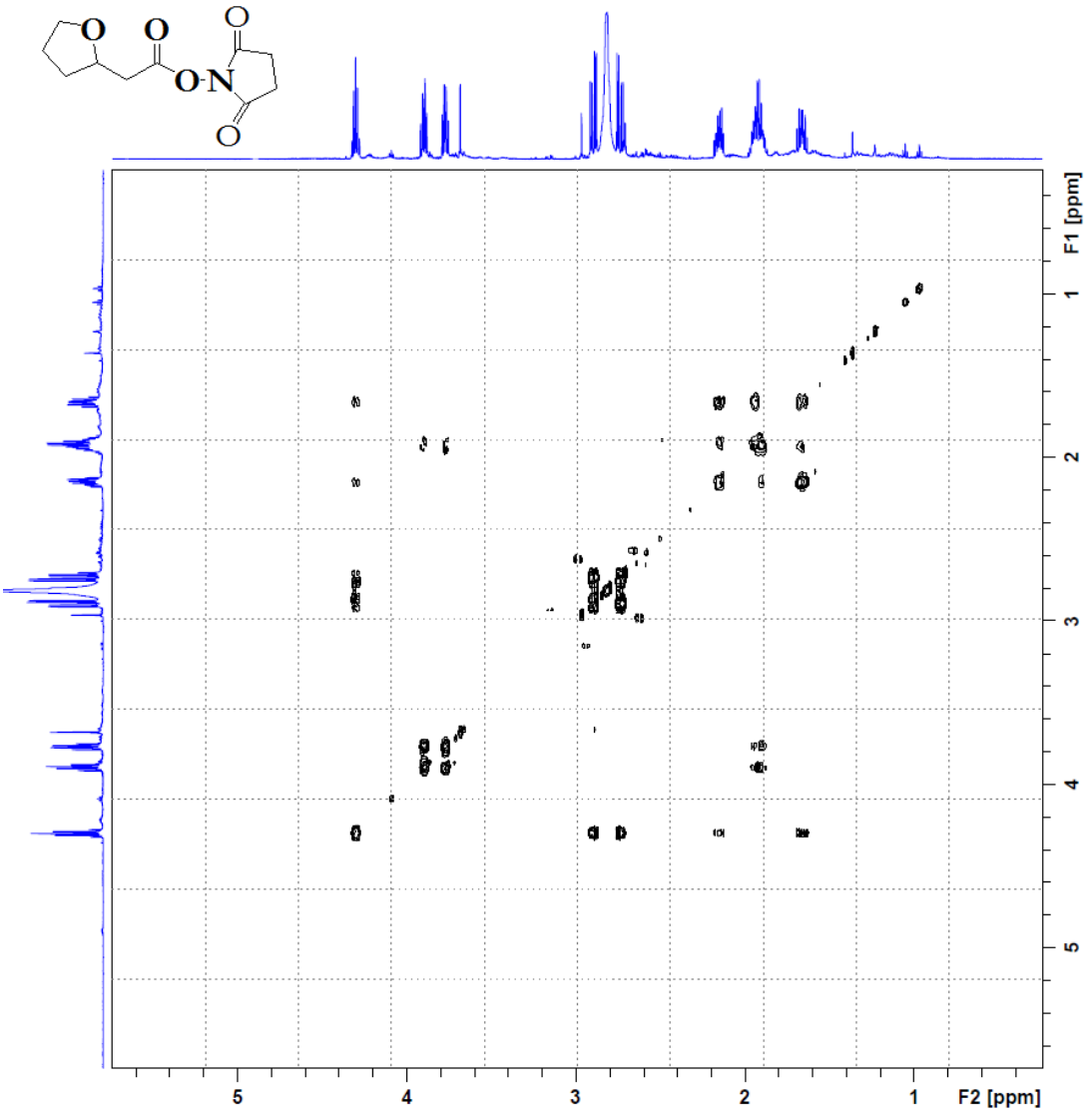

Figure A6. COSY of 2-tetrahydrofuranacetyl-succinimide ester in $CDCl_3$ at 600 MHz.

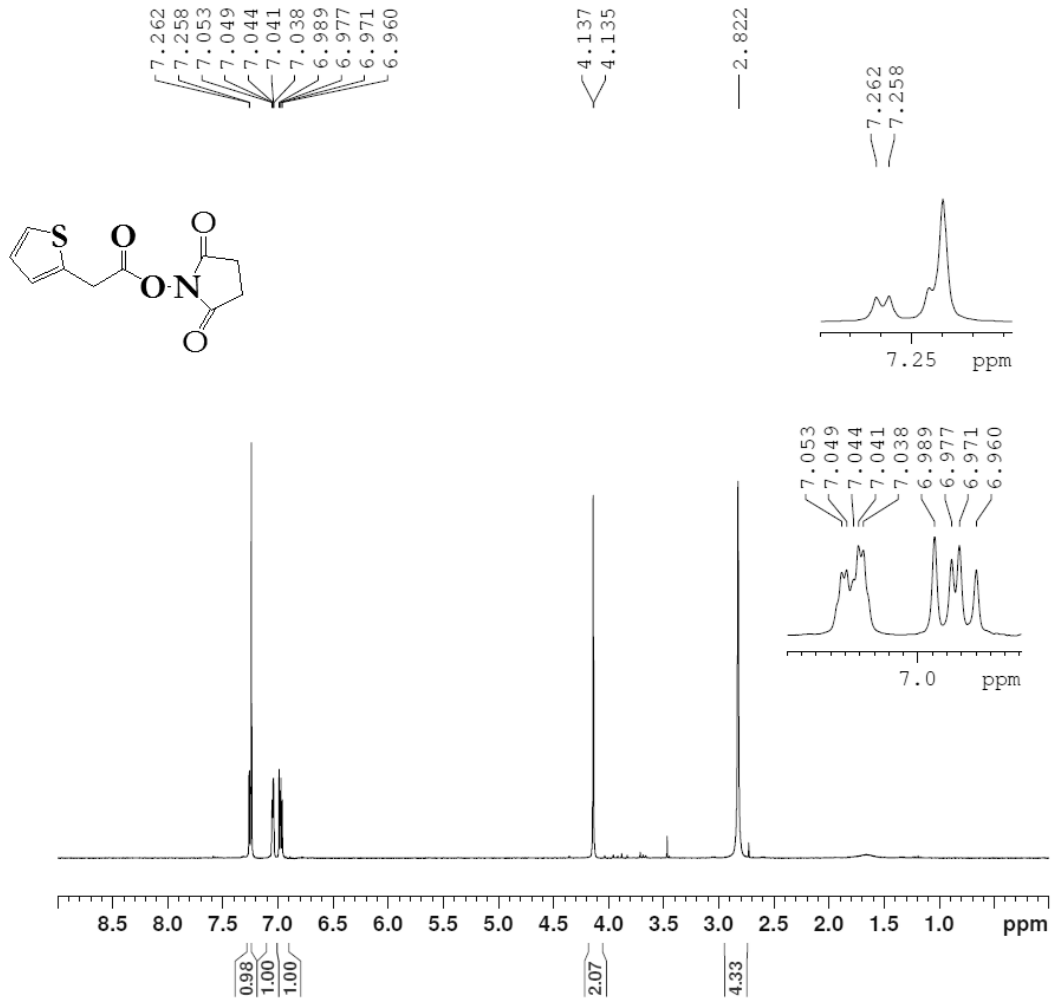

Figure A7. ^{1}H NMR of 2-thiopheneacetyl-succinimide ester in $CDCl_3$ at 300 MHz.

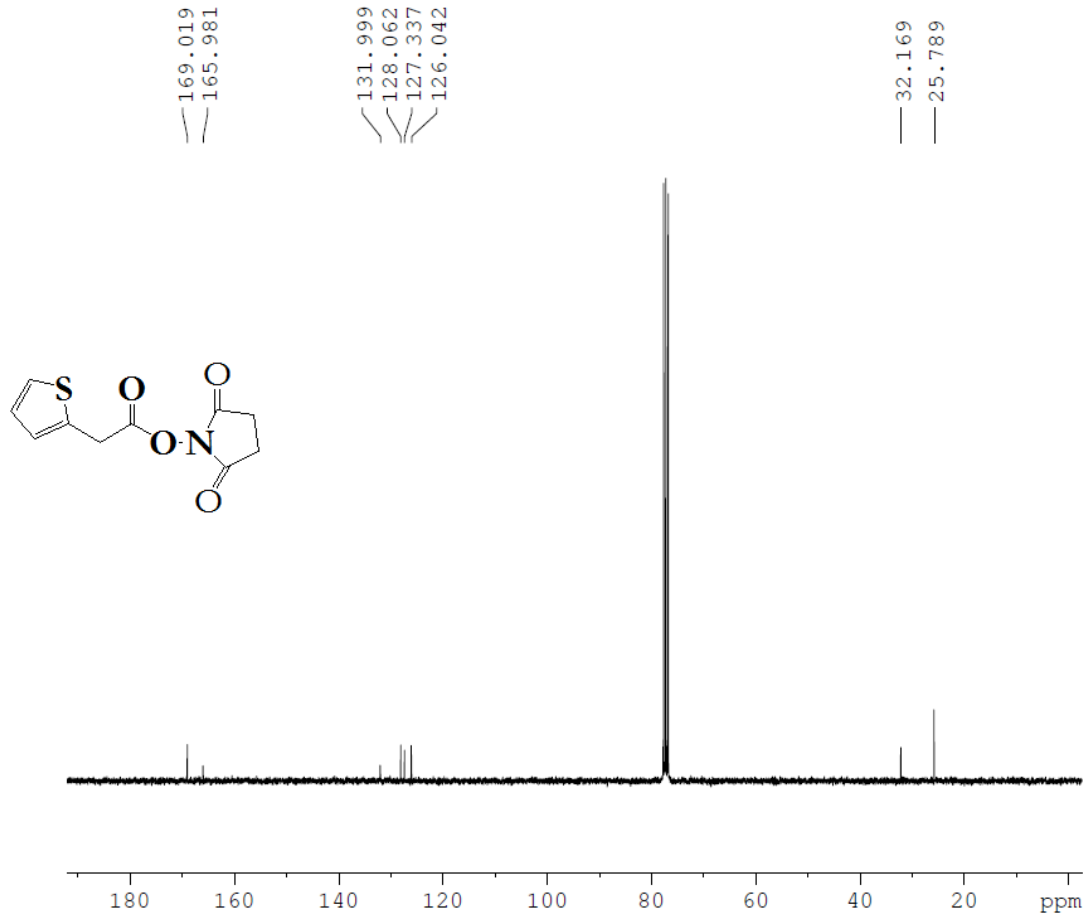

Figure A8. ^{13}C NMR of 2-thiopheneacetyl-succinimide ester in $CDCl_3$ at 300 MHz.

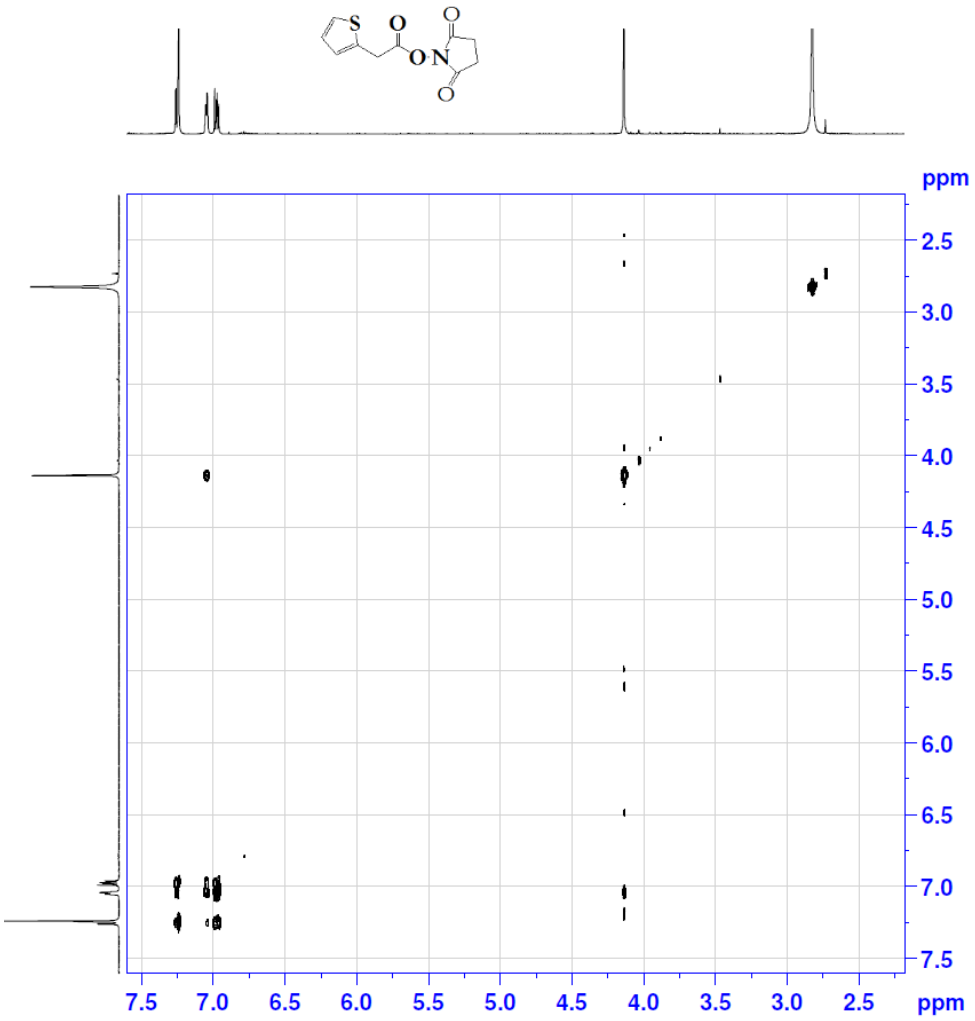

Figure A9. COSY of 2-thiopheneacetyl-succinimide ester in $CDCl_3$ at 300 MHz.

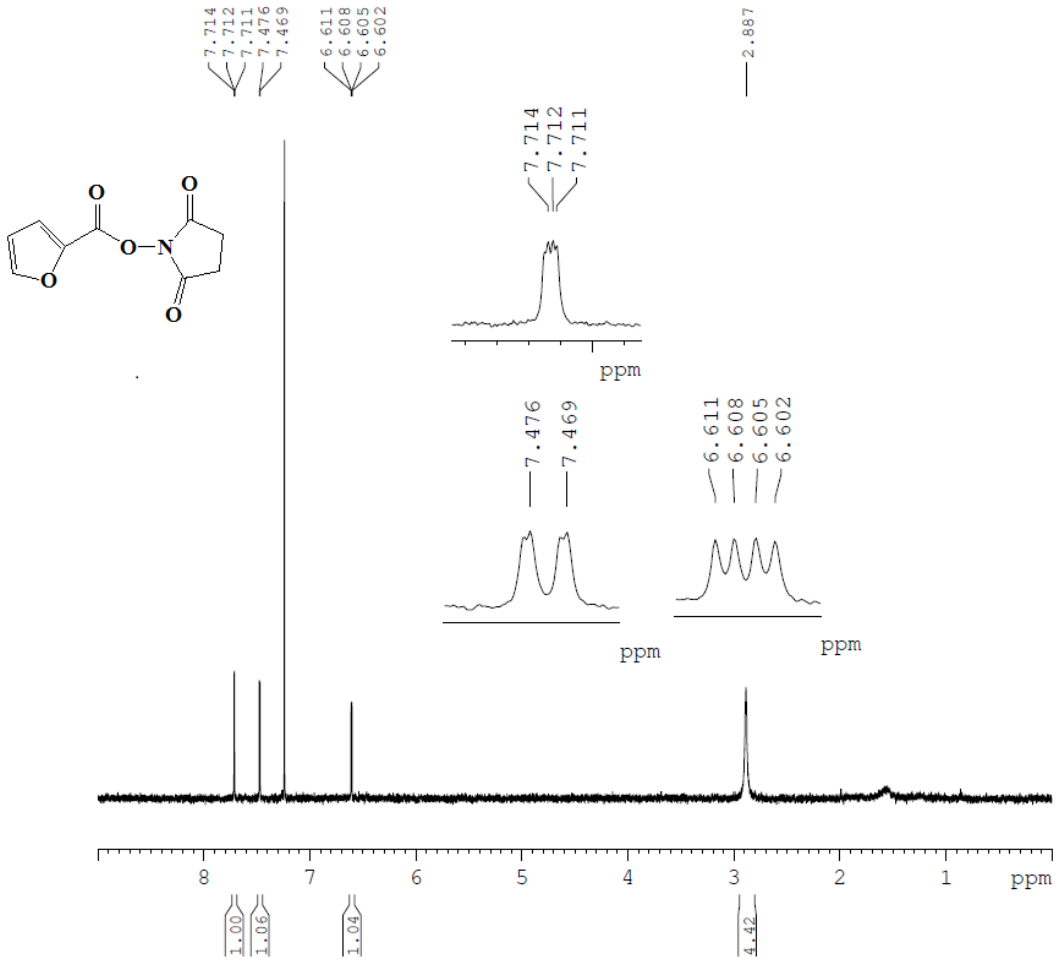

Figure A10. ^{1}H NMR of 2-furoyl-succinimide ester in $CDCl_3$ at 600 MHz.

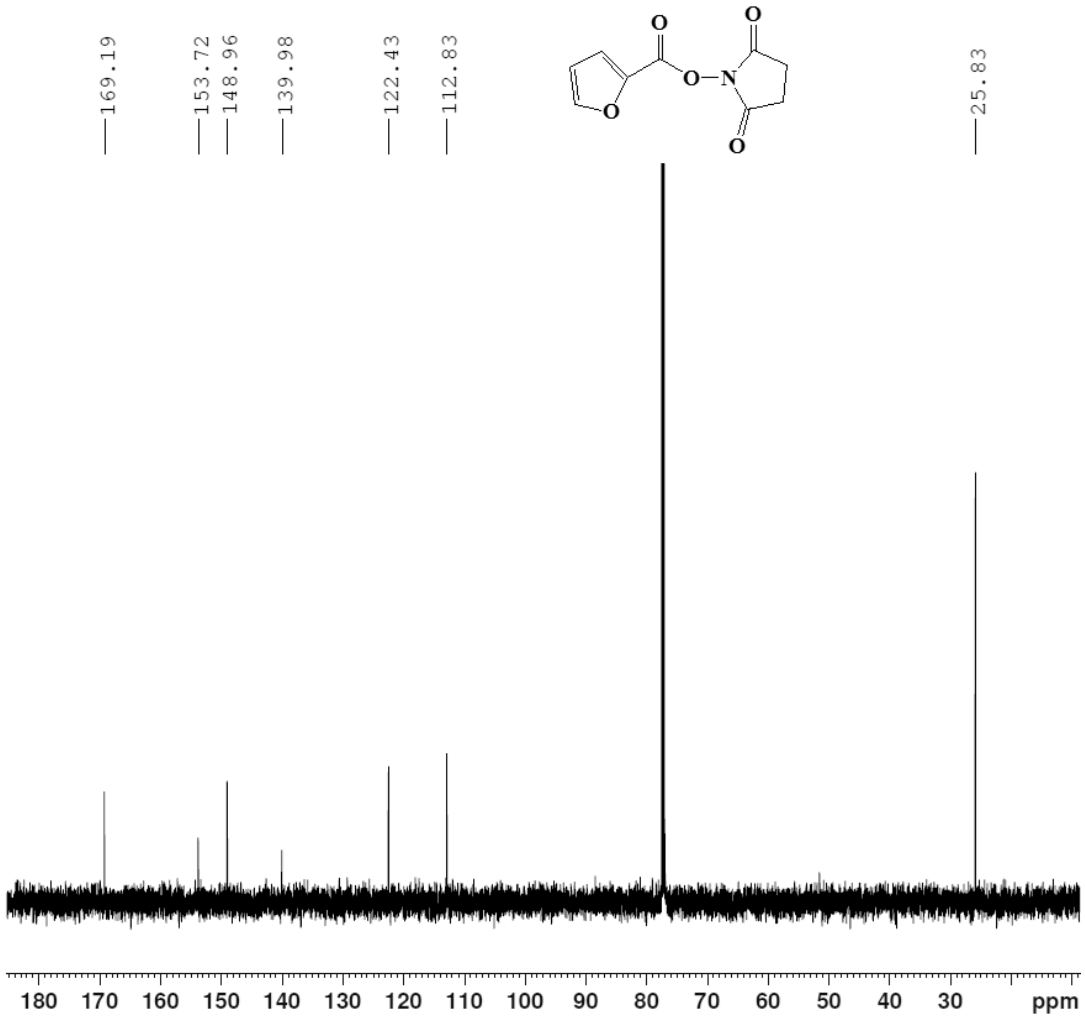

Figure A11. **^{13}C NMR of 2-furoyl-succinimide ester in $CDCl_3$ at 600 MHz.**

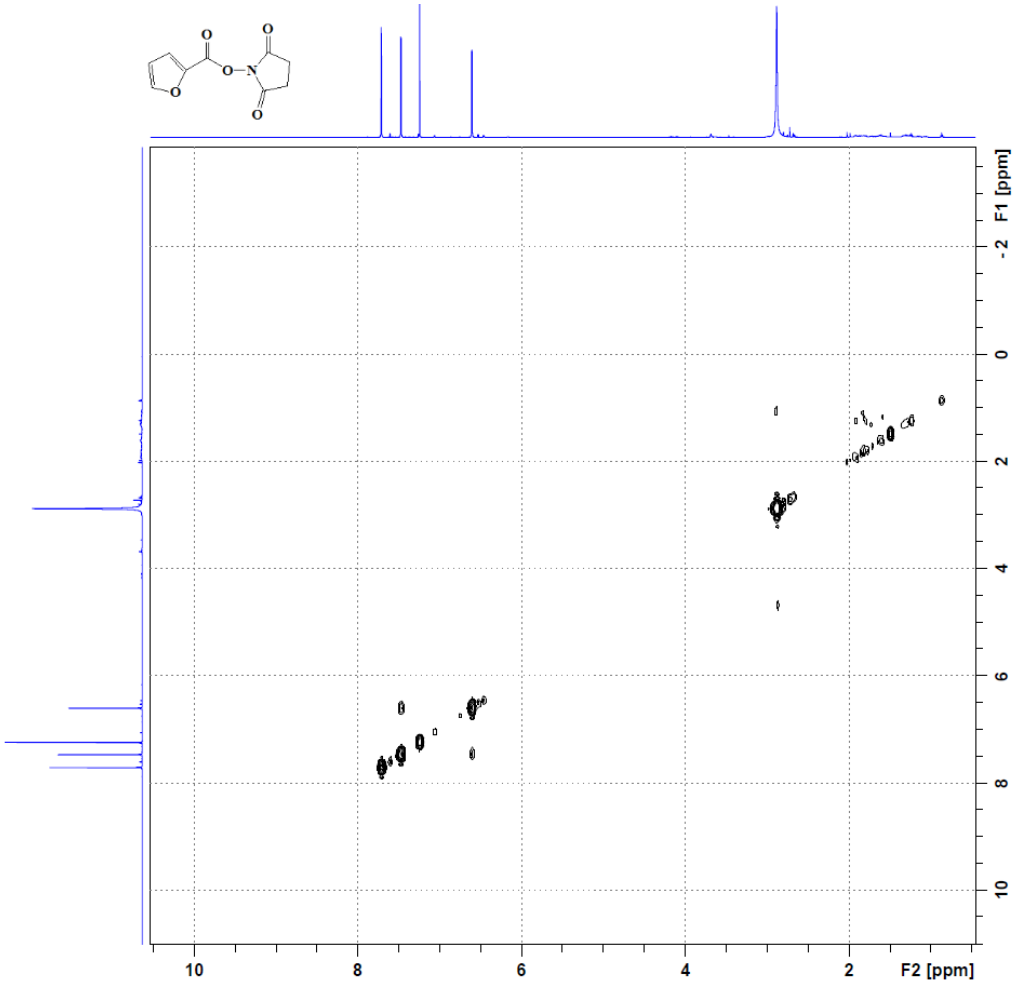

Figure A12. COSY of 2-furoyl-succinimide ester in $CDCl_3$ at 600 MHz.

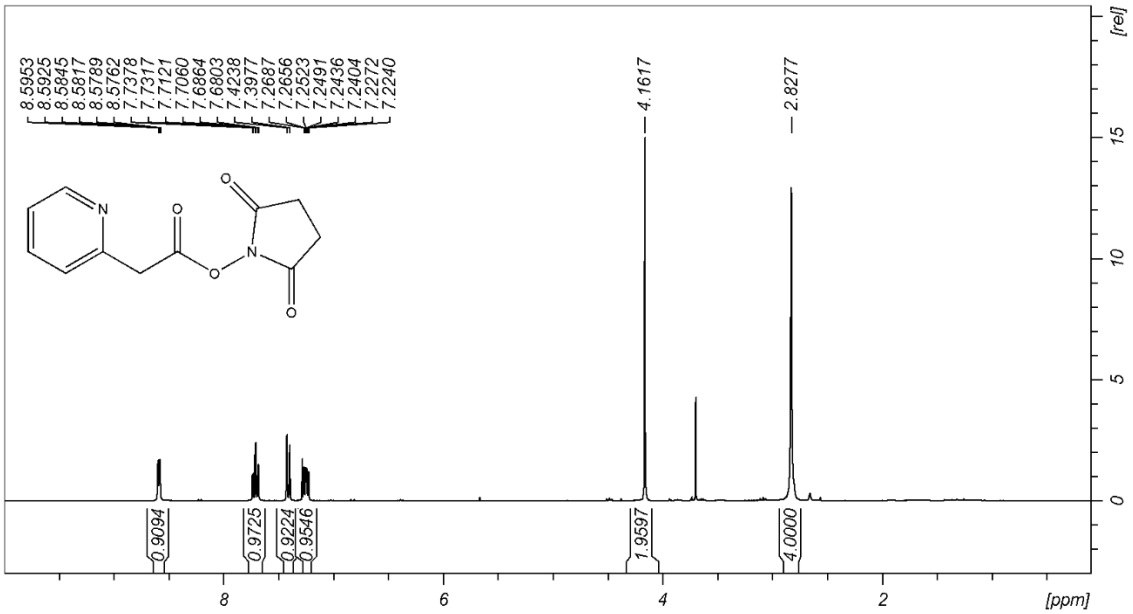

Figure A13. ^{1}H NMR of 2-pyridylacetyl-succinimide ester in $CDCl_3$ at 600 MHz.

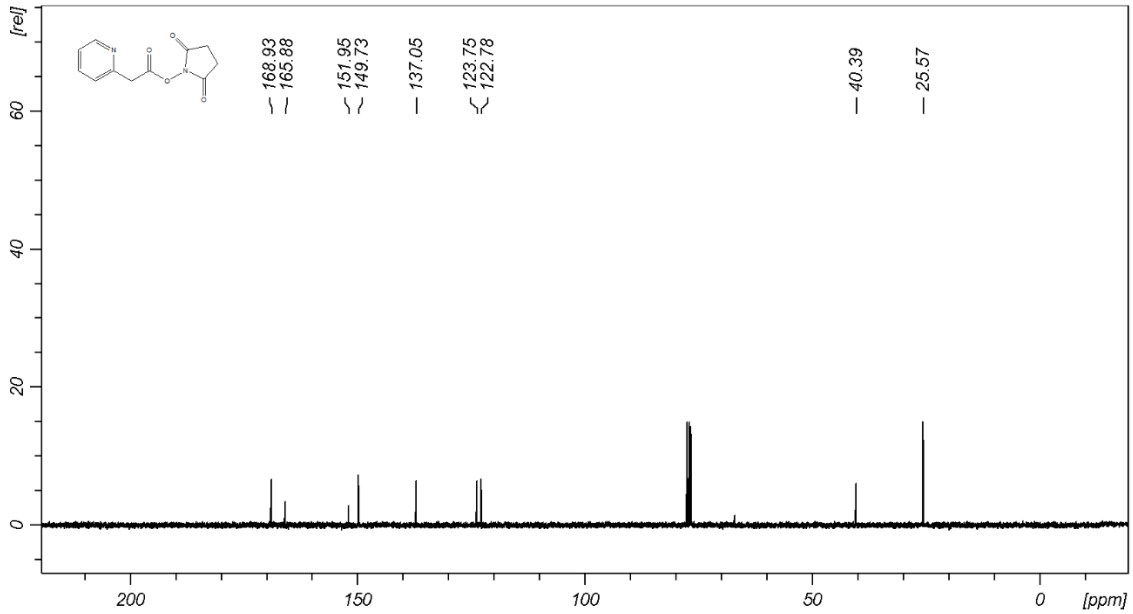

Figure A14. ^{13}C NMR of 2-pyridylacetyl-succinimide ester in $CDCl_3$ at 600 MHz.

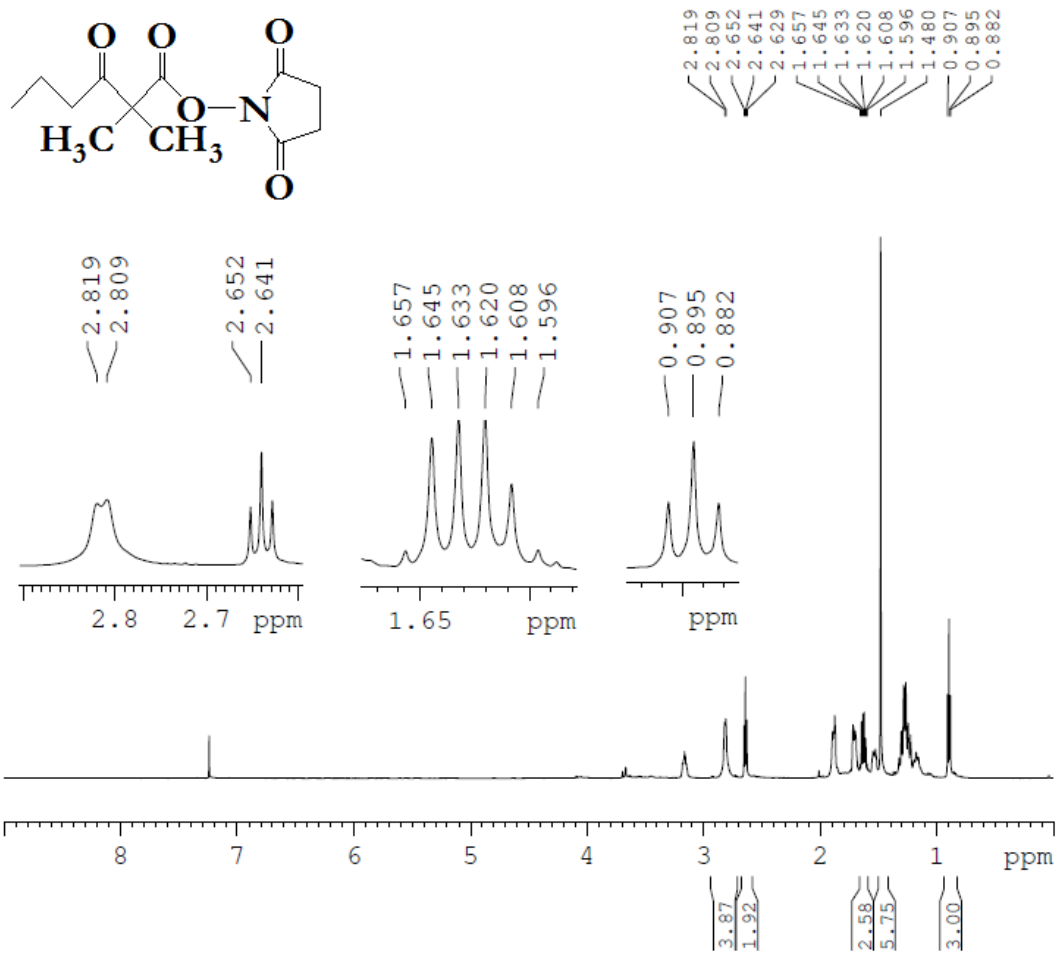

Figure A15. ^{1}H NMR of 2,2´-dimethyl-3-oxohexanoyl-succinimide ester in $CDCl_3$ at 600 MHz.

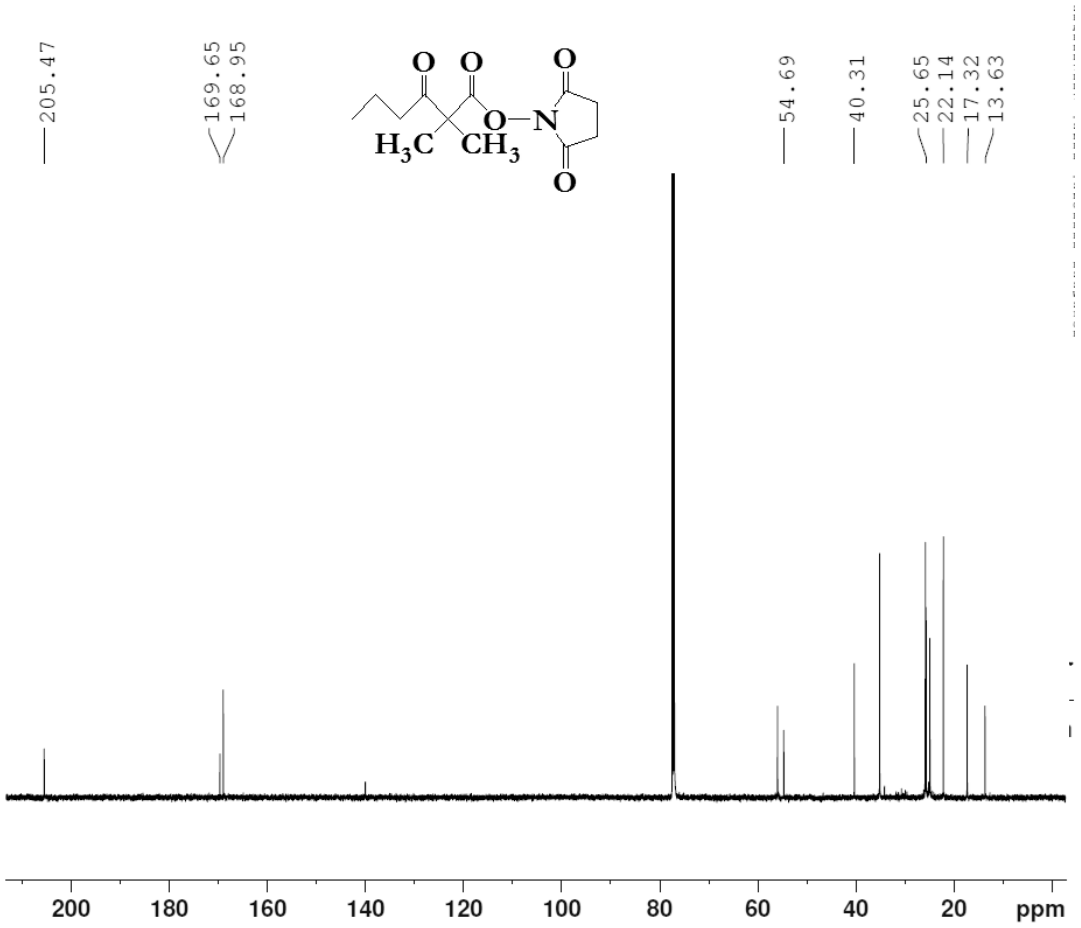

Figure A16. ^{13}C NMR of 2,2´-dimethyl-3-oxohexanoyl-succinimide ester in $CDCl_3$ at 600 MHz.

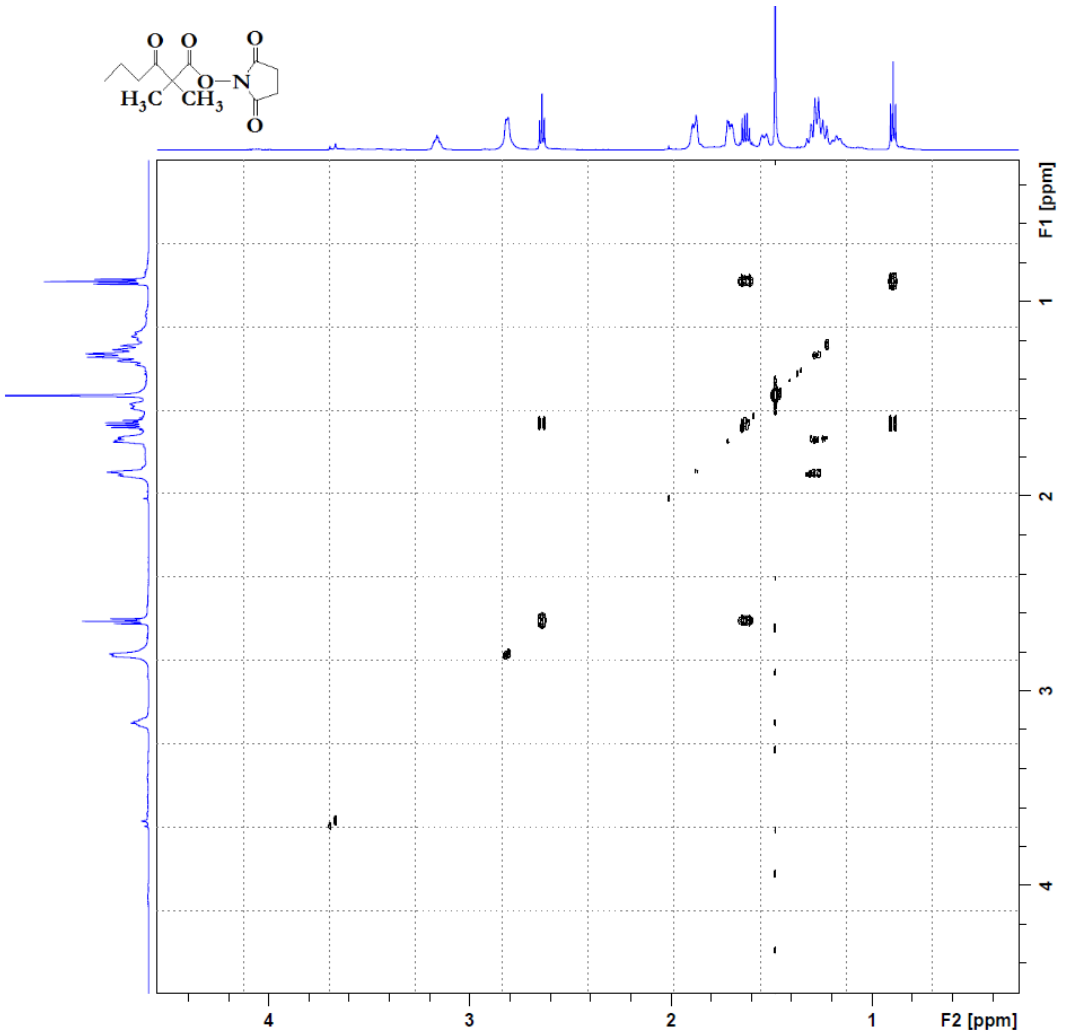

Figure A17. COSY of 2,2´-dimethyl-3-oxohexanoyl-succinimide ester in $CDCl_3$ at 600 MHz.

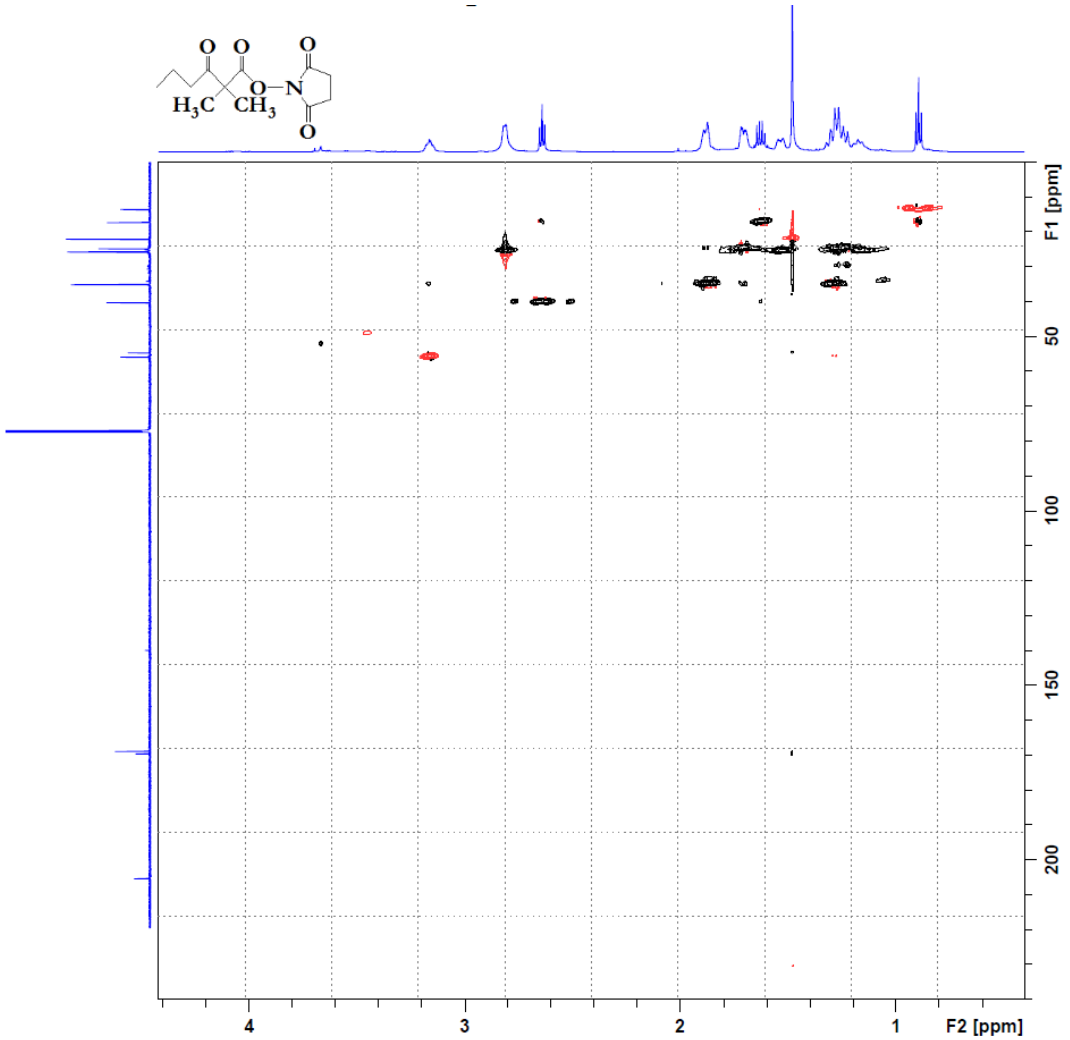

Figure A18. HSQC of 2,2´-dimethyl-3-oxohexanoyl-succinimide ester in $CDCl_3$ at 600 MHz.

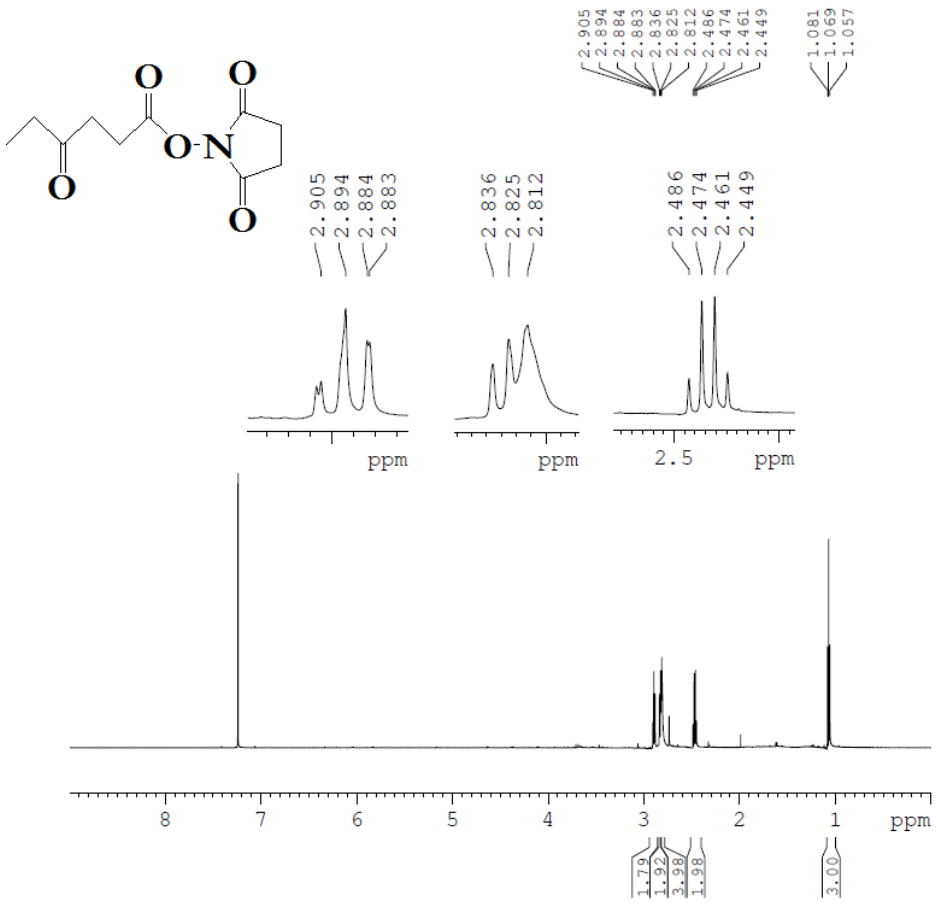

Figure A19. ^{1}H NMR of 4-oxohexanoyl-succinimide ester in $CDCl_3$ at 600 MHz.

.

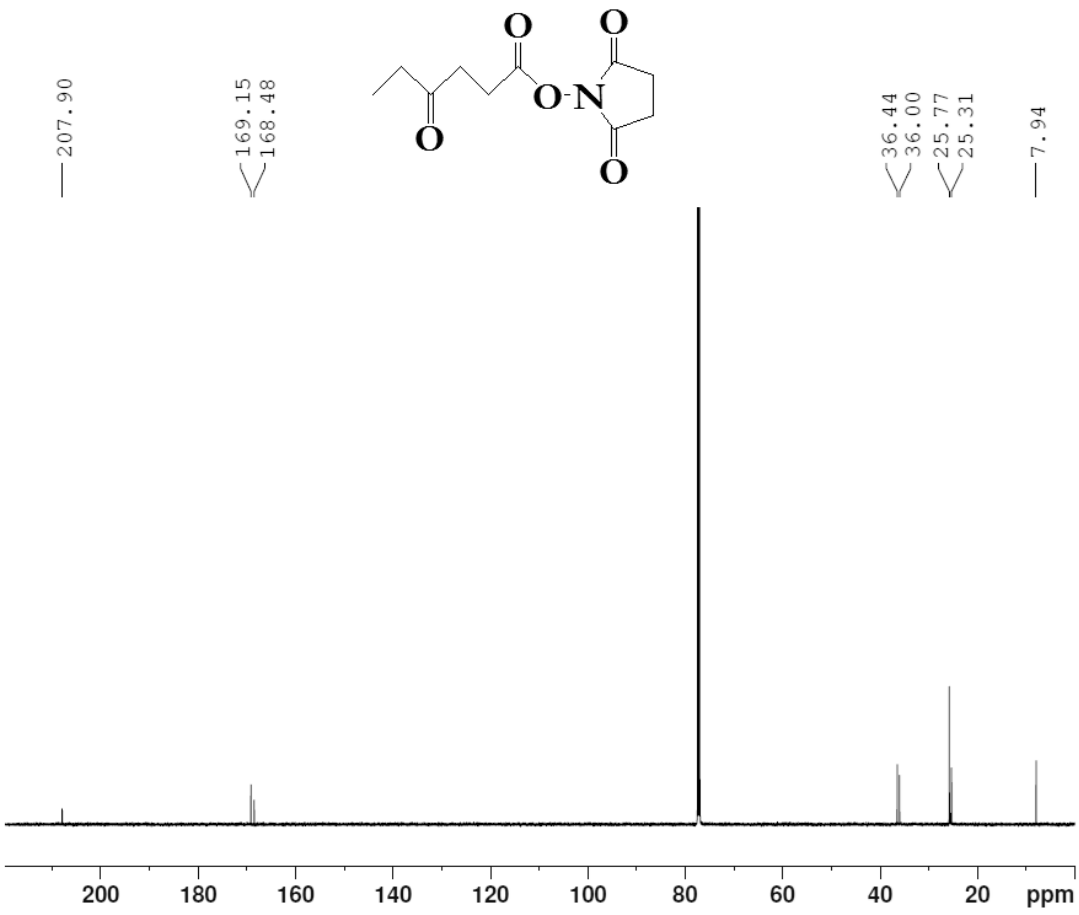

Figure A20. ^{13}**C NMR of 4-oxohexanoyl-succinimide ester in** $CDCl_3$ **at 600 MHz.**

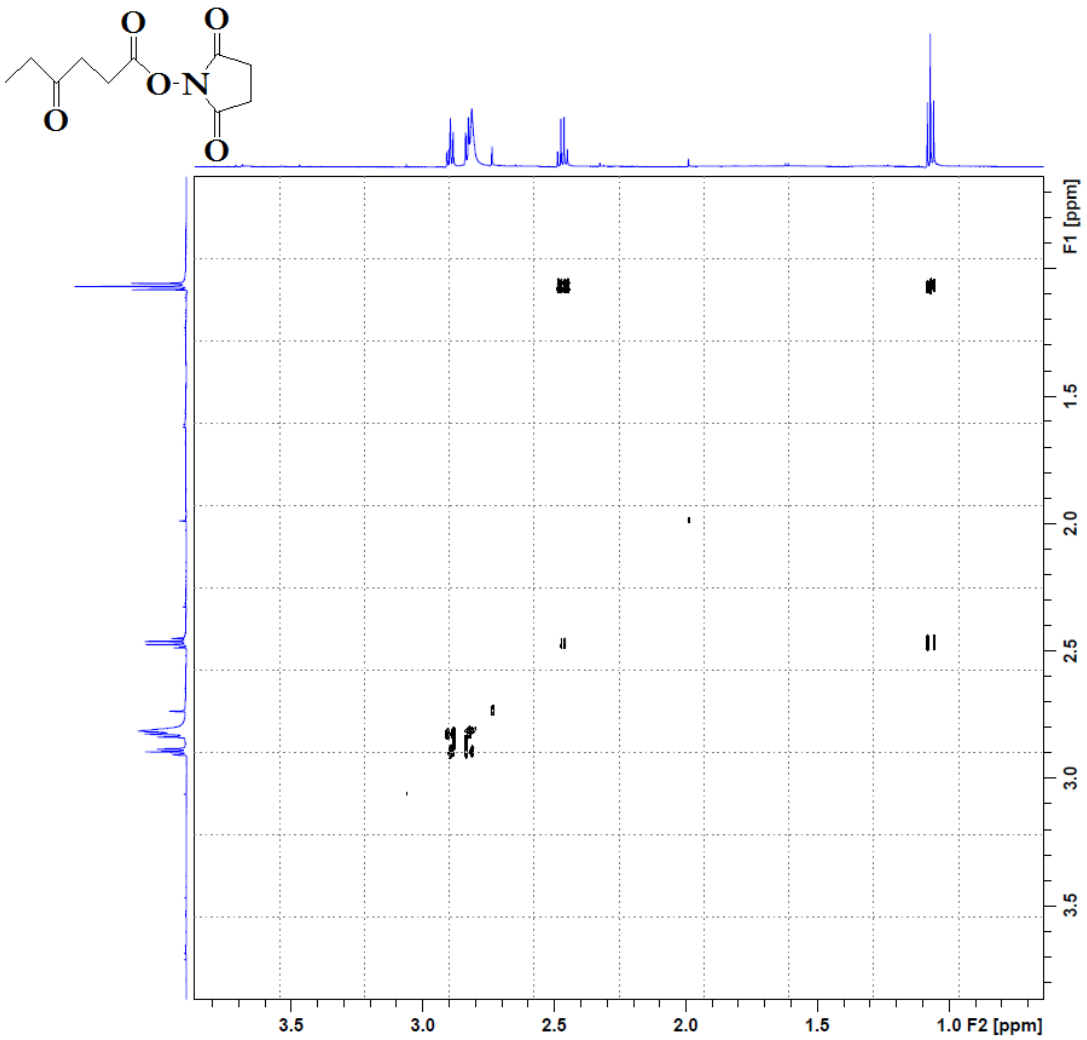

Figure A21. COSY of 4-oxohexanoyl-succinimide ester in $CDCl_3$ at 600 MHz.

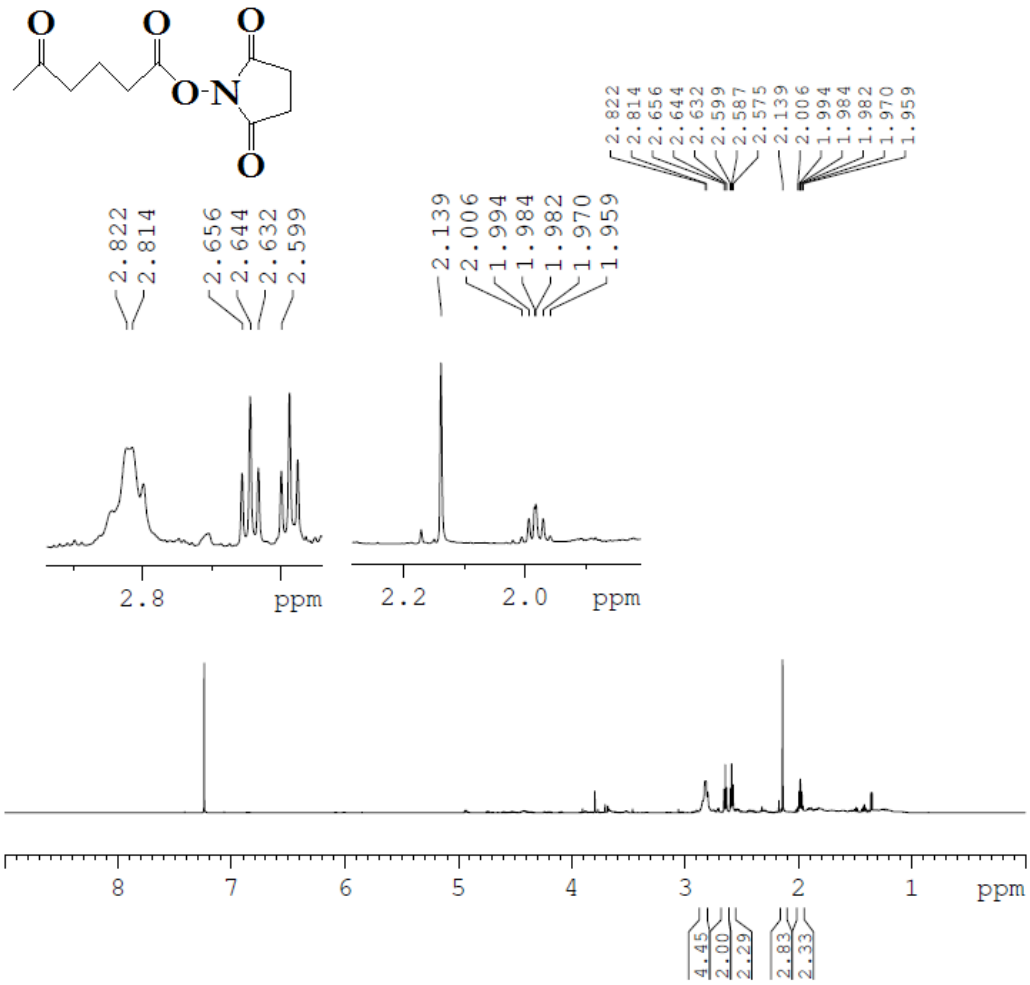

Figure A22. ^{1}H NMR of 5-oxohexanoyl-succinimide ester in $CDCl_3$ at 600 MHz.

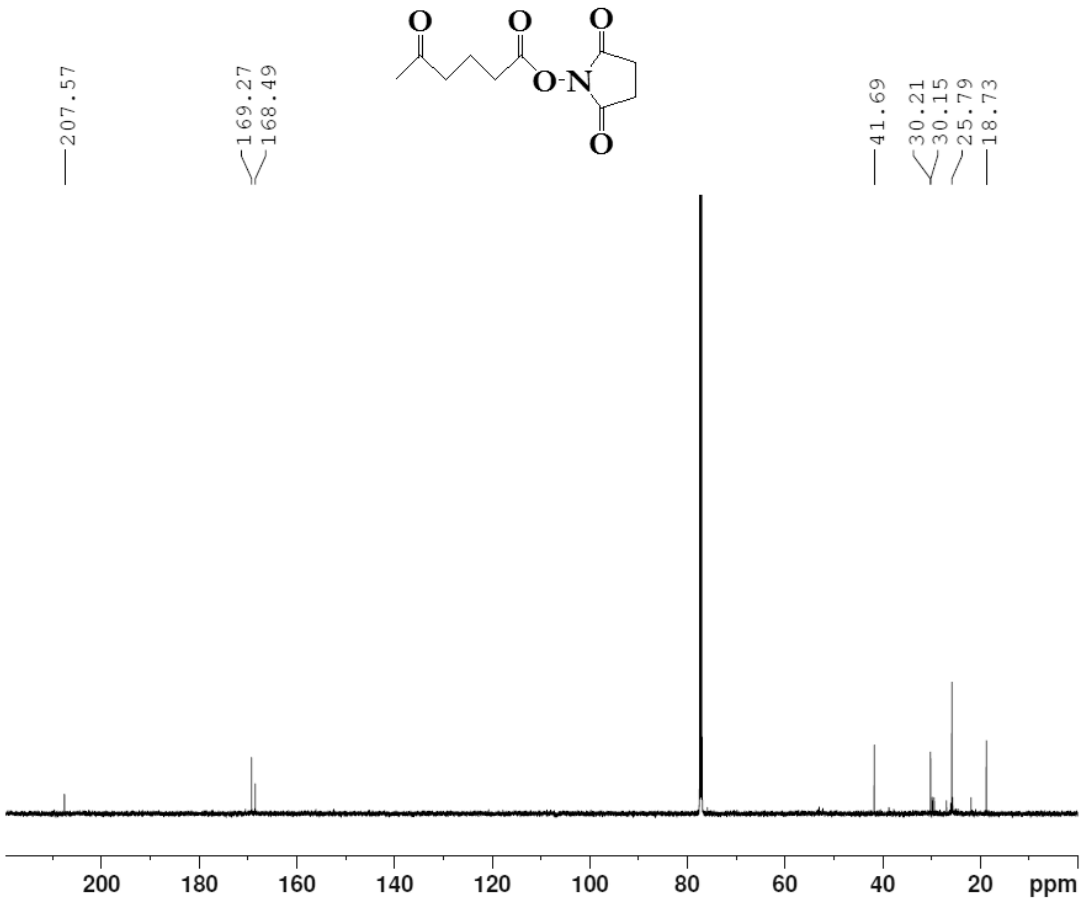

Figure A23. ^{13}**C NMR of 5-oxohexanoyl-succinimide ester in** $CDCl_3$ **at 600 MHz.**

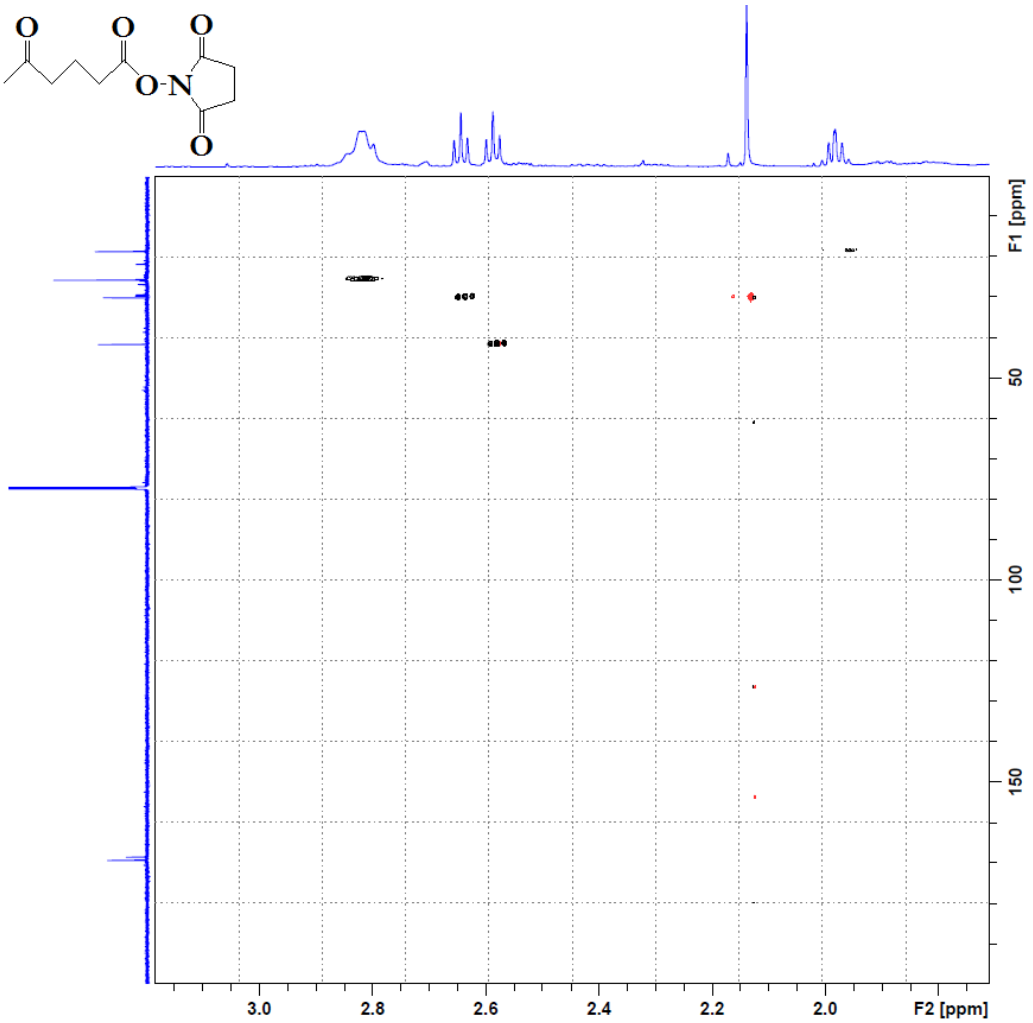

Figure A24. HSQC of 5-oxohexanoyl-succinimide ester in $CDCl_3$ at 600 MHz.

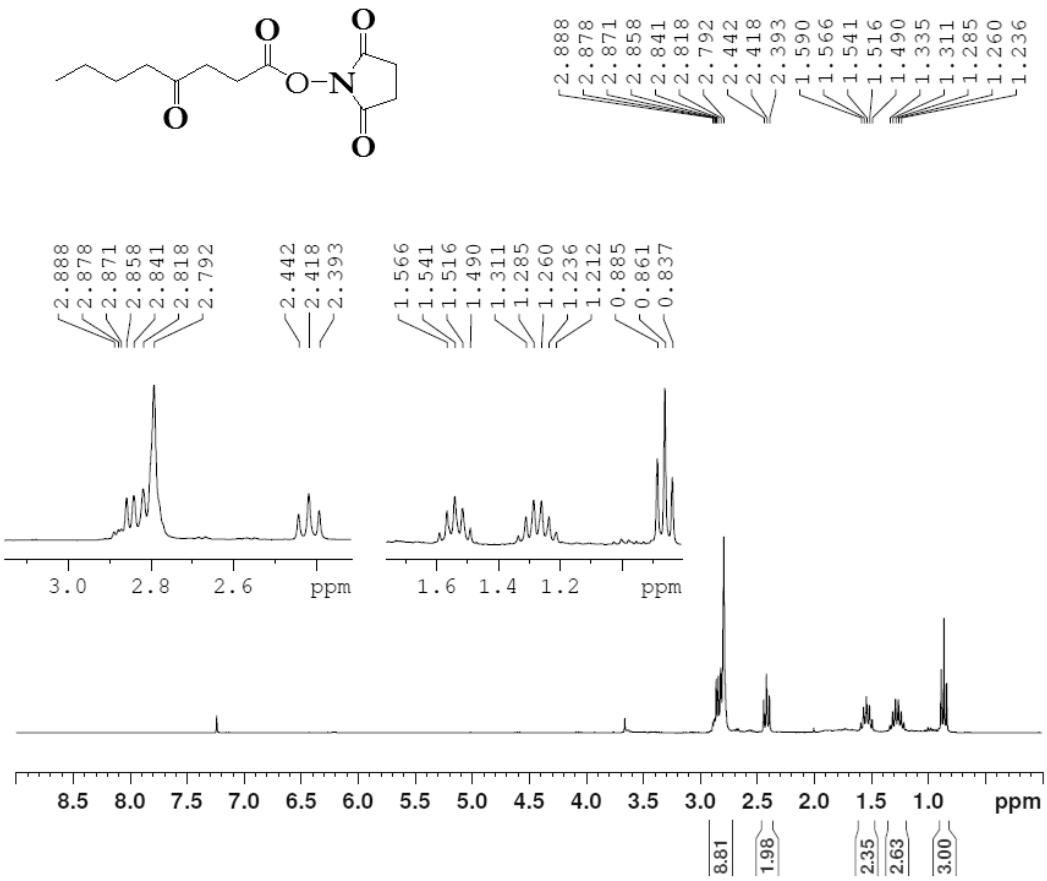

Figure A25. ^{1}H NMR of 4-oxooctanoyl-succinimide ester in $CDCl_3$ at 300 MHz.

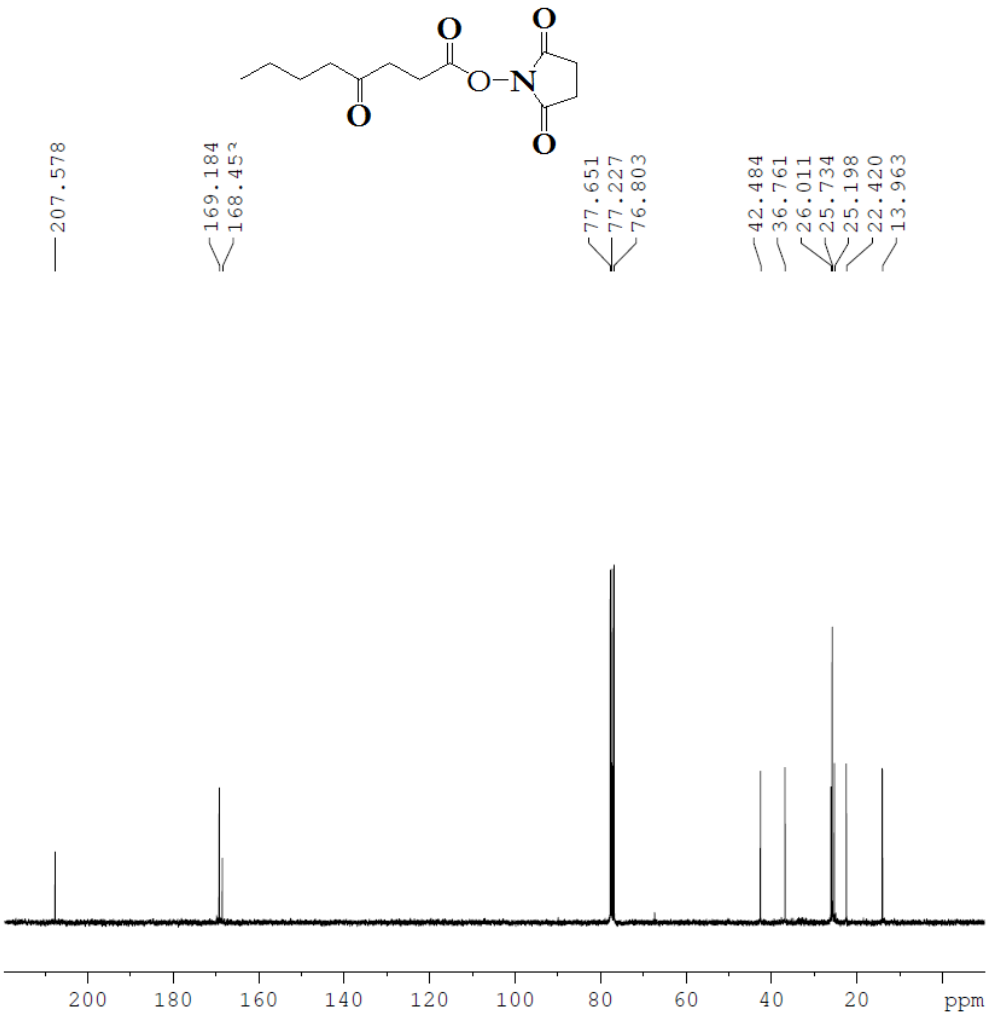

Figure A26. ^{13}C NMR of 4-oxooctanoyl-succinimide ester in $CDCl_3$ at 300 MHz.

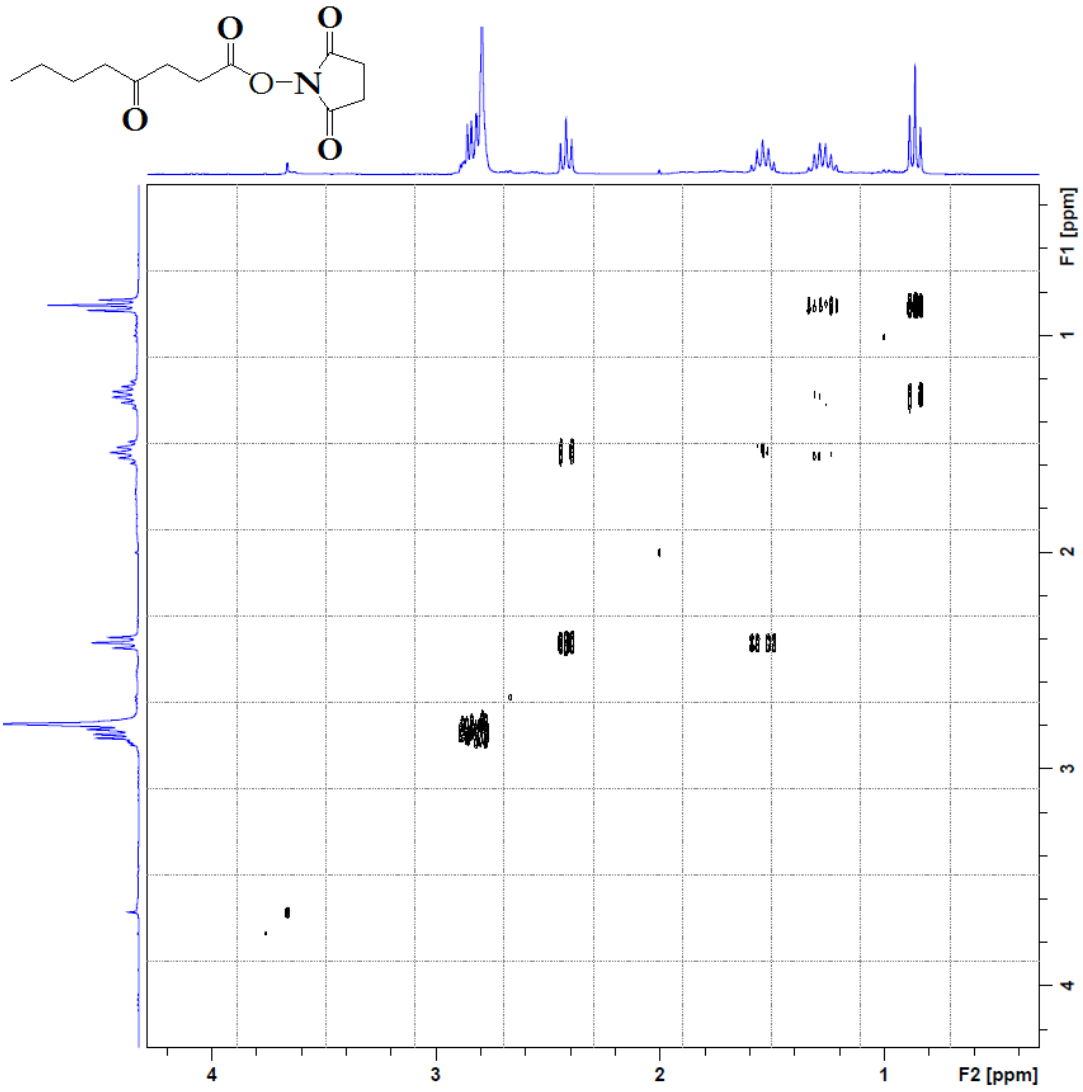

Figure A27. COSY of 4-oxooctanoyl-succinimide ester in $CDCl_3$ at 300 MHz.

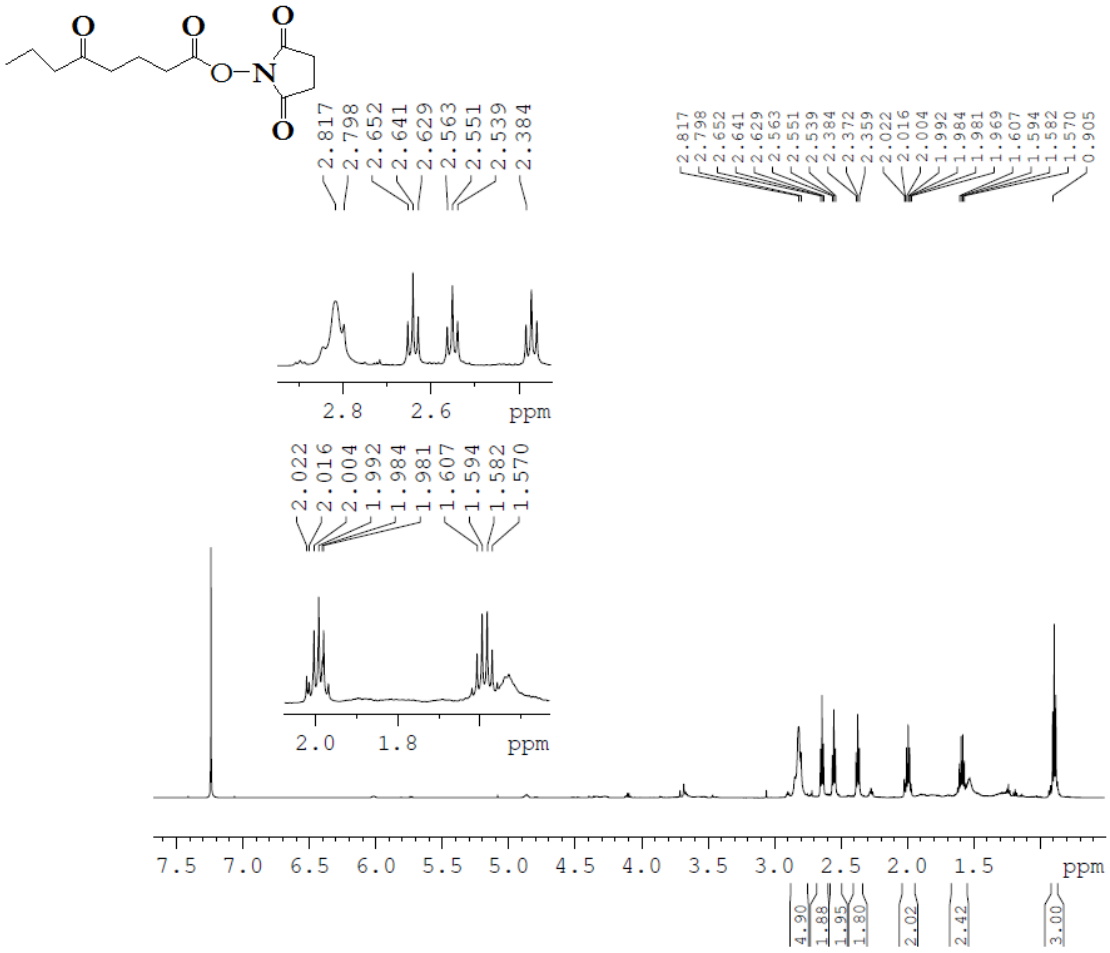

Figure A28. ^{1}H NMR of 5-oxooctanoyl-succinimide ester in $CDCl_3$ at 600 MHz.

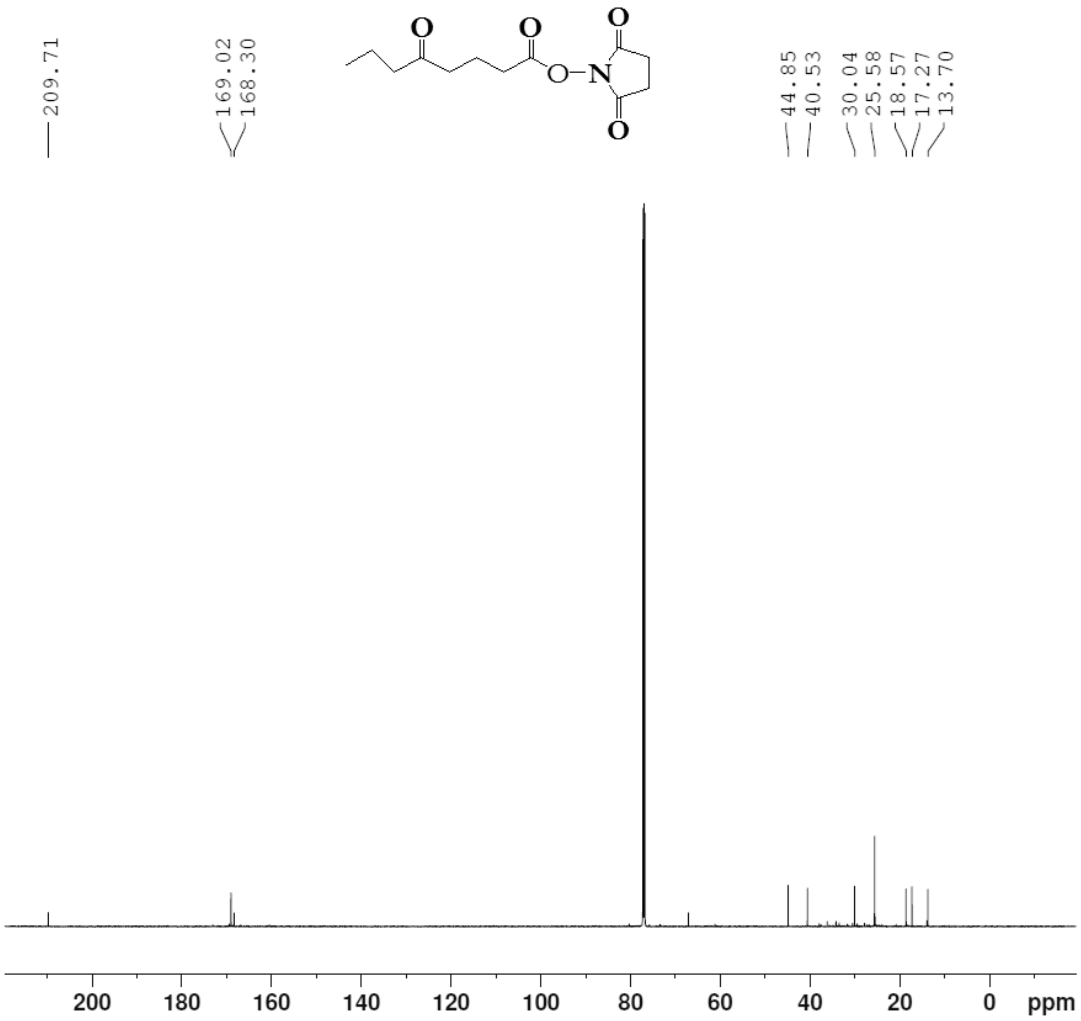

Figure A29. ^{13}C NMR of 5-oxooctanoyl-succinimide ester in $CDCl_3$ at 600 MHz.

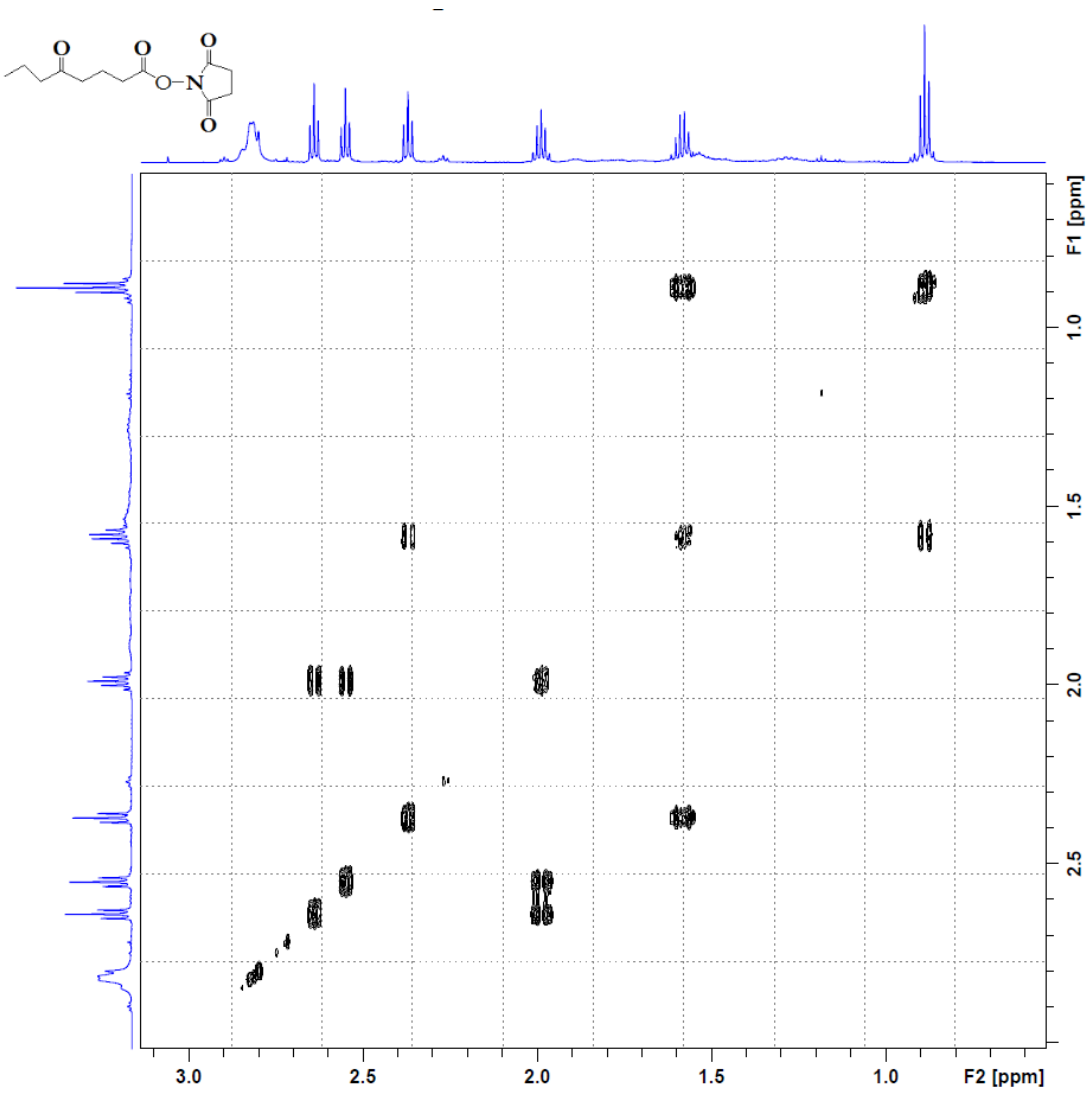

Figure A30. COSY of 5-oxooctanoyl-succinimide ester in $CDCl_3$ at 600 MHz.

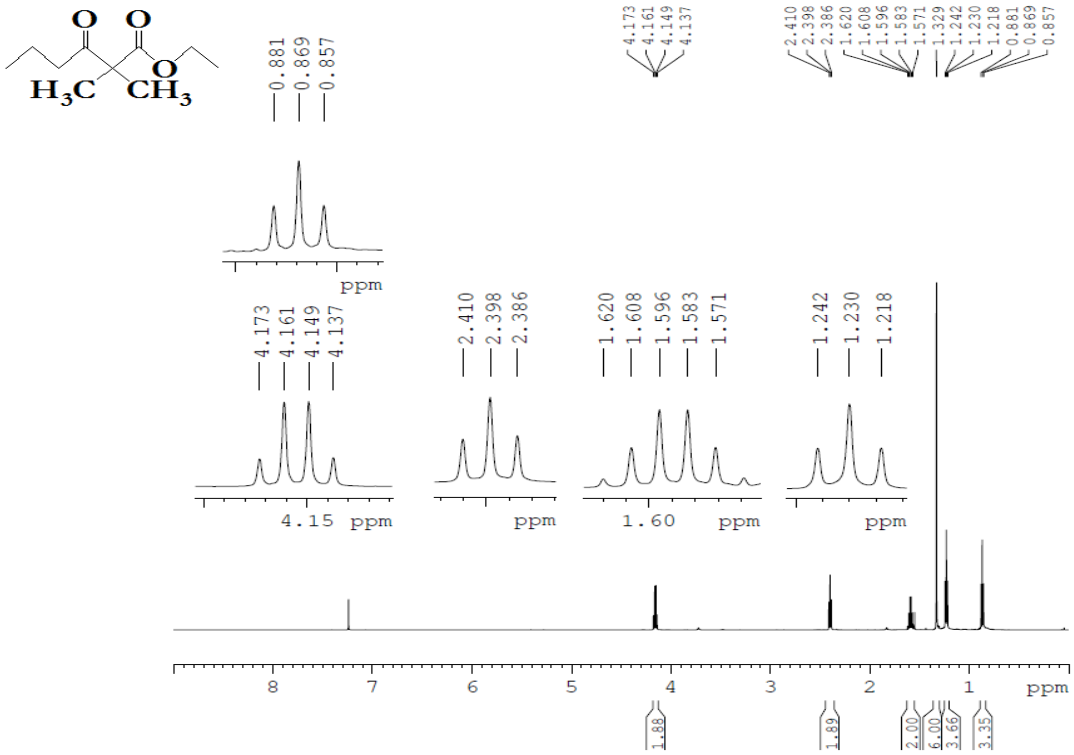

Figure A31. ^{1}H NMR of ethyl-2,2´-dimethyl-3-oxohexanoate in $CDCl_3$ at 600 MHz.

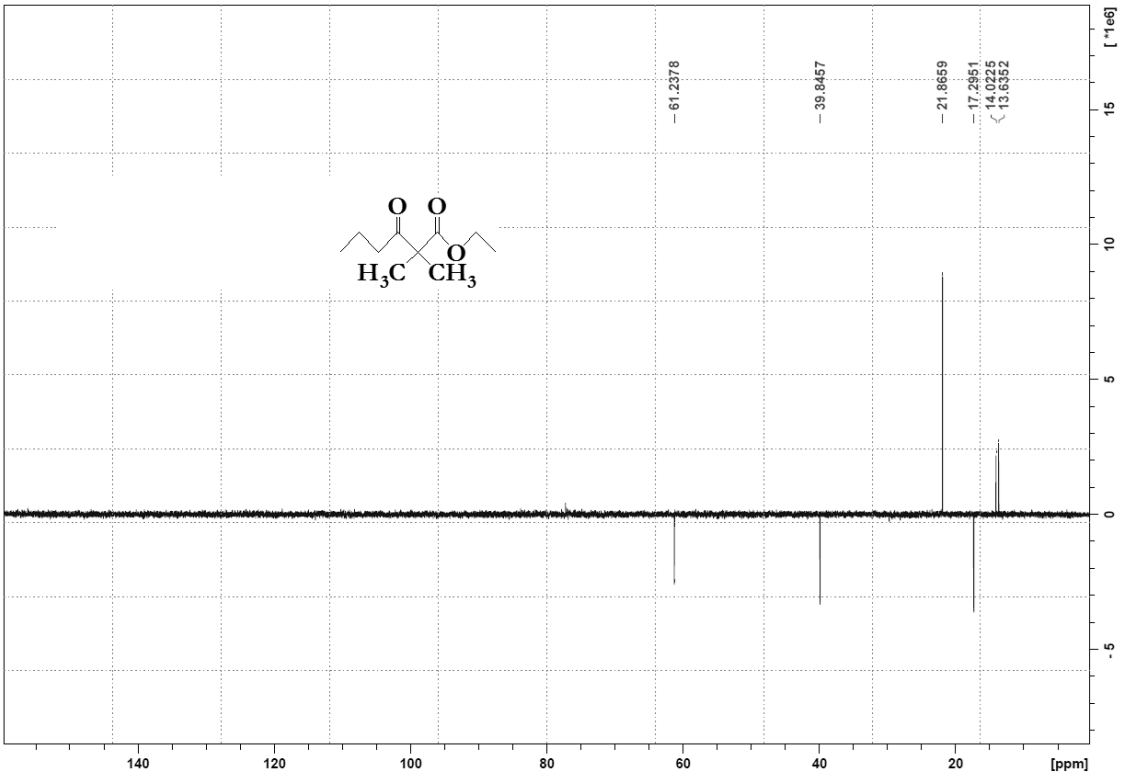

Figure A32. DEPT-135 NMR of ethyl-2,2´-dimethyl-3-oxohexanoate in $CDCl_3$ at 600 MHz.

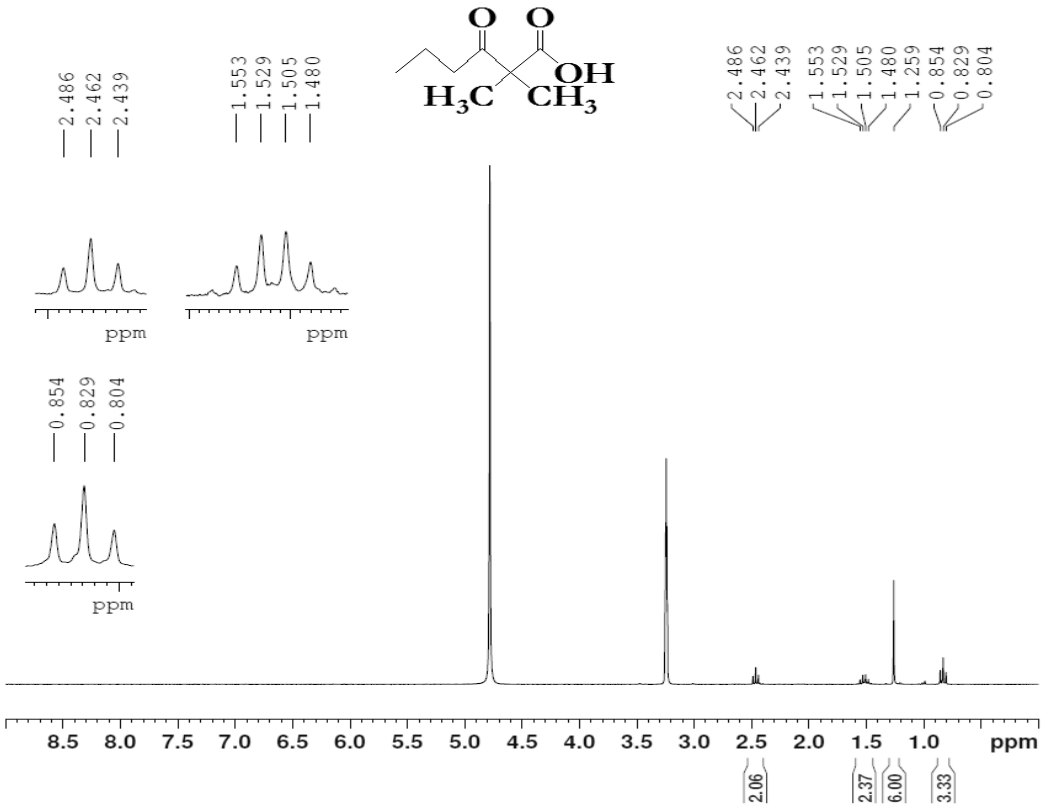

Figure A33. ^{1}H NMR of 2,2´-dimethyl-3-oxohexanoic acid in MeOD-d$_4$ at 300 MHz.

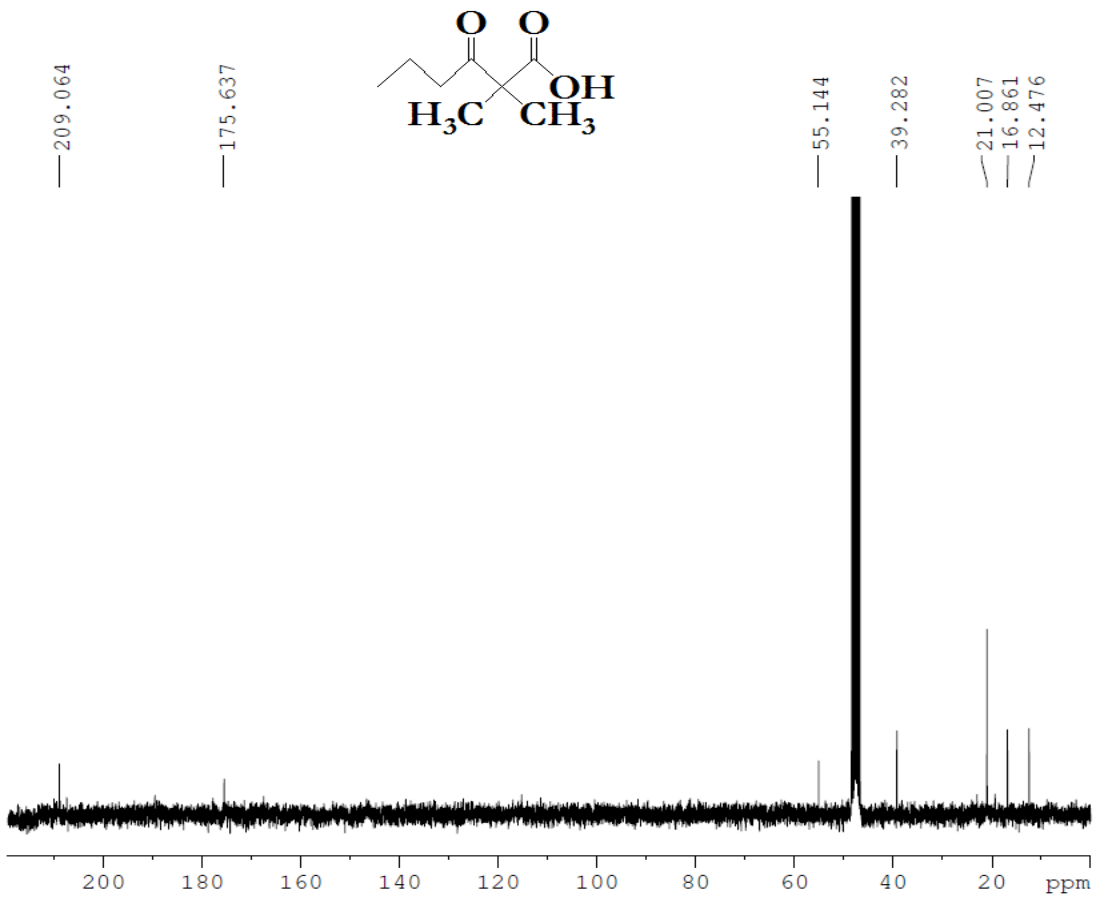

Figure A34. ^{13}C NMR of 2,2´-dimethyl-3-oxohexanoic acid in MeOD-d$_4$ at 300 MHz.

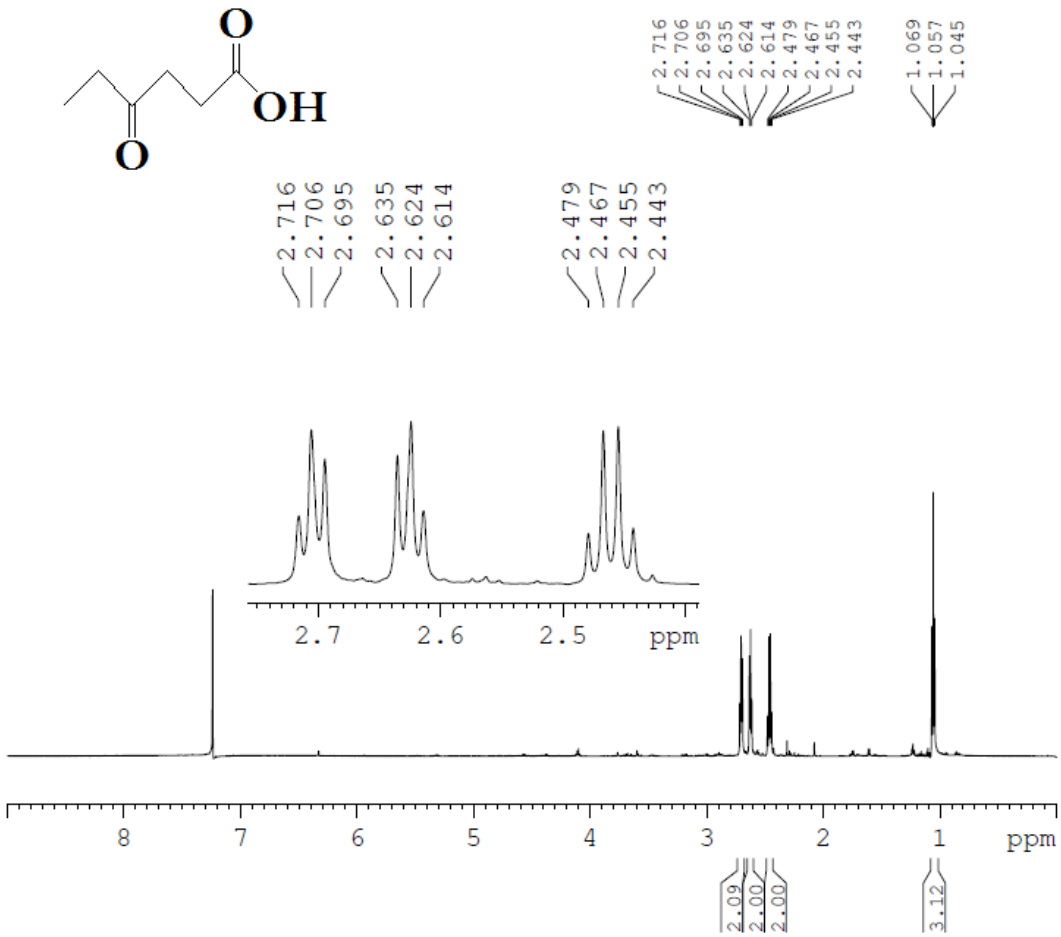

Figure A35. ^{1}H NMR of 4-oxohexanoic acid in $CDCl_3$ at 600 MHz.

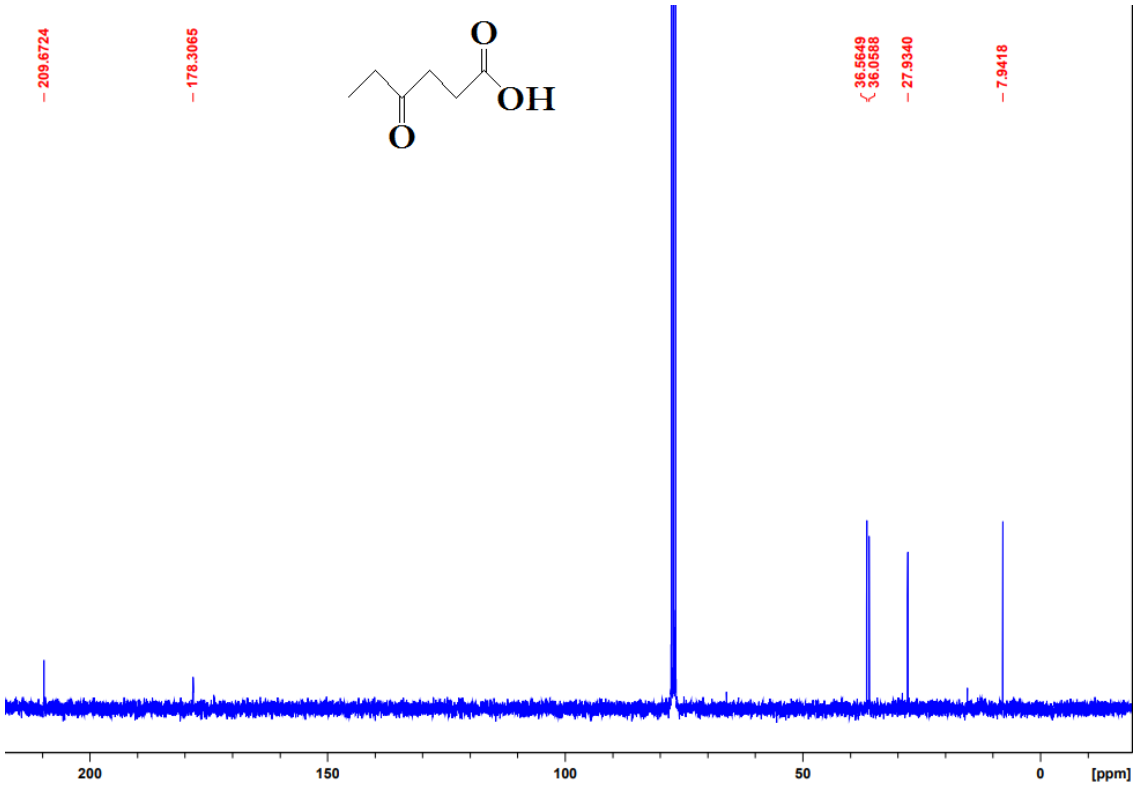

Figure A36. ^{13}**C NMR of 4-oxohexanoic acid in** $CDCl_3$ **at 600 MHz.**

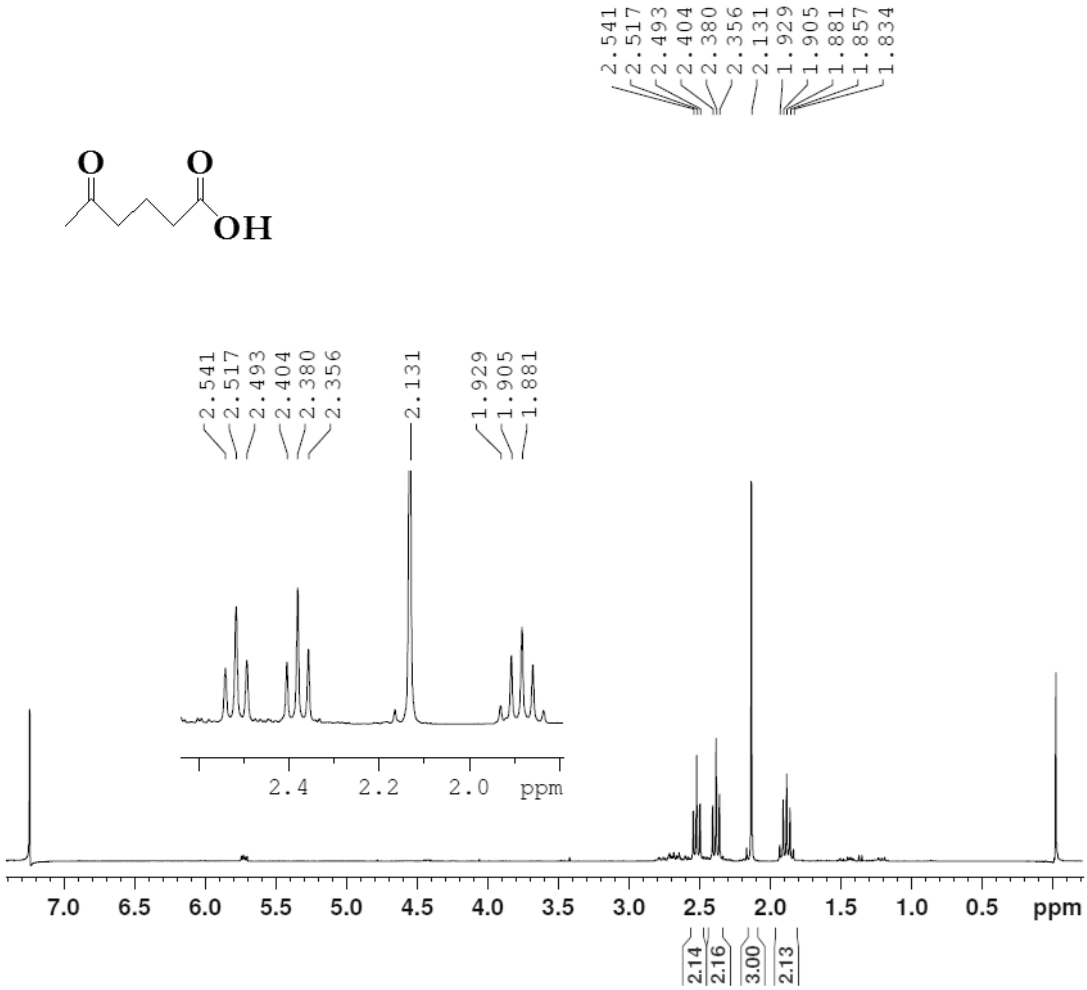

Figure A37. ^{1}H NMR of 5-oxohexanoic acid in $CDCl_3$ at 300 MHz.

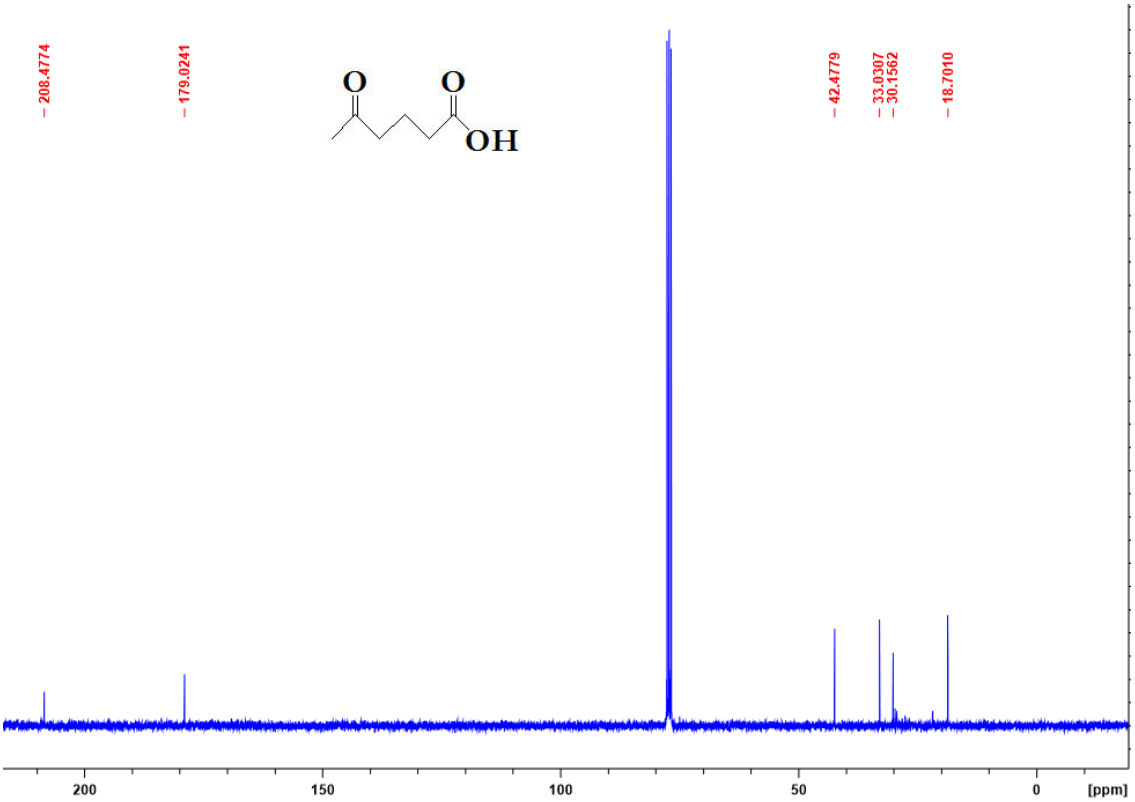

Figure A38. ^{13}C NMR of 5-oxohexanoic acid in $CDCl_3$ at 300 MHz.

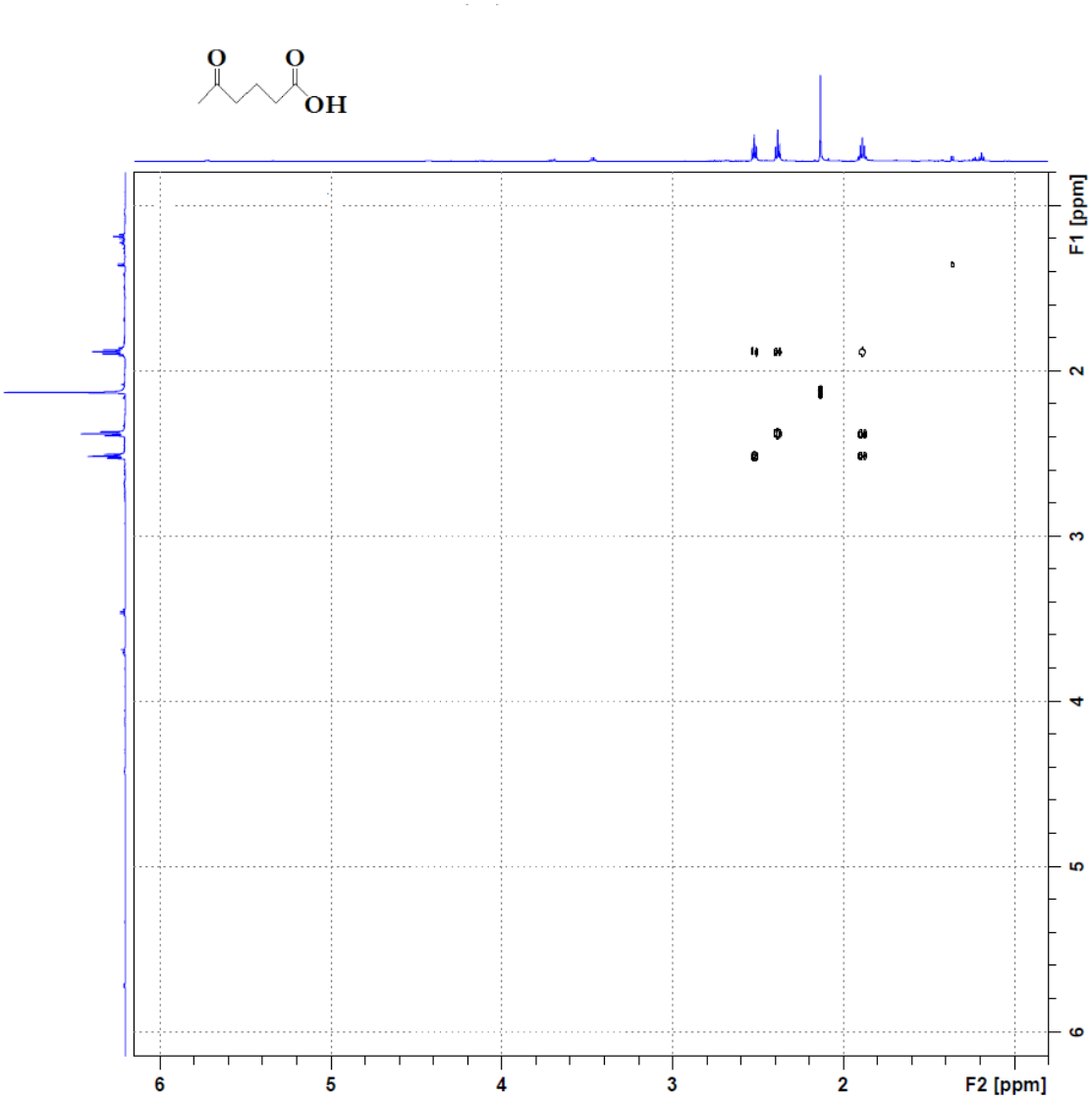

Figure A39. COSY of 5-oxohexanoic acid in $CDCl_3$ at 300 MHz.

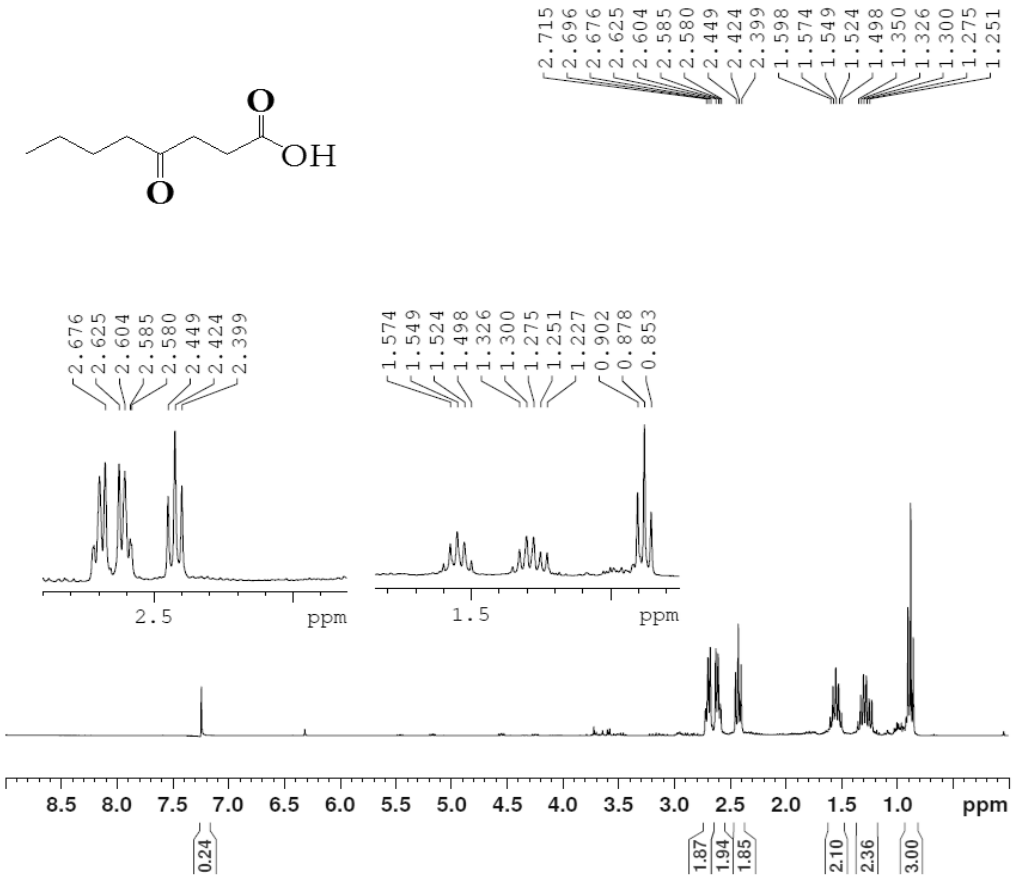

Figure A40. ^{1}H NMR of 4-oxooctanoic acid in $CDCl_3$ at 300 MHz.

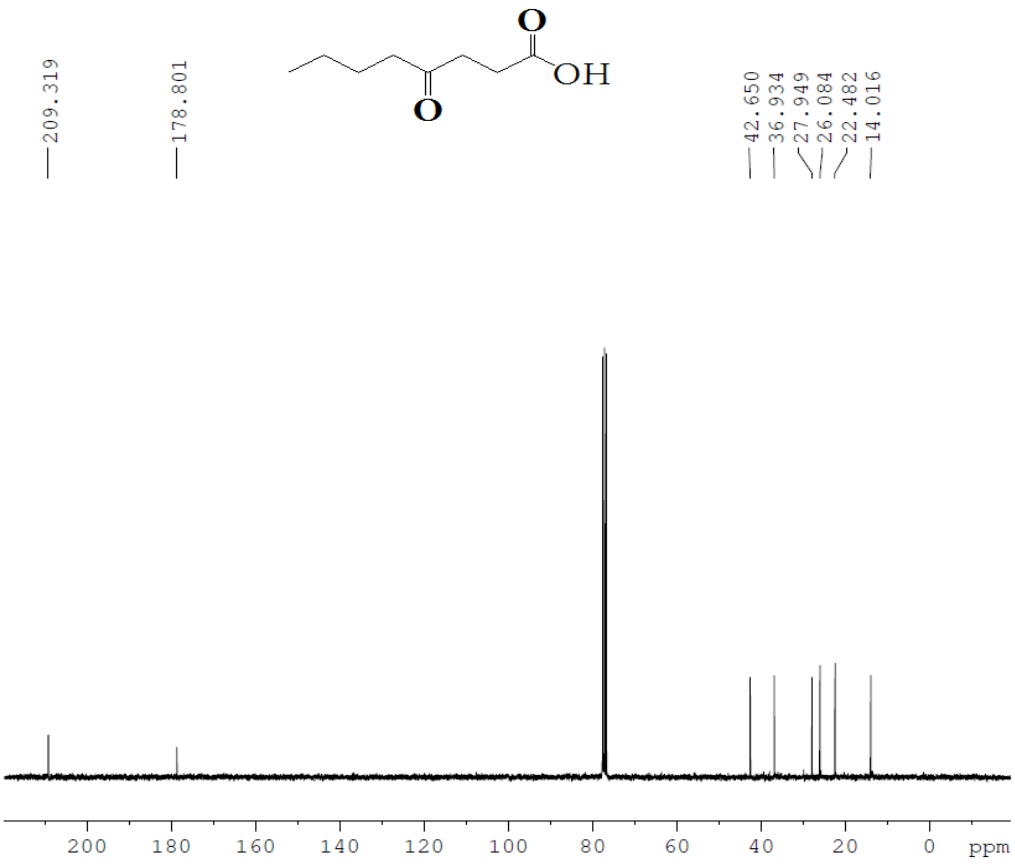

Figure A41. ^{13}C NMR of 4-oxooctanoic acid in $CDCl_3$ at 300 MHz.

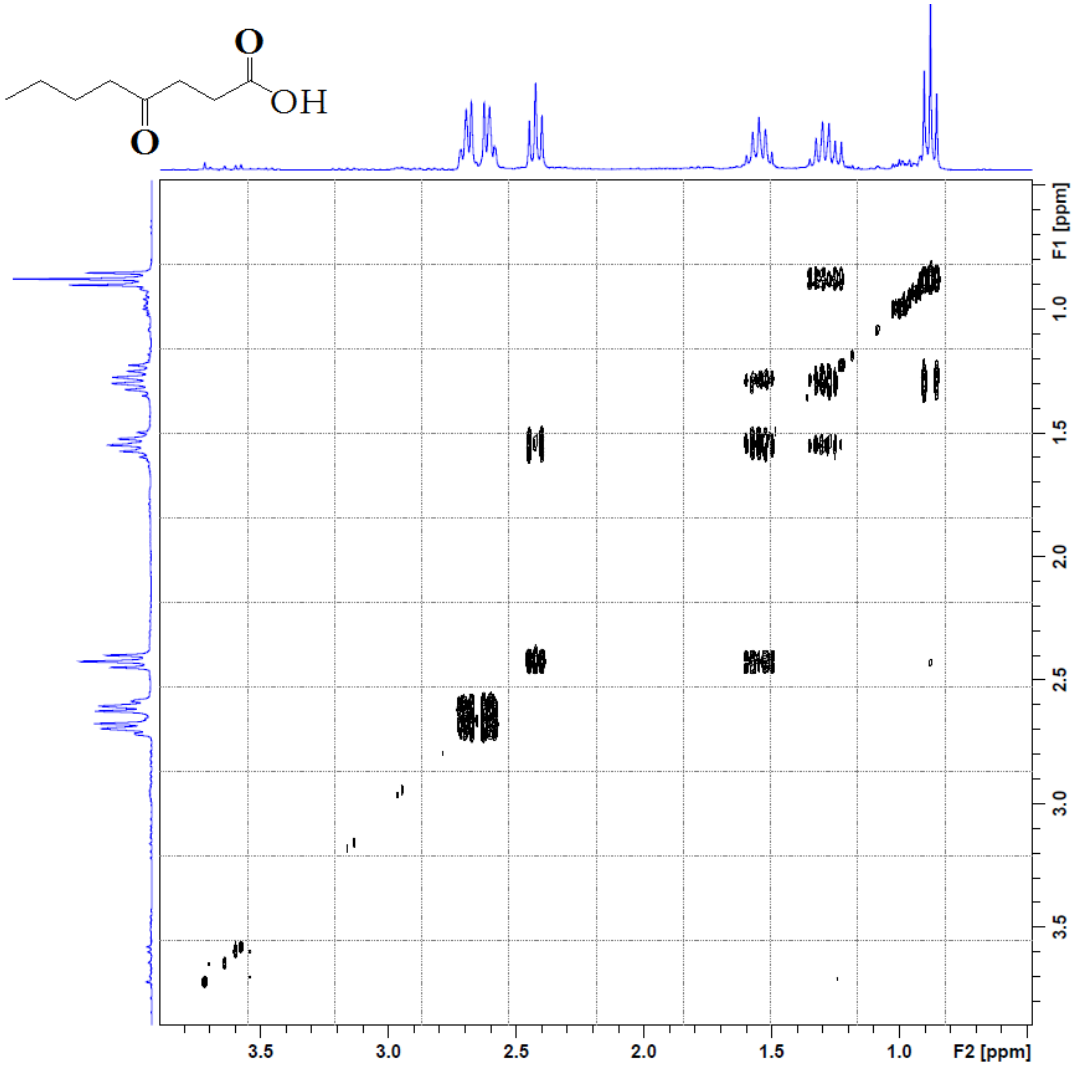

Figure A42. COSY of 4-oxooctanoic acid in $CDCl_3$ at 300 MHz.

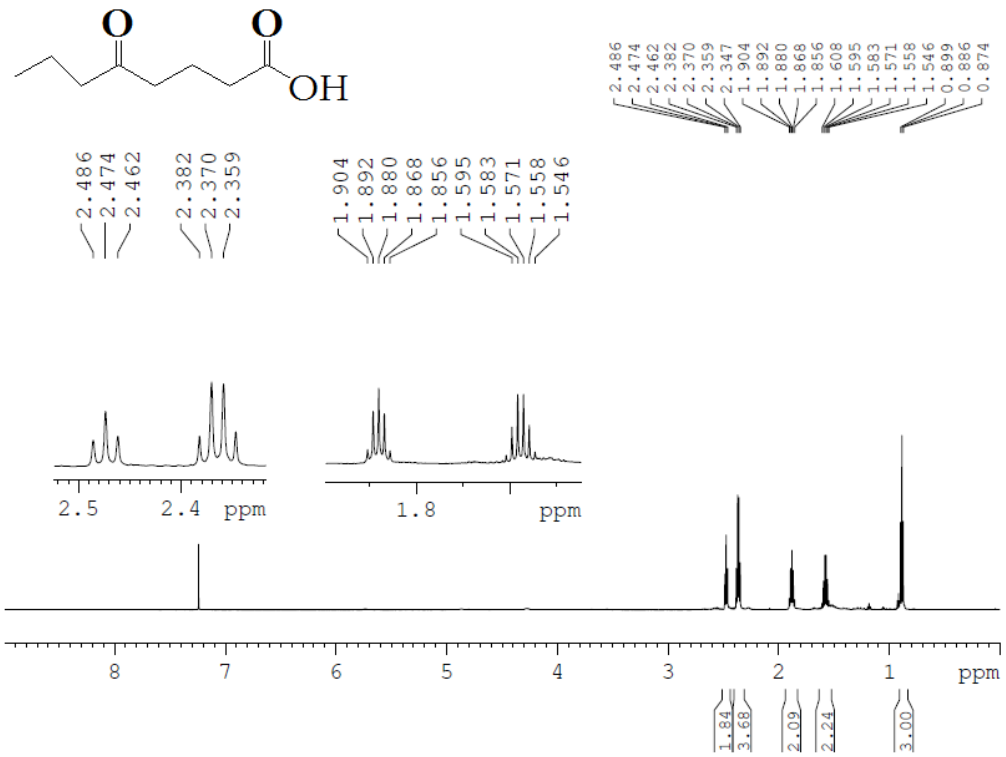

Figure A43. ^{1}H NMR of 5-oxooctanoic acid in $CDCl_3$ at 600 MHz.

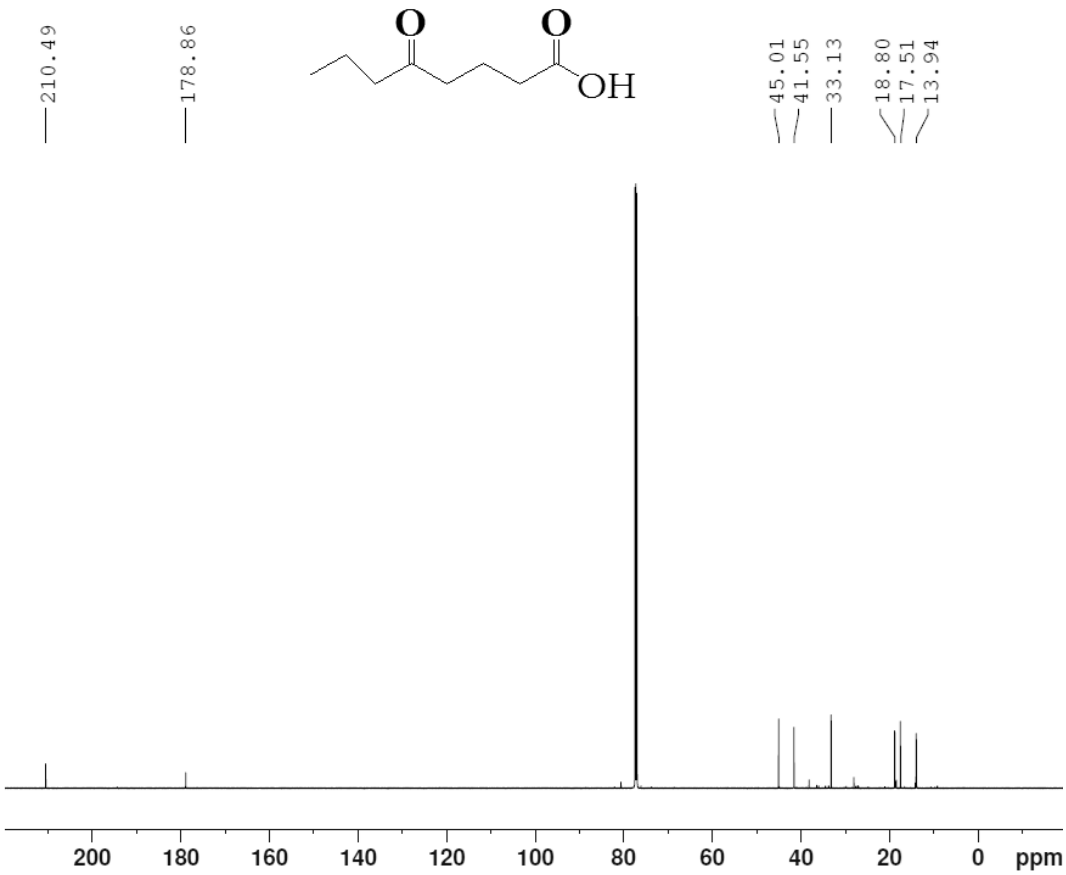

Figure A44. ^{13}**C NMR of 5-oxooctanoic acid in** $CDCl_3$ **at 600 MHz.**

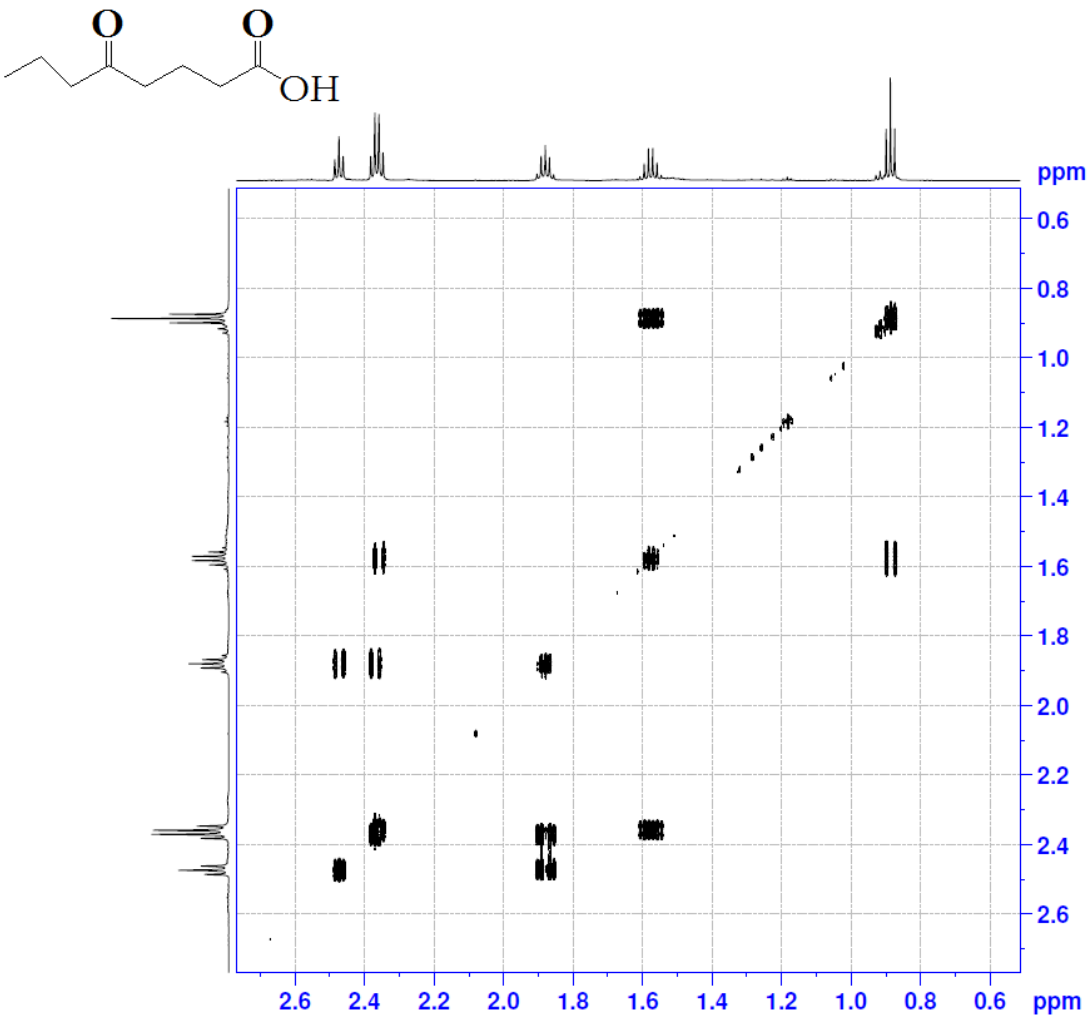

Figure A45. COSY of 5-oxooctanoic acid in $CDCl_3$ at 600 MHz.

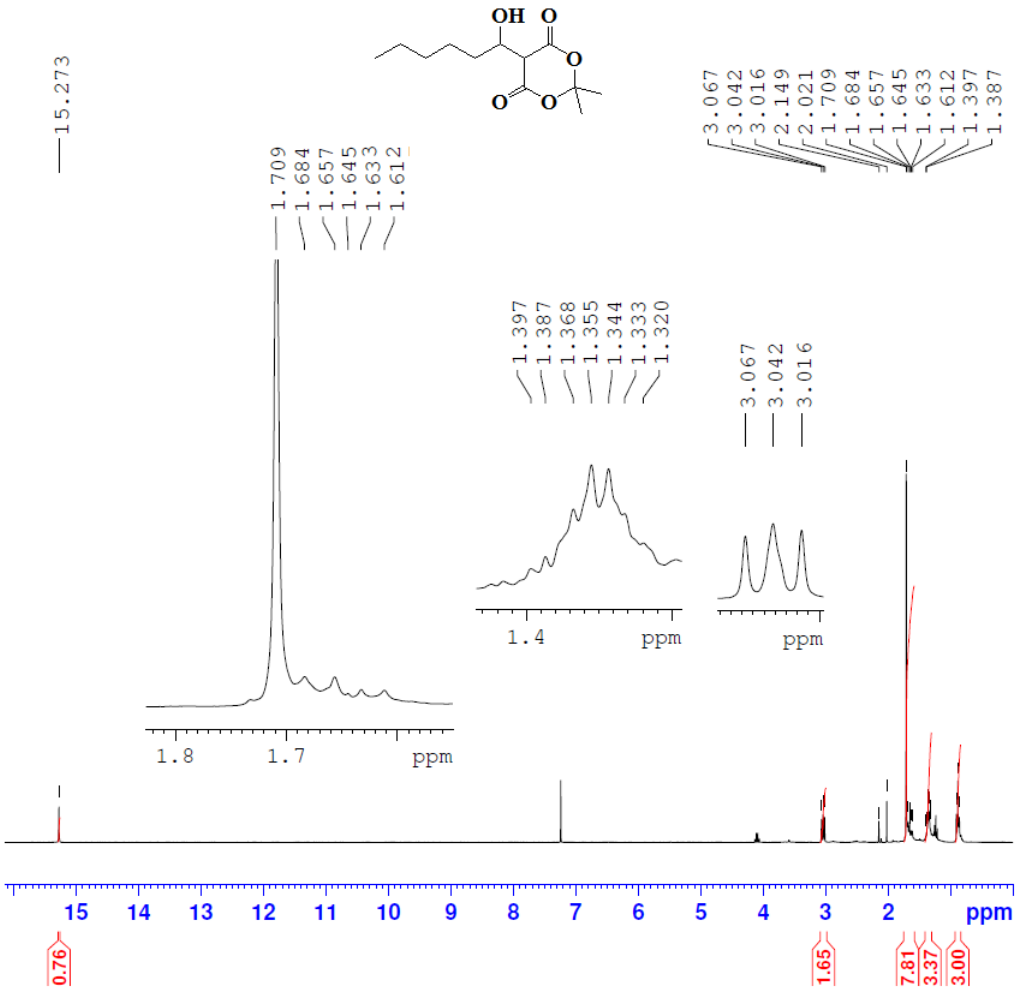

Figure A46. ^{1}H NMR of hexyl-Meldrum's acid in $CDCl_3$ at 300 MHz.

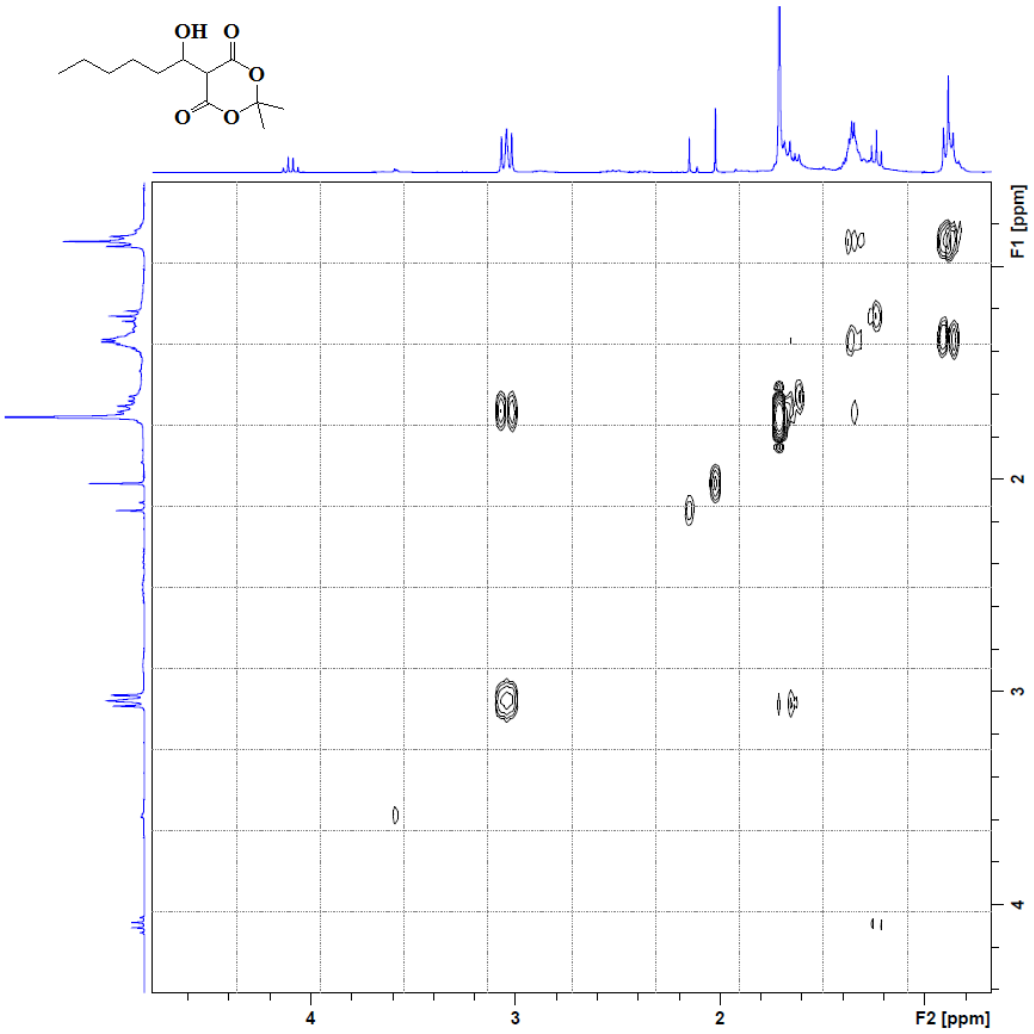

Figure A47. COSY of hexyl-Meldrum's acid in $CDCl_3$ at 300 MHz.

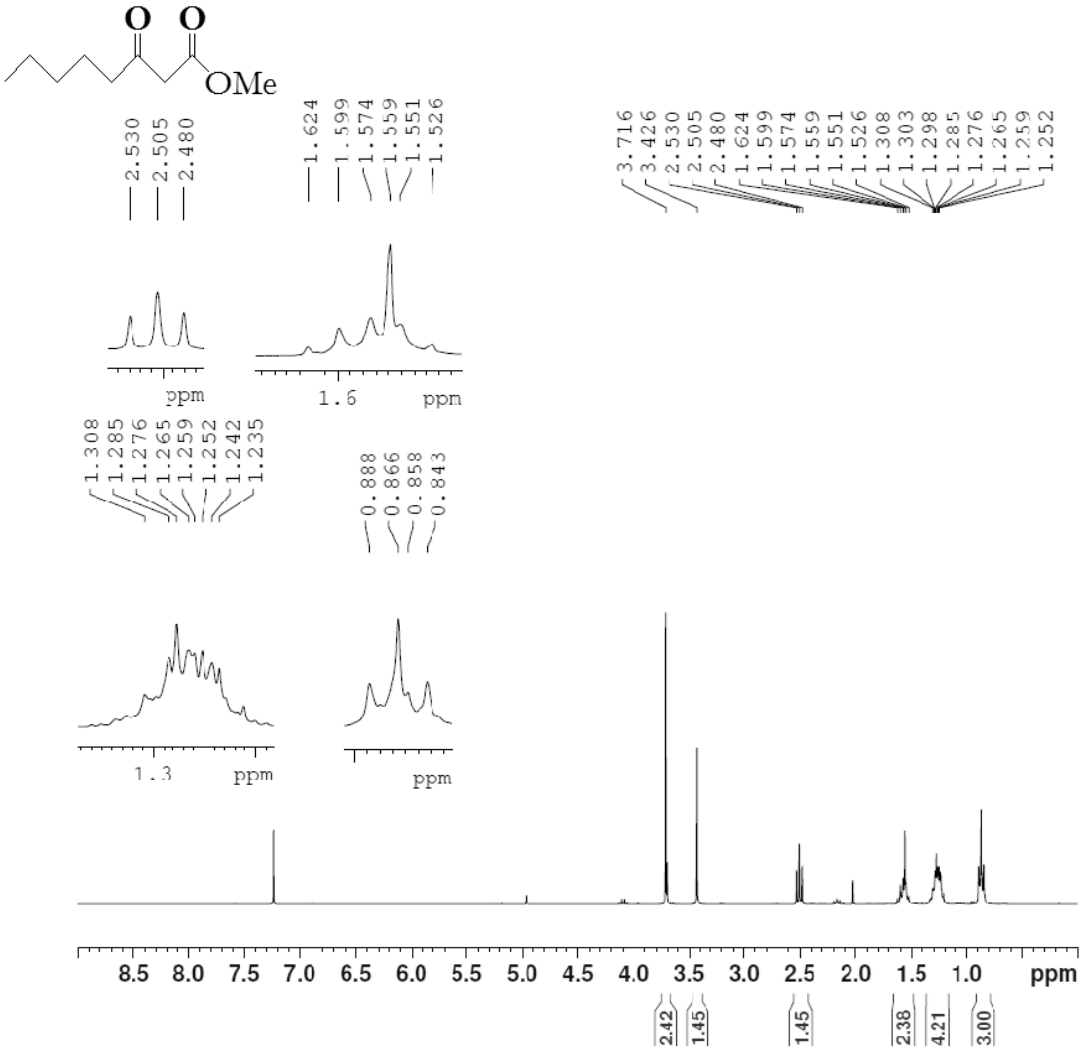

Figure A48. ^{1}H NMR of methyl-3-oxooctanoate in $CDCl_3$ at 300 MHz.

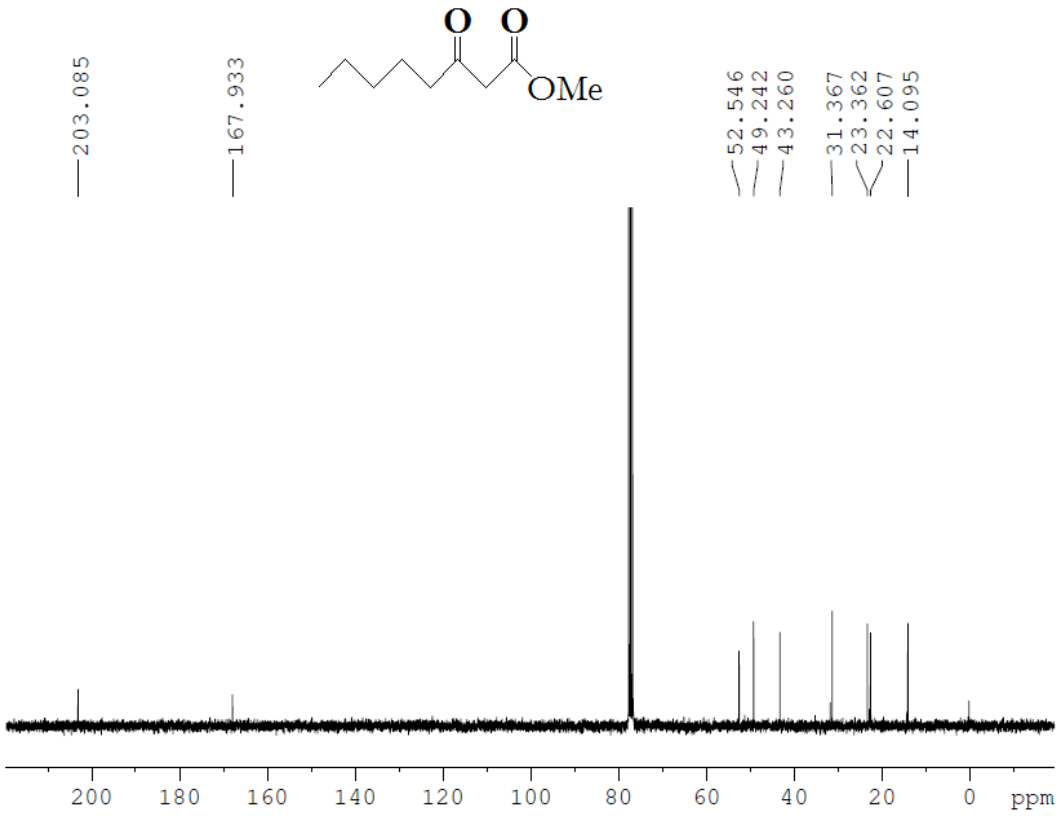

Figure A49. ^{13}C NMR of methyl-3-oxooctanoate in $CDCl_3$ at 300 MHz.

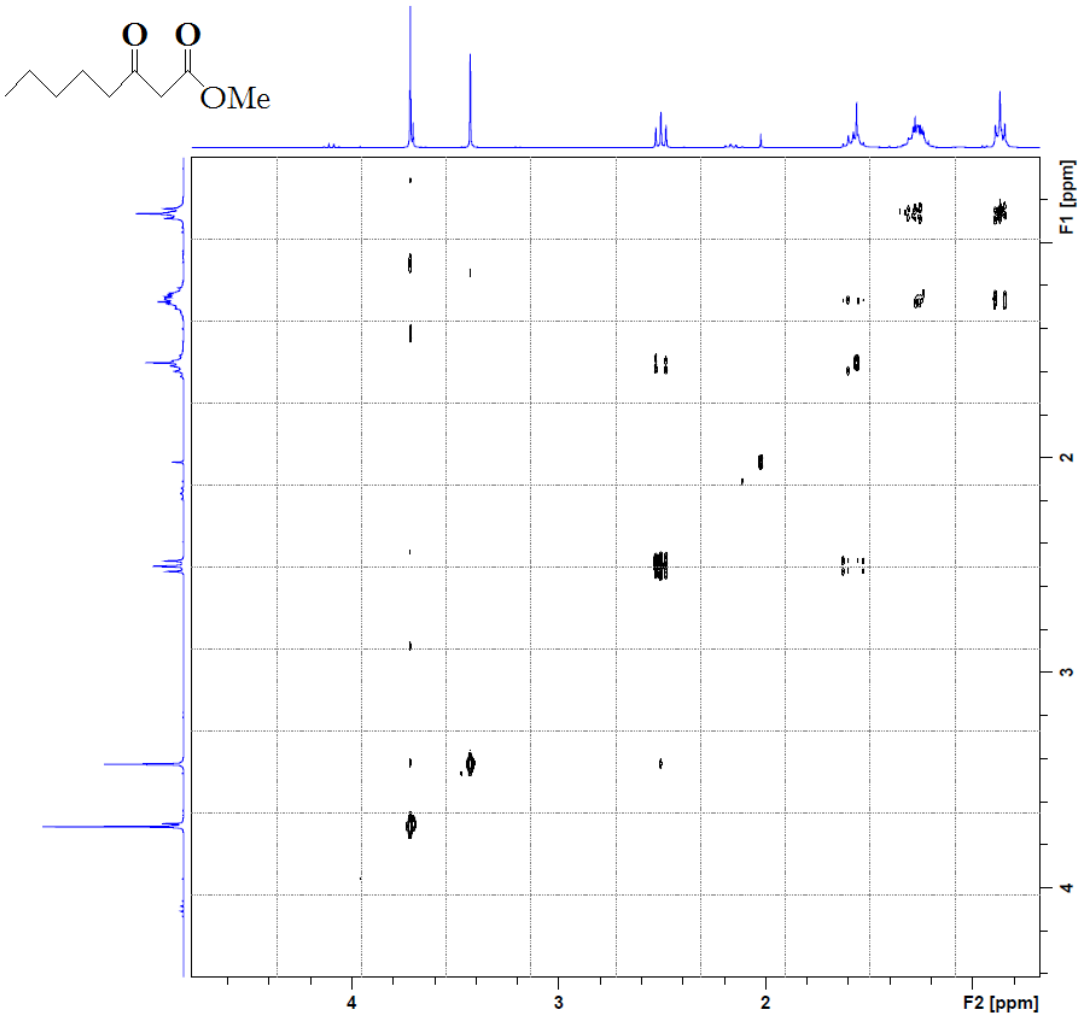

Figure A50. COSY of methyl-3-oxooctanoate in $CDCl_3$ at 300 MHz.

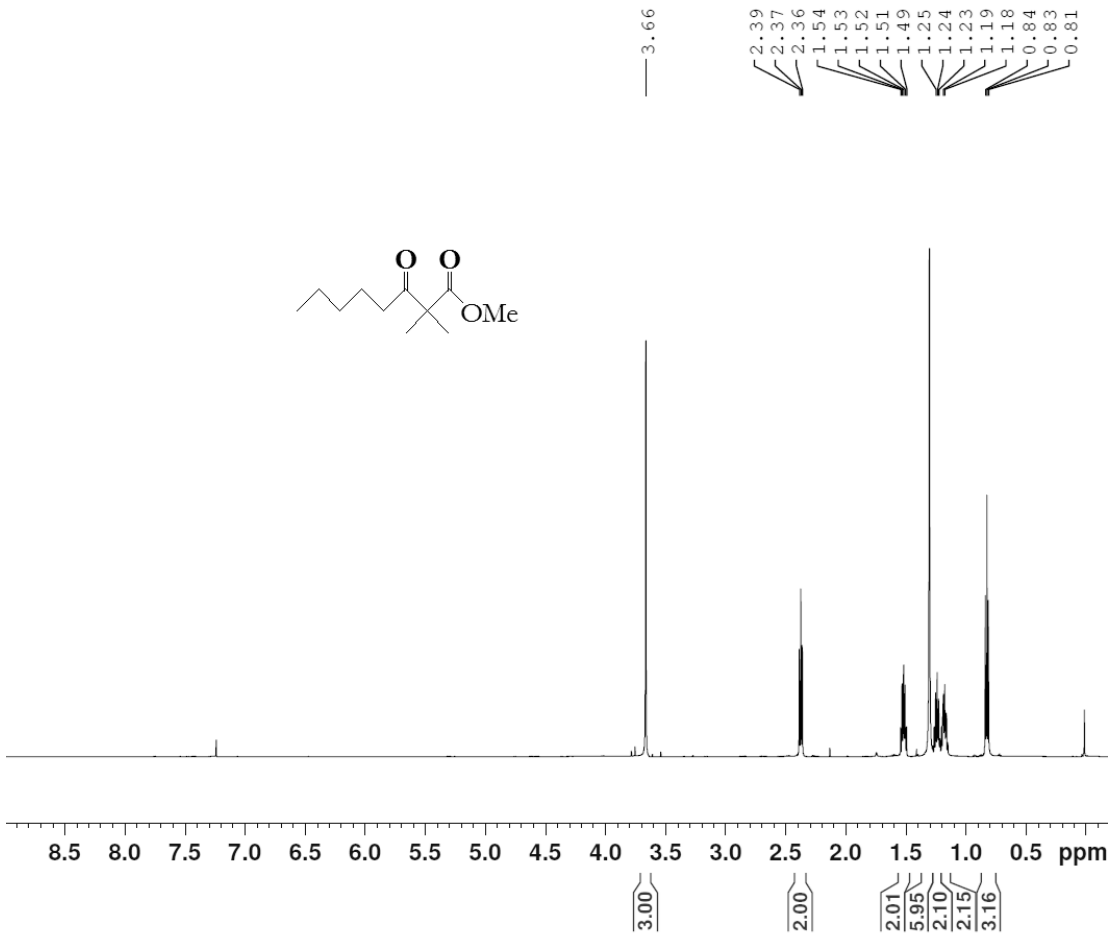

Figure A51. ^{1}H NMR of methyl-2,2′-dimethyl-3-oxooctanoate in $CDCl_3$ at 600 MHz.

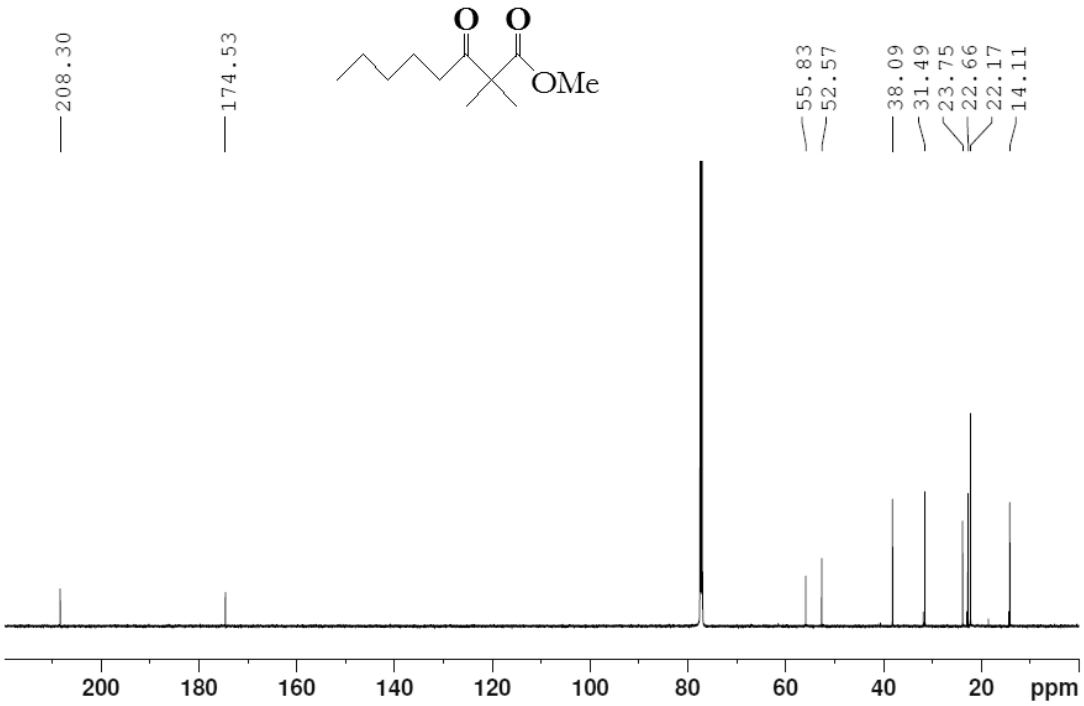

Figure A52. ^{13}C NMR of methyl-2,2′-dimethyl-3-oxooctanoate in $CDCl_3$ at 600 MHz.

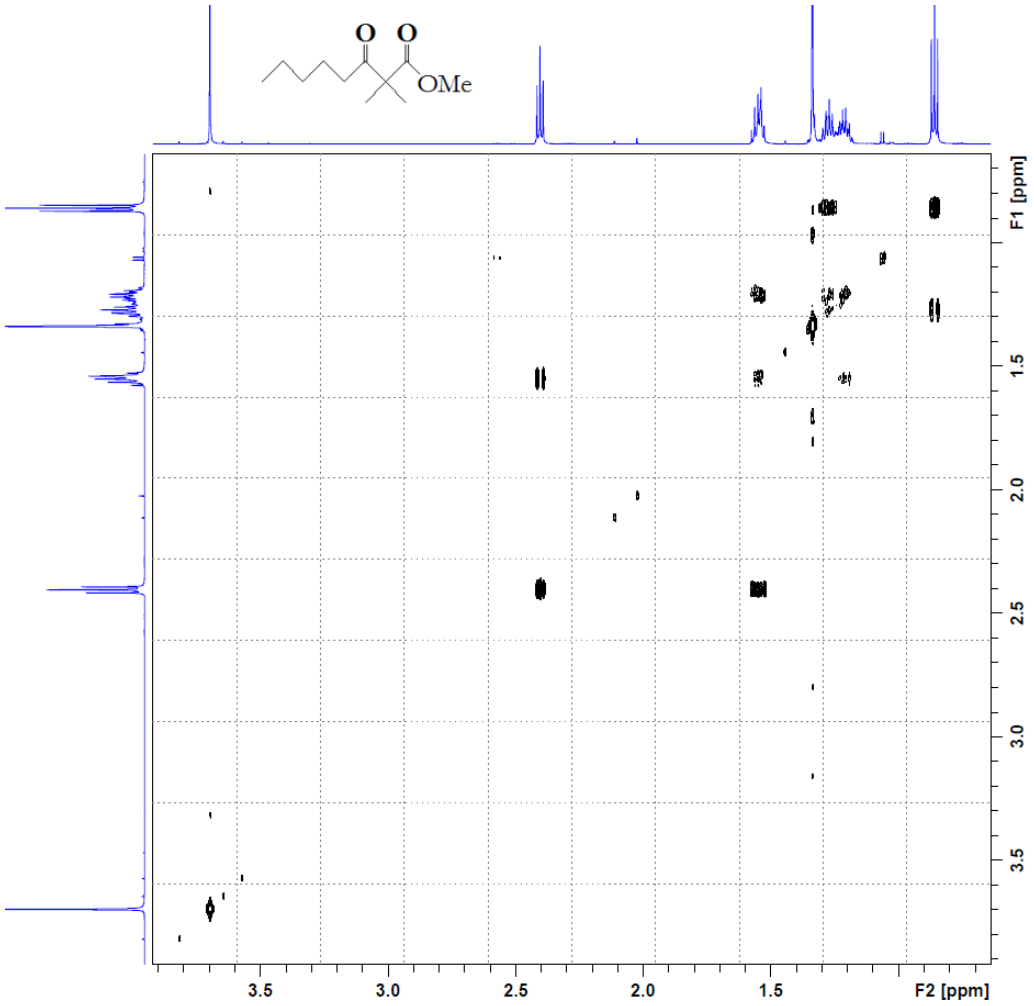

Figure A53. COSY of methyl-2,2′-dimethyl-3-oxooctanoate in $CDCl_3$ at 600 MHz.

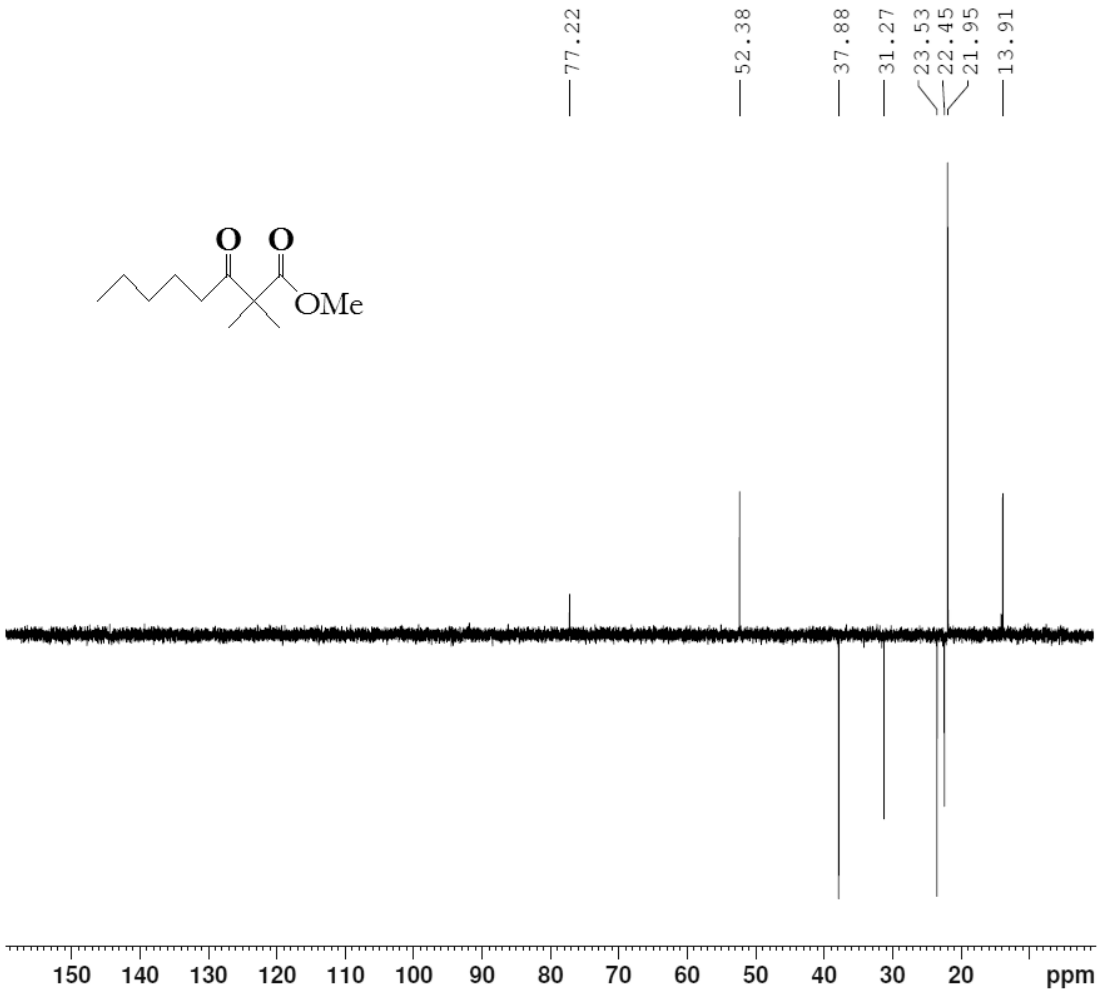

Figure A54. DEPT-135 NMR of methyl-2,2′-dimethyl-3-oxooctanoate in $CDCl_3$ at 600 MHz.

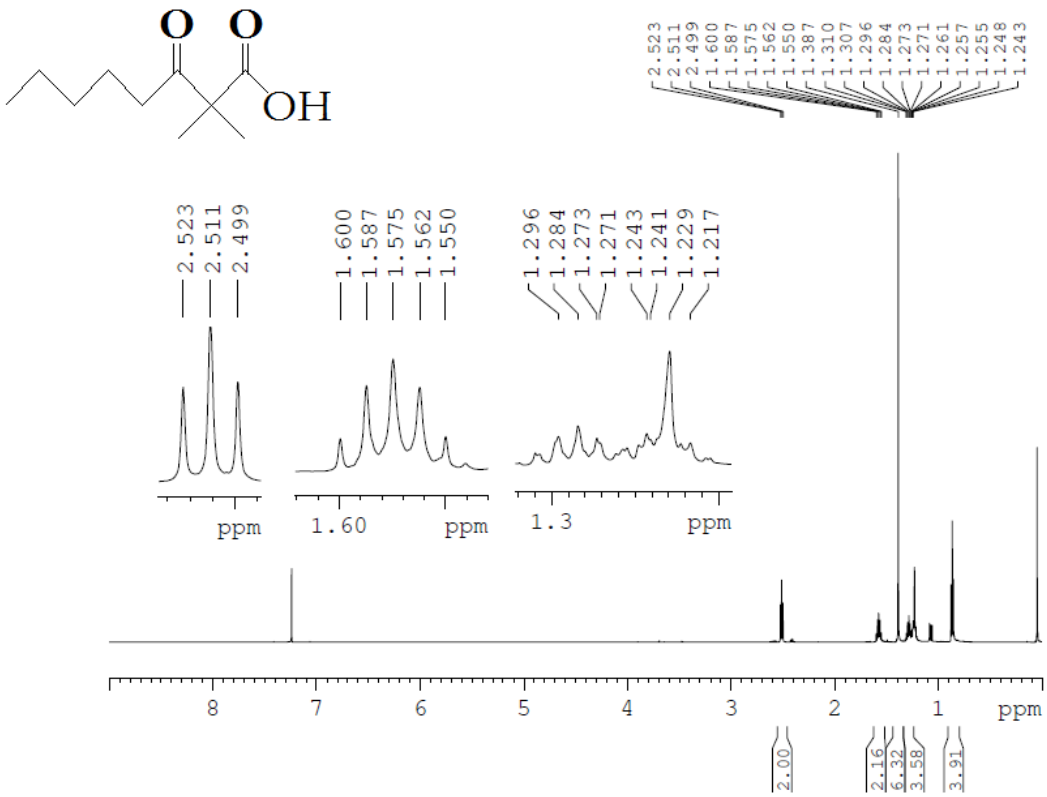

Figure A55. ^{1}H NMR of 2,2′-dimethyl-3-oxooctanoic acid in $CDCl_3$ at 600 MHz.

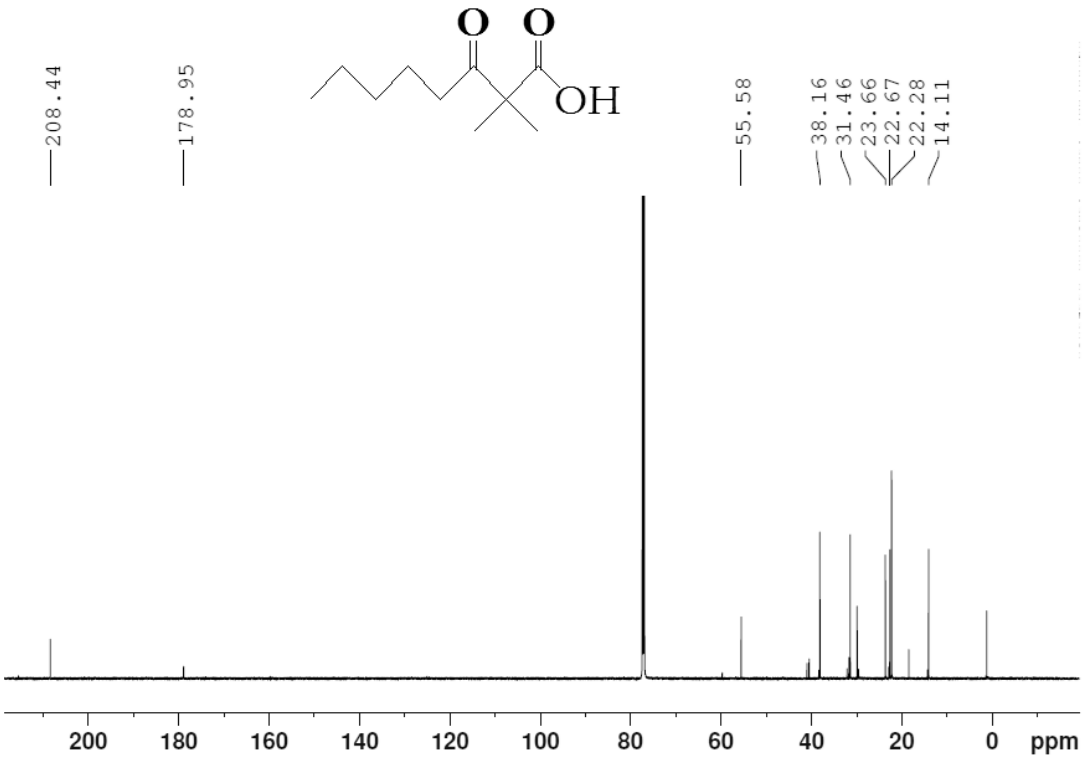

Figure A56. ^{13}C NMR of 2,2′-dimethyl-3-oxooctanoic acid in $CDCl_3$ at 600 MHz.

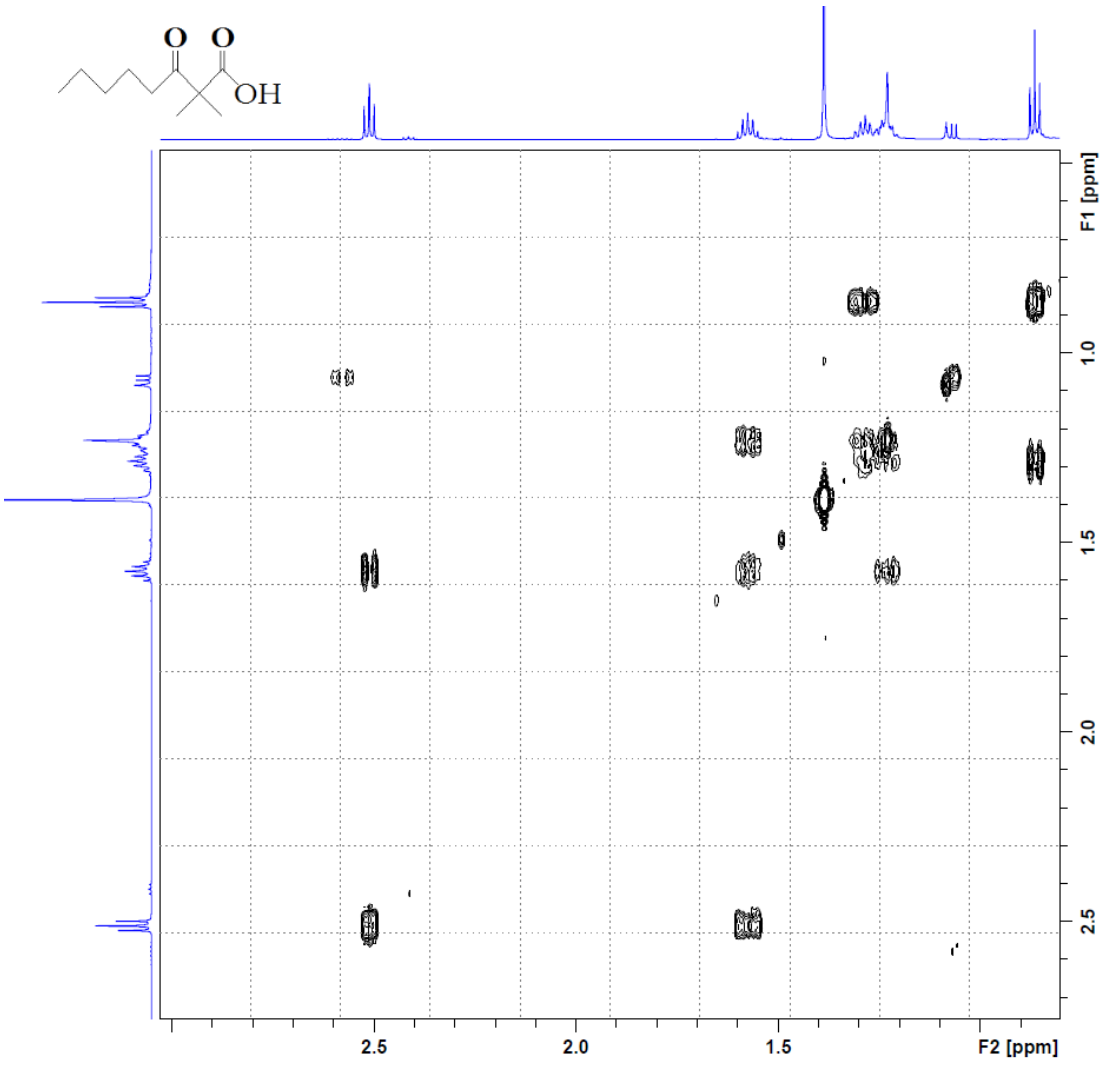

Figure A57. COSY of 2,2′-dimethyl-3-oxooctanoic acid in $CDCl_3$ at 600 MHz.

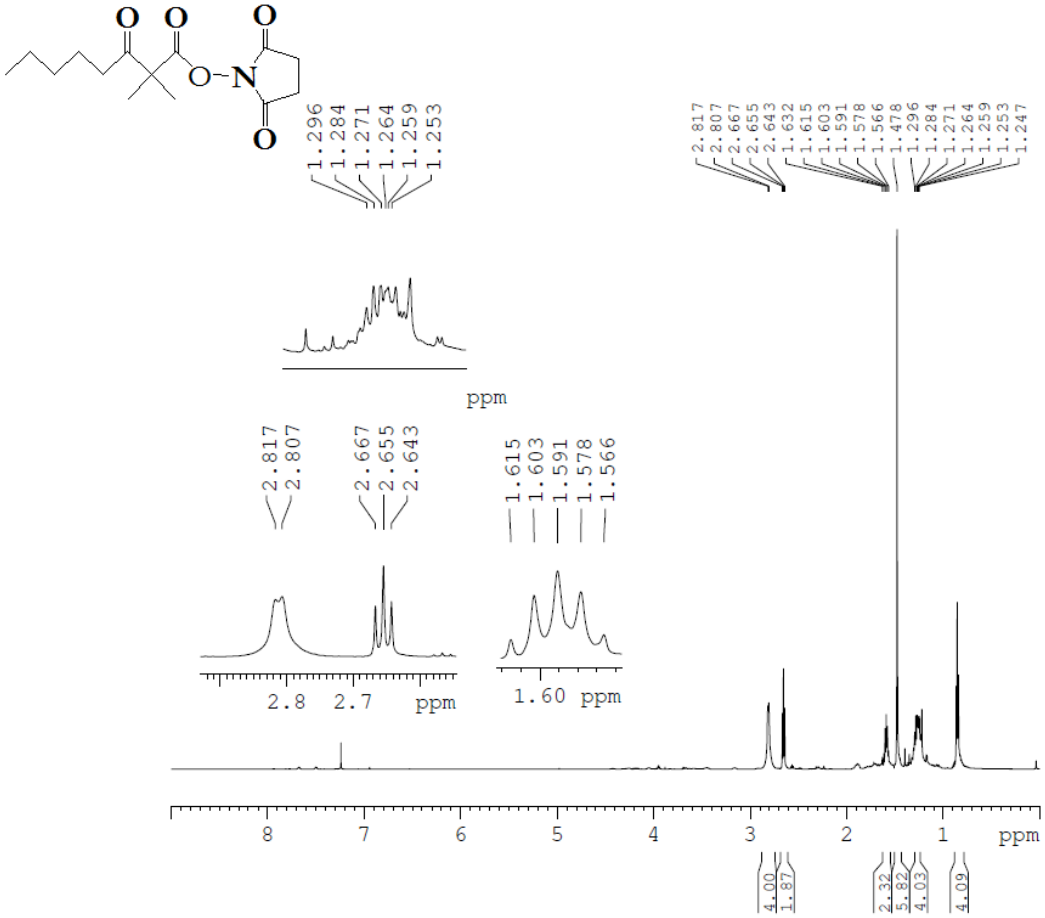

Figure A58. ^{1}H NMR of 2,2′-dimethyl-3-oxooctanoyl-succinimide ester in $CDCl_3$ at 600 MHz.

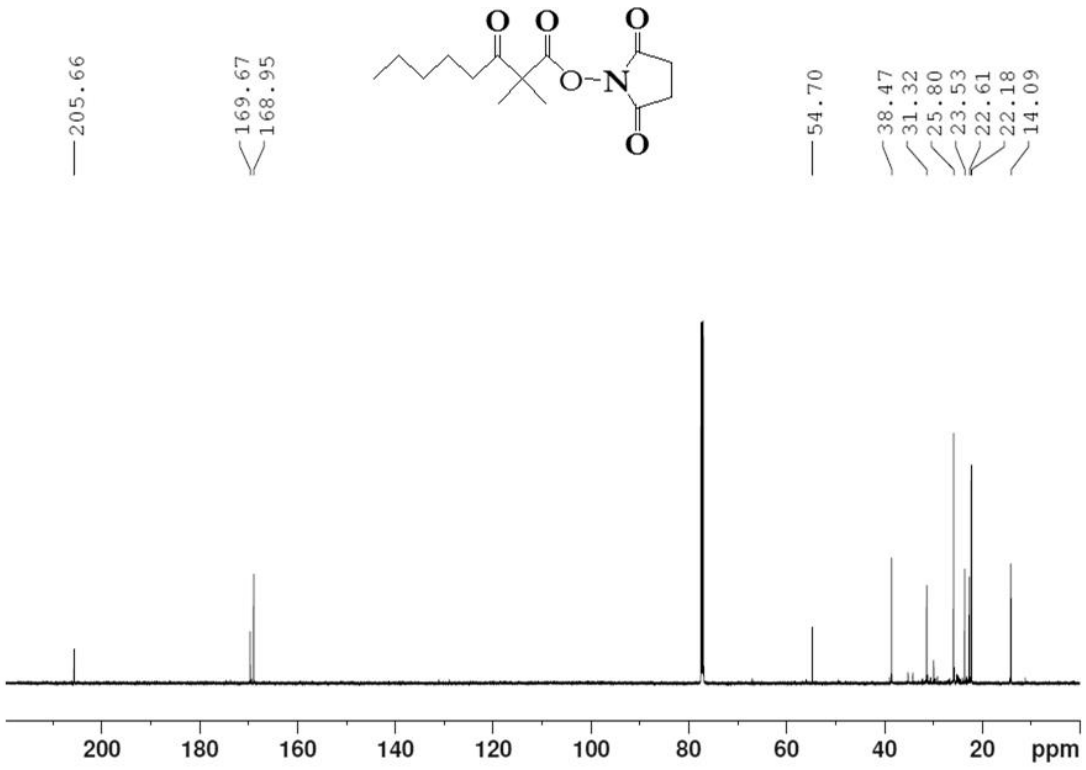

Figure A59. ^{13}C NMR of 2,2′-dimethyl-3-oxooctanoyl-succinimide ester in $CDCl_3$ at 600 MHz.

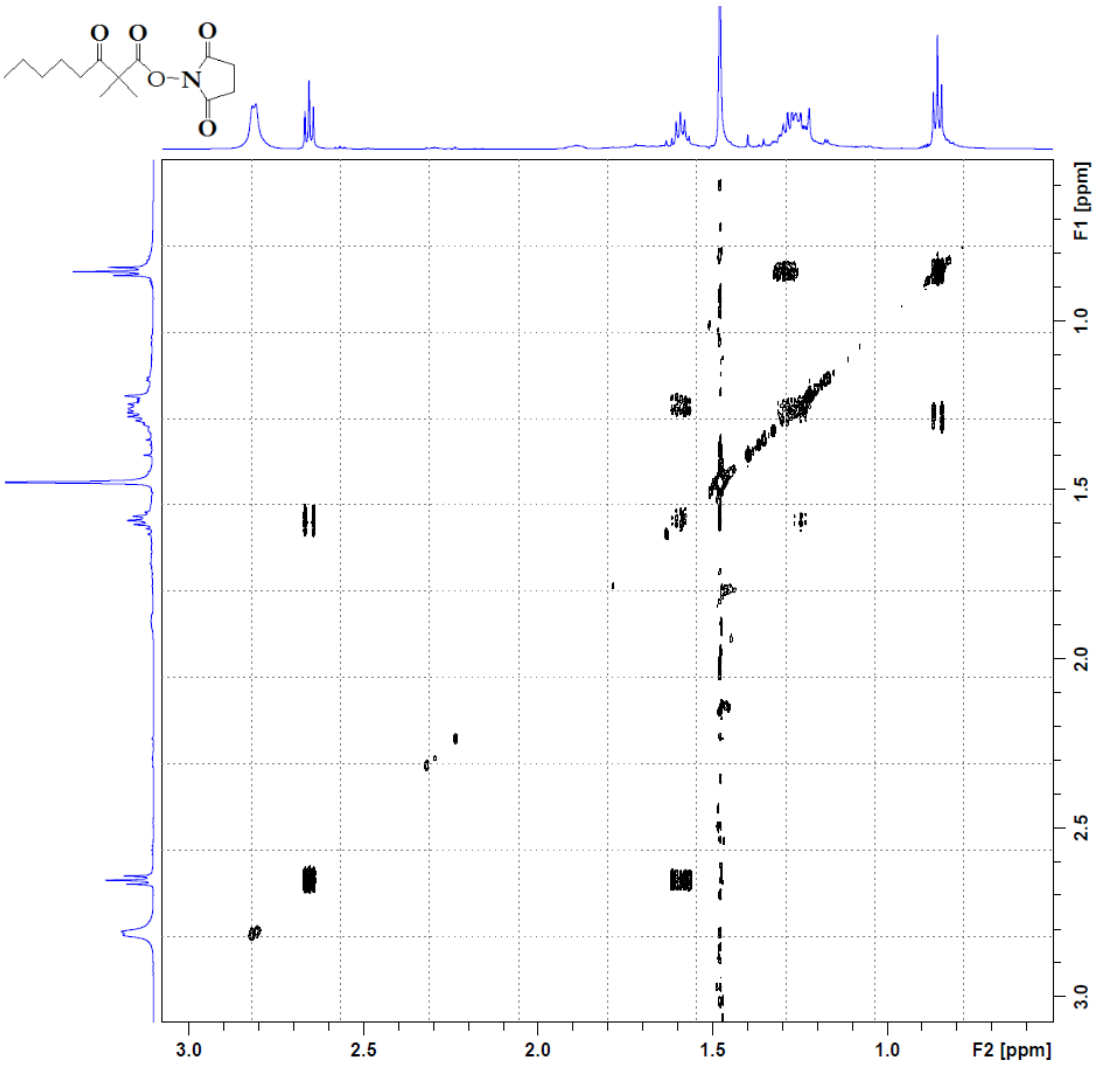

Figure A60. COSY of 2,2′-dimethyl-3-oxooctanoyl-succinimide ester in $CDCl_3$ at 600 MHz.

APPENDIX B

Mass Spectrometry Data

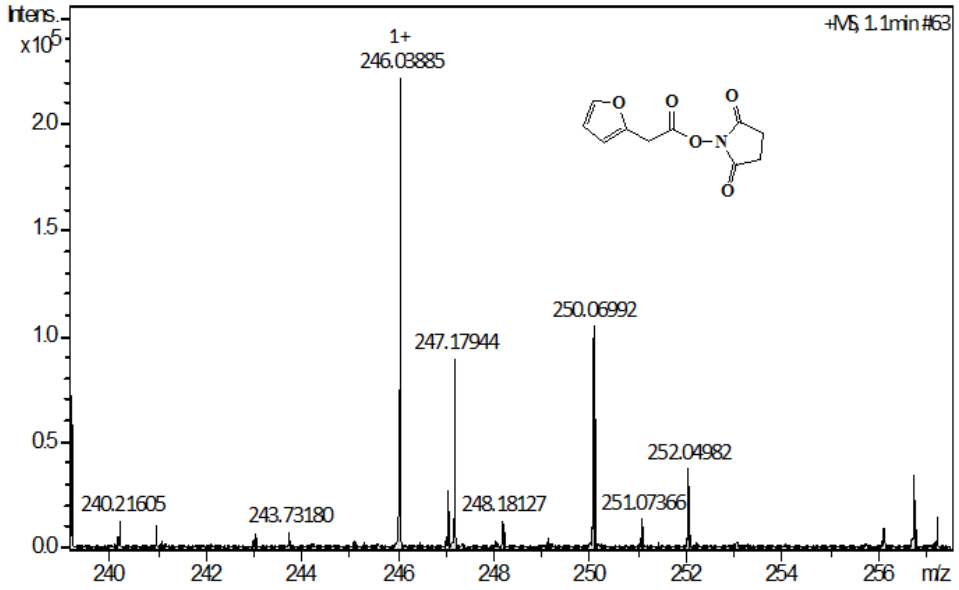

Figure B1. Mass spectrum of 2-furanacetyl-succinimide ester.

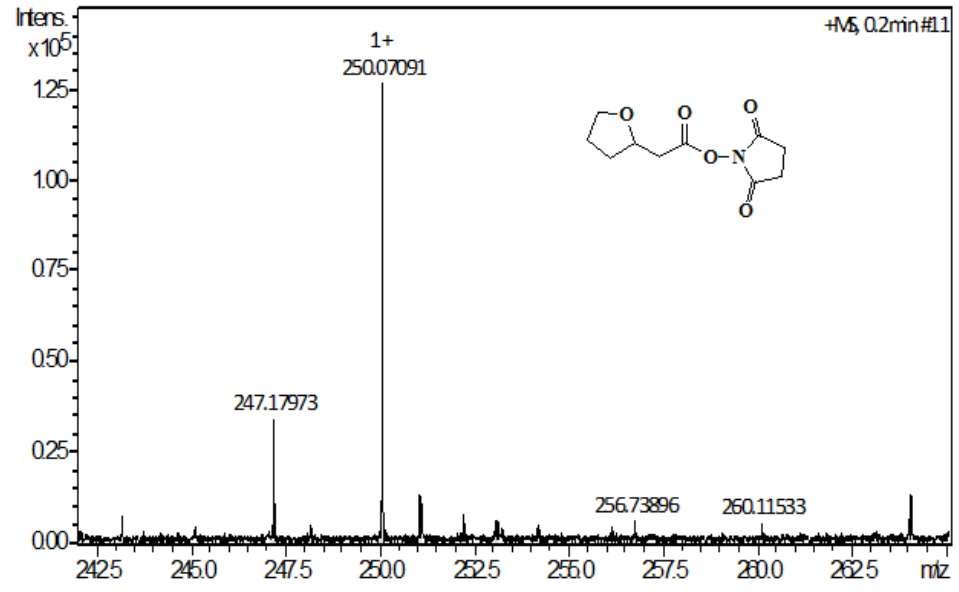

Figure B2. Mass spectrum of 2-tetrahydrofuranacetyl-succinimide ester.

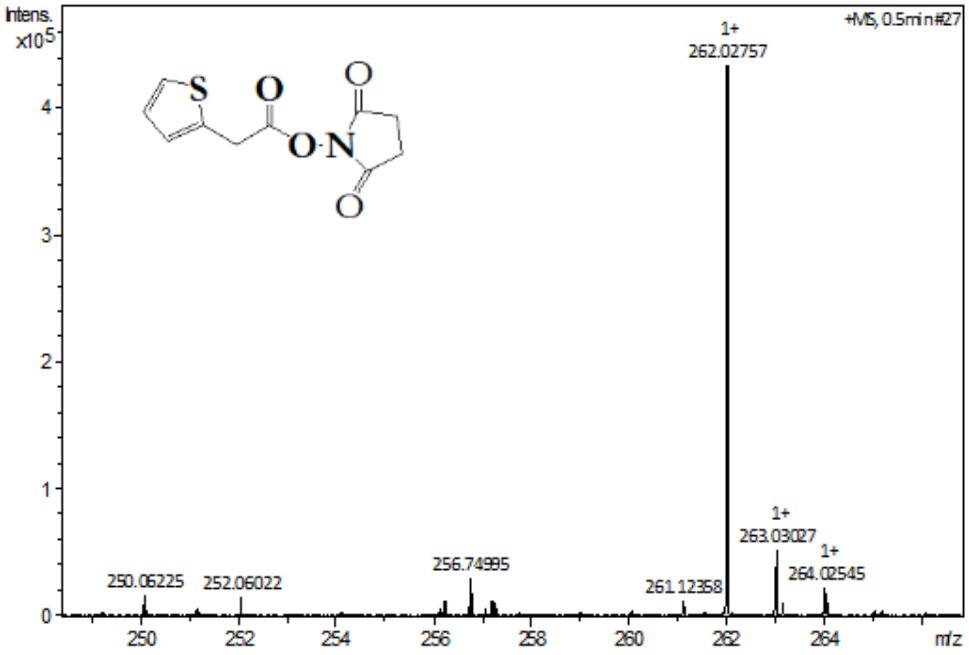

Figure B3. Mass spectrum of 2-thiopheneacetyl-succinimide ester.

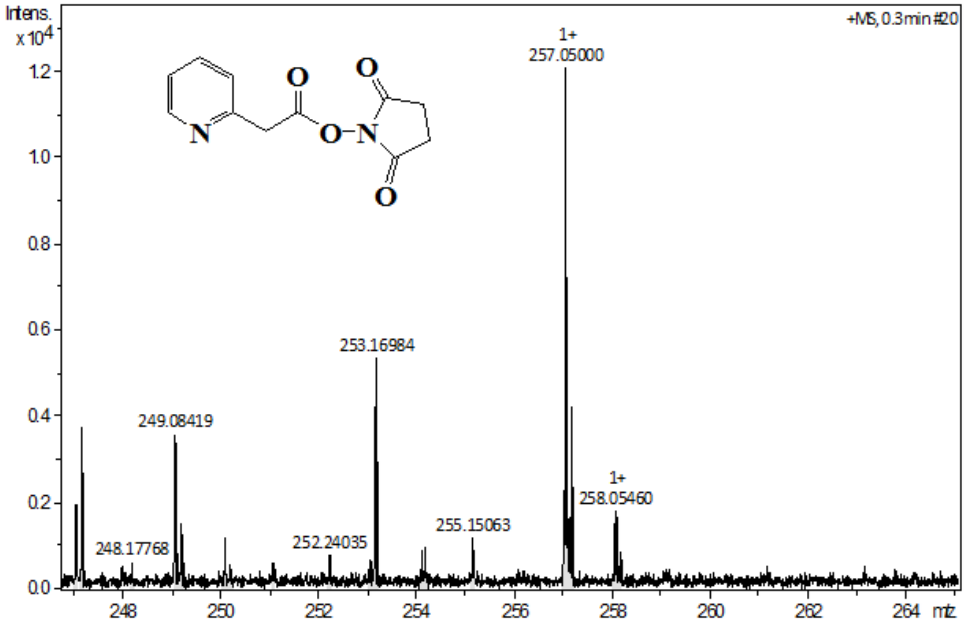

Figure B4. Mass spectrum of 2-pyridylacetyl-succinimide ester.

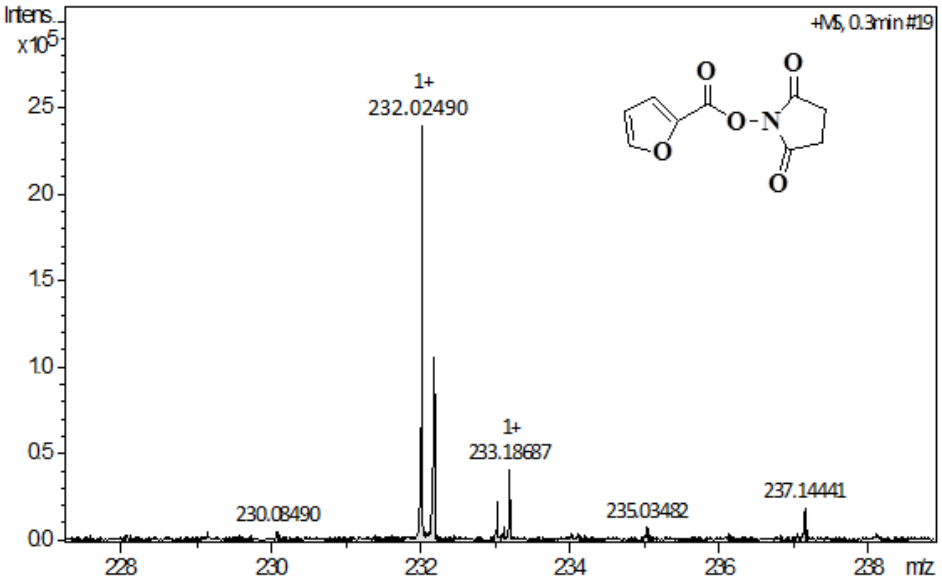

Figure B5. Mass spectrum of 2-furoyl-succinimide ester.

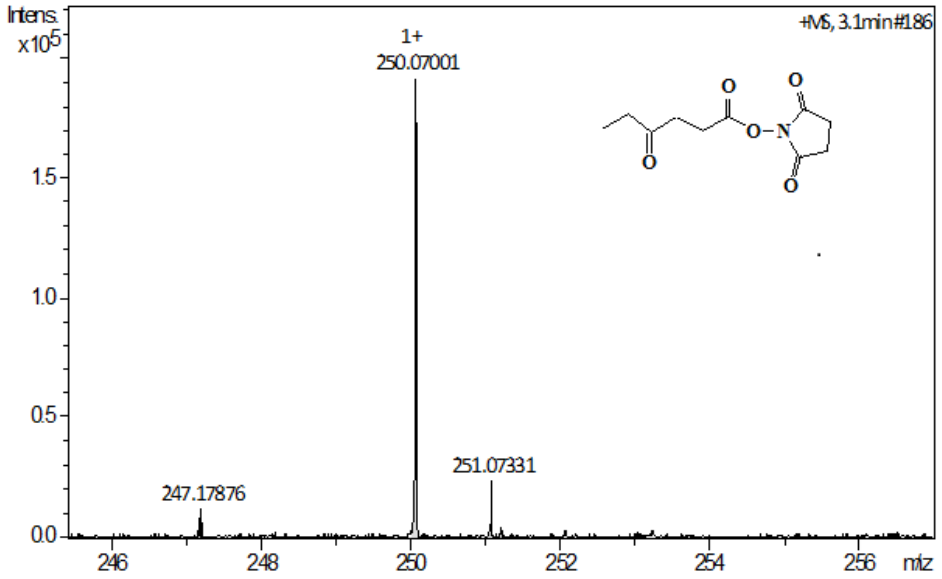

Figure B6. Mass spectrum of 4-oxohexanoyl-succinimide ester.

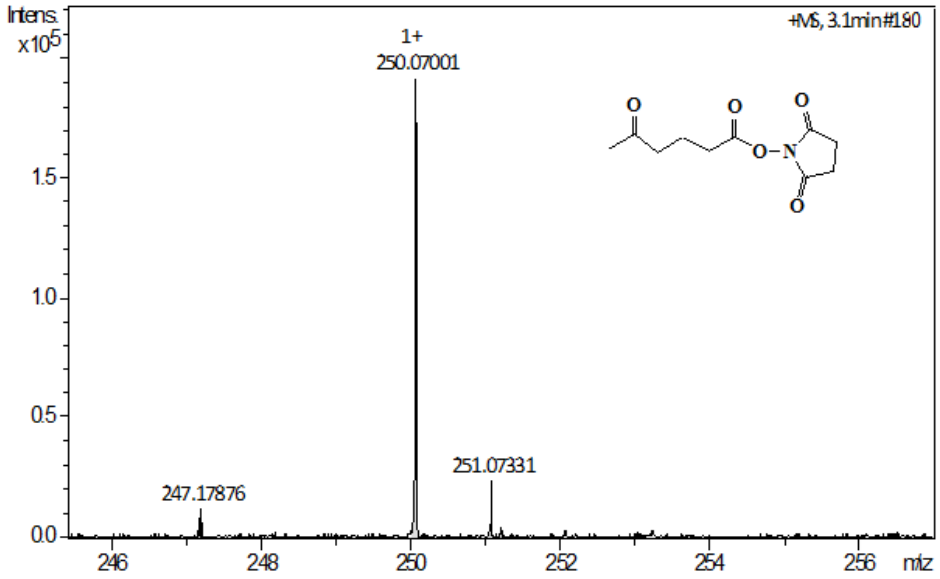

Figure B7. Mass spectrum of 5-oxohexanoyl-succinimide ester.

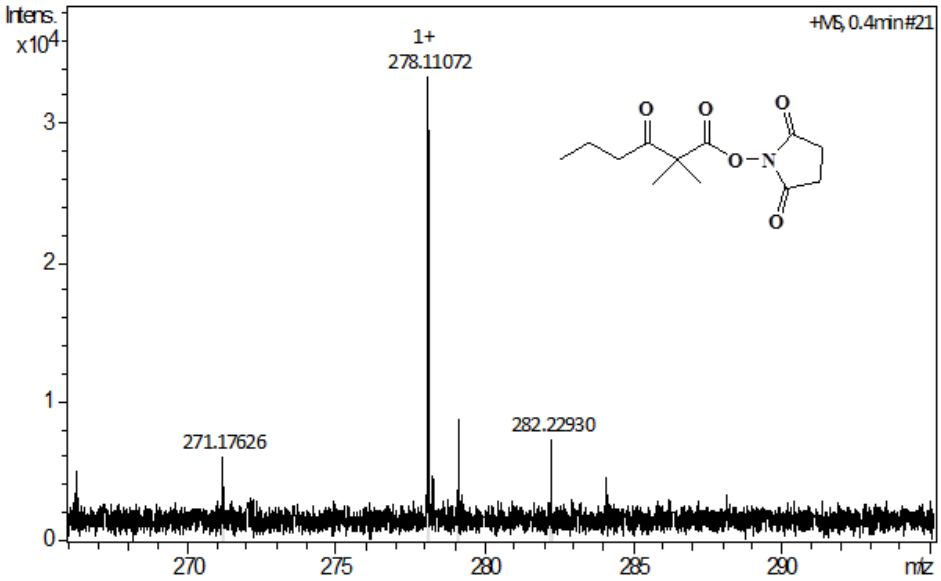

Figure B8. Mass spectrum of 2,2´-dimethyl-3-oxohexanoyl-succinimide ester.

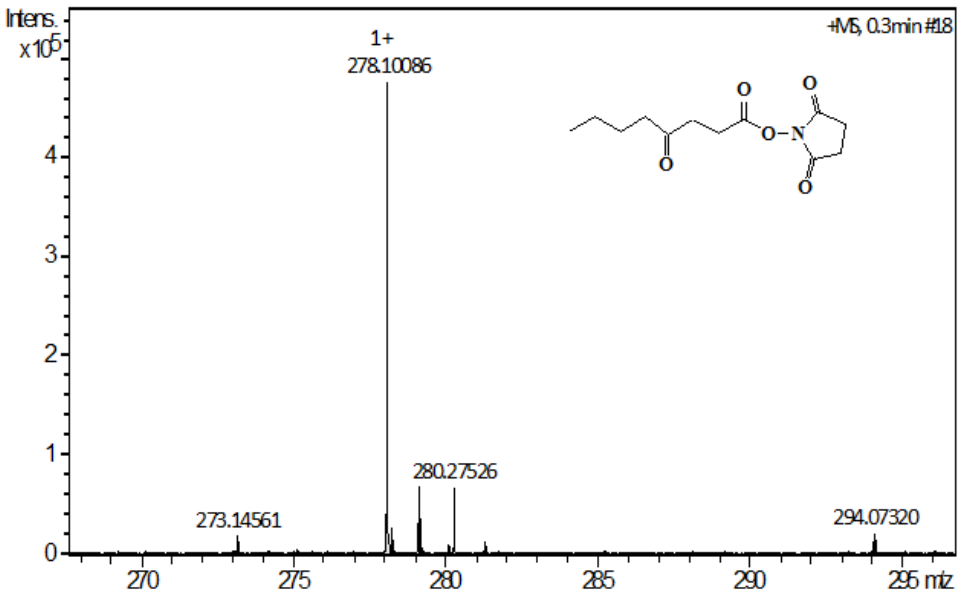

Figure B9. Mass spectrum of 4-oxooctanoyl-succinimide ester.

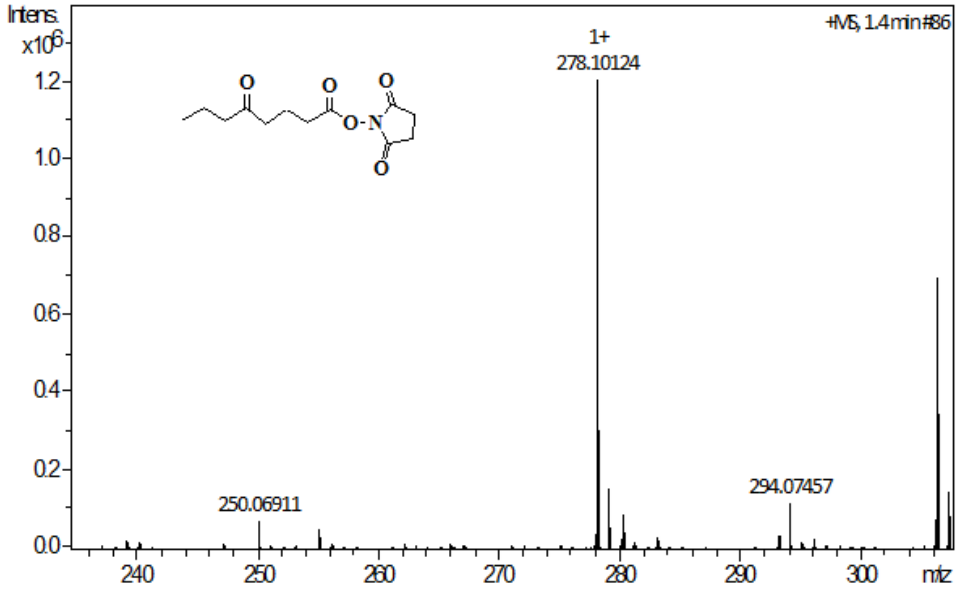

Figure B10. Mass spectrum of 5-oxooctanoyl-succinimide ester.

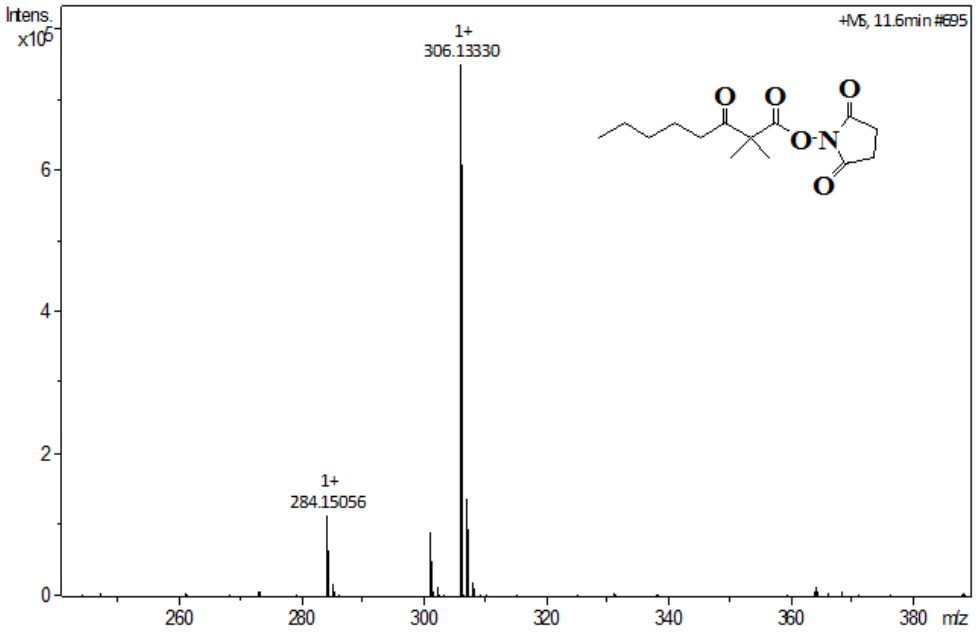

Figure B11. Mass spectrum of 2,2´-dimethyl-3oxooctanoyl-succinimide ester.

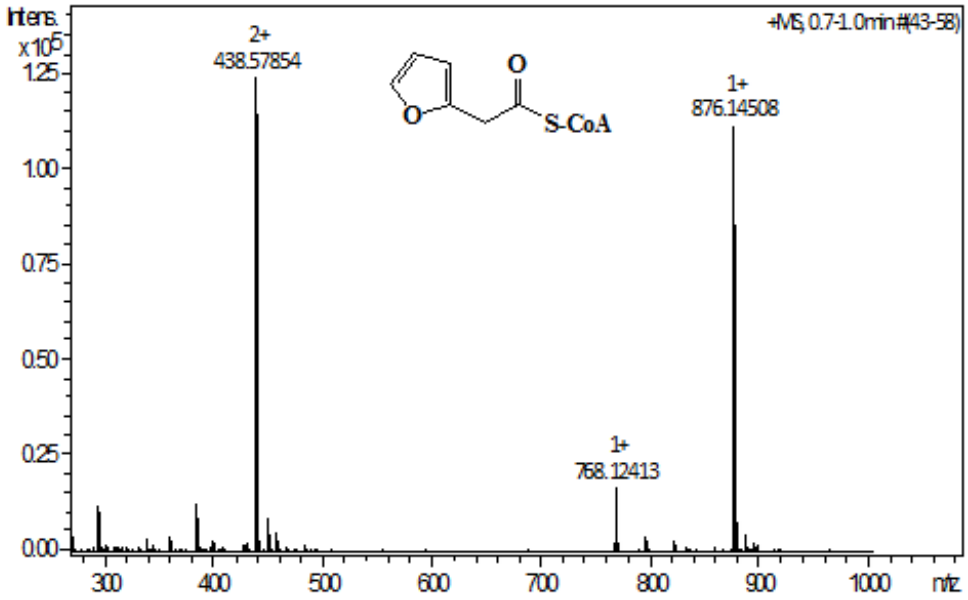

Figure B12. Mass spectrum of 2-furanacetyl-CoA.

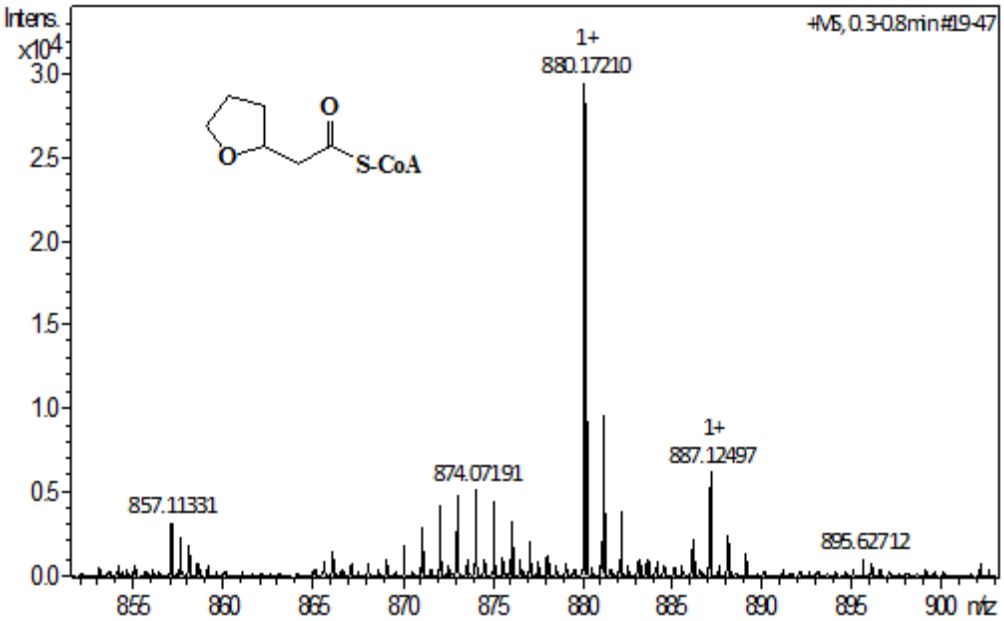

Figure B13. Mass spectrum of 2-tetrahydrofuranacetyl-CoA.

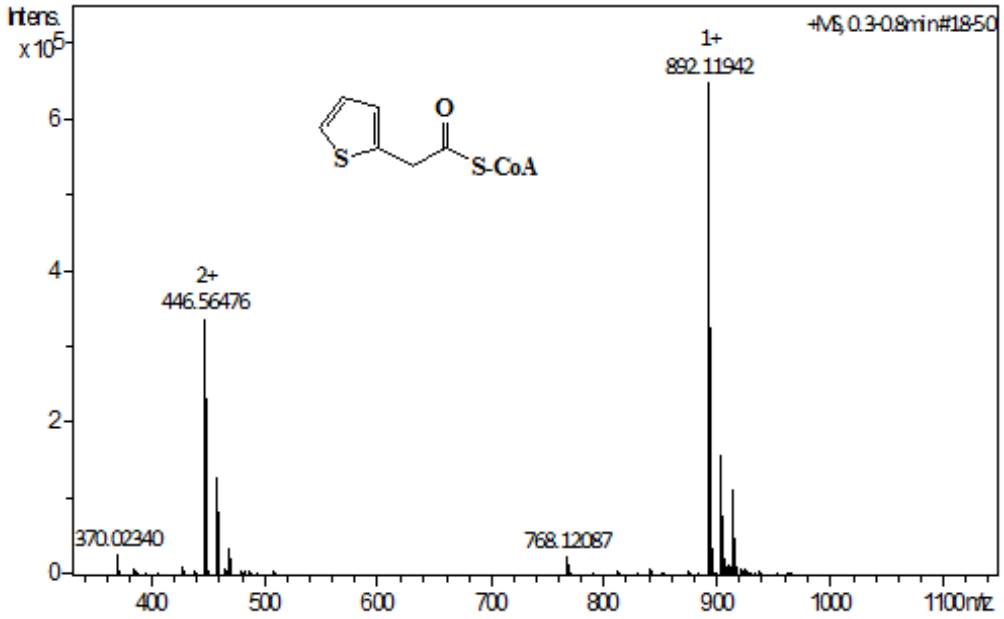

Figure B14. Mass spectrum of 2-thiophenacetyl-CoA.

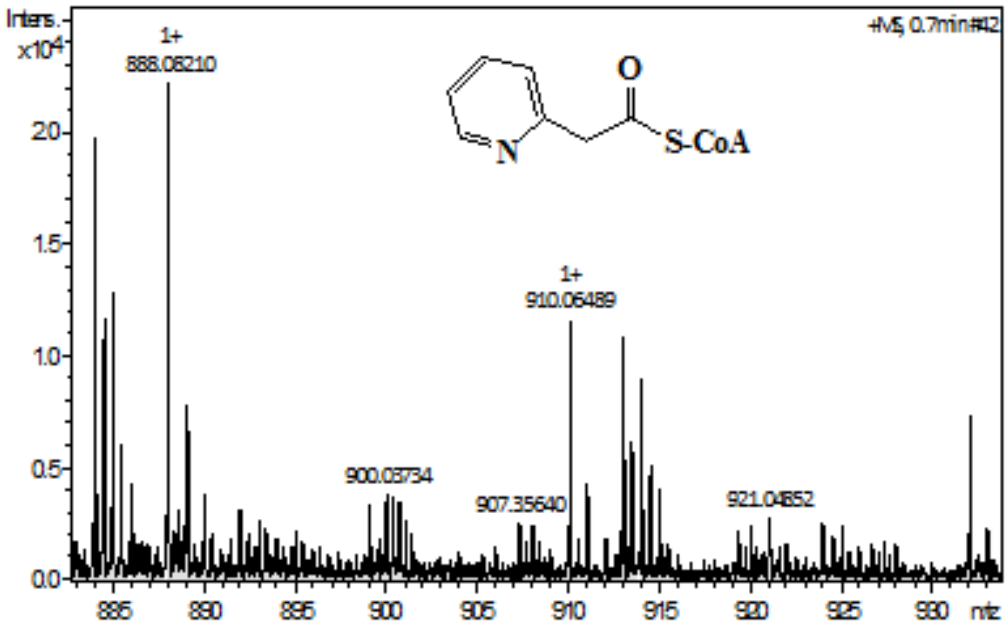

Figure B15. Mass spectrum of 2-pyridylacetyl-CoA.

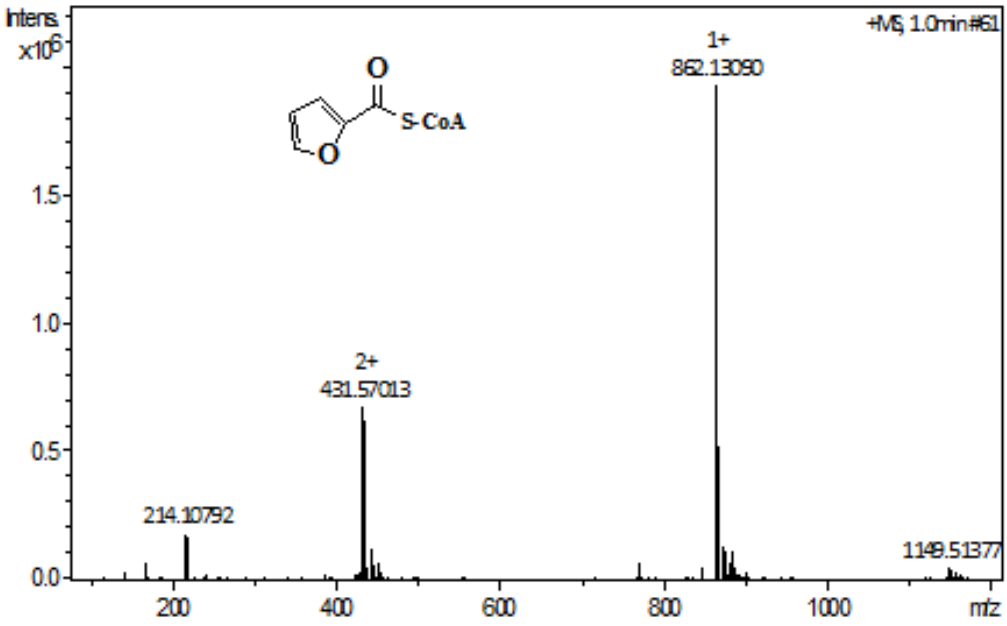

Figure B16. Mass spectrum of 2-furoyl-CoA.

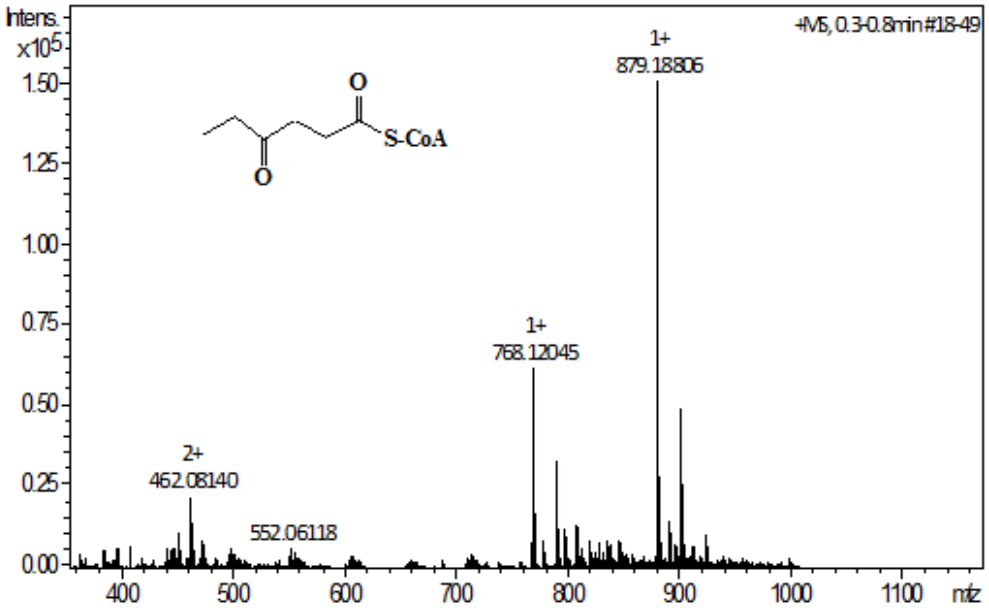

Figure B17. Mass spectrum of 4-oxohexanoyl-CoA.

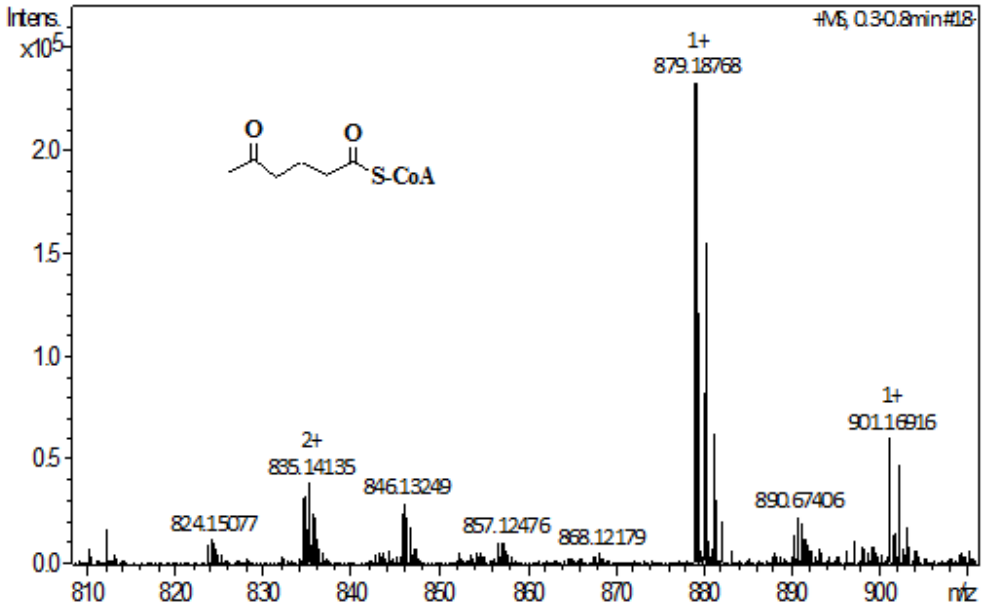

Figure B18. Mass spectrum of 5-oxohexanoyl-CoA.

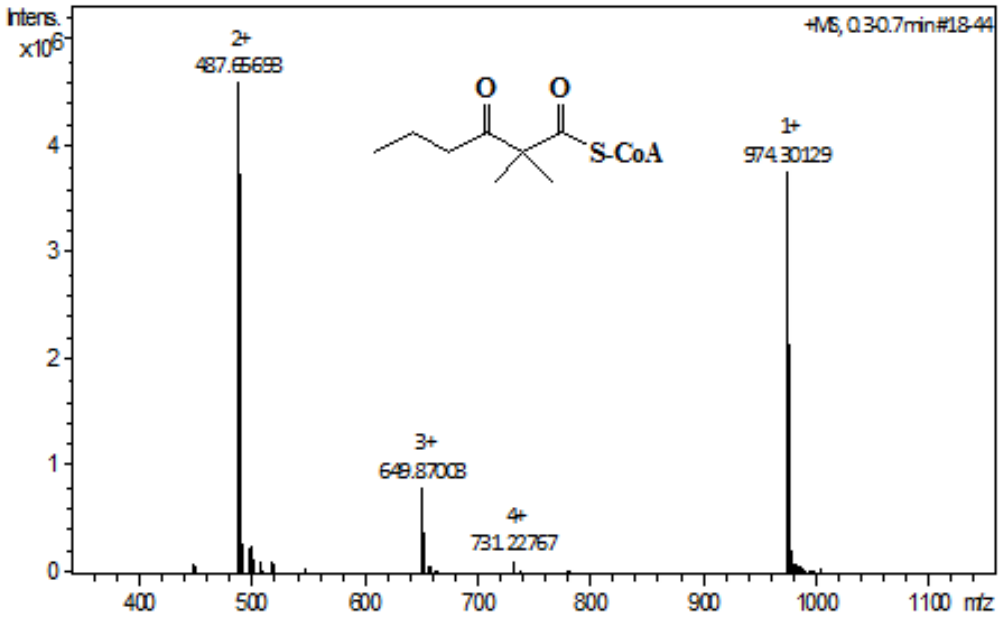

Figure B19. Mass spectrum of 2,2´-dimethyl-3-oxohexanoyl-CoA.

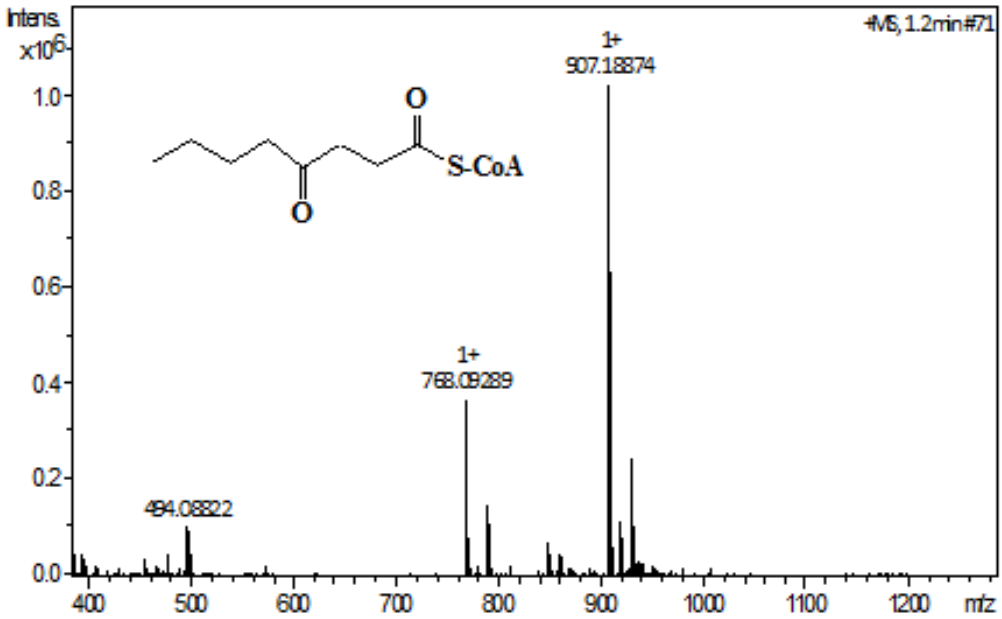

Figure B20. Mass spectrum of 4-oxooctanoyl-CoA.

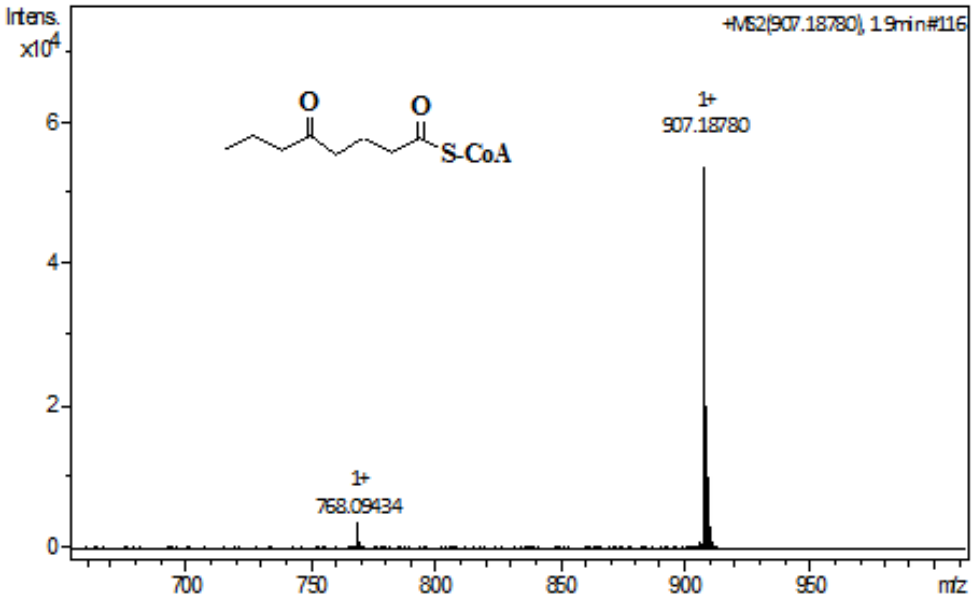

Figure B21. Mass spectrum of 5-oxooctanoyl-CoA.

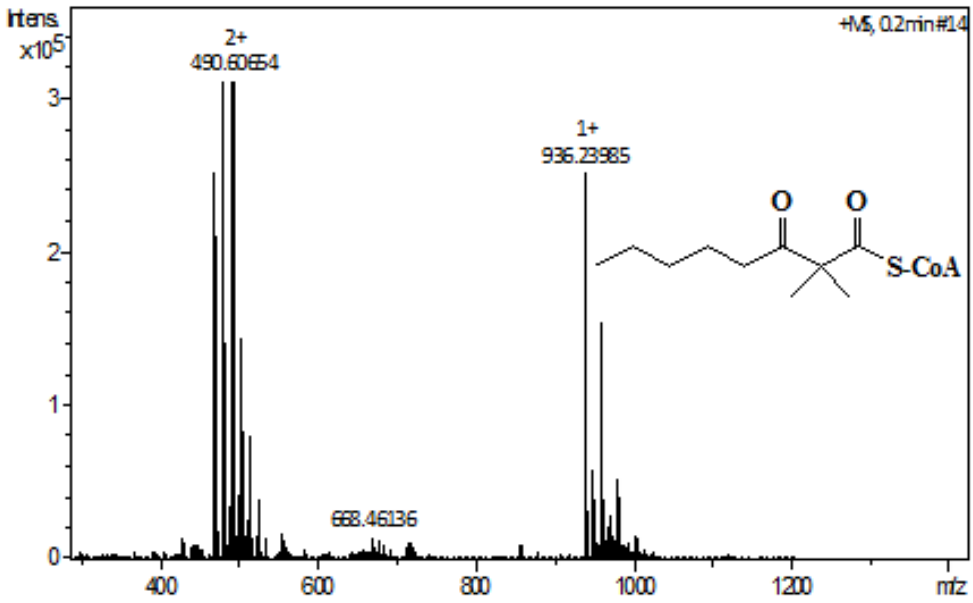

Figure B22. Mass spectrum of 2,2´-dimethyl-3-oxooctanoyl-CoA.

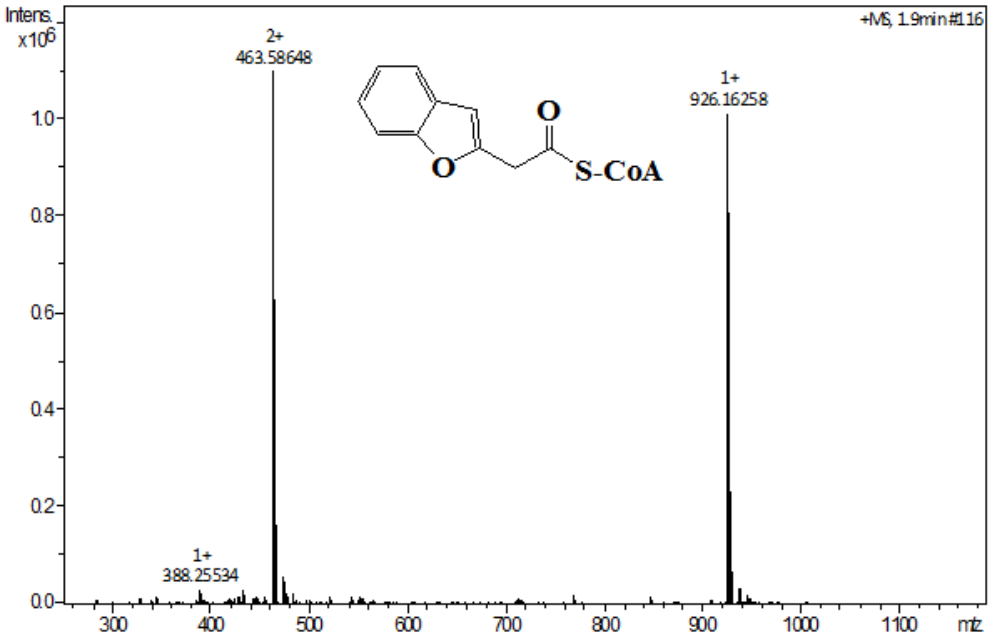

Figure B23. Mass spectrum of 2-benzofuranacetyl-CoA.

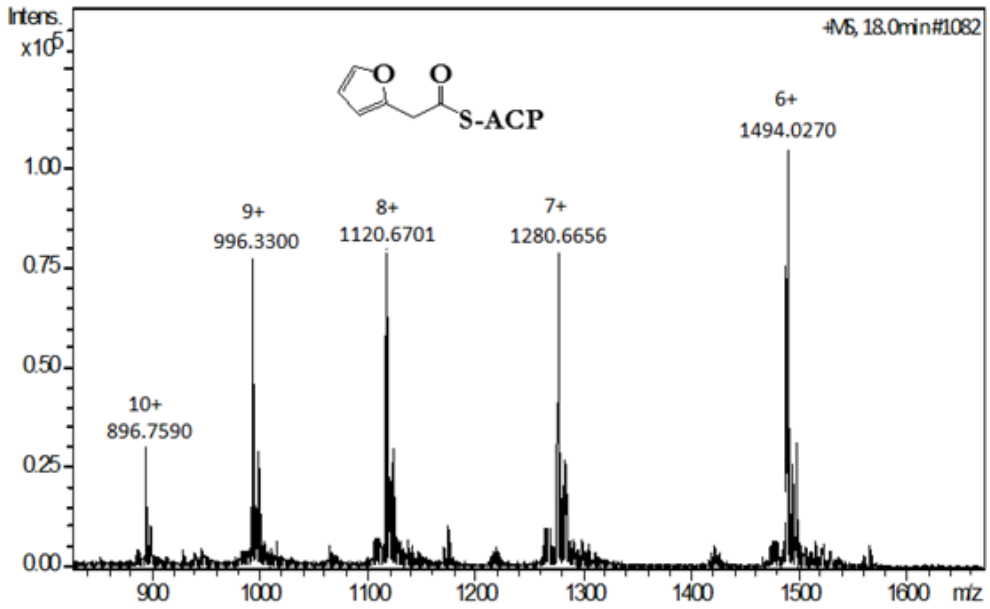

Figure B24. Mass spectrum of 2-furanacetyl-ACP.

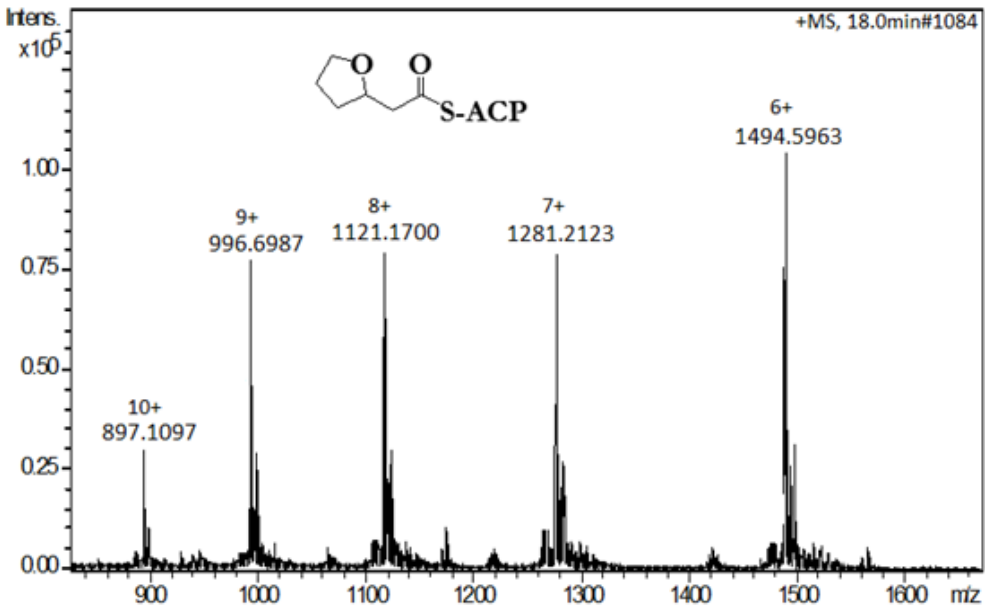

Figure B25. Mass spectrum of 2-tetrahydrofuranacetyl-ACP.

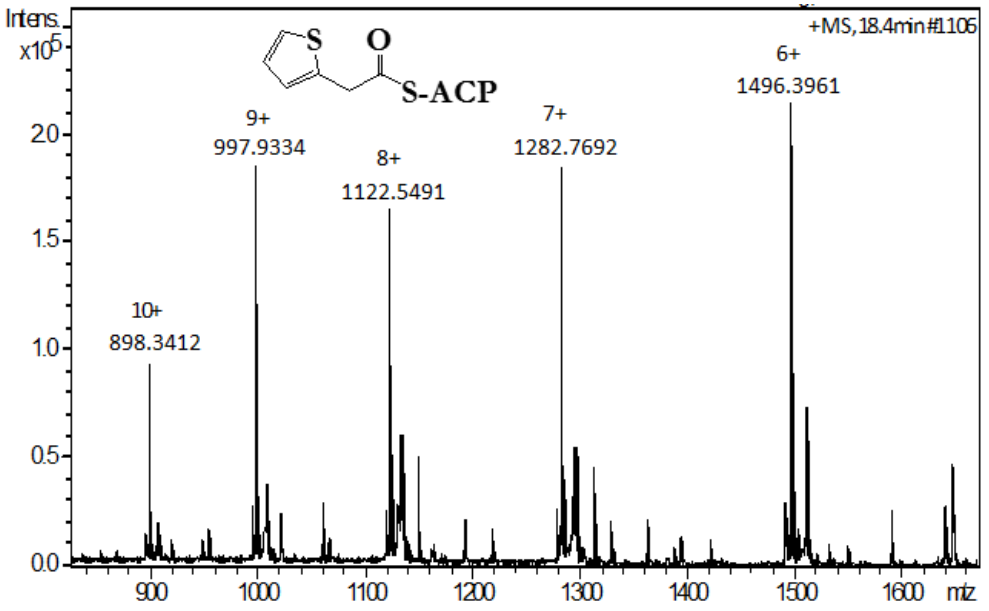

Figure B26. Mass spectrum of 2-thiopheneacetyl-ACP.

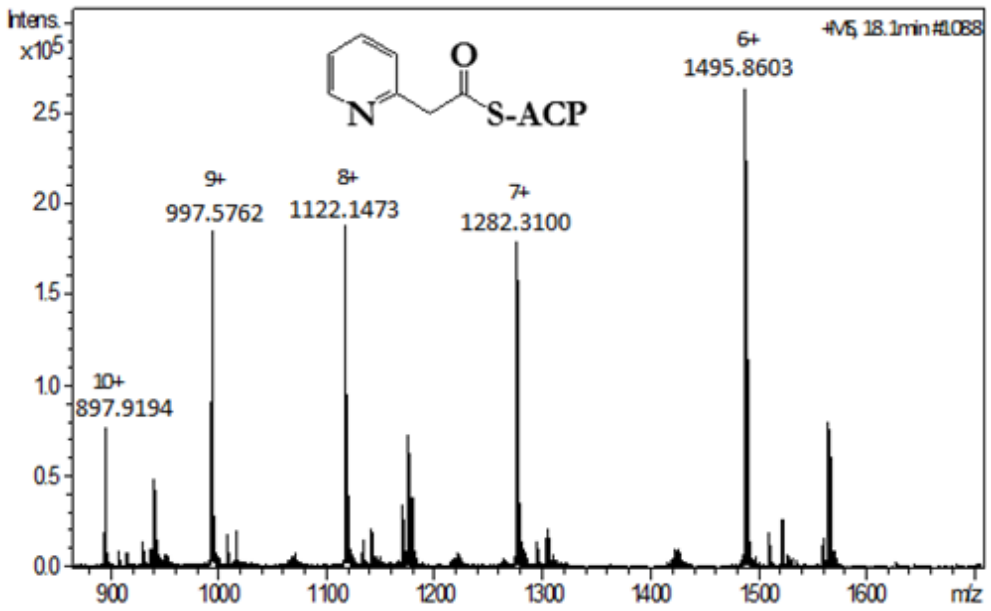

Figure B27. Mass spectrum of 2-pyridylacetyl-ACP.

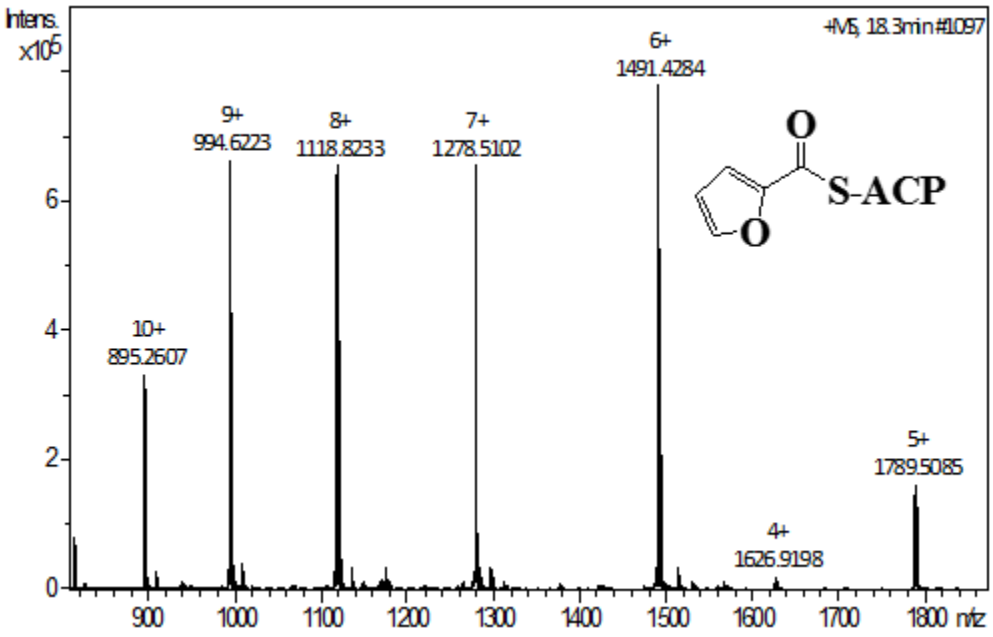

Figure B28. Mass spectrum of 2-furoyl-ACP.

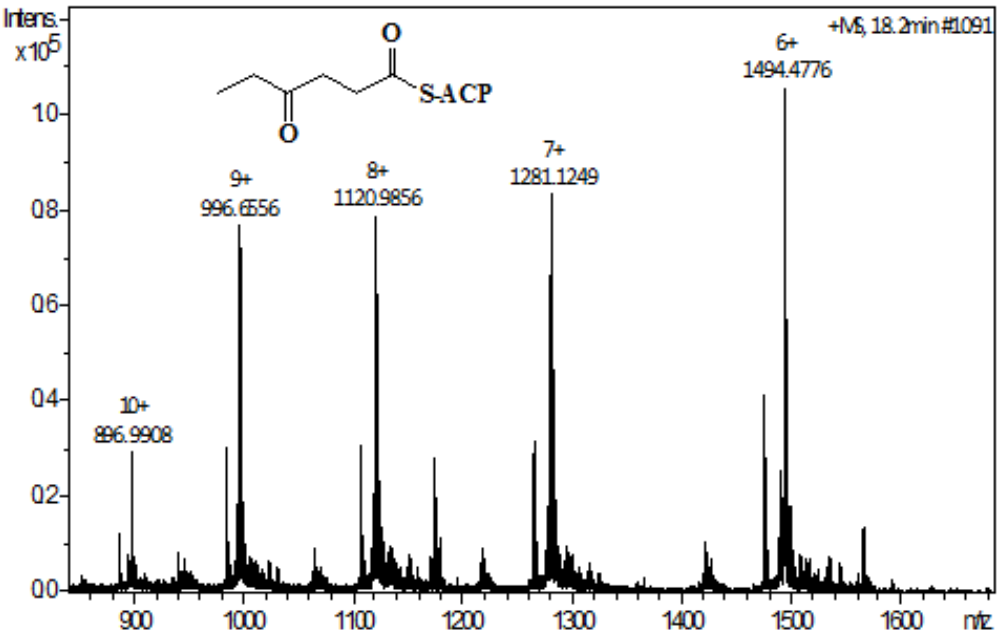

Figure B29. Mass spectrum of 4-oxohexanoyl-ACP.

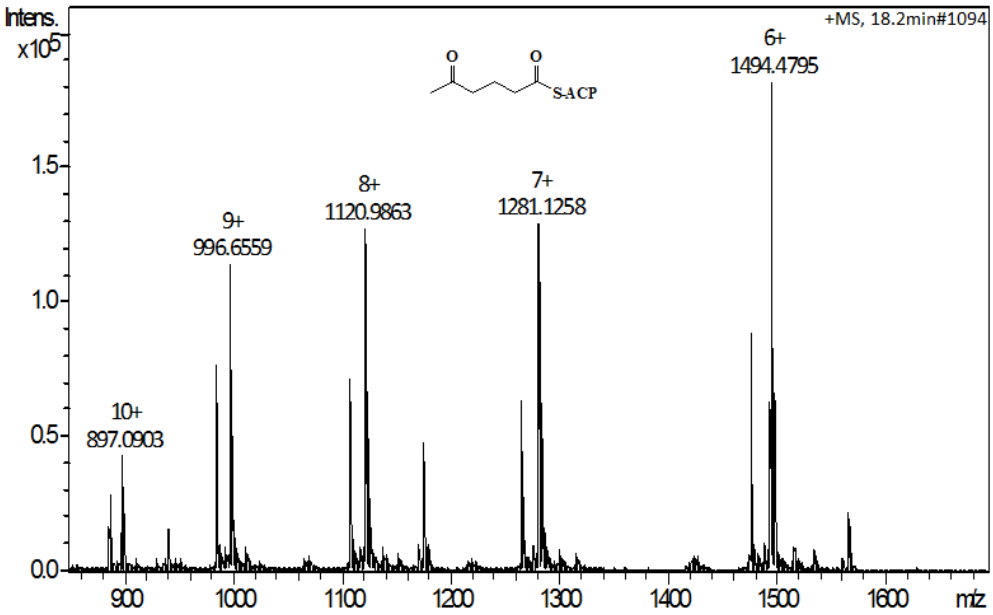

Figure B30. Mass spectrum of 5-oxohexanoyl-ACP.

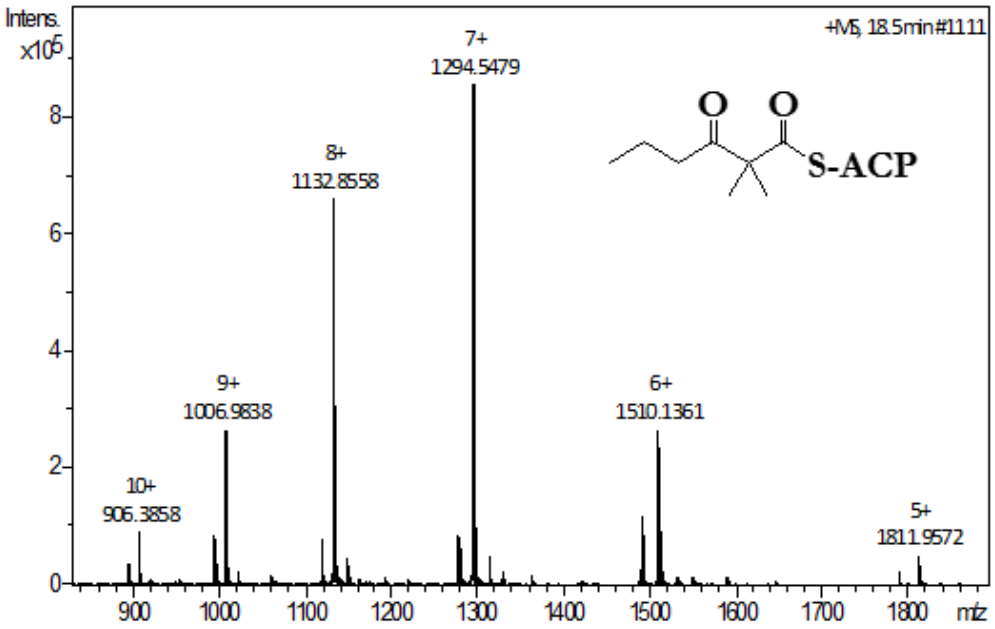

Figure B31. Mass spectrum of 2,2´-dimethyl-3-oxohexanoyl-ACP.

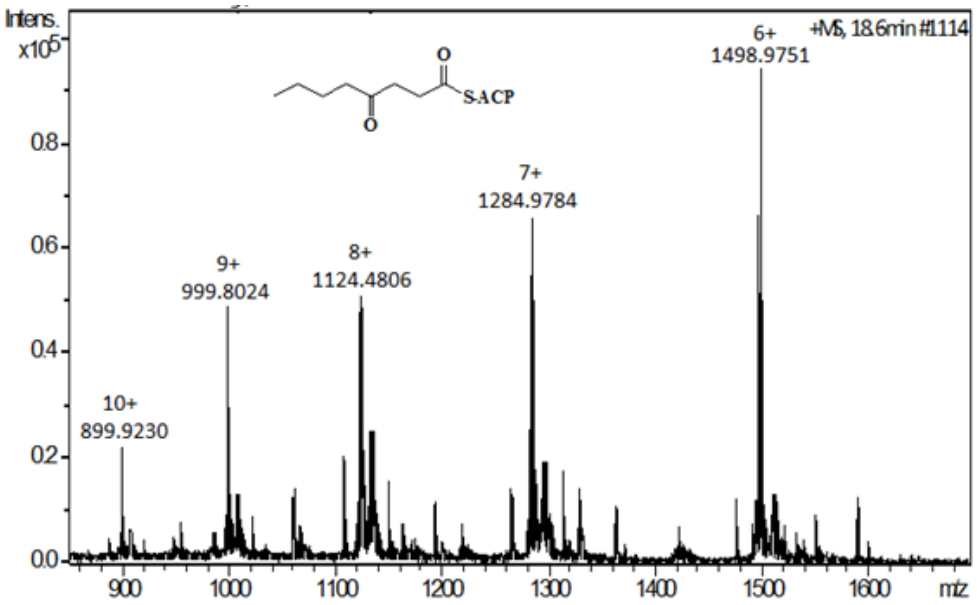

Figure B32. Mass spectrum of 4-oxooctanoyl-ACP.

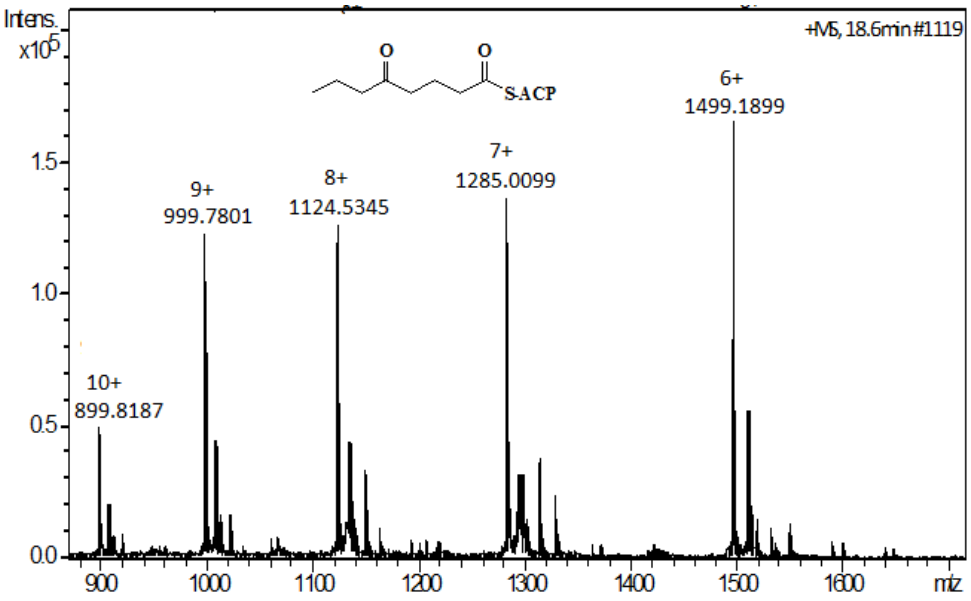

Figure B33. Mass spectrum of 5-oxooctanoyl-ACP.

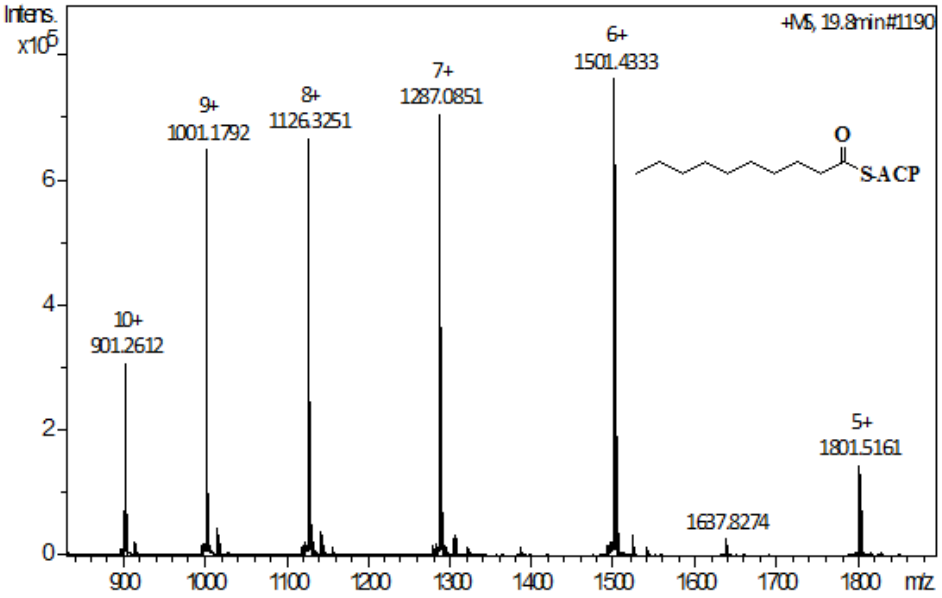

Figure B34. Mass spectrum of decanoyl-ACP.

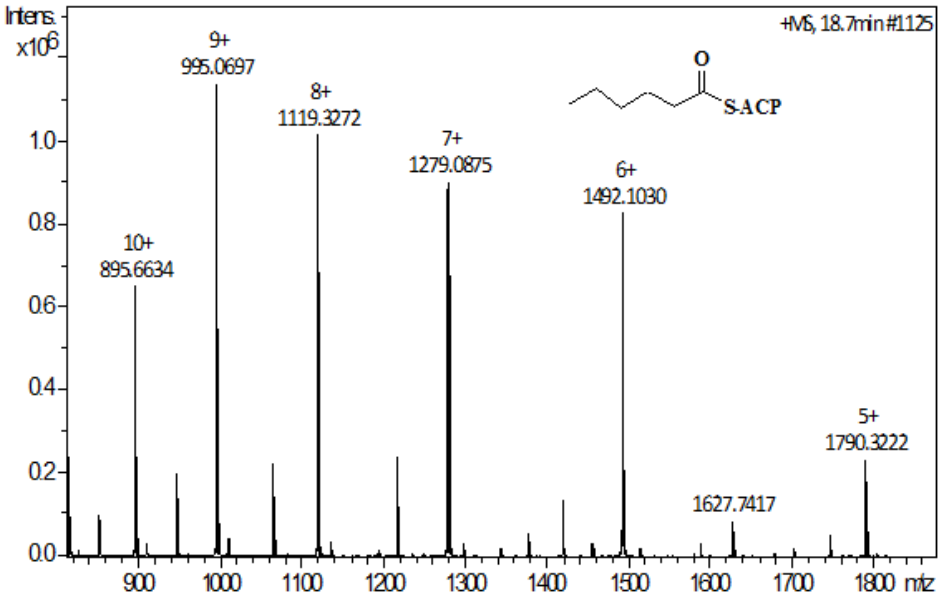

Figure B35. Mass spectrum of hexanoyl-ACP.

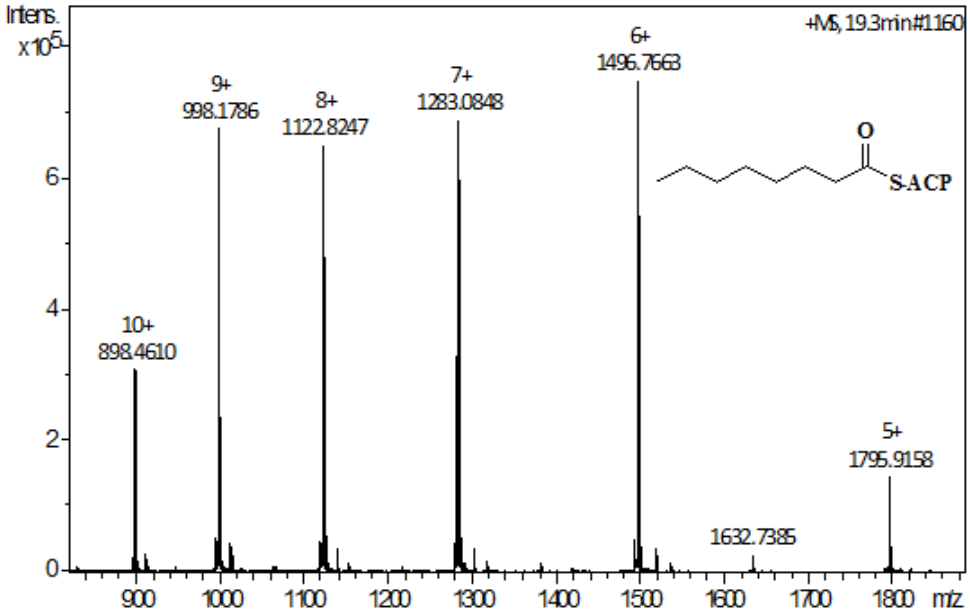

Figure B36. Mass spectrum of octanoyl-ACP.

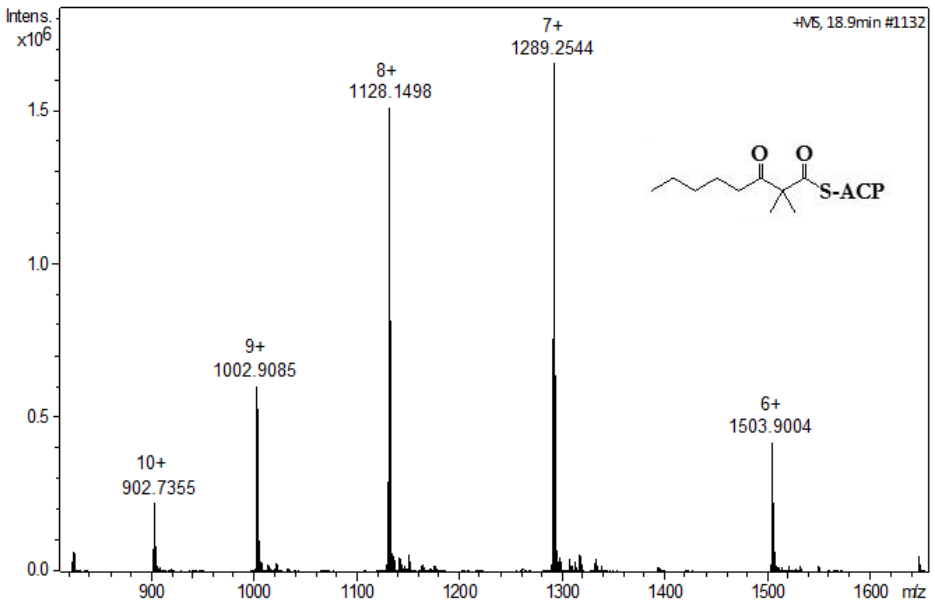

Figure B37. Mass spectrum of 2,2´-dimethyl-3-oxoC8-ACP.

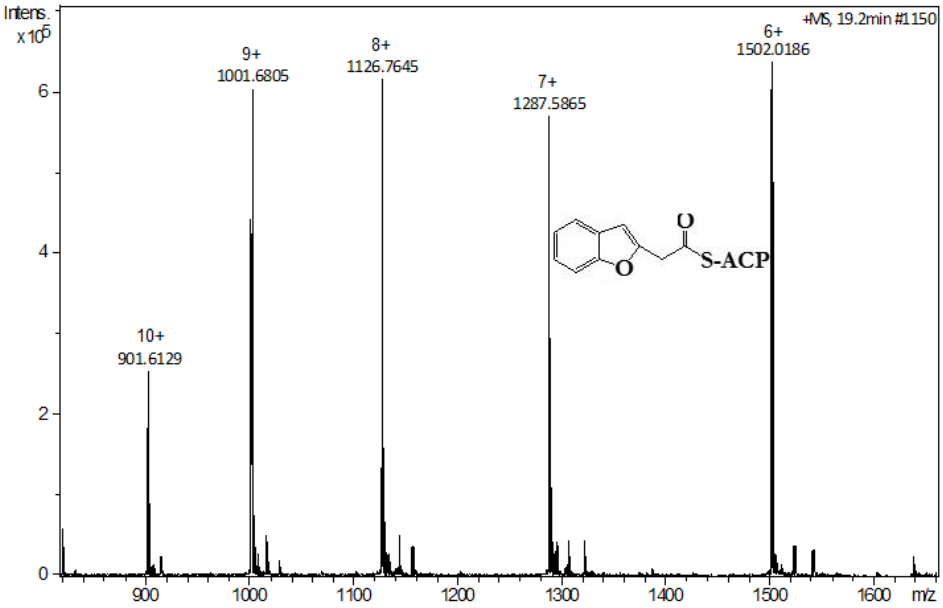

Figure B38. Mass spectrum of 2-benzofuranacetyl-ACP.

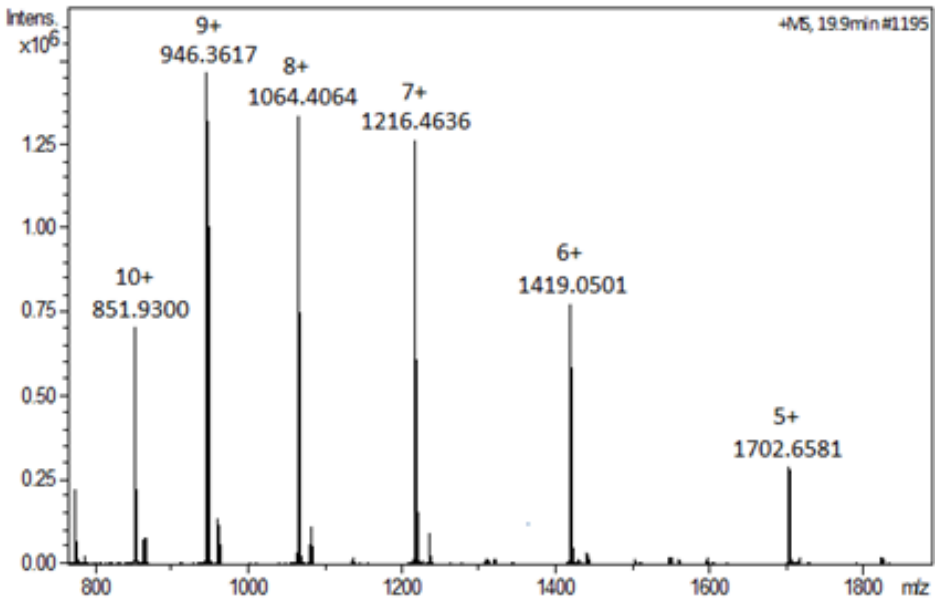

Figure B39. Mass spectrum of apo-ACP.

APPENDIX C

Enzyme-kinetic data

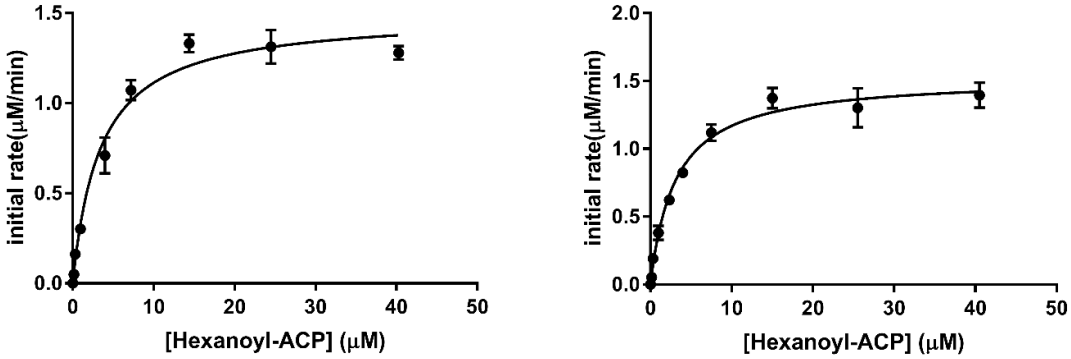

Figure C1. Substrate-velocity curve for EsaI T140A with C6-ACP following (left) lactonization and (right) acylation.

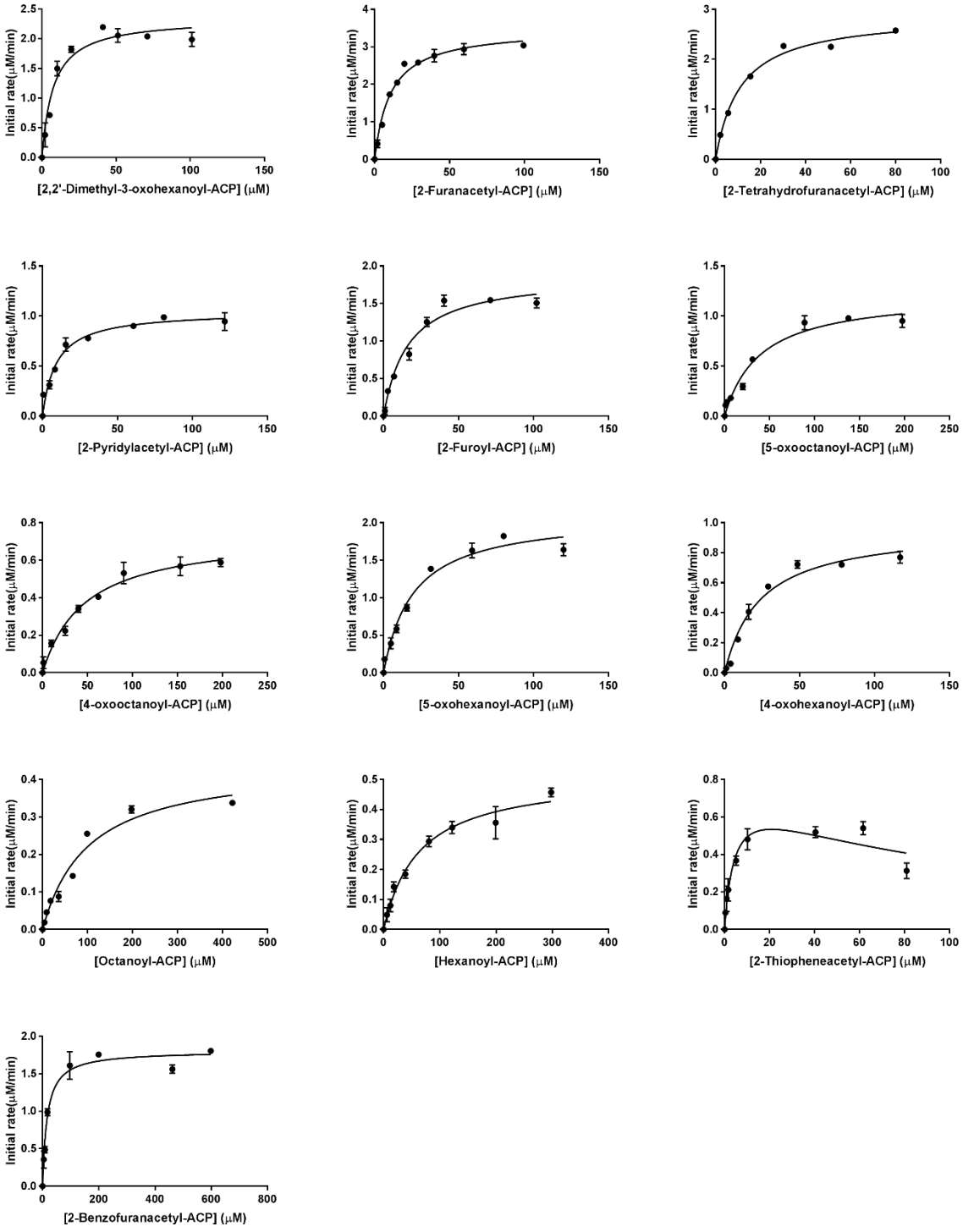

Figure C2. Substrate-velocity curves of alternative 3-oxoacyl-ACP substrates in EsaI-catalyzed reaction by following lactonization assay.

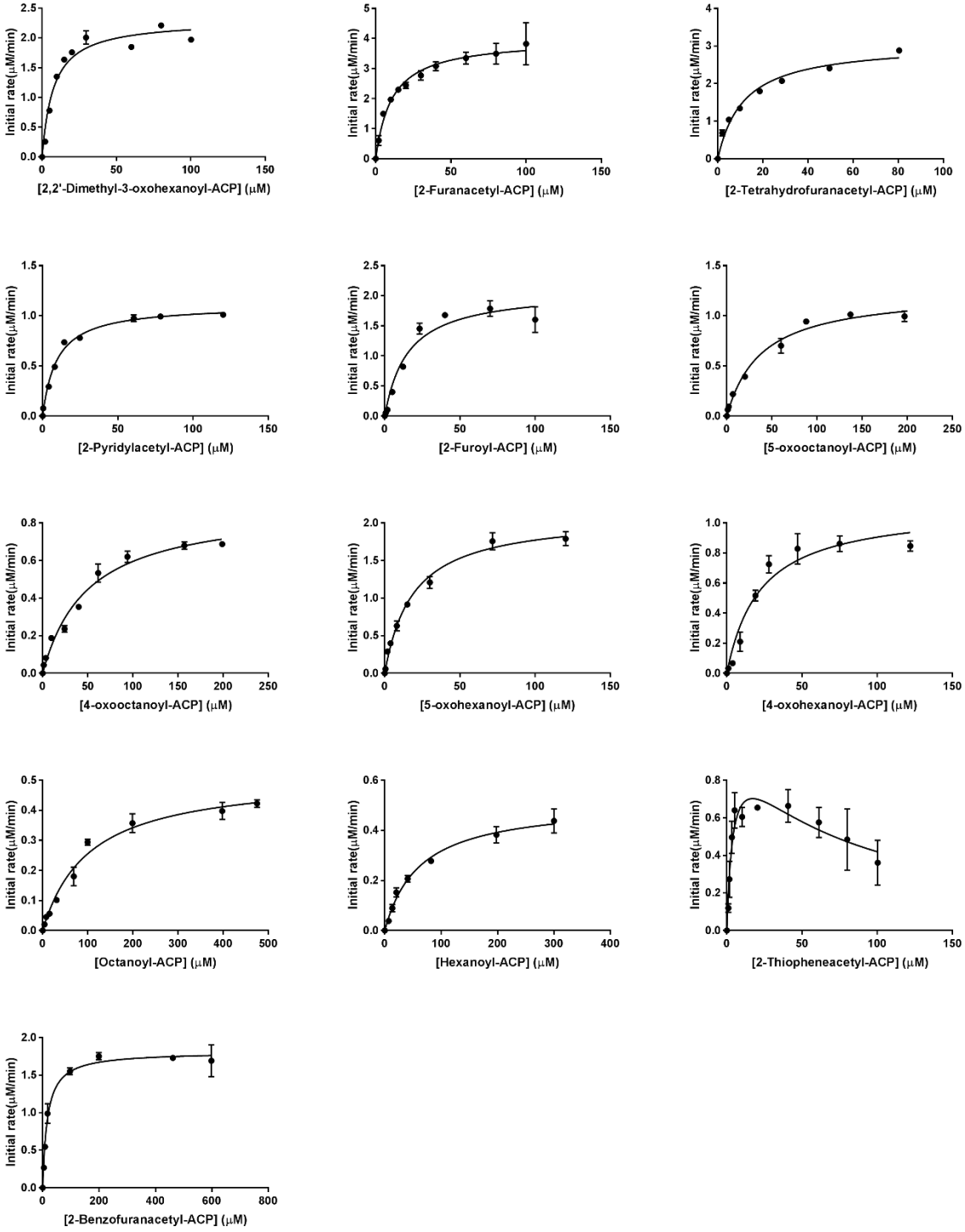

Figure C3. Substrate-velocity curves of alternative 3-oxoacyl-ACP substrates in EsaI-catalyzed reaction by following acylation assay.

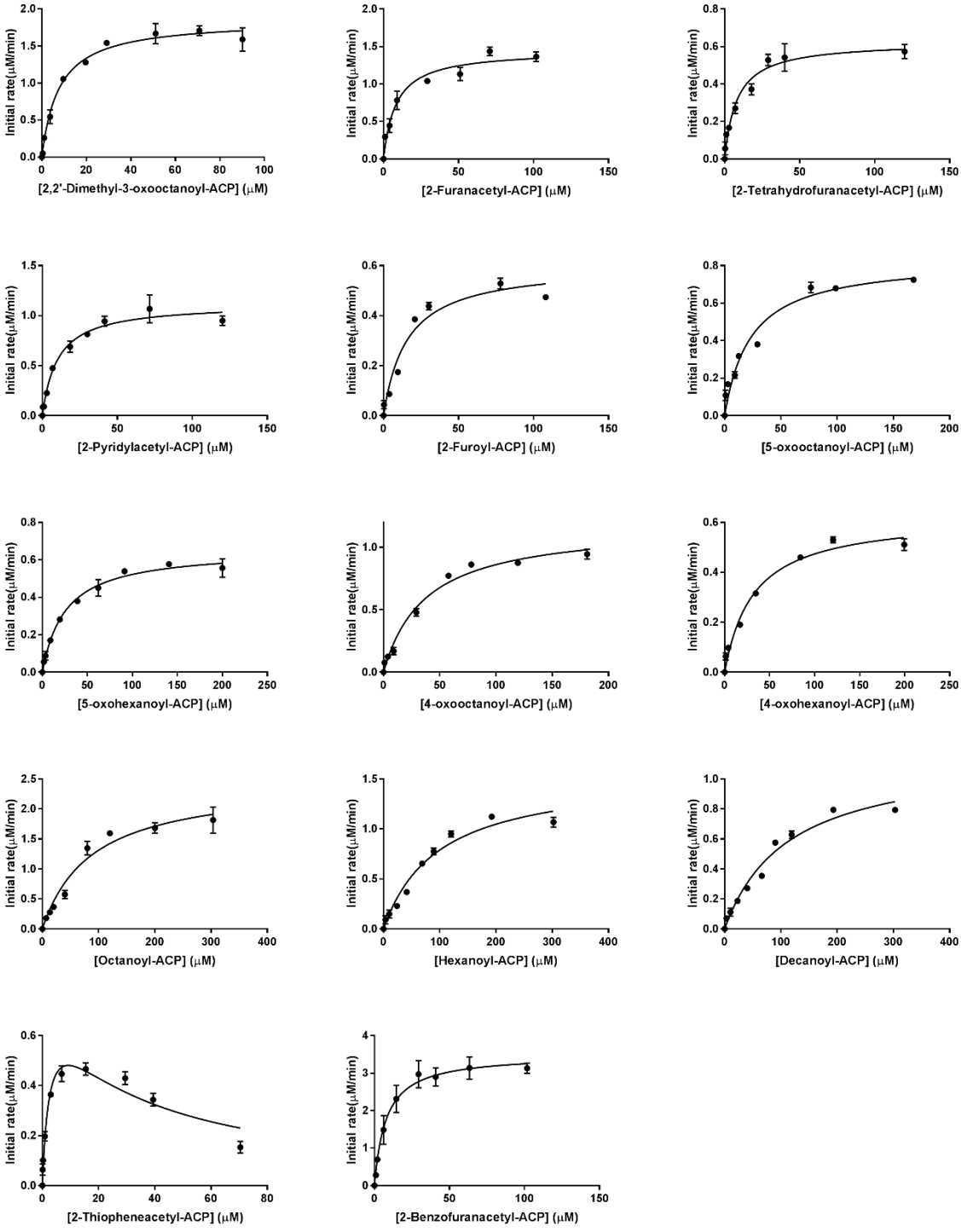

Figure C4. Substrate-velocity curves of alternative 3-oxoacyl-ACP substrates in YspI-catalyzed reaction by following lactonization assay.

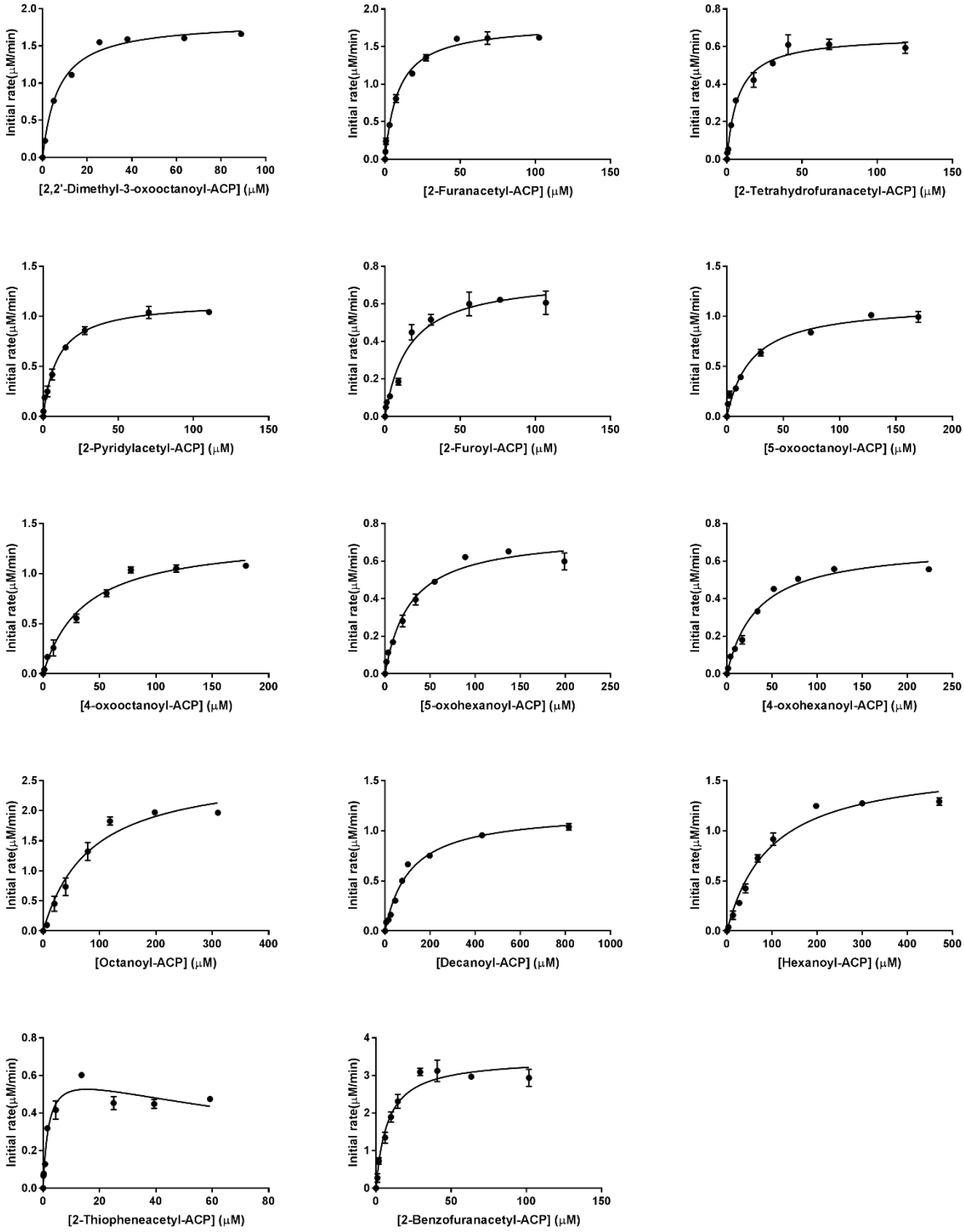

Figure C5. Substrate-velocity curves of alternative 3-oxoacyl-ACP substrates in YspI-catalyzed reaction by following acylation assay.

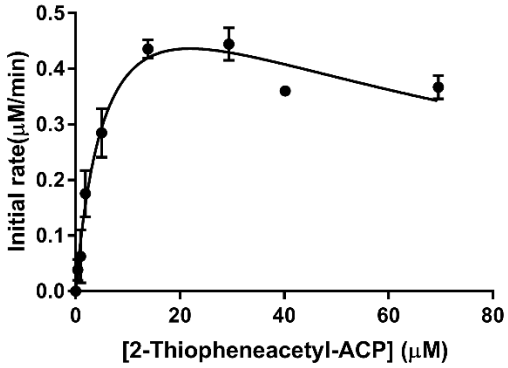

Figure C6. Substrate-velocity curve of 2-thiopheneacetyl-ACP in EsaI-catalyzed reaction following lactonization. SAM and EsaI concentrations were fixed at 50 μM and 1.02 μM, respectively. Kinetic parameters were summarized in table 3.

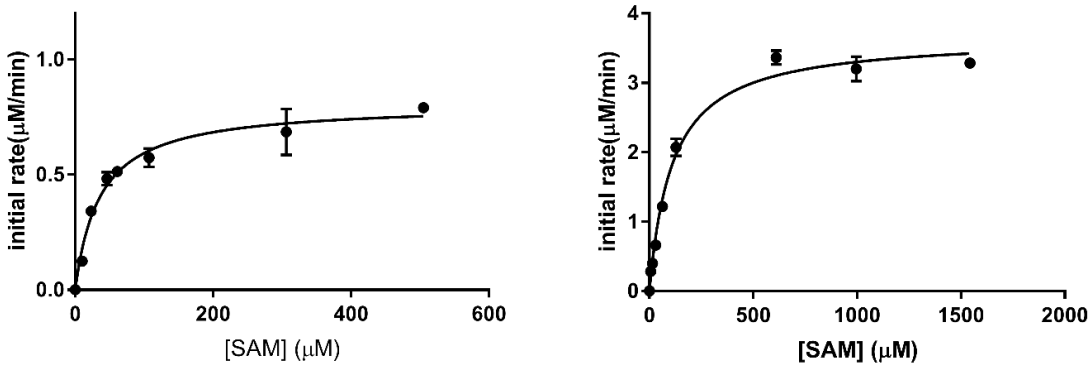

Figure C7. Determination of $\mathbf{K_m^{SAM}}$ in EsaI-catalyzed reaction. (Left) 2-Thiopheneacetyl-ACP and EsaI concentrations were fixed at 40 μM and 1.01 μM, respectively. The value of $\mathbf{K_m^{SAM}}$ was 36.09 ± 4.69 μM, k_{cat} was 0.796 ± 0.029 min^{-1}, k_{cat}/K_m was 0.0221 ± 0.0029 $\mu M^{-1}min^{-1}$. (Right) 2-Furanacetyl-ACP and EsaI concentrations were fixed at 103 μM and 1.01 μM, respectively. The value of $\mathbf{K_m^{SAM}}$ was 111.3 ± 10.7 μM, k_{cat} was 3.64 ± 0.09 min^{-1}, k_{cat}/K_m was 0.0327 ± 0.0032 $\mu M^{-1}min^{-1}$.

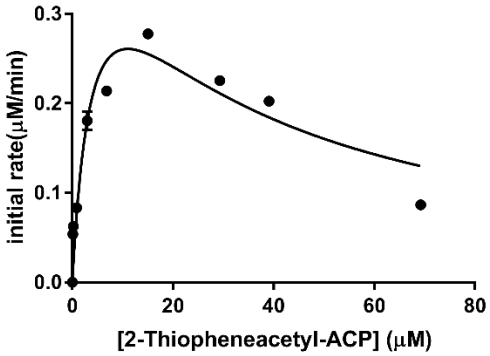

Figure C8. Substrate-velocity curve of 2-thiopheneacetyl-ACP in YspI-catalyzed reaction following lactonization. SAM and YspI concentrations were fixed at 50 μM and 1 μM, respectively. Kinetic parameters were summarized in table 5.

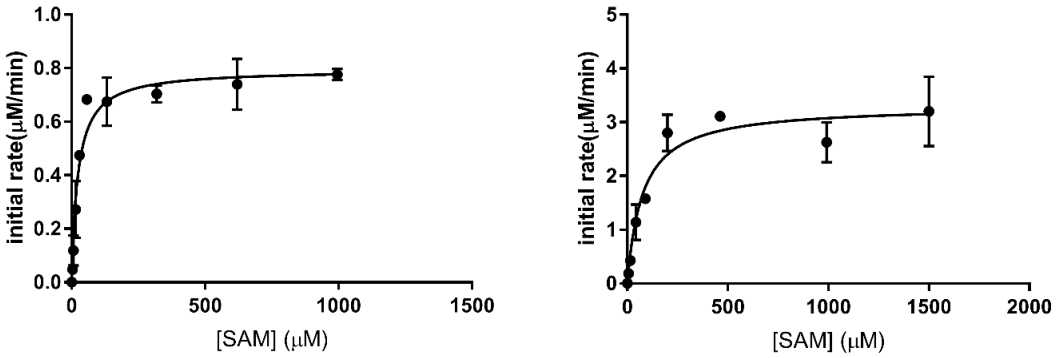

Figure C9. Determination of $\mathbf{K_m^{SAM}}$ in YspI-catalyzed reaction. (Left) 2-Thiopheneacetyl-ACP and YspI concentrations were fixed at 40 μM and 1.04 μM, respectively. The value of $\mathbf{K_m^{SAM}}$ was 23.52 ± 4.03 μM, k_{cat} was 0.764 ± 0.029 min-1, k_{cat}/K_m was 0.0325 ± 0.0057 $\mu M^{-1}min^{-1}$. (Right) 2-Benzofuranacetyl-ACP and YspI concentrations were fixed at 80 μM and 1.03 μM, respectively. The value of $\mathbf{K_m^{SAM}}$ was 75.98 ± 17.49 μM, k_{cat} was 3.21 ± 0.18 min-1, k_{cat}/K_m was 0.0423 ± 0.0100 $\mu M^{-1}min^{-1}$.